Fast Atom Bombardment and Electron Impact Mass Spectrometry Studies of Some Aryltin Compounds and Ferrocenes

Yongchong Luo, B.Sc. (Hons.)

A Thesis

submitted to the Department of Chemistry

in partial fulfillment of the requirements

for the degree of

Master of Science

August 1993

Brock University

St. Catharines, Ontario

To my parents
for their affection, encouragement and endurance
during those hard times!

ABSTRACT

Both EI MS and FAB MS behavior of two groups of compounds, aryltin and ferrocene compounds, have been studied.

For the aryltin compounds, the effect of substituent group position, substituent group type and ligand type on the EI spectra have been explored in the EI MS studies. The fragmentation mechanism has been investigated under EI with linked scans, such as fragment ion scans(B/E), parent ion scans(B^2/E) and constant neutral radical loss scans($B^2(1-E)/E^2$). In the FAB MS studies, matrix optimization experiments have been carried out. The positive ion FAB MS studies focused on the effect of substituent group position, substituent group type and ligand type on the spectra. The fragmentation mechanisms of all the samples under positive ion FAB have been studied by means of the linked scans. The CA positive ion FAB fragmentation studies were also carried out for a typical sample. Negative ion FAB experiments of all the compounds have been done. And finally, the comparison of the EI MS and FAB MS has been made.

For ferrocenes, the studies concentrated on the fragmentation mechanism of each compound under EI with linked scan techniques in the first field-free region and the applicability of positive/negative ion FAB MS to this group of compounds. The fragmentation mechanisms under positive ion FAB of those ferrocenes which can give positive ion FAB MS spectra were studied with the linked scan techniques. The CA +ve FAB fragmentation studies were carried out for a typical sample. Comparison of the EI MS and FAB MS has been made.

ACKNOWLEDGMENTS

This author like to give sincere thanks to Professor Jack M. Miller for his teaching, support and encouragement which was so generously provided throughout the course of this project.

I would also like to express my gratitude to Professor J. Stephen Hartman, Professor Dave C. Moule, Professor Eugene A. Cherniak and Professor Kathleen M. Gough for the guidance and advice they provided me during my M.Sc. studies.

I am greatly indebted to Professor I. Wharf for his provision of the aryltin compounds and Professor Z. R. Lin for his provision of ferrocene samples for this study.

Very special appreciation goes to Mr. Tim Jones for his great help and teaching in operating the necessary instruments in this project. Without his help, to finish this thesis is impossible. Thanks also go to my friends who have given me help and inspiration.

And finally, I would like to give my special thanks to my wife and my son for their assistance in my study period.

Table of Contents

List of Figures

List of Tables

List of Schemes

Schemes **Page**

Schemes **Page**

Schemes **Page**

.1.

INTRODUCTION

1.1. Mass Spectrometry

1.1.1. Brief Review of Mass Spectrometry

The generation of mass spectra goes back to the late nineteenth and early twentieth centuries. In 1886, Goldstein [1] first observed visible streamers of light in a low pressure electric discharge tube. He suggested that there must be some type of rays or particles associated with them that traveled in a direction opposite to that of the usual cathode rays. In 1898, W. Wien [2] demonstrated that these rays could be deflected by strong electric and magnetic fields, and concluded that they are consisted of positively charged particles. Thomson [3] had done more detailed investigation into the properties of the positive rays using a positive-ray parabola apparatus in 1913. In his experiment, the positive rays formed in a low pressure discharge tube were accelerated and collimated by a fine-bore brass tube and then proceeded into a low-pressure region along an axis between two electrostatic plates and the pole pieces of an electromagnet. The ions were stopped by a fluorescent screen that allowed direct observation of the final focal point of any particular ion trajectory. With a similar apparatus, Thomson first demonstrated the existence of two stable neon isotopes [4].

Dempster [5] and Aston [6] built the first sophisticated instruments. In 1918, Dempster made a mass analyzing system using a semi-circular magnetic field instead of a circular field. The positively charged particles were deflected through 180° circle and detected. At almost the same time, Aston developed a different type of instrument which he called the "mass spectrograph". This instrument could not only separate particles according to their m/z (mass/charge) ratios, but also focus them by filtering out unwanted velocities. Dempster's instruments provided a more accurate measurement of ion abundance. With his apparatus, Dempster made an accurate abundance determination of the isotopes of magnesium, lithium, potassium etc.. Aston's machine, on the other hand, permitted more accurate mass measurements. Using his equipment, Aston provided unequivocal proof that neon consists of two isotopes, mass number 20 and 22. In 1934, Mattauch and Herzog [7,8] combined an electrostatic lens and a magnet to provide both direction and velocity focusing properties, thereby providing a relatively good mass and ion abundance measurement. Moreover, they derived general focusing equations for radial electric and homogeneous magnetic fields which made it possible to design high resolution, double focusing mass spectrographs.

The work of these scientists established the foundation of modern mass spectrometry. Since the 1940s, mass spectrometry has gradually become an important tool for quantitative analysis, because it can provide remarkably reproducible mass spectra for gases and some volatile hydrocarbons. Around 1950, the commercial availability of mass spectrometers increased dramatically [9] as the introduction of heatable sample inlet systems provided the capability required to obtain the mass spectra of low volatility compounds [10].

In recent years, with the advance of technology and the introduction of various new ionization techniques, as well as the advent of various hyphenated techniques such as GC-MS, LC-MS, etc., mass spectrometry has become a very powerful analytical tool in both fundamental studies and routine analysis. The development of mass spectrometry gradually

developed from two-dimensional spectra into three- and four-dimensional spectra [11]. Figure 1 is a schematic diagram of historical progress of high resolution mass spectrometer designs from photoplate detector, to electrical detection and ultimately to MS-MS designs.

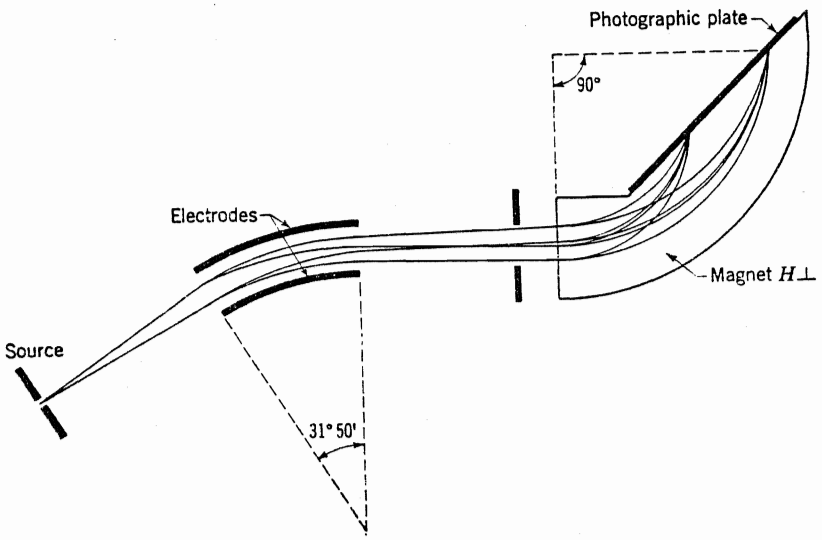

Figure 1.(a) Double-focusing mass spectrometer of Mattauch-Herzog type (1934)

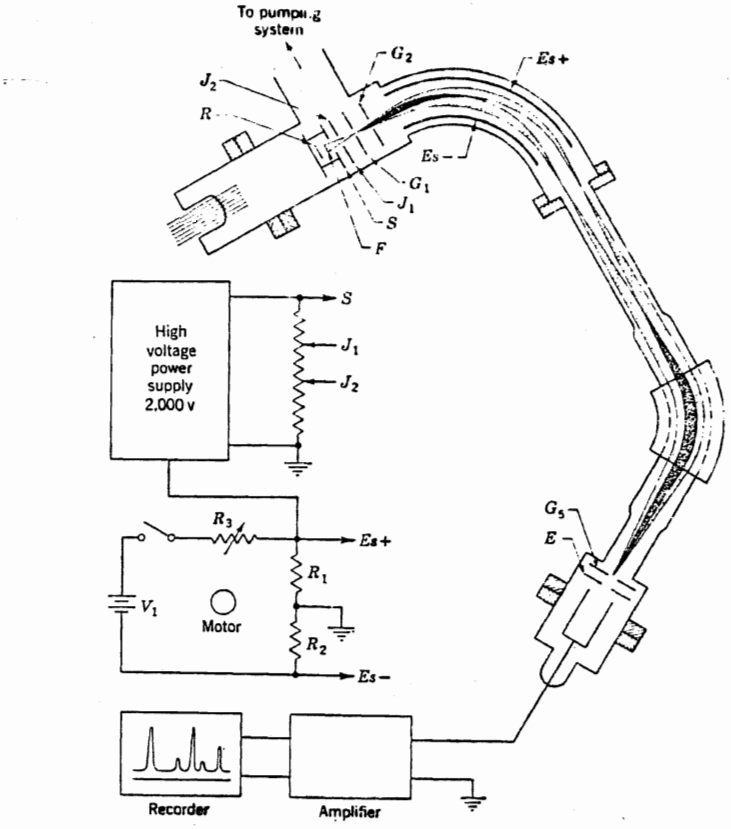

1. (b). Double-focusing mass spectrometer of Nier-Robert type (1951)

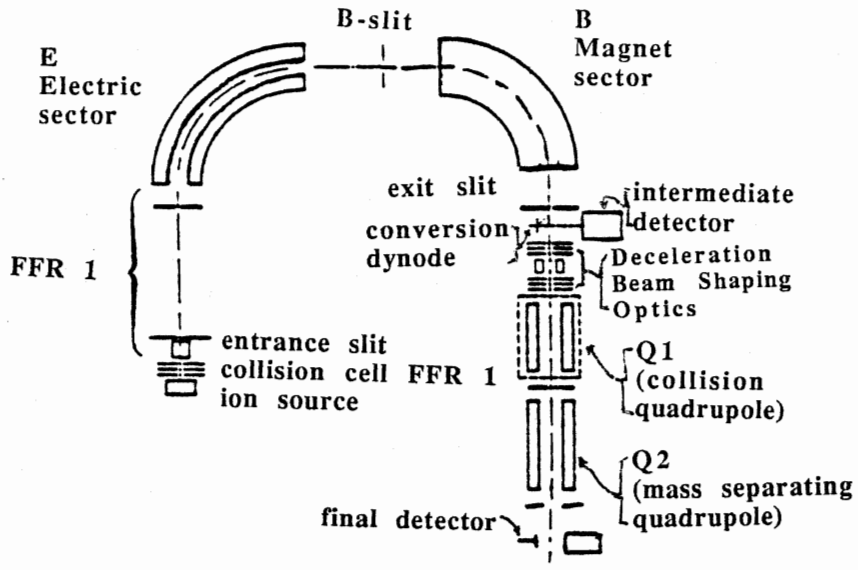

1.(c). EBQQ mass spectrometer (1190)

Figure 1. Historical progress of mass spectrometer designs

1.1.2. Electron Impact (EI)

Among the three major parts of a mass spectrometer (ionization source, analyzer, and collector), the ionization source is considered to be the "heart of the mass spectrometer". It is the region in which the sample ions to be analyzed are generated. Hence, the development of new ion sources to provide both molecular ions and plenty of fragment ions always becomes the focal point of mass spectrometry. During the last two decades, more than ten different types of ion sources, plus numerous variations on each theme have appeared. The frequently used ionization sources include electron impact (EI), chemical ionization (CI), atmospheric pressure ionization (API) techniques, field desorption (FD), plasma desorption (PD), laser desorption (LD), secondary ion mass spectrometry (SIMS) (solid or liquid) and fast atom bombardment (FAB) ionization etc.. This section will introduce electron impact (EI) ionization source. Section 1.1.3 will discuss fast atom bombardment (FAB) source. Section 1.1.4. will briefly introduce the rest of the ionization sources mentioned above.

Electron impact (EI) ionization [12] is one of the oldest and most commonly used techniques in the production of positive ions. In electron impact ionization, milligram to nanogram amounts of sample are introduced, as a vapor, into the source at the operating pressure (ca. 10-6 torr). The vapor is allowed to pass through a slit, A, into the ionization chamber (Fig. 2), where it is bombarded with a beam of electrons accelerated from a hot filament. The energy of the electron beam can be varied from 0 to 100eV. The energy imparted to the molecules by the impact of the ionizing electrons, is usually greater than the ionization energy; excess energy may remain in the molecular ion ($M^{+\cdot}$) making the molecular ion very unstable. Generally, these energies can be used to break one or more bonds of the molecular ion. Depending on the energy available, molecular ions may remain

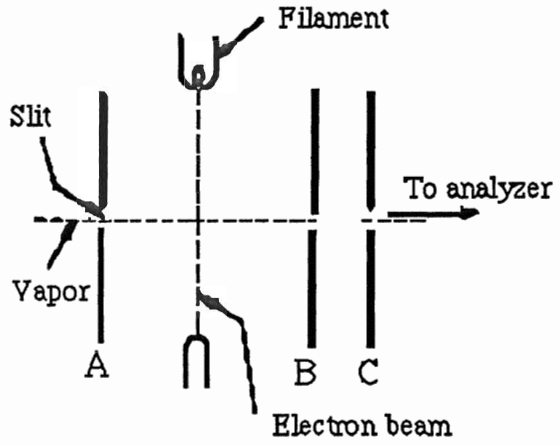

Figure 2. Schematic diagram of simplified EI source [12]

or dissociate either by eliminating a radical or by losing an even-electron molecule. The entire process can be illustrated as follows:

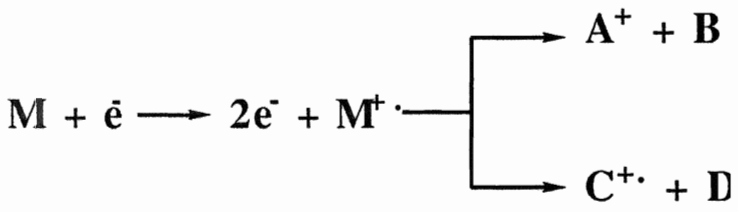

where :

	M	is the analyte molecule ;
	e^-	is a 70-100 eV electron;
	$M^{+\cdot}$	is an excited state radical (the molecular ion);
	A^+	is a charged even-electron fragment ion;

$B\cdot$ is a neutral radical;

$C^{+}\cdot$ is a charged odd-electron fragment ion;

D is an even-electron molecule.

Depending on their internal energies, the fragment ions A^{+} and $C^{+}\cdot$ also have the possibility of fragmenting.

The extent to which the molecular ions fragment is usually relatively large when electron impact ionization is employed. Sometimes, it is impossible to detect an appreciable abundance of the molecular ion. This problem is a serious drawback of electron impact ionization. In some cases, it is possible to increase the relative abundance of the molecular ion by reducing the energy of the ionizing beam of electrons. When the energy of the ionizing electrons approaches the ionization energy of the molecule, the excess energy remaining in the molecular ion is small and fragmentation is decreased. However, the large degree of fragmentation, associated with electron impact ionization, is often advantageous. In fact, a wealth of information concerning the structure of the molecule under investigation may be deduced from the fragmentation pattern.

In addition, the electron impact process requires the sample to be in the vapor state. For some compounds such as ionic materials, high molecular weight compounds, metal cluster complexes, thermally labile systems and polymeric systems, volatilization is impractical [13]. The application of electron impact ionization to these compounds is restricted.

1.1.3. Fast Atom Bombardment (FAB)

Barber and his co-workers [14, 15] first introduced the fast atom bombardment (FAB) ionization method in 1981. FAB shares similar principles with SIMS. The difference between them is that FAB uses an energetic beam of fast neutral atoms of an

inert gas as the bombarding source, and samples are dissolved in a suitable matrix to get better spectra. Readily fitted to high-mass, high-resolution magnetic mass spectrometers, this technique has become more and more popular and powerful [16]. The applications of FAB MS have been widely explored from high molecular weight substances to thermally labile biological compounds, ionic and polymeric systems and metal cluster organo-metallic compounds [16-20]. Among the materials which successfully afforded spectra were vitamin B_{12} and its coenzyme [21], which had been described as a "milestone" [22, 13] in history of mass spectrometry.

In FAB MS experiments, an energetic fast neutral atom beam is directed onto a sample deposited on the metal tip of a direct-insertion probe, such that the sputtered ion beam can go through the entrance slits into the mass analyzer to be separated and analyzed by a conventional mass spectrometer.

Figure 3 is the schematic diagram of FAB source. The atom gun is the core component of the source. The atom gun typically can handle argon or xenon atoms with 6-10KeV kinetic energy and more recently, Cs^+ ion sources with energies of about 30KeV have become more and more common, especially for high molecular weight biopolymers. These are used in the so-called liquid SIMS source. The heavier the bombarding atom or ion, the greater the sensitivity, which is roughly proportional to the atomic weight [23]. A power supply is needed for the source which can provide voltage of 2-10KV to accelerate the ions produced. The ions are then neutralized through collision with the inert gas to produce the fast energetic atoms. A modified direct insertion probe is used to introduce the samples into the FAB ion source. It is normally made of copper or stainless steel. The recent development of the continuous-flow probe allows a continuous stream of solvent (containing a small amount of matrix) to enter the source [24]. Wider spacings in the collimating and focusing electrodes are used, compared with those in an EI source, allowing for greater dispersion of the sputtered ions [16]. At Brock we have pioneered the use of FAB source with some of the extra opening closed up.

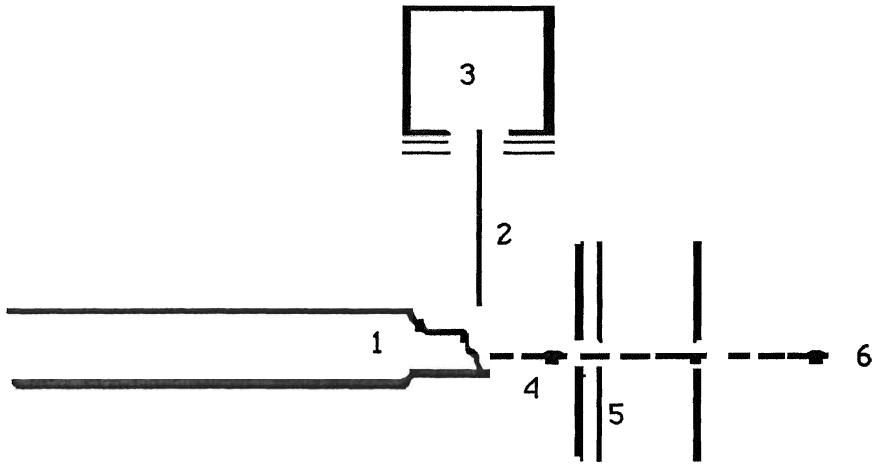

Figure 3. Schematic diagram of FAB source [16]:

(1) probe,

(2) fast-atom beam,

(3) atom gun,

(4) sputtered secondary ion beam,

(5) source ion optics,

(6) to mass analyzer.

The use of the liquid matrix is an integral part of the FAB technique and certainly choosing the matrix is the most critical, yet difficult part. Basically, choice of matrix and co-solvent depends on polarity of sample to be analyzed. The general characteristics of an "ideal" matrix have been summarized by De Pauw as follows [17]: **a.** The sample should be soluble in the matrix or solution of matrix and co-solvent; **b.** The matrix should have a low vapor pressure in vacuum (usually b.p. > 100^{o} C at 1 Torr.); **c.** The matrix should have a low enough viscosity to ensure good sample mobility, yet retain sufficient surface

tension to remain on the probe tip during FAB analyses; **d.** The matrix should not contain major ion peaks in the desired mass ranges of the samples being analyzed; **e.** The matrix should be chemically inert towards the samples.

In general, hydroxylated matrices work well with polar molecules and organic salts because their high dielectric constants favor the dissociation of ion pairs, lowering the coulombic interaction. For inorganic and organometallic complexes, aprotic solvents will normally be used where acid-base reactions and solvolysis must be avoided. In the case of less polar samples, redox matrices can be employed. Oxidizing matrices have high electron affinities and reducing matrices have low ionization energies. Besides, in some cases, doping the matrix liquid with a trace of acid or base or adding the sodium or chloride salts may help to obtain positive- or negative- ion spectra.

Finally, performing FAB experiments on solid materials without the presence of a matrix liquid is also possible but in most cases, the lifetime of the observed spectra is much shorter although often adequate to characterize the material of interest.

Compared with ionization techniques, the FAB ionization method provides the following advantages:

(1). No heating is required to bring the analyte into gas phase since sample ions are sputtered from the solution surface. Therefore, FAB MS is the right choice for such compounds which are thermally liable or ionic;

(2). The bombarding atom beam is neutral, so problems such as surface charging and beam steering are avoided;

(3). FAB allows the analysis of both positive and negative ionic species by providing both positive and negative spectra;

(4). Unlike either EI MS (which normally lacks the capability to provide the molecular ion mass) or CI, FD MS etc. (which often give little structural information), FAB MS can provide both the molecular ion mass and plenty of fragment ions;

(5). Preparation of the analyte as a solution in a liquid matrix allows for longer lived

spectra, accurate mass measurement and metastable scanning as well as repeated analyses when a reproducibility check is needed;

(6). The amount of sample needed is small. Sample preparation is relatively simple and the technique is very easy to learn. Moreover, it can be retrofitted to virtually any mass spectrometer at minimal cost.

Based on these advantages, FAB MS has become the favorite technique for the analysis of both organic and organometallic compounds.

1.1.4. Other Ionization Techniques

Chemical Ionization (CI)

Chemical ionization (CI) [25] is an ionization method in which a molecular sample is ionized via an ion-molecule reaction. Reagent ions are generated by electron bombardment of reactant gases such as methane in a high-pressure ion source. These reagent ions formed in the molecular reaction, such as $C_2H_5^+$, CH_5^+ and $C_3H_5^+$, are usually far more numerous than the sample molecules. The "pseudo molecular" ions which form as a result of the addition or loss of a proton to the molecule, coming from ion-molecule reaction between reagent gas and sample molecules, $(M+H)^+$ or $(M-H)^-$ respectively have lower internal energies and are usually more stable toward fragmentation than those ions formed in electron impact. As a result, it is easier to deduce the molecular ion mass using either $(M+H)^+$ or $(M-H)^-$, while at the same time it is harder to deduce the fragmentation mechanism as there are only a few fragment ions available. In addition, chemical ionization is a sensitive technique, even for negative ion formation. The main problems with the classical CI technique are still the need for the analyte to be in the gas phase and the high-pressure conditions under which chemical ionization must take place. The latter condition may lead to high accelerating voltage discharges in the ion source.

Atmospheric Pressure Ionization (API)

Atmospheric pressure ionization (API) combined with mass spectrometry (APIMS) provides many advantages, including reliable mixture analysis ability and enhanced sensitivity and selectivity, although at first it seems impractical to couple ionization conducted at atmospheric pressure with mass analysis and detection carried out under high vacuum [26].

The atmospheric pressure ionization ion source region is separated from the high-vacuum mass analyzer region by an orifice which must be large enough to introduce as many ions as possible from the atmospheric pressure region into the vacuum region while maintaining a low enough pressure to allow efficient operation of the mass spectrometer. Samples are ionized through either a gas-phase ionization method or a liquid-phase ionization method. When the sample ions enter the high-vacuum region, they suffer a free-jet expansion and undergo considerable adiabatic cooling, something the ions in conventional mass spectrometer ion source systems do not experience.

One of the most important applications of APIMS is in combination with some powerful separation techniques such as gas chromatography, liquid chromatography, supercritical fluid chromatography, capillary electrophoresis, and ion chromatography in the analysis of mixture of compounds.

The biggest problem with the APIMS is the tendency to generate low molecular weight cluster ion adducts that will produce high chemical noise, which can in turn interfere with the trace detection of low molecular mass compounds.

Field Desorption (FD)

EI, CI and API require samples to be in the gas phase prior to ionization. To avoid the necessity of volatilization of sample prior to its ionization, several techniques have been developed. Since these techniques lead to less thermal decomposition, they are called "soft

ionization" techniques. Field desorption (FD), introduced in 1969, is one of such techniques. FD is an ionization technique in which the sample, deposited directly on an emitter, is entered into the proximity of an intense electric field in order to be ionized [27]. The sample is normally deposited as a thin film on carbon microneedles, grown on a fine tungsten wire as an activated anode and then inserted into the field ionization source through a vacuum lock; the field is then switched on. An electron is ejected from a sample molecule to the anode, and the cation thus formed migrates toward the microneedle tip where it is desorbed or field evaporated.

Field desorption mass spectra often exhibit intense molecular ion and cluster ion peaks, but there are several major problems. One is that the total ion current obtained is normally very low compared to other ionization methods, which results in low sensitivity. Another disadvantage is that the desorbed ions have very little internal energy resulting in few fragment ions. In addition to the expensive, difficult-to-make and easy-to-break micro crystals coated on the activated emitter, poor reproducibility due to the variability of the carbon microneedle surface is always a problem [28].

Plasma Desorption (PD)

The plasma desorption (PD), introduced by Macfarlane and Torgerson in 1974 [29], is a "soft ionization" technique. PD uses the high-energy fragments, typically ^{142}Ba and ^{106}Tc with energies of 79 and 104MeV, respectively, emitted by the spontaneous fission of ^{252}Cf to desorb and ionize sample molecules with high molecular weight for mass analysis [30].

In PD, the sample to be analyzed is deposited on a thin foil, usually made of nickel, which placed in the ion source in front of a ^{252}Cf fission fragment source. ^{252}Cf nuclei break up quickly and spontaneously to give high energy fragments with unequal masses and energies. When these high-energy fission fragments pass through the sample foil, extremely rapid localized heating occurs, producing a temperature in the region of

10,000K. As a result, the sample molecules in the plasma zone are desorbed, with the production of both positive and negative ions. Because of its wide mass range, high ion transmission, and ability to record different mass ions simultaneously, PD source is most commonly used with time-of-flight (TOF) mass analyzer.

The major advantage of the technique is that it is extremely useful for obtaining mass spectra of thermally sensitive or involatile compounds. It is potentially capable of yielding molecular ions for biomolecules of relatively high mass. The disadvantage comes from the low mass resolution of the time-of-flight mass analyzer used with the plasma source which makes it impossible to determine the isotopic contributions to the molecular ion signal in PDMS spectra.

Laser Desorption (LD)

Laser desorption (LD), introduced in the field of mass spectrometry in 1963 [31], is a very useful ionization technique when analyzing biochemical samples due to its wide mass range. LD uses a high-intensity laser pulse to vaporize and ionize a small amount of sample, with the production of both molecular and fragment ions. The lasers used can produce photon energies from the infrared to the ultraviolet and pulse widths from picoseconds to continuous wave [32]. Very recently, the development of matrix-assisted laser desorption ionization (MALDI) [33, 34] further expands the scope of application of LDMS and makes the accessible mass range in the range of several hundred thousand daltons. It would therefore appear that MALDI will evolve as the most sensitive analytical technique in protein analysis.

Laser desorption ion sources are usually combined with time-of-flight (TOF) mass spectrometers. However, the growing popularity of the combination of the laser desorption source and fourier transform mass spectrometer (FTMS) has made LDMS more and more powerful and useful [35]. One of the advantages of LDMS is its ability to analyze large molecule very rapidly with high sensitivity. Both molecular ions and

fragment ions show up in either positive or negative ion mass spectra.

The major disadvantage of LDMS is its limited mass resolution with TOF mass analyzer. Sometimes it is very difficult to distinguish several possible molecular ions. Poor reproducibility and chemical interferences are also among the disadvantages. Moreover, for MALDI, the method of sample preparation has a very strong influence on the quality of the spectra.

Secondary Ion Mass Spectrometry (SIMS)

Secondary Ion Mass Spectrometry (SIMS) [36] uses a beam of ions (typically Ar^+, Xe^+, or Cs^+) with 2-30 KeV energy to bombard a target coated with the sample or to bombard a sample dissolved in a liquid matrix. In consequence, the sample is sputtered, during which process part of the sample enters the gas phase as ions, which can be analyzed and detected. The latter sometimes is called liquid secondary ion mass spectrometry (LSIMS) or fast ion bombardment (FIB). The kinetic energy of the collision creates a cascade of secondary ions for mass analysis [37].

The process involved in the production of secondary ions is not completely clear [38-40]. The sputtering process itself is not absolutely understood and there are two main schools of thought concerning the ionization process: one considers preformed ions in the "solution", which will be transferred to the gas phase and the analyzer, and the other a gas-phase ionization process not unlike that of chemical ionization. It seems likely that both processes may be operational, depending on the sample and experimental conditions.

SIMS has many advantages: (1) wide range of elemental analysis capabilities covering the spectrum from hydrogen to uranium; (2) isotopic characterization; (3) easy analysis of various kinds of solid organic and inorganic compounds and (4) very high sensitivity (the ability to detect 10^{-15} to 10^{-19} gram of compound). However, SIMS also has some drawbacks, such as low ion currents due to the lowered incident beam flux, surface charging of insulating compounds, and difficulties in steering a charged ion beam

(the bombarding ions) onto a surface at the accelerating voltage needed in magnetic instruments [41]. But with the application of liquid matrix, and especially with the use of a high voltage Cs^+ gun, the SIMS or LSIMS can produce identical or even better spectra compared with FAB MS [42].

1.1.5. E/B SECTOR DOUBLE FOCUSING MASS ANALYZER

Dempster's first mass spectrometer [5] was a single-focusing mass analyzer in which the positive ions were deflected through 180° in a magnetic field (B). The instrument focused the ions either in direction or in velocity. It is clear that certain m/z ions will follow a particular path of radius r_m at a given magnetic field strength B and accelerating voltage V governed by the mass equation $m/z= B^2r_m^2e/2V$. Ions leaving the source exhibit the full spread of possible translational energies, resulting in limited mass resolving power. To improve the resolving power, Nier [43] designed a new mass spectrometer. Nier's instrument consists of a 90° electrostatic analyzer followed by a 90° magnetic sector, with a slit between electric and magnetic fields. The electric field is created by the electrostatic analyzer, which contains two oppositely charged metal plates with a voltage E between them. Ions entering the electrostatic analyzer will follow a circular path which meets the equation

$$\mathbf{zeE = mv^2/r_e}$$

where E is the electric voltage , r_e is the radius of the electrostatic analyzer. Combined with the equation

$$\mathbf{zeV = mv^2/2}$$

which applies in the accelerating region, we get

$$\mathbf{r_e = 2V/E}$$

From this equation we can see that ions of different energies will follow paths of different radii r_e with a constant electric field E. If the electric field E and the analyzer radius

r_e are preset, only ions with a certain energy can pass through the electrostatic analyzer; the others either collide with the analyzer walls or the jaws of the slit. It is characteristic of "normal double-focusing" sector instruments (i.e. E/B sector double focusing) (cf. Figure 4), in which ions are focused twice using both their initial direction and their energy. Much higher resolution can be attained by using this type of mass spectrometer than by using a single-focusing instrument, even for very high molecular weight compounds. Such an instrument makes the exact mass determination of sample possible.

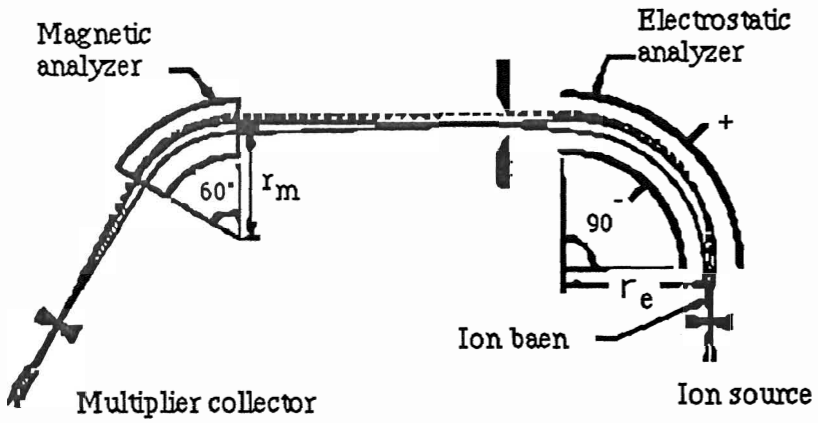

Figure 4. Conventional geometry of double-focusing mass spectrometer (E/B) [12]

1.1.6. Metastable Ions and Linked Scans

Metastable Ions

Metastable ions are those that are sufficiently stable to leave the ionization chamber, but will decompose before reaching the collector. Metastable ions can decompose anywhere along their path through the mass spectrometer, after leaving the ion source. Ions

that decompose in the field-free region are brought to a focus and give rise to the so-called metastable peaks which are usually denoted by asterisks m^*. Metastable peaks are readily identified in a normal mass spectrum because they need not have integral m/z values and they are almost always much broader than normal peaks with relatively lower abundance. Metastable ion peaks appear at mass unit $m^* = m_2^2/m_1$ (m_1 means parent ion, m_2 means fragment ion). Modern computer data systems actually remove these "normal" metastable ions and "raw data" acquisition is required to observe them.

Metastable ions usually have lifetimes of several tens of microseconds, and their internal energies are only several tenths of an electron volt greater than those of the lowest energy dissociation fragments. Therefore, metastable ions generally produce only a few fragment ions in their dissociative reactions, all of them resulting from the lowest energy dissociation mechanisms. Meanwhile, if a rearrangement reaction has a critical energy less than that of the lowest energy dissociation reaction, the rearrangement can occur before the ion fragments. This makes the interpretation of mass spectra more complex.

Since only the lowest energy dissociation reactions can be observed for metastable ions, rearrangement reactions which may give less structural information than that of simple bond cleavage will dominate the spectra due to their lower energy pathways. Several methods of ionic excitation have been developed to increase the amount of their internal energies resulting in more diagnostic simple-cleavage reactions. Among them, the collision of a high-velocity ion with a target gas molecule, referred to as collisional activation (CA), is the most common one. Ions with large translational energies collide inelastically with neutral atoms or molecules, normally hydrogen, helium, or air converting part of the translational energy of the ion into internal energy, and this subsequently causes decomposition of the ion [44-46].

Linked Scans

In an E/B double-focusing mass spectrometer, there are three field-free regions

(sometimes called drift regions) in which the ions are not acted on by either magnetic or electric fields. These field-free regions are located before the electric analyzer but after the acceleration region, between the electric and magnetic analyzers, and after the magnetic analyzer but before the detector . They are referred to as the first, second, and third field-free regions (denoted by $^{1}m^{*}$, $^{2}m^{*}$, and $^{3}m^{*}$ region) of a double-focusing mass spectrometer respectively (Figure 5). The dimensions of these regions can range from a few centimeters to more than a meter in length.

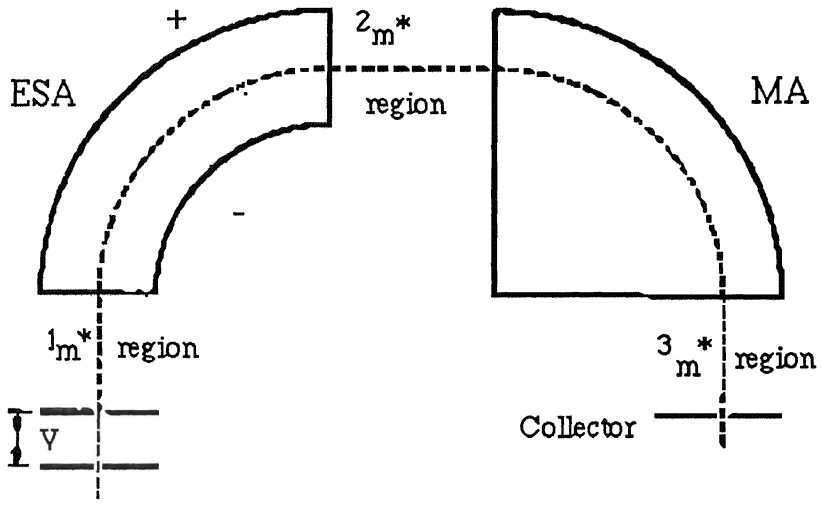

Figure 5. Schematic diagram of field-free regions in E/B mass spectrometer [12]

To induce the ion dissociation, collision cells may be set in these defined field-free regions to allow the use of a collision gas. A typical collision cell is about 1cm long, with its entrance slit normally located at an ion optical focal point. Differential pumping systems have been used to minimize the gas load in the rest of the mass spectrometer [47]. Metastable ions which dissociate in the first, second, and third field-free regions give rise

to first, second and third field-free region metastable peaks ($^1m^*$, $^2m^*$, $^3m^*$), respectively. Metastable peaks arising from decomposition in each of the three field-free regions may be detected in principle, however, in practice, for instrumental reasons, metastable transitions are usually only observed in either the first or second field-free regions. Due to the limited scope of this thesis, the following discussion will focus on the metastable transition in the first field-free region. Figure 6 shows the metastable transitions in the first field-free region. Metastable transitions can be expressed by the following equation, where m_1^+ is parent ion, m_2^+ daughter ion, n neutral radical.

$$m_1^+ \longrightarrow m_2^+ + n$$

There are several methods (called linked scans) available to detect all of the parent ions giving rise to the fragment ion m_2^+, and all daughter ions coming from the ion m_1^+ or all the parent and daughter ion pairs, which lose a constant total mass of n units.

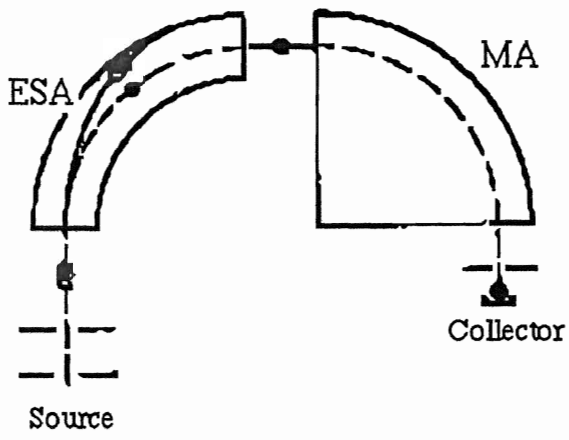

Figure 6. Metastable transitions in the first field-free region [12]

a. Fragment Ion Scans (B/E)

These scans sweep the ESA and the magnetic field such that the ratio B/E remains constant. They are also called B/E scans. This type of scan records all fragment ions which originate from a specified precursor ion. This gives maximum sensitivity and good resolution.

In such experiments, the ion m_1^+ is first tuned through the electric analyzer E and magnetic analyzer B, fixing the ratio of B_1/E_1. In order to make the fragment ions m_2^+ go through the electric analyzer E and the magnetic analyzer B, the following equations should be satisfied.

$$E_2 = E_1(m_2/m_1)$$

$$r_m B_2 e = m_2 v_2$$

Since the ion m_1^+ fragments in the reaction region and experiences no further acceleration or deceleration, the velocity of the daughter ion is the same as that of the parent ion, $v_1=v_2$, together with

$$r_m B_1 e = m_1 v_1.$$

We have

$$B_2/B_1 = E_2/E_1 = m_2/m_1,$$

thus

$$B_2/E_2 = B_1/E_1 = \text{constant } K(m_1)$$

By employing constant ratio B_1/E_1, we ensure that all of the daughter ions produced in the first field-free region by the ion m_1^+ will be detected.

b. Precursor Ion Scans (B^2/E)

These scans sweep the ESA potential (E) and the magnetic field (B) simultaneously such that the ratio B^2/E remains constant. In this way, the B^2/E scan provides all of the parent ions of a certain daughter ion m_2^+, while keeping the accelerating voltage V constant

to give maximum sensitivity and good resolution.

In experiment, the ion m_2^+ is carried through the electric analyzer E and magnetic analyzer B, thereby setting the value of B_2^2/E_2. Suppose in the first field-free region, we have

$$m_1'^+ \longrightarrow m_2^+ + n'$$

$$m_1''^+ \longrightarrow m_2^+ + n''$$

In order to make fragment ion m_2^+ go through the electric analyzer E and magnetic analyzer B, the following conditions have to be met:

$$eE_2' = (m_2v_2^2)/r_e$$

$$r_mB_2'e = m_2v_2$$

By $(2)^2/(1)$, we get:

$$B_2'^2/E_2' = (m_2r_e)/(r_m^2e)$$

Since m_2, r_e, r_m are all fixed, $B_2'^2/E_2'$ is constant. Thus because the ratio of the electric field to the square of the magnetic field is constant, all ions that dissociate to a given daughter ion in the reaction region are detected.

c. Constant Neutral Loss (CNL) Scans ($B^2(1-E)/E^2$)

These scans sweep the ESA and the magnetic field such that the ratio $B^2(1-E)/E^2$ remains constant. Only fragment ions produced by loss of a specific neutral species are detected. This type of scan records either the masses of all precursor ions that lose a particular neutral species, or the masses of all fragment ions produced by loss of this neutral species.

In the experiment, in order to make the parent ion m_1^+ go through the accelerating area, and the fragment ion m_2^+ pass through the electric and magnetic sector, the following equations must be satisfied:

$$eV = (m_1v_1^2)/2$$

$$E = m_2/m_1 = 1\text{-}m_n/m_1$$

$$ev_2B = (m_2v_2^2)/r_m$$

together with $v_1 = v_2$, we have

$$m^* = m_2^2/m_1 = (B^2r_m^2e)/2V$$

$$m^* = m_2^2/m_1 = m_nE^2/(1\text{-}E)$$

That is,

$$(B^2r_m^2e)/2V = (m_nE^2)/(1\text{-}E)$$

So, we get

$$B^2(1\text{-}E)/E^2 = (2Vm_n)/r_m^2e$$

Since V, m_n, and r_m are fixed, $B^2(1\text{-}E)/E^2$ is a constant. Thus, by scanning both the electric and magnetic sectors with constant $B^2(1\text{-}E)/E^2$, all parent and daughter ions with the same neutral fragment loss are collected [48-49].

There are several advantages associated with observing metastable transitions in the first field-free region as opposed to the second field-free region of an E/B instrument. First, each transition in the first field-free region is normally unequivocally identified in terms of the mass of parent and daughter ions; secondly, all of the precursor ions of m_2^+, all of the daughter ions of m_1^+ and all parent-daughter ion pairs with constant neutral mass loss can be detected in each scan, respectively; third, normal ions generally do not interfere and the artifact peaks are readily identified due to their unique narrow peak characteristics; and finally, in the absence of normal ions, the electron multiplier (collection sensitivity) can be increased and so weak transitions may be detected.

1.2. Mass Spectrometric Studies Related to This Thesis

1.2.1. Aryltin Compounds

The earliest mass spectrometric studies of organotin compounds were done by Dibeler [50] , Hobrock and Kiser [51], giving the mass spectrum of tetramethyltin in general studies of the fragmentation of Group IVB tetramethyls. The first mass spectrometric study of aryltin compounds was reported by Occolowitz [52] in 1966. In his paper, Occolowitz gave partial spectral data of tetraphenyltin and other organotin compounds and summarized three major modes of fission of organotin compounds: (1) fragmentation of the molecular ion by elimination of a ligand radical; (2) ligand loss by elimination of an unsaturated hydrocarbon with hydrogen rearrangement; (3) the elimination of neutral ligand pairs.

Chambers et al. [53] reported the fragmentation behavior of aryltin compounds [$SnPh_nEt_{4-n}$ (n=0-4), $SnPh_3(CH_2CH_2Ph)$, $SnPh_3X$ (X=F, Cl, Br, or I), Sn_2R_6 (R=Et, Ph)] at 70eV EI. They found that parent ions are always of low abundance and decompose mainly by elimination of an odd-electron neutral fragment, whereas Ar_3Sn^+ ions are of high abundance and lose even-electron fragments. Most of the ion current is carried by metal-containing species.

In 1969, Miller [54] reported the mass spectrometric studies of $(C_6F_5)_4Sn$. He observed bond forming rearrangements, involving fluorine abstraction by the central atom, forming perfluorophenylene ions and neutral metal fluoride species. The bulk of the ion current is carried by metal fluoride ions, while SnF^+ formed the base peaks in the spectrum. Later on, his group [55] recorded the mass spectra of $Ph_3SnSC_6F_5$ and $Ph_3SnOC_6F_5$ and compared with the corresponding pentafluoropheny derivatives. They

found that sulfur and oxygen compounds show fewer rearrangements leading to the formation of metal fluoride than do simple C_6F_5 derivatives. The ions Ar_3Sn^+ are usually observed as the base peaks in their studies. Ions containing Sn-S appear more stable than Sn-O species.

Gielen et al.[56] recorded the mass spectra of a series of compounds of alkyldimethyl-sec-butytin, alkyldimethyl(α-methylbenzyl)tin, alkyltriisobutyltin, and trimethyltin halides. Their results confirmed the fragmentation rules described earlier [52, 53]. Harrison et al. [57] reported the mass spectra of $Me_2Sn(SMe)_2$, $(R_3Sn)_2S$ (R=Me or Ph) and $(R_2SnR)_3$ (R=Me, Bu or Ph). They found the fragmentation patterns were similar to those of other organotin derivatives and showed no unusual features attributable to possible S-Sn π-bonding effects and confirmed $(R_2SnR)_3$ are cyclic trimers.

Wharf et al. [58] reported the EI mass spectrometric results of the hexamethyphosphoramide (HMPA) adducts $Ph_3SnX{\cdot}HMPA$ (X=Cl, Br, I, and NCS), $Ph_2SnX_2{\cdot}2HMPA$ (X=Cl, Br, I, and NCS), and $Ph_2SnX_2{\cdot}HMPA$ (X=Cl, Br and I [59]). They observed that the Sn-HMPA bond in the parent ions becomes stronger in the order I<Br<Cl and that the Sn-HMPA bond in $Ph_3Sn{\cdot}HMPA^+$ is weaker than in $Ph_2SnX{\cdot}HMPA^+$.

HMPA (hexamethylphosphoramide) adducts of phenyltin (IV) [$Ph_3SnX \cdot HMPA$ (X = Cl, Br, I), $Ph_2SnX_2 \cdot HMPA$ (X = Br, I); $Ph_2SnX_2 \cdot 2HMPA$ (X = Br, I) were studied [60] with FAB in glycerol/HMPA matrix and EI. Neither EI nor FAB give parent ions, but for FAB there is a much higher proportion of the metal-containing ions. The main difference in the FAB spectra is the preferential loss of halide compared to phenyl, the reverse of that observed in the EI spectra. Such preferential loss has been discussed by Miller et al.[65]. in term of preferential solvation of halide ions by the FAB matrix.

The mass spectrometric investigation of the thermal decomposition of tetrakis(N, N-diethylthiocarbamato)tin (IV) in vacuum was carried by Bratspies et al.[61]. Mass spectra were recorded for $p\text{-}CH_2SnMePhC_6H_4CMe{:}NNHCO_2R$ [R=(-)-menthyl],

$PhSnMeRCH_2Ph$ (R= Me, Et, CH_2Ph), $MeSnPh_2R$ [R=Me, Bu, $(CH_2)_{11}Me$], $(MeSnPh_2CH_2)_2CH_2$ and p-$ClSnMePhC_6H_4COMe$ by Gielen [62]. [SnL][$SnCl_4$] (L=o-HOC_6H_4:$N(CH_2)_nN$:CHC_6H_4OH-o, n=2,4,6) were characterized by mass spectrometric methods [63].

Another group of aryltin compounds ($SnClPh_3$, $SnPh_nCl_{4-n}$) [64] were studied in order to compare EI and FAB spectra as well as various matrix liquids (eg. sulfolane, glycerol, thioglycerol, diamylphenol, 18-crown-6/tetra-glyme, p-nitrophenyloctylether) used in the FAB ionization technique. Little difference was obtained between EI and FAB mass spectra with a low abundance of molecular ion being found in both cases. Only one major difference was cited involving the loss of halide preferentially over the loss of phenyl in FAB and the opposite trend in the case of EI. Similarly, no significant parent ions were seen for various matrices including glycerol and sulfolane, although there were some ions in which a sulfolane molecule was coordinated to the organometallic halide.

The electron impact (EI) and fast atom bombardment (FAB in a p-nitrophenyl-n-octyl ether (NPOE) matrix) mass spectra of the tris-p-fluorophenyl and tris-p-chlorophenyl tin halides (X=Cl, Br, I) are reported [65], along with the mass spectral data for their mono-hexamethylphosphoramide (HMPA) adducts. Parent ions are absent in both EI and FAB spectra for the adducts, and for the free Lewis acids in FAB and in some of the EI spectra. NPOE as a FAB matrix liquid is observed to weakly complex with the free Lewis acids. For the HMPA adducts, little ligand displacement is observed. Metal-HMPA fragments are of higher abundance than observed for analogous systems when using excess HMPA as a matrix liquid. Fluoride and chloride migrations to tin are observed for both the free organometallics and their HMPA adducts in the EI spectra. However, they are only observed in the FAB spectra for the free organometallics.

Recently, Iskander et al.[66] recorded the EI mass spectra of dimethyltin (IV) complexes with N-salicylidene derivatives of aroylhydrazines, S-methyldrazine carbodithioate and 4-substituted thiosenricarbazides and studied the fragmentation patterns

of these compounds under EI.

1.2.2. Ferrocenes

Ferrocene and its derivatives have been studied by mass spectrometry since Friedman et al. reported the results of a mass spectral study of the new and interesting class of compound of formula $M(C_5H_5)_2$ in 1955 [67]. Since then much information on the mass spectra has been reported and several fragmentation routes have been proposed [68-69]. In 1969, Junk and Svec [69] summarized the results of mass spectrometric studies of ferrocenes up to then.

In 1970's and 80's, a lot of mass spectrometric studies of ferrocene derivatives were done. The mass spectra of some mono-substituted ferrocenes [70-72] were reported. Sheley [73] and Imai [74] recorded the mass spectra of some di-substituted ferrocene derivatives. The high-resolution mass spectra of the syn- and anti-forms of the acylferrocene oximes [75] were examined at various ionizing voltages, the fragmentation patterns were presented and discussed. Mysove et al.[76] studied the fragmentation of symmetrically substituted methylferrocenes under electron impact. Hisatome et al.[77] reported the mass spectra of ferrocenophanes.

In 1980, Zagorevskii et al.[78] studied the mass spectrometry behavior of dimethyiaminoalkyl derivatives of ferrocene. Zhuk et al.[79] observed the effect of the structure of alkylferrocenes on their fragmentation types upon electron impact. Chen [80] reported the mass spectra of some N-substituted ferrocenylmethyl adenines. Patil et al. [81] have done the mass spectral studies on ferrocenyl arylhydrazones. In 1985, Rapic' et al. got the electron impact mass spectra of some bridged ferrocene derivatives [82]. They also studied the behavior of some ferrocene derivatives under electron impact [83]. In 1988, Thiele et al.[84] studied $CpM(FcN)_2$ and $(C_5Me_5)_2Ti(FcN)Cl$ (M=Ti, Zr, Hf; FcN=2-(dimethylaminomethyl)-ferrocenyl) with mass spectra. Mirek et al.[85] studied the fragmentation of 3-spiro[5]ferrocenophane-1,5-diones upon electron impact. In 1989,

Kruger et al.[86] characterized the $(FcN)_2M$ complexes (M=Zn, Cd, Hg) and FcNHgCl with mass spectra.

The mass spectra of ferrocene and its derivatives are, in fact, very simple, generally showing a small number of ions with overwhelming relative abundance. This led to the assumption of very simple fragmentation pathways, and arguments [87] about the substituent effect on the dissociation energy of the bond between the iron atom and the ring have been advanced. The recent studies of this class of complex also confirmed the assumption, except in few cases.

Most of the mass spectral studies of ferrocene and its derivatives were carried out with conventional electron impact (EI) method using the direct insertion probe. The ionizing voltages used were in 10-70eV ranges. Chemical ionization (CI) was also used in some cases. However, as well as the above mentioned methods, there are some other methods which have been used to do the mass spectral studies of ferrocene and its derivatives recently. Shildcrout [88] has recorded high-pressure mass spectra of ferrocenes. Innorta et al.[89] have used metastable ion spectra to study the fragmentation pathways and ionic structures of some substituted ferrocenes. Filipovic'-Marinic' et al. [90] reported the mass analyzed kinetic energy (MIKE) spectra of some monosubstituted ferrocenes derivatives. Nelson et al.[91] have done doubly charged ion mass spectrometric studies of ferrocenes. Drewello et al.[92] have used neutralization-reionization mass spectrometry (NRMS) to study formation and detection of neutral half-sandwich complexes MC_5H_5 (M=Fe, Co, Ni). Cloke et al.[93] studied the FAB MS spectra of a series of bis(pentamethyl-cyclopentadienyl) metal derivatives (M=Mo, W, Re, Fe, Ru), but no mass spectral data and matrix information is available. Lappert et al.[94] recorded the FAB MS spectra of the complexes $[FeCp(CO)_2\{M(X)R_2\}]$ (R = $CH(SiMe_3)_2$, Cp=η-C_5H_5; M=Sn and X= H, F, Cl, Br, I or OMe; or M = Pb and X =I), however, no mass spectra, matrix materials or discussion are given. Barfuss et al. [95] have done a mass spectrometric investigation of chloro-, bromo- and methylferrocenes by electron and photon impact

ionization.

To comprehensively review the mass spectrometric studies of ferrocenes is far beyond the scope of this thesis, only a few which are related to this project are mentioned here.

1.3. Scope of the Thesis

The purposes of this thesis are to study the mass spectrometric behavior of two groups of organometallic compounds and the applicability of atom fast bombardment mass spectrometry to these compounds. Group one consists of twenty aryltin compounds; group two includes fourteen ferrocene derivatives.

For the aryltin compounds, the studies have been focused on their EI MS and FAB MS behavior. In the EI MS studies, the effect of substituent group position, substituent group type of ligand and ligand type on the EI spectra has been explored. The fragmentation mechanism of each sample in the group has been investigated under EI with linked scans, such as fragment ion scans (B/E), parent ion scans (B^2/E) and constant neutral radical loss scans ($B^2(1\text{-}E)/E^2$). In the FAB MS studies, matrix optimization experiments have been carried out. The positive ion FAB MS studies have been focused on the effect of substituent group position, substituent group type and ligand type on the spectra. The fragmentation mechanism of all the samples under positive ion FAB has been studied by means of the linked scans. The CA +ve FAB fragmentation studies has been carried out for a typical sample. Negative ion FAB experiments of all the compounds have been done. And finally, the comparison of the results of EI MS and those of FAB MS has been made.

For ferrocenes, the studies have been concentrated on the fragmentation mechanism of each compound under EI with linked scan techniques in the first field-free region and the applicability of positive/negative ion FAB MS to this group of compounds. The fragmentation mechanism under positive ion FAB of those ferrocenes which give positive ion FAB MS spectra has been studied with the linked scan techniques. The CA +ve FAB fragmentation studies have been carried out for a typical sample. The comparison of the results of EI MS and those of FAB MS studies has been made.

.2.

EXPERIMENTAL

2.1. Instrumentation

All positive/negative ion FAB, EI and their linked scan mass spectra were recorded on a Kratos Concept IS double focusing mass spectrometer with a combined EI/CI and FAB sources (see Figure 7). The samples were introduced by a heated solid probe for EI and an unheated probe for FAB. For collecting normal EI and EI linked scan mass spectra, an accelerating voltage of 8KV was used with a corresponding mass range of 10 to 1000 mass units. When collecting positive/negative ion and positive ion linked scan FAB mass spectra, an accelerating voltage 6KV was used. The resolving power used was 1000 and the magnet was scanned at 10 seconds/decade for all spectra recording.

For electron impact mass analysis, samples were admitted via a direct insertion probe into the source area which was heated to 180°C. A 70eV ionization energy was used for bombardment. Calibration of both normal and linked scan mass spectra was performed using perfluorokerosene (PFK).

For fast atom bombardment mass analysis, samples which were dissolved in the matrix were bombarded with energetic fast atoms produced by an Ion Tech Ltd. saddle-field type fast atom gun, without heating the sample. Xenon was used as the bombarding atom and the gun was operated at approximately 1.0mA providing fast atoms with an energy of 7.5KeV. Calibration was achieved using Tris-(perfluoroheptyl)-S-triazine for

positive ion FAB mass analysis. For negative ion FAB analysis, CsI was used to calibrate the instrument.

For recording linked scan spectra, the electric (E) and the magnetic (B) fields were scanned in such a way that the value B/E (fragment ion scans), B^2/E (precursor ion scans) and $B^2(1-E)/E^2$ (constant neutral loss scans) remained constant. Metastable transitions in the first field-free region were observed (the region before the electrostatic analyzer but after the accelerating region of the ion source). For recording the collision activation positive ion FAB linked scan spectra, helium was used as the collision gas at a pressure sufficient to attenuate the main ion beam by 50% of its original value.

Data was collected with a Kratos DS-90 data system and all computations were carried out with a Kratos mach 3 data system. Ions were identified by pattern matching of isotope clusters, using deconvolution when necessary. In all the FAB spectra the data system was used for the background subtraction of the matrix peaks. At low masses in particular for aryltin compounds, the matrix subtraction did not always completely remove the matrix peaks, a result of the variation of the matrix spectrum with concentration.

Figure 7. The picture of Kratos Concept IS double focusing mass spectrometer [98]

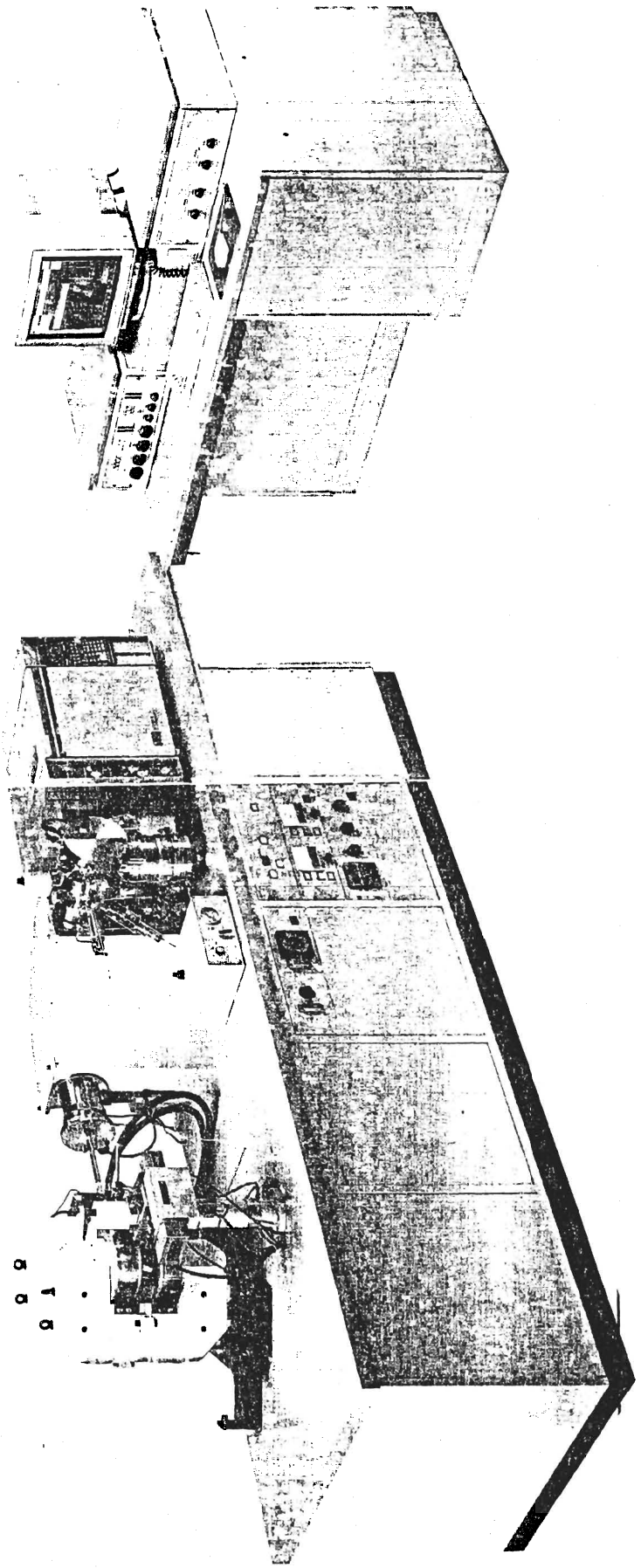

2.2. Compounds Analyzed

2.2.1. Aryltin Compounds

All of aryltin compound samples were supplied by Prof. Ivor Wharf, McGill University, Canada. No further purification were done. Preparations of some of these compounds have appeared elsewhere [96,97]. The samples analyzed are listed in Table I.

Table I. Samples of Aryltin Compounds

Formula	Mol. Weight
Ar_4Sn:	
$(o\text{-}CH_3C_6H_4)_4Sn$	483.22
$(m\text{-}CH_3C_6H_4)_4Sn$	483.22
$(p\text{-}CH_3C_6H_4)_4Sn$	483.22
$(m\text{-}CF_3C_6H_4)_4Sn$	699.11
$(p\text{-}CF_3C_6H_4)_4Sn$	699.11
$(o\text{-}CH_3OC_6H_4)_4Sn$	547.22
$(m\text{-}CH_3OC_6H_4)_4Sn$	547.22
$(p\text{-}CH_3OC_6H_4)_4Sn$	547.22
$(p\text{-}CH_3SC_6H_4)_4Sn$	611.46
$(3,5\text{-}Cl_2C_6H_3)_4Sn$	702.67
$(3,5\text{-}F_2C_6H_3)_4Sn$	571.04
$(3,5\text{-}(CH_3)_2C_6H_3)_4Sn$	539.33
$(m\text{-}FC_6H_4)_4Sn$	499.07
Ar_3SnX:	
$(o\text{-}CH_3C_6H_4)_3SnI$	518.99
$(o\text{-}CH_3OC_6H_4)_3SnBr$	519.99
$(o\text{-}CH_3OC_6H_4)_3SnI$	566.99
$(2,4,6\text{-}(CH_3)_3C_6H_2)_3SnCl$	511.70
$(2,4,6\text{-}(CH_3)_3C_6H_2)_3SnBr$	556.15
$(2,4,6\text{-}(CH_3)_3C_6H_2)_3SnI$	603.15
$(2,4,6\text{-}(CH_3)_3C_6H_2)_3SnO_2CCH_3$	535.29

Note: All aryltin compounds supplied by Prof. Ivor Wharf, Chemistry Department, McGill University, Montreal, PQ, Canada H3A 2K6.

2.2.2. Ferrocenes

A list of the ferrocene samples analyzed in this thesis is given in Table II. Some of these samples were provided by Prof. Zan Ru Lin, Sichuan Normal University, Peoples Republic of China. The rest of them were purchased from the Aldrich Chemical Company and Sigma Chemical Company, USA. No further purification was carried out.

Table II. Samples of Ferrocenes

Chemical	Formula	Mol.Weight
$C_5H_5FeC_5H_4R$:		
ferrocene[a]	$(C_5H_5)_2Fe$	186.04
ferrocenecarboxaldehyde[b]	$C_5H_5FeC_5H_4CHO$	214.05
ferrocenemethanol[b]	$C_5H_5FeC_5H_4CH_2OH$	216.06
ferroceneacetonitrile[b]	$C_5H_5FeC_5H_4CH_2CN$	225.08
acetylferrocene[c]	$C_5H_5FeC_5H_4COCH_3$	228.07
ferrocenecarboxylic acid[b]	$C_5H_5FeC_5H_4COOH$	230.05
ferroceneacetic acid[b]	$C_5H_5FeC_5H_4CH_2COOH$	244.07
benzoylferrocene[c]	$C_5H_5FeC_5H_4COC_6H_5$	290.14
$(C_5H_4R)_2Fe$:		
1,1'-ferrocenedimethanol[b]	$(C_5H_4CH_2OH)_2Fe$	246.09
1,1'-diacetylferrocene[a]	$(C_5H_4COCH_3)_2Fe$	270.11
1,1'-ferrocenedicarboxylic acid[a]	$(C_5H_4COOH)_2Fe$	274.06
1,1'-dimethylferrocenedicarboxylate[a]	$(C_5H_4COOCH_3)_2Fe$	302.11
1,1'-dibenzoylferrocene[c]	$(C_5H_4COC_6H_5)_2Fe$	394.25
1,1'-bis(diphenylphosphino)ferrocene[b]	$(C_5H_4PPh_2)_2Fe$	554.39

Note: a. Prof. Lin, Chemistry Department, Sichuan Normal University, Chengdu, P.R. China 610066;
b. Aldrich Chemical Co., Milwaukee, Wisconsin, USA;
c. Sigma Chemical Co., St. Louis, Missouri, USA.

2.3. FAB Sample Preparation

First, the samples were prepared for analysis by premixing 1-5μg of the solid analyte with about 10μl of matrix. Table III lists the various matrix materials used in this study and their supplier. Then, the appropriate solution was applied to the surface of a stainless steel probe tip 2mm in diameter until the entire surface was covered. This required about 2μl. The probe tip was then inserted into the end of the unheated probe, which was in turn inserted through a series of vacuum locks into the source area.

Table III. Other Chemicals Used in This Thesis

Chemical	Formula	Supplier
Matrixes		
Glycerol (GLY)	$C_3H_8O_3$	Aldrich Chemical Co. Milwaukee, Wisconsin
3-Nitrobenzyl alcohol (NBA)	$C_7H_7NO_3$	Aldrich Chemical Co. Milwaukee, Wisconsin
2-Nitrophenyl octylether (NPOE)	$C_{14}H_{21}NO_3$	Fluka, AG, CH-9470 Switzerland
Monothioglycerol (TGL)	$C_3H_8O_2S$	Sigma Chemical Co. St. Louis, Missouri
Tetramethylene Sulfone (SUL)	$C_4H_8O_2S$	Aldrich Chemical Co. Milwaukee, Wisconsin
1,3-Dimethyl-3,4,5,6, -tetrahydro-2(1H)- Pyrimidinone (DTP)	$C_6H_{12}N_2O$	Aldrich Chemical Co. Milwaukee, Wisconsin
2,2'-Thiodiethanol (TDl)	$C_4H_6O_4S$	Aldrich Chemical Co. Milwaukee, Wisconsin
Diamylphenol (DPL)		ICN Pharmaceuticals, Inc. Life Sciences Group, Plainview, New York
Other Chemicals		
Tris(perfluoroheptyl) -S-triazine	$C_{24}F_{45}N$	PCR Inc. Gainesville, Florida
Perfluoroalkane	C_nF_{2n+2}	Pierce Chemical Co. Gainesville, Florida
Xenon	Xe	Matheson Gas Products Canada
Caesium iodide	CsI	BDH Chemical Ltd. Poole, England
Helium	He	Union Carbide Canada Ltd. Toronto, Canada

.3.

RESULTS AND DISCUSSION

3.1. Aryltin Compounds

3.1.1. Electron Impact MS Studies

a. EI Spectra

The partial EI mass spectral data of all aryltin compounds are listed in Table IV. For convenience in studying the effects of substituent group position, substituent group type of ligands and ligand type on the EI spectra, these aryltin compounds are classified into nine groups (see Table IV (1)-(9)). Since the intensities of ligand related peaks are very low (about 10-35% of total intensity), only metal-containing data are given in the table. Ion currents of all metal-containing ions in a spectrum have been summed. Each ion is expressed as a percentage of this sum. The ion current of an ion is the sum of all its isotopes contributions.

Like R_4Sn, $R'_2R_2''Sn$ and other Ar_4Sn, Ar_3SnX (X=Cl, Br, I) compounds studied earlier [50-65], the EI spectra of this group of aryltin compounds in Table I show the following common features. All of the spectra are fairly simple, with almost over 70% of total intensity belonging to tin-containing peaks. More than half of the spectra have not shown molecular ion peaks. If they appear, they have only very low abundance. For most of these compounds, Ar_3Sn^+ is the highest peak, observed either as base peak or as the highest peak among metal-containing peaks. In all cases, the even-electron ions, Ar_3Sn^+,

and $ArSn^+$, are the most abundant. Parent ions decompose mainly by elimination of an odd-electron neutral fragment, while Ar_3Sn^+ ions decompose by elimination of even-electron neutral fragments. Unimolecular decomposition and rearrangement reactions are dominant reaction patterns. More detailed discussion on fragmentation patterns will be given in Section 3.1.4.

The common observed peaks of ligand-related ions in the EI spectra are Ar^+, Ar_2^+, $(Ar_2\text{-}H)^+$, $(Ar_2\text{-}F)^+$, $(Ar\text{-}F)^+$, $(Ar+H)^+$ and some rearrangement peaks of pieces of ligands with low abundances.

b. Effect of the Substituent Group Positions in Ligands on the EI Spectra

The effect of the substituent group positions in the ligands on the EI spectra can be seen from the spectral data of the following three groups of aryltin compounds: (1).(o-$CH_3C_6H_4)_4Sn$, (m-$CH_3C_6H_4)_4Sn$, (p-$CH_3C_6H_4)_4Sn$ (cf. Table IV (1)); (2).(m-$CF_3C_6H_4)_4Sn$, (p-$CF_3C_6H_4)_4Sn$ (cf. Table IV (2)); (3). (o-$CH_3OC_6H_4)_4Sn$, (m-$CH_3OC_6H_4)_4Sn$, (p-$CH_3OC_6H_4)_4Sn$ (cf. Table IV (3)).

For (x-$CH_3C_6H_4)_4Sn$ (x= o, m, p) compounds (Table IV(1)), the substituent group position does not have much influence on the mass spectra. The spectra of these three compounds are quite similar, except for some difference in intensities of the corresponding peaks, like Ar_3Sn^+, $ArSn^+$, Sn^+, etc. The major difference observed among this group of compounds is that (m-$CH_3C_6H_4)_4Sn$ and (p-$CH_3C_6H_4)_4Sn$ have an intense peak of Ar_2Sn^+, while (o-$CH_3C_6H_4)_4Sn$ possess an intense peak $(Ar_2Sn\text{-}H)^+$. The reason for the difference is due to the "ortho effect" [105] in (o-$CH_3C_6H_4)_4Sn$, which can give stable $(Ar_2Sn\text{-}H)^+$ ion.

For (x-$CF_3C_6H_4)_4Sn$ (x=m, p) compounds (Table IV(2)), the effect of substituent group position on the EI mass spectra is also small. Like (x-$CH_3C_6H_4)_4Sn$ (x= o, m, p) compounds, only some differences in intensities of the corresponding peaks ($(M\text{-}F)^+$, Ar_3Sn^+, Ar_2SnF^+, $ArSn^+$, SnF^+, Sn^+, etc) of these two compounds are

observed. Their spectra look very similar. However, the ligand-related peaks are quite intense in these two spectra. These peaks include $(Ar_2\text{-}F)^+$, $(Ar_2\text{-}2F)^+$, $(Ar_2\text{-}2F\text{-}HF)^+$, $(Ar+2F)^+$, Ar^+, $(Ar\text{-}F)^+$, and $(Ar\text{-}2F)^+$. The fluorine abstraction by the central atom forming metal fluoride ions is observed(eg. Ar_2SnF^+, SnF^+), just as for $(C_6F_5)_4Sn$ [54].

Noticeable effect of substituent group position on the EI mass spectra is observed among $(x\text{-}CH_3OC_6H_4)_4Sn$ (x= o, m, p) compounds. $(m\text{-}CH_3OC_6H_4)_4Sn$ gives an intense molecular ion peak, $(p\text{-}CH_3OC_6H_4)_4Sn$, a very small molecular ion peak, while $(o\text{-}CH_3OC_6H_4)_4Sn$ gives a tiny $(M\text{-}H)^+$ peak instead of a molecular ion peak. Unlike the other two compounds, $(o\text{-}CH_3OC_6H_4)_4Sn$ has more intense Ar_2Sn^+ peaks rather than $ArSn^+$ peaks. Differences in fragmentation patterns can be easily observed just from their spectral data. Each compound of this group of compounds has some unique peaks.

From the spectral data for the above three groups of compounds, it is clear that the spectra patterns of m-, p- isomers of each group of compounds are quite similar, while that of o- isomer show bigger differences. This suggests that the "ortho effect" of sample can affect the spectra a lot. Moreover, the polarity and the size of the substituent group are the factors which affect spectral forms. The larger the polarity of the substituent group (CH_3O > CF_3 > CH_3), the larger the effect of its position on the EI spectra. Similarly, the bigger or more flexible the substituent group on the ligand (CH_3O > CF_3 > CH_3), the larger the effect of its position on the EI spectra. Therefore, as the polarity and the size of the substituent group become larger, the similarity of the spectra of o-, m-, p- isomers gets less.

c. Effect of the Substituent Group Type on the EI Spectra

The effect of the substituent group type on the EI spectra can be obtained from the spectral data of the three groups of aryltin compounds: (1).$(3,5\text{-}F_2C_6H_3)_4Sn$, $(3,5\text{-}Cl_2C_6H_3)_4Sn$, $(3,5\text{-}(CH_3)_2C_6H_3)_4Sn$ (cf. Table IV (4)); (2).$(p\text{-}CH_3C_6H_4)_4Sn$, $(p\text{-}CF_3C_6H_4)_4Sn$, $(p\text{-}CH_3OC_6H_4)_4Sn$, $(p\text{-}CH_3SC_6H_4)_4Sn$ (cf. Table IV (5)); (3). $(m\text{-}FC_6H_4)_4Sn$, $(m\text{-}CF_3C_6H_4)_4Sn$, $(m\text{-}CH_3C_6H_4)_4Sn$, $(m\text{-}CH_3OC_6H_4)_4Sn$ (cf. Table IV

(6)).

For $(3,5\text{-}X_2C_6H_3)_4Sn$ (X= F, Cl, CH_3) compounds, the effect of substituent group type on the EI spectra is quite obvious. From F to CH_3, the spectra of the corresponding compounds become more complicated. Due to the large electronegativity of F and Cl, SnX^+ (X=F,Cl) are very intense peaks in both spectra. In fact, this peak forms the base peak in spectrum of $(3,5\text{-}Cl_2C_6H_3)_4Sn$. The spectrum shows no Ar_2Sn^+ peak. However, a tiny $(Ar_2Sn\text{-}2H)^+$ peak is observed. In the spectrum of $(3,5\text{-}F_2C_6H_3)_4Sn$, a small Ar_2Sn^+ is observed, while in the spectrum of $(3,5\text{-}(CH_3)_2C_6H_3)_4Sn$, the Ar_2Sn^+ is very intense. Like other groups of compounds studied in this thesis, the molecular ion peaks of this group of compounds either appear with low abundance (e.g. spectrum of $(3,5\text{-}F_2C_6H_3)_4Sn$) or wholly disappear.

The effect of substituent group type on the EI spectra is also quite obvious among $(p\text{-}XC_6H_4)_4Sn$ (X=CH_3, CF_3, CH_3O, CH_3S) compounds. Compared with the spectrum of $(p\text{-}CH_3OC_6H_4)_4Sn$, the spectra of the rest of this group of compounds are simpler. Molecular ion peaks are observed in the spectra of $(p\text{-}CH_3OC_6H_4)_4Sn$ and $(p\text{-}CH_3SC_6H_4)_4Sn$, the peak in the latter being very intense. Intense Ar_2Sn^+ peaks appear in the spectra of $(p\text{-}CH_3C_6H_4)_4Sn$ and $(p\text{-}CH_3OC_6H_4)_4Sn$. The spectrum of $(p\text{-}CH_3SC_6H_4)_4Sn$ has a strong $(Ar_2Sn\text{-}CH_3)^+$ peak.

For the last group of compounds, $(m\text{-}XC_6H_4)_4Sn$ (X=F, CF_3, CH_3, CH_3O), the effect of substituent group type on the EI spectra is still great. In this group of compounds, only the spectrum of $(m\text{-}CH_3OC_6H_4)_4Sn$ has a molecular ion peak and most fragment peaks. As in spectra of $(3,5\text{-}F_2C_6H_3)_4Sn$ and $(3,5\text{-}Cl_2C_6H_3)_4Sn$, the spectrum of $(m\text{-}FC_6H_4)_4Sn$ shows a very intense SnF^+ peak, while $(m\text{-}CF_3C_6H_4)_4Sn$ has only a fair one just as that of $(p\text{-}CF_3C_6H_4)_4Sn$. This can be explained in that the migration of the fluorine on benzene ring to Sn is easier than that from the CF_3 group attached to the benzene ring, due to that the loss of the fluorine on benzene ring is easier than that of the fluorine on the CF_3 group. Like $(3,5\text{-}F_2C_6H_3)_4Sn$, $(m\text{-}FC_6H_4)_4Sn$ has a large Sn^+ peak in its spectrum.

Compared with the effect of the substituent group positions in ligands on the EI spectra, the effect of the substituent group type is much bigger. The extent of the effect depends on the the polarity, ionization energy, bonding energy of the substituent group, also depends on the size of the substituent group.

d. Effect of the Ligand Type on the EI Spectra

To study the effect of the ligand type on the EI spectra, three groups of compounds are considered: (1). $(o\text{-}CH_3C_6H_4)_3SnI$, $(o\text{-}CH_3OC_6H_4)_3SnI$, $(2,4,6\text{-}(CH_3)_3C_6H_2)_3SnI$ (cf. Table IV (7)); (2). $(o\text{-}CH_3OC_6H_4)_3SnBr$, $(o\text{-}CH_3OC_6H_4)_3SnI$, $(o\text{-}CH_3OC_6H_4)_4Sn$ (cf. Table IV (8)); (3). $(2,4,6\text{-}(CH_3)_3C_6H_2)_3SnCl$, $(2,4,6\text{-}(CH_3)_3C_6H_2)_3SnBr$, $(2,4,6\text{-}(CH_3)_3C_6H_2)_3SnI$, $(2,4,6\text{-}(CH_3)_3C_6H_2)_3SnO_2CCH_3$ (cf. Table IV (9)). Group (1) are Ar_3SnI type compounds, where Ar = $o\text{-}CH_3C_6H_4$, $o\text{-}CH_3OC_6H_4$, $2,4,6\text{-}(CH_3)_3C_6H_3$. Group (2) are $(o\text{-}CH_3OC_6H_4)_3SnX$ type compounds, X = Br, I, $o\text{-}CH_3OC_6H_4$. While group (3) are $(2,4,6\text{-}(CH_3)_3C_6H_3)_3SnX$, where X= Cl, Br, I, O_2CCH_3. In addition to the difference in X's, the Ar group in group (3) is larger than that in group (2).

For group (1) compounds, the spectrum of each compound is quite different from that of another both in the fragmentation patterns and in relative ion intensities. However, some similarity still can be found among them. Both $(o\text{-}CH_3C_6H_4)_3SnI$ and $(2,4,6\text{-}(CH_3)_3C_6H_2)_3SnI$ have tiny molecular peaks and $(Ar_2Sn\text{-}H)^+$ peaks. All these compounds have no Ar_2Sn^+ peaks.

In group (2), the spectra of $(o\text{-}CH_3OC_6H_4)_3SnBr$ and $(o\text{-}CH_3OC_6H_4)_3SnI$ have some similarities. Both spectra have Ar_2SnX^+, $(Ar_2Sn\text{-}CH_3)^+$, SnX^+(X=Br, I), $SnOCH_3^+$ peaks and some rearrangement peaks of ligand, such as $(C_6H_4)_2O^+$, $(Ar+CH_2)^+$, $(Ar+H)^+$, but no Ar_2Sn^+ peaks appear. However, difference is still big. $(o\text{-}CH_3OC_6H_4)_3SnBr$ has a tiny molecular peak and a very strong Ar_2^+ peak in its spectrum, while $(o\text{-}CH_3OC_6H_4)_3SnI$ gets an intense $C_6H_5Sn^+$ peak and no molecular peak shows in its spectrum. Unlike these two compounds, $(o\text{-}CH_3OC_6H_4)_4Sn$ has more low

abundance fragment peaks, even though no molecular peak.

For group (3) compounds, the difference among the spectra is very obvious. $(2,4,6\text{-}(CH_3)_3C_6H_2)_3SnI$ has a very strong Ar_3Sn^+ peak (base peak), while the rest of this group of compounds show no strong Ar_3Sn^+ peaks. Only in this group of compounds no strong Ar_3Sn^+ peaks appear. $(2,4,6\text{-}(CH_3)_3C_6H_2)_3SnCl$ and $(2,4,6\text{-}(CH_3)_3C_6H_2)_3SnBr$ have strong $(Ar_2SnX\text{-}H)^+$ and SnX^+ peaks, but $(2,4,6\text{-}(CH_3)_3C_6H_2)_3SnI$ hasn't. Similar phenomena have been observed for $(C_6H_5)_3SnI$ [53] and $(p\text{-}FC_6H_4)_3SnI$, $(p\text{-}ClC_6H_4)_3SnI$ [65], they produce only very small Ar_2SnX^+ and SnX^+ peaks. The difference come from the larger ligand $2,4,6\text{-}CH_3C_6H_2$. $(2,4,6\text{-}(CH_3)_3C_6H_2)_3SnO_2CCH_3$ has an intense Ar_2SnX^+ peak in its spectrum. In the spectra of $(2,4,6\text{-}(CH_3)_3C_6H_2)_3SnCl$ and $(2,4,6\text{-}(CH_3)_3C_6H_2)_3SnBr$, the $(Ar_2\text{-}H)^+$ peaks form base peaks. The Ar^+ peak is the base peak in spectrum of $(2,4,6\text{-}(CH_3)_3C_6H_2)_3SnO_2CCH_3$. If not base peak, the $(Ar_2\text{-}H)^+$ and Ar^+ peaks are still quite intense in the spectra of the rest of this group of compounds.

Based on the above analysis and data in Table IV, it can be concluded that ligand types have biggest effect, while the substituent group types have bigger effect than the substituent group position on the EI spectra. Such effect comes from many factors. These factors include the steric orientation, the polarity, ionization energy, bonding energy, etc. of substituent group, ligand and the compound studied.

* Note: text continues on page 52.

Table IV. EI Mass Spectral Data* of Aryltin Compounds

(1) $(x\text{-}CH_3C_6H_4)_4Sn$ (x=o, m, p)

ION^+	Ar= o-$CH_3C_6H_4$	= m-$CH_3C_6H_4$	= p-$CH_3C_6H_4$
$(M\text{-}H)^+$	0.2	0.9	0.1
Ar_3Sn^+	58.7	47.1	49.2
Ar_2Sn^+	-	24.6	23.1
$(Ar_2Sn\text{-}H)^+$	11.1	-	-
$ArSn^+$	19.3	12.5	12.5
Sn^+	10.7	14.9	15.0

* Percentage of the total positive ion current carried by tin-containing ions.

(2) $(x\text{-}CF_3C_6H_4)_4Sn$ (x=m, p)

ION^+	Ar= m-$CF_3C_6H_4$	= p-$CF_3C_6H_4$
$(M\text{-}F)^+$	4.1	3.6
Ar_3Sn^+	55.3	68.5
Ar_2SnF^+	3.3	2.4
Ar_2Sn^+	1.8	1.2
$ArSn^+$	20.4	16.1
$(ArSn\text{-}HF)^+$	4.0	-
SnF^+	7.7	5.0
Sn^+	3.4	3.3

* Percentage of the total positive ion current carried by tin-containing ions.

Table IV (cont.) (3) $(x\text{-}CH_3OC_6H_4)_4Sn$ (x=o, m, p)

ION$^+$	Ar= o-$CH_3OC_6H_4$	= m-$CH_3OC_6H_4$	= p-$CH_3OC_6H_4$
M^+	-	7.9	0.7
$(M-H)^+$	0.7	-	-
$Ar_3SnO(CH_3)_2^+$	-	-	2.3
Ar_3Sn^+	54.2	51.9	33.8
$(Ar_3Sn-CH_4)^+$	-	-	0.4
$(Ar_3Sn-2CH_3)^+$	0.6	-	-
Ar_2Sn^+	10.1	7.7	9.3
$(Ar_2Sn-CH_3)^+$	6.8	8.0	5.1
$(Ar_2Sn-OCH_3)^+$	-	1.0	2.6
$(Ar_2Sn-2CH_3)^+$	4.3	-	-
$(Ar_2Sn-CH_3O-CH_2)^+$	2.1	-	-
$ArSn(OCH_3)_2^+$	-	0.9	-
$ArSnOCH_3 \cdot H_2O^+$	-	-	4.6
$ArSn^+$	4.7	11.4	17.1
$(ArSn-CH)^+$	3.2	-	-
$(ArSn-CH_3)^+$	-	-	2.6
$(ArSn-OCH_3)^+$	6.6	-	6.3
$C_6H_3Sn^+$	-	3.2	-
$SnOCH_3^+$	2.6	-	4.1
$(CH_3O)_2SnH_2^+$	-	-	2.8
$C_2H_5Sn^+$	-	3.1	-
$SnCH_3^+$	1.1	-	-
Sn^+	2.8	5.0	8.5

* Percentage of the total positive ion current carried by tin-containing ions.

Table IV (cont.) (4) $(3,5\text{-}X_2C_6H_3)_4Sn$ (X=F, Cl , CH_3)

ION$^+$	Ar= $3,5\text{-}F_2C_6H_3$	= $3,5\text{-}Cl_2C_6H_3$	= $3,5\text{-}(CH_3)_2C_6H_3$
M^+	0.1	-	-
$(M\text{-}H)^+$	-	-	0.9
$(M\text{-}3H)^+$	-	1.9	-
$(M\text{-}CH_3)^+$	-	-	0.3
$Ar_3Sn{\cdot}CH_2^+$	-	-	0.6
Ar_3Sn^+	34.8	35.1	25.9
$(Ar_3Sn\text{-}CH_3)^+$	-	-	1.2
$(Ar_3Sn\text{-}HCl)^+$	-	0.5	-
Ar_2SnX^+	-	1.0	-
Ar_2Sn^+	2.1	-	20.5
$(Ar_2Sn\text{-}2H)^+$	-	1.1	-
$(Ar_2Sn\text{-}CH_3)^+$	-	-	1.0
$ArSn^+$	19.8	18.1	14.0
$(ArSn\text{-}CH_3)^+$	-	-	7.5
$(ArSn\text{-}2CH_3)^+$	-	-	7.5
SnX^+	23.4	35.1	-
Sn^+	19.8	7.0	20.7

(X=F,or Cl)

* Percentage of the total positive ion current carried by tin-containing ions.

Table IV (cont.) (5) $(p\text{-}XC_6H_4)_4Sn$ (X=CH_3, CF_3, CH_3O, CH_3S)

ION$^+$	Ar=p-$CH_3C_6H_4$	=p-$CF_3C_6H_4$	= p-$CH_3OC_6H_4$	= p-$CH_3SC_6H_4$
M^+	-	-	0.7	10.5
$(M-H)^+$	0.1	-	-	-
$(M-F)^+$	-	3.6	-	-
$Ar_3SnO(CH_3)_2^+$	-	-	2.3	-
Ar_3Sn^+	49.2	68.5	33.8	48.4
$(Ar_3Sn-CH_4)+$	-	-	0.4	-
$Ar_2Sn{\cdot}F^+$	-	2.4	-	-
$Ar_2SnCH_3^+$	-	-	-	0.2
Ar_2Sn^+	23.1	-	9.3	-
$(Ar_2Sn-CH_3)^+$	-	-	5.1	17.0
$(Ar_2Sn-OCH_3)^+$	-	-	2.6	-
$(Ar_2Sn-2HF)^+$	-	1.2	-	-
$ArSnOCH_3{\cdot}H_2O$	-	-	4.6	-
$ArSn^+$	12.5	16.1	17.1	12.3
$(ArSn-CH_3)^+$	-	-	2.6	-
$(ArSn-OCH_3)^+$	-	-	6.3	-
$SnOCH_3^+$	-	-	4.1	-
$(CH_3O)_2SnH_2^+$	-	-	2.8	-
SnF^+	-	5.0	-	-
Sn^+	15.0	3.0	8.5	11.5

* Percentage of the total positive ion current carried by tin-containing ions.

Table IV (cont.) (6) $(m\text{-}XC_6H_4)_4Sn$ (X=F, CF_3, CH_3, CH_3O)

ION^+	$Ar=m\text{-}FC_6H_4$	$=m\text{-}CF_3C_6H_4$	$=m\text{-}CH_3C_6H_4$	$=m\text{-}CH_3OC_6H_4$
M^+	-	-	-	7.9
$(M-H)^+$	-	-	0.9	-
$(M-F)^+$	-	4.1	-	-
Ar_3Sn^+	28.4	55.3	47.1	51.9
$Ar_2Sn{\cdot}F^+$	-	3.3	-	-
Ar_2Sn^+	2.6	1.8	24.6	7.7
$(Ar_2Sn\text{-}CH_3)^+$	-	-	-	8.0
$(Ar_2Sn\text{-}OCH_3)^+$	-	-	-	1.0
$ArSn(OCH_3)_2^+$	-	-	-	0.9
$ArSn^+$	19.7	20.4	12.5	11.4
$ArSn^+$	-	4.0	-	-
$C_6H_3Sn^+$	-	-	-	3.2
$C_2H_5Sn^+$	-	-	-	3.1
SnF^+	22.2	7.7	-	-
Sn^+	27.1	3.4	14.9	5.0

* Percentage of the total positive ion current carried by tin-containing ions.

(7) Ar_3SnI ($Ar=o\text{-}CH_3C_6H_4$, $o\text{-}CH_3OC_6H_4$, $2,4,6\text{-}(CH_3)_3C_6H_2$)

ION^+	$Ar=o\text{-}CH_3C_6H_4$	$=o\text{-}CH_3OC_6H_4$	$=2,4,6\text{-}(CH_3)_3C_6H_2$
$(M-H)^+$	0.1	-	0.1
Ar_3Sn^+	59.2	63.5	62.1
Ar_2SnI^+	6.4	3.4	-
$(Ar_3Sn\text{-}3CH_3)^+$	-	0.7	-
$(ArSnI{+}CH_3)^+$	-	0.5	-
$(Ar_2Sn\text{-}CH_3)^+$	-	2.7	-
$(ArSnI\text{-}H)^+$	1.9	-	-
$(Ar_2Sn\text{-}H)^+$	3.0	-	13.2
SnI^+	4.5	2.3	-
$ArSn^+$	18.3	6.7	18.0
$C_6H_5Sn^+$	-	10.9	-
$SnOCH_3^+$	-	4.7	-
Sn^+	6.8	4.7	6.7

* Percentage of the total positive ion current carried by tin-containing ions.

Table IV (cont.) (8) $(o\text{-}CH_3OC_6H_4)_3SnX$ (X=Br, I, $o\text{-}CH_3OC_6H_4$)

ION^+	X=Br	=I	$=o\text{-}CH_3OC_6H_4$
M^+	0.4	-	-
$(M-H)^+$	-	-	0.7
Ar_3Sn^+	51.4	63.5	54.2
Ar_2SnX^+	12.8	3.4	-
$(Ar_3Sn\text{-}2CH_3)+$	-	-	0.6
$(Ar_3Sn\text{-}3CH_3)^+$	-	0.7	-
Ar_2Sn^+	-	-	10.1
$(ArSnX+CH_3)^+$	-	0.5	-
$(Ar_2Sn\text{-}CH_3)^+$	2.4	2.7	6.8
$(Ar_2Sn\text{-}2CH_3)^+$	-	-	4.3
$(Ar_2Sn\text{-}CH_3O\text{-}CH_2)^+$	-	-	2.1
$(ArSn\text{-}CH)^+$	-	-	3.2
$(ArSn\text{-}OCH_3)^+$	-	-	6.6
$ArSn^+$	7.4	6.7	4.7
~SnX^+	15.1	2.3	1.1
$C_6H_5Sn^+$	-	10.9	-
$SnOCH_3^+$	4.9	4.7	2.6
Sn^+	5.6	4.7	2.8

X=Br, I, CH_3

* Percentage of the total positive ion current carried by tin-containing ions.

~ For $(o\text{-}CH_3OC_6H_4)_3SnBr$, this abundance includes those of $C_6H_5Sn^+$ and $SnBr^+$.

Table IV (cont.) (9) $(2,4,6\text{-}(CH_3)_3C_6H_2)_3SnX$ (X=Cl, Br, I, O_2CCH_3)

ION$^+$	X= Cl	=Br	= I	= O_2CCH_3
M^+	-	-	-	0.7
$(M\text{-}H)^+$	0.3	0.2	0.1	-
Ar_3Sn^+	2.0	3.1	62.1	7.8
$(M\text{-}C_6H_3)^+$	0.9	-	-	-
Ar_2SnX^+	-	-	-	22.2
$(Ar_2SnX\text{-}H)^+$	40.4	39.7	-	-
$(Ar_2SnX\text{-}CH_3)^+$	-	-	-	2.5
$Ar_2Sn{\cdot}H_2O^+$	-	-	-	2.3
$(Ar_2SnX\text{-}CH_4)^+$	6.2	3.9	-	-
$(Ar_2SnX\text{-}3CH_3)^+$	-	3.7	-	-
$(Ar_2Sn\text{-}H)^+$	4.7	4.7	13.2	22.5
$(Ar_2Sn\text{-}OH)^+$	-	-	-	1.4
(ArSnX-H)+	2.9	2.4	-	-
$ArSnCH_2^+$	-	-	-	1.0
$ArSn^+$	21.8	19.2	18.0	18.8
SnX^+	10.6	12.6	-	4.1
$SnCH_3^+$	-	-	-	3.7
Sn^+	10.3	11.4	6.7	9.6

* Percentage of the total positive ion current carried by tin-containing ions.

3.1.2. Positive Ion FAB MS Studies

a. Matrix Optimization

In FAB MS studies, choosing a suitable matrix to dissolve the samples is the most critical part of getting better spectra. Since different compounds may need different matrices, comparative experiments to choose the best matrix is necessary. De Pauw [17] has summarized some basic characteristics of an "ideal" matrix (cf. Section 1.1.3).

For the aryltin compounds, the following compounds (see Table III) have been studied to choose the better matrices. They are glycerol (GLY), 3-nitrobenzyl alcohol (NBA), 2-nitrophenyl octyl ether (NPOE), monothioglycerol (TGL), tetramethylene sulfone (SUL), 1,3-dimethyl-3,4,5,6-tetrahydro-2(1H)-pyrimidinone (DTP), 2,2'-thiodiethanol (TDL), and diamylphenol (DPL). For comparison, mass spectra are recorded under nearly identical operating conditions with approximately the same sample concentrations (10μg of the sample is dissolved in 10μl of the matrix), the same mass calibration and other important parameters.

Due to either poor solubility of samples or the very high vapor pressure of matrices, some spectra give only matrix peaks or very tiny sample peaks; while with some other matrices, good spectra only last two or three scans before the ion current suddenly collapses. In addition, even for those two or three "good" scans, the huge matrix background is obvious, resulting in little fragmentation information.

Among this group of matrices, only 3-nitrobenzyl alcohol (NBA) and 2-nitrophenyl octyl ether (NPOE) give better spectra. Of these two, 3-nitrobenzyl alcohol (NBA) provides much better spectra. For comparison, the partial positive ion FAB spectral data in 3-nitrobenzyl alcohol (NBA) and 2-nitrophenyl octyl ether (NPOE) are listed in Table V and Table VI, respectively.

Therefore, of the eight major matrices commonly used, 3-nitrobenzyl alcohol

(NBA) seems the best one for the aryltin compounds studied in this project. The following discussion will focus on the positive ion FAB studies of aryltin compounds in NBA matrix.

b. FAB Spectra in NBA matrix

The partial positive ion FAB mass spectral data of the aryltin compounds in Table I in NBA matrix are listed in Table V. In most of the +ve FAB spectra, no molecular ion peaks show up. Even in those spectra in which molecular ion peaks appear, they usually have low abundance. The only exception to this is that (p-$CH_3SC_6H_4)_4Sn$ has a much more intense molecular ion peak in its spectrum. Ar_3Sn^+ peaks are the strongest tin-containing peaks in all of the spectra. Ar_2SnI^+ (of (o-$CH_3C_6H_4)_3SnI$ and (o-$CH_3OC_6H_4)_3SnI$) and Ar_2SnBr^+ (of (o-$CH_3OC_6H_4)_3SnBr$) have higher abundance in corresponding spectra. Intense $ArSn^+$ peaks are observed in all of the spectra but those of (p-$CH_3SC_6H_4)_4Sn$ and (o-$CH_3OC_6H_4)_4Sn$, which fail to produce such peaks. SnF^+ peaks in spectra of (p-$CF_3C_6H_4)_4Sn$ and (3,5-$F_2C_6H_3)_4Sn$ are intense. Contrast to their EI counterparts, no SnF^+ peaks exist in the +ve FAB spectra of (m-$FC_6H_4)_4Sn$ and (m-$CF_3C_6H_4)_4Sn$. Ar_2Sn^+ peaks have low abundance if they show up. When they appear, Sn^+ peaks are usually strong. Even electron ion peaks dominate all of the +ve FAB spectra, similar to those observed in the EI spectra. In all of the +ve FAB spectra, matrix related peaks are few and are in high mass range with lower abundance.

c. Effect of the Substituent Group Positions in Ligands on the FAB Spectra

To study the effect of the substituent group positions in ligands on the +ve FAB spectra in NBA matrix, three groups of aryltin compounds are considered. The classification is the same as that in section 3.1.1.b. Partial spectral data of these compounds are listed in Table V(1), (2), (3).

For compounds (x-$CH_3C_6H_4)_4Sn$ (x=o,m,p) (Table V(1)), (m-$CH_3C_6H_4)_4Sn$

gives a much better spectrum, while the other two produce poorer spectra. In all of the spectra of this group of compounds, molecular ion peaks either show as very tiny peaks (e.g. $(m\text{-}CH_3C_6H_4)_4Sn$, $(p\text{-}CH_3C_6H_4)_4Sn$) or disappear (e.g. $(o\text{-}CH_3C_6H_4)_4Sn$). Ar_3Sn^+'s are base peaks in spectra of $(m\text{-}CH_3C_6H_4)_4Sn$ and $(p\text{-}CH_3C_6H_4)_4Sn$, but $(Ar_2\text{-}2H)^+$ is the base peak in the spectrum of $(o\text{-}CH_3C_6H_4)_4Sn$. No Sn^+ peak is observed in spectrum of $(p\text{-}CH_3C_6H_4)_4Sn$. All of the spectra show very intense Ar_3Sn^+ and $ArSn^+$ peaks. Peaks related to matrix adducts or their fragment pieces are quite weak (e.g. $Ar_3Sn{\cdot}NBA^+$, $Ar_2Sn{\cdot}OH^+$), if they appear. Differences among the spectra of this group of compounds is large, compared with those in EI spectra. However, some similarities exist between spectra of $(o\text{-}CH_3C_6H_4)_4Sn$ and $(p\text{-}CH_3C_6H_4)_4Sn$. This probably indicates the ortho- and para- effects on benzene ring under +ve FAB in NBA have great influence.

In spectra of $(m\text{-}CF_3C_6H_4)_4Sn$ and $(p\text{-}CF_3C_6H_4)_4Sn$ (Table V(2)), $(M\text{-}F)^+$ peaks appear instead of molecular ion peaks. The Ar_3Sn^+ peaks are base peaks and $ArSn^+$ peaks the second most intense peaks in both of the spectra. The two spectra look quite similar, except for some difference observed in low mass range. $(p\text{-}CF_3C_6H_4)_4Sn$ has more intense ligand related peaks, such as $(Ar_2\text{-}F)^+$, $(Ar_2\text{-}2F)^+$, $(Ar_2\text{-}3F)^+$, $(Ar\text{-}F)^+$, and $(Ar\text{-}2F)^+$, while $(m\text{-}CF_3C_6H_4)_4Sn$ shows only fairly intense $(Ar_2\text{-}F)^+$, $(Ar_2\text{-}2F)^+$ and $(Ar\text{-}F)^+$ peaks. SnF^+ and Sn^+ are only observed in spectrum of $(p\text{-}CF_3C_6H_4)_4Sn$. The matrix related peaks observed in these spectra are $Ar_3Sn{\cdot}NBA^+$.

For $(x\text{-}CH_3OC_6H_4)_4Sn$ (x=o,m,p) compounds (Table V(3)), $(m\text{-}CH_3OC_6H_4)_4Sn$ and $(p\text{-}CH_3OC_6H_4)_4Sn$ show very low abundance molecular ion peaks in their spectra, while $(o\text{-}CH_3OC_6H_4)_4$ gives a tiny $(M\text{-}H)^+$ peak instead of molecular ion peak. In the spectrum of $(o\text{-}CH_3OC_6H_4)_4Sn$, the only observed four tin-containing peaks are: $(Ar_3Sn{\cdot}NBA\text{-}H)^+$, $(M\text{-}H)^+$, Ar_3Sn^+ and $(Ar_3Sn\text{-}CH_3)^+$, with Ar_3Sn^+ being the base peak. More resemblance between spectra of $(m\text{-}CH_3OC_6H_4)_4Sn$ and $(p\text{-}CH_3OC_6H_4)_4Sn$ is observed. In these two spectra, Ar_3Sn^+ (base peaks) and $ArSn^+$ are still dominant peaks. Ar_2Sn^+ and Sn^+ have low abundance. In low mass range, $(m\text{-}CH_3OC_6H_4)_4Sn$ has more

fragment peaks.

From above analysis, we can conclude that substituent group positions of the ligands have larger effect on their +ve FAB spectra than on their EI spectra. This perhaps is due to the addition of matrix, which may partially change the steric orientation of sample molecules through complexing at sample molecules. Moreover, when the polarity and size of the substituent group are small, the spectra of the ortho- and para- isomers have some similarities, as shown in Table V(1). When the polarity and size of the substituent group of the substituent group are larger, however, only the spectra of meta- and para- isomers show similarities as in Table V(2) and (3). The reason for the difference mainly comes from the "ortho effect" [105]

d. Effect of the Substituent Group Type on the FAB Spectra

In order to study the effect of the substituent group type on the positive ion FAB spectra in NBA matrix, we can analyze the spectral data in Table V(4), (5), (6) of the following three groups of compounds: (1). $(3,5\text{-}X_2C_6H_3)_4Sn$ (X=F, Cl, CH_3); (2). $(p\text{-}XC_6H_4)_4Sn$ (X=CH_3, CF_3, CH_3O, CH_3S); (3). $(m\text{-}XC_6H_4)_4Sn$ (X=F, CF_3, CH_3, CH_3O).

For group (1) compounds (Table V(4)), no molecular ion peaks are observed. $(3,5\text{-}(CH_3)_2C_6H_3)_4Sn$ shows a low abundance $(M\text{-}H)^+$ peak and a lot of fragment peaks. $(3,5\text{-}F_2C_6H_3)_4Sn$ gives few fragment peaks. In all of these spectra, Ar_3Sn^+ and $ArSn^+$ are major tin-containing peaks. SnX^+ is only observed in spectrum of $(3,5\text{-}F_2C_6H_3)_4$. Peaks related to matrix are $Ar_3Sn{\cdot}NBA^+$, $(Ar_3Sn{\cdot}NBA\text{-}H)^+$, $M{\cdot}NO_2^+$ and Ar_3SnCHO^+. Greater differences exist among these spectra.

In the spectra of group (2) compounds (Table V(5)), only $(p\text{-}CH_3OC_6H_4)_4Sn$ and $(p\text{-}CH_3SC_6H_4)_4$ show molecular ion peaks. $(p\text{-}CH_3C_6H_4)_4Sn$ and $(p\text{-}CH_3SC_6H_4)_4$ yield fewer fragment peaks than the other two compounds do. Even electron ion peaks, such as Ar_3Sn^+, $ArSn^+$, SnF^+, are predominant in these spectra. Matrix related peaks are observed in higher mass range (e.g. $(M{\cdot}NBA\text{-}2H)^+$, $(M{\cdot}NBA\text{-}NO_2)^+$, $Ar_3Sn{\cdot}NBA^+$).

In spectra of group (3) compounds (Table V(6)), a molecular ion peak is only observed in (m-$CH_3OC_6H_4)_4Sn$. Ar_3Sn^+ and $ArSn^+$ are dominant peaks in all of these spectra. Sn^+ peaks have higher abundance in spectra of (m-$FC_6H_4)_4Sn$ and (m-$CH_3C_6H_4)_4Sn$. Differences among the spectra are quite obvious in both fragmentation patterns and ion intensities of peaks.

Compared with the effect of substituent position of the ligands on the +ve FAB spectra, substituent type has larger influence on their corresponding +ve FAB spectra.

e. Effect of Ligand Type on the FAB Spectra

To observe the effect of ligand type on FAB spectra, the partial +ve FAB MS spectral data in Table V(7), (8), (9) can provide such information. These data belong to the following three groups of aryltin compounds: (1). (o-$CH_3C_6H_4)_3SnI$, (o-$CH_3OC_6H_4)_3SnI$, (2,4,6-$(CH_3)_3C_6H_2)_3SnI$; (2). (o-$CH_3OC_6H_4)_3SnBr$, (o-$CH_3OC_6H_4)_3SnI$, (o-$CH_3OC_6H_4)_4Sn$; (3). (2,4,6-$(CH_3)_3C_6H_2)_3SnCl$, (2,4,6-$(CH_3)_3C_6H_2)_3SnBr$, (2,4,6-$(CH_3)_3C_6H_2)_3SnI$, (2,4,6-$(CH_3)_3C_6H_2)_3SnO_2CCH_3$. Group (1) are Ar_3SnI type compounds, where Ar = o-$CH_3C_6H_4$, o-$CH_3OC_6H_4$, 2,4,6-$(CH_3)_3C_6H_3$. Group (2) are (o-$CH_3OC_6H_4)_3SnX$ type compounds, X = Br, I, o-$CH_3OC_6H_4$. While group (3) are (2,4,6-$(CH_3)_3C_6H_3)_3SnX$, where X= Cl, Br, I, O_2CCH_3. In addition to the difference in X's, the Ar group in group (3) is larger than that in group (2).

In the spectra of group (1) compounds (Table V(7)), only (o-$CH_3C_6H_4)_3SnI$ has a tiny molecular ion peak. Ar_3Sn^+ peaks are the strongest tin-containing peaks in all of these spectra. Both (o-$CH_3C_6H_4)_3SnI$ and (o-$CH_3OC_6H_4)_3SnI$ have an intense Ar_2SnI^+ peak, while (2,4,6-$(CH_3)_3C_6H_2)_3SnI$ doesn't exhibit such a peak. (o-$CH_3C_6H_4)_3SnI$ and (2,4,6-$(CH_3)_3C_6H_3)_3SnI$ give strong $ArSn^+$ peaks. In all of the spectra, Sn^+ peaks are in fairly high abundance. The matrix related peaks observed are $(Ar_3Sn{\cdot}NBA+C_2H_2)^+$, $Ar_3Sn{\cdot}NBA^+$, $Ar_2SnI{\cdot}NBA^+$, $(Ar_3Sn{\cdot}NBA-H_2O)^+$, $(Ar_3Sn{\cdot}NO_2+CH)^+$, and

$(Ar_3Sn{\cdot}NO_2{+}H)^+$. Bigger differences exist among these spectra.

For group (2) compounds (Table V(8)), no molecular ion peaks show up in their spectra. Ar_3Sn^+ ion peaks are the most intense tin-containing peaks in all of the spectra. In spectra of $(o\text{-}CH_3OC_6H_4)_3SnBr$ and $(o\text{-}CH_3OC_6H_4)_3SnI$, very strong Ar_2SnX^+ (X=Br, I) peaks are observed. Some similarities are observed in spectra of $(o\text{-}CH_3OC_6H_4)_3SnBr$ and $(o\text{-}CH_3OC_6H_4)_3SnI$, while a bigger difference appear between the spectrum of $(o\text{-}CH_3OC_6H_4)_4Sn$ and that of $(o\text{-}CH_3OC_6H_4)_3SnBr$ or that of $(o\text{-}CH_3OC_6H_4)_3SnI$. $(o\text{-}CH_3OC_6H_4)_4Sn$ gives only few tin-containing peaks. $(ArSn{\cdot}NBA{+}C_2H_2)^+$, $Ar_3Sn{\cdot}NBA^+$ and $(Ar_3Sn{\cdot}NO_2{+}CH)^+$ are the matrix related peaks observed in these spectra.

$(2,4,6\text{-}(CH_3)_3C_6H_2)_3SnX$ (X=Cl, Br, I, O_2CCH_3) compounds (Table V(9)) don't have the molecular ion in their spectra. However, $(2,4,6\text{-}(CH_3)_3C_6H_2)_3SnCl$ and $(2,4,6\text{-}(CH_3)_3C_6H_2)_3SnBr$ yield low abundance $(M\text{-}H)^+$ peaks. In all of these spectra, Ar_3Sn^+ and $ArSn^+$ are dominant peaks. Spectra of $(2,4,6\text{-}(CH_3)_3C_6H_2)_3SnCl$ and $(2,4,6\text{-}(CH_3)_3C_6H_2)_3SnBr$ bear some similarities, while a much bigger difference is observed when comparing them with the other two spectra. The spectra of $(2,4,6\text{-}(CH_3)_3C_6H_2)_3SnI$ and $(2,4,6\text{-}(CH_3)_3C_6H_2)_3SnO_2CCH_3$ are also quite different (see Table V(9)).

Based on above discussion and the data in Table V, we can conclude that the effect of ligand type on +ve FAB spectra is the biggest, then the effect of substituent type, finally the effect of substituent position of the ligands. However, when the polarity and size of the substituent group become larger, substituent group position also has a bigger effect on the +ve FAB spectra.

* Note: text continues on page 71.

Table V. Positive Ion FAB Mass Spectral Data* of Aryltin Compounds in NBA Matrix

(1) $(x\text{-}CH_3C_6H_4)_4Sn$ (x=o, m, p)

ION^+	Ar= o-$CH_3C_6H_4$	= m-$CH_3C_6H_4$	= p-$CH_3C_6H_4$
$Ar_3Sn{\cdot}NBA^+$	-	2.3	2.1
$(M\text{-}H)^+$	-	1.5	0.7
$Ar_3Sn{\cdot}CH_2^+$	-	2.1	-
Ar_3Sn^+	73.9	53.6	81.6
$Ar_2Sn{\cdot}OH^+$	-	2.9	-
$(Ar_2Sn\text{-}H)^+$	-	5.9	-
$(Ar_2Sn\text{-}2H)+$	-	-	1.1
$ArSn^+$	15.0	17.5	14.6
Sn^+	11.1	14.3	-

* Percentage of the total positive ion current carried by tin-containing ions.

(2) $(x\text{-}CF_3C_6H_4)_4Sn$ (x=m, p)

ION^+	Ar= m-$CF_3C_6H_4$	= p-$CF_3C_6H_4$
$Ar_3Sn{\cdot}NBA^+$	5.5	5.3
$(M\text{-}F)^+$	4.0	1.5
$(Ar_3SnHF+2H)^+$	4.3	8.0
Ar_3Sn^+	54.9	39.6
$(Ar_3Sn\text{-}F)^+$	2.7	2.4
$(Ar_3Sn\text{-}CHF_3)^+$	1.1	1.4
$(Ar_2Sn{\cdot}F\text{-}2H)^+$	4.0	3.0
$(Ar_2Sn\text{-}HF\text{-}H)^+$	2.9	0.6
$ArSn^+$	20.6	17.5
SnF^+	-	11.3
Sn^+	-	9.6

* Percentage of the total positive ion current carried by tin-containing ions.

Table V (cont.) (3) $(x\text{-}CH_3OC_6H_4)_4Sn$ (x=o, m, p)

ION$^+$	Ar= o-$CH_3OC_6H_4$	= m-$CH_3OC_6H_4$	= p-$CH_3OC_6H_4$
$(Ar_3Sn\cdot NBA\text{-}H)^+$	0.3	-	-
$(M\cdot NBA\text{-}2H)^+$	-	0.5	0.9
M^+	-	2.7	1.3
$(M\text{-}H)^+$	0.4	-	-
$Ar_3SnO(CH_3)_2^+$	-	-	0.6
$Ar_3Sn\cdot CH_2^+$	-	-	1.4
Ar_3Sn^+	96.9	55.2	60.2
$(Ar_3Sn\text{-}CH_4)^+$	-	1.3	1.8
$(Ar_3Sn\text{-}OCH_3)^+$	-	-	2.1
$Ar_2Sn\cdot OH^+$	-	1.5	-
$Ar_2SnCH_3^+$	-	-	1.9
Ar_2Sn^+	-	4.6	5.9
$(Ar_2Sn\text{-}CH_3)^+$	2.4	4.4	3.1
$ArSn(OCH_3)_2^+$	-	0.9	-
$ArSn^+$	-	14.5	16.3
$C_6H_5SnH_2^+$	-	-	2.0
$C_6H_3Sn^+$	-	2.3	-
$C_2H_5Sn^+$	-	2.8	-
$SnCH_3^+$	-	6.9	-
Sn^+	-	6.6	2.3

* Percentage of the total positive ion current carried by tin-containing ions.

Table V (cont.) (4) $(3,5\text{-}X_2C_6H_3)_4Sn$ (X=F, Cl , CH_3)

ION$^+$	Ar= 3,5-$F_2C_6H_3$	= 3,5-$Cl_2C_6H_3$	= 3,5-$(CH_3)_2C_6H_3$
$Ar_3Sn{\cdot}NBA^+$	6.2	-	-
$(Ar_3Sn{\cdot}NBA\text{-}H)^+$	-	10.2	-
$M{\cdot}NO_2^+$	-	-	1.1
$(M\text{-}H)^+$	-	-	4.0
$Ar_3Sn{\cdot}CHO^+$	-	1.6	-
$Ar_3Sn{\cdot}CH_2^+$	-	-	4.8
Ar_3Sn^+	48.1	61.5	46.0
$(Ar_3Sn\text{-}CH_3)^+$	-	-	1.2
$(Ar_3Sn\text{-}Cl)^+$	-	3.2	-
Ar_2SnX^+	-	0.9	3.0
Ar_2Sn^+	-	-	8.9
$(Ar_2Sn\text{-}CH_3)^+$	-	-	1.4
$ArSnCH_3^+$	-	-	1.1
$ArSn^+$	20.3	22.7	16.1
$(ArSn\text{-}CH_3)^+$	-	-	5.2
SnX^+	14.4	-	-
Sn^+	11.0	-	7.1

(X=F, Cl, CH_3)

* Percentage of the total positive ion current carried by tin-containing ions.

Table V (cont.) (5) $(p\text{-}XC_6H_4)_4Sn$ (X=CH_3, CF_3, CH_3O, CH_3S)

ION^+	Ar=p-$CH_3C_6H_4$	=p-$CF_3C_6H_4$	= p-$CH_3OC_6H_4$	= p-$CH_3SC_6H_4$
$(M\cdot NBA\text{-}2H)^+$	-	-	0.9	-
$(M\cdot NBA\text{-}NO_2)^+$	-	-	-	9.6
$Ar_3Sn\cdot NBA^+$	2.1	5.3	-	-
M^+	-	-	1.3	18.4
$(M\text{-}H)^+$	0.7	-	-	-
$(M\text{-}F)^+$	-	1.5	-	-
$Ar_3SnO(CH_3)_2^+$	-	-	0.6	-
$(Ar_3SnHF+2H)^+$	-	8.0	-	-
$Ar_3Sn\cdot CH_2^+$	-	-	1.4	-
Ar_3Sn^+	81.6	39.6	60.2	72.0
$(Ar_2Sn\text{-}2H)+$	1.1	-	-	-
$(Ar_3Sn\text{-}CH_4)^+$	-	-	1.8	-
$(Ar_3Sn\text{-}F)^+$	-	2.4	-	-
$(Ar_3Sn\text{-}OCH_3)^+$	-	-	2.1	-
$(Ar_3Sn\text{-}CHF_3)+$	-	1.4	-	-
$Ar_2SnCH_3^+$	-	-	1.9	-
$(Ar_2Sn\cdot F\text{-}2H)^+$	-	3.0	-	-
Ar_2Sn^+	-	-	5.9	-
$(Ar_2Sn\text{-}CH_3)^+$	-	-	3.1	-
$(Ar_3Sn\text{-}F)^+$	-	0.6	-	-
$ArSn^+$	14.6	17.5	16.3	-
$C_6H_5SnH_2^+$	-	-	2.0	-
SnF^+	-	11.3	-	-
Sn^+	-	9.6	2.3	-

* Percentage of the total positive ion current carried by tin-containing ions.

Table V (cont.) (6) $(m\text{-}XC_6H_4)_4Sn$ (X=F, CF_3, CH_3, CH_3O)

ION$^+$	Ar=m-FC_6H_4	=m-$CF_3C_6H_4$	= m-$CH_3C_6H_4$	= m-$CH_3OC_6H_4$
$Ar_3Sn{\cdot}NBA^+$	4.5	5.5	2.3	0.5
M^+	-	-	-	2.7
$(M-H)^+$	-	-	1.5	-
$(M-F)^+$	-	4.0	-	-
$Ar_3Sn{\cdot}OCH_2^+$	7.1	-	-	-
$(Ar_3SnHF+2H)^+$	-	4.3	-	-
$Ar_3Sn{\cdot}CH_2^+$	-	-	2.1	-
Ar_3Sn^+	43.5	54.9	53.6	55.2
$(Ar_3Sn-CH_4)^+$	-	-	-	1.3
$(Ar_3Sn-F)^+$	-	2.7	-	-
$(Ar_3Sn-CHF_3)+$	-	1.1	-	-
$(Ar_2Sn{\cdot}F-2H)^+$	-	4.0	-	-
$Ar_2Sn{\cdot}OH^+$	-	-	2.9	1.5
Ar_2Sn^+	-	-	-	4.6
$(Ar_2Sn-H)^+$	-	-	5.9	-
$(Ar_2Sn-CH_3)^+$	-	-	-	4.4
$(Ar_2Sn-F)^+$	-	2.9	-	-
$ArSn(OCH_3)_2^+$	-	-	-	0.9
$ArSn^+$	28.2	20.6	17.5	14.5
$C_6H_3Sn^+$	-	-	-	2.3
$SnCH_3^+$	-	-	-	6.9
Sn^+	16.7	-	14.3	6.6

* Percentage of the total positive ion current carried by tin-containing ions.

Table V (cont.) (7) Ar_3SnI (Ar=o-$CH_3C_6H_4$, o-$CH_3OC_6H_4$, 2,4,6-$(CH_3)_3C_6H_2$)

ION$^+$	Ar=o-$CH_3C_6H_4$	=o-$CH_3OC_6H_4$	=2,4,6-$(CH_3)_3C_6H_2$
$(Ar_3Sn{\cdot}NBA{+}C_2H_2)^+$	-	0.9	-
$Ar_3Sn{\cdot}NBA^+$	0.7	-	-
$Ar_2SnI{\cdot}NBA^+$	0.6	-	-
$(Ar_3Sn{\cdot}NBA{-}H_2O)^+$	-	-	0.7
M^+	0.6	-	-
$Ar_3SnC_6H_3^+$	1.8	-	-
$(Ar_3Sn{\cdot}NO_2{+}CH)^+$	-	1.3	-
$(Ar_3Sn{\cdot}NO_2{+}H)^+$	-	-	6.1
$Ar_3Sn{\cdot}CH_4^+$	-	-	3.2
Ar_3Sn^+	37.0	54.7	35.3
Ar_2SnI^+	18.9	18.6	-
$Ar_2SnCH_3^+$	1.4	-	-
$(Ar_2Sn{-}H)^+$	4.5	-	7.6
$(Ar_2Sn{-}CH_3)^+$	-	1.0	-
SnI^+	2.7	-	-
$ArSnCH_2^+$	-	-	3.0
$ArSn^+$	22.3	8.4	28.0
$SnOCH_3^+$	-	3.8	-
Sn^+	9.4	11.2	16.0

* Percentage of the total positive ion current carried by tin-containing ions.

Table V (cont.) (8) $(o\text{-}CH_3OC_6H_4)_3SnX$ (X=Br, I, $o\text{-}CH_3OC_6H_4$)

ION^+	X=Br	=I	$=o\text{-}CH_3OC_6H_4$
$(Ar_3Sn\cdot NBA+C_2H_2)^+$	1.8	0.9	-
$Ar_3Sn\cdot NBA^+$	-	-	0.3
$(Ar_3Sn\cdot NO_2+CH)^+$	0.5	1.3	-
$(M-H)^+$	-	-	0.4
Ar_3Sn^+	51.8	54.7	96.9
Ar_2SnX^+	32.7	18.6	-
$(Ar_2Sn-CH_3)^+$	-	1.0	2.4
$ArSn^+$	6.8	8.4	-
SnX^+	2.4	-	-
$SnOCH_3^+$	-	3.8	-
Sn^+	4.0	11.2	-

* Percentage of the total positive ion current carried by tin-containing ions.

Table V (cont.) (9) $(2,4,6\text{-}(CH_3)_3C_6H_2)_3SnX$ (X=Cl, Br, I, O_2CCH_3)

ION$^+$	X= Cl	=Br	= I	= O_2CCH_3
$(Ar_3Sn{\cdot}NBA\text{-}2H)^+$	-	-	-	0.5
$(Ar_3Sn{\cdot}NBA\text{-}H_2O)^+$	-	-	0.7	-
$(M{\cdot}X\text{-}H)^+$	-	-	-	-
$(M\text{-}H)^+$	3.6	2.8	-	-
$(Ar_3Sn{\cdot}NO_2{+}H)^+$	-	-	6.1	2.2
$(Ar_3Sn{\cdot}NO_2\text{-}CH_2)^+$	-	-	-	1.5
$Ar_3Sn{\cdot}CH_4^+$	0.1	-	3.2	-
$Ar_3Sn{\cdot}CH_2^+$	-	1.5	-	2.0
Ar_3Sn^+	21.8	20.8	35.3	39.2
$(Ar_3Sn\text{-}CH_4)^+$	-	-	-	0.8
$Ar_2SnXCH_2^+$	2.2	1.9	-	-
Ar_2SnX^+	21.7	-	-	1.8
$(Ar_2SnX\text{-}H)^+$	-	17.6	-	-
$Ar_2Sn{\cdot}H_2O^+$	-	-	-	4.1
$(Ar_2SnX\text{-}CH_4)^+$	2.4	0.6	-	-
$Ar_2SnCH_3^+$	-	2.5	-	-
$(Ar_2Sn\text{-}H)^+$	3.2	5.0	7.6	10.4
$(Ar_2Sn\text{-}CH_5)^+$	0.1	1.2	-	1.4
(ArSnX-H)+	1.8	1.5	-	-
$ArSnCH_2^+$	1.4	2.6	3.0	2.1
$ArSn^+$	18.4	18.9	28.0	23.7
SnX^+	5.3	4.7	-	-
$SnCH_3^+$	8.5	10.3	-	4.6
Sn^+	7.8	8.2	16.0	6.0

* Percentage of the total positive ion current carried by tin-containing ions.

Table VI. Positive Ion FAB Mass Spectral Data* of Aryltin Compounds in NPOE Matrix

(1) $(x\text{-}CH_3C_6H_4)_4Sn$ (x=o, m, p)

ION^+	Ar= o-$CH_3C_6H_4$	= m-$CH_3C_6H_4$	= p-$CH_3C_6H_4$
$Ar_3Sn{\cdot}NPOE^+$	-	4.4	2.1
$(M+2H)^+$	1.5	-	-
$(M-H)^+$	-	3.4	-
$Ar_3SnCH_2^+$	-	28.5	1.9
Ar_3Sn^+	36.3	48.7	68.2
$(Ar_3Sn\text{-}CH_3)^+$	-	1.2	-
Ar_2SnOH^+	-	3.6	-
$Ar_2SnCH_3^+$	-	-	2.6
$(Ar_2Sn\text{-}H)^+$	-	5.5	7.1
$ArSn^+$	10.6	17.7	18.2
Sn^+	51.5	12.6	-

* Percentage of the total positive ion current carried by tin-containing ions.

(2) $(x\text{-}CH_3OC_6H_4)_4Sn$ (x=o, m, p)

ION^+	Ar= o-$CH_3OC_6H_4$	= m-$CH_3OC_6H_4$	= p-$CH_3OC_6H_4$
$(Ar_3Sn{\cdot}NPOE\text{-}2H)^+$	-	-	2.5
M^+	-	3.4	2.5
Ar_3Sn^+	98.4	78.1	55.0
$(Ar_3Sn\text{-}CH_2)^+$	-	-	3.8
$(Ar_3Sn\text{-}2CH_3)^+$	-	-	3.0
Ar_2Sn^+	-	2.3	8.8
$(Ar_2Sn\text{-}CH_3)^+$	-	2.1	3.5
$ArSn^+$	1.6	14.1	15.1
$SnCH_3^+$	-	-	2.3
Sn^+	-	-	3.5

* Percentage of the total positive ion current carried by tin-containing ions.

Table VI (cont.) (3) $(x\text{-}CF_3C_6H_4)_4Sn$ (x=m, p)

ION^+	Ar= m-$CF_3C_6H_4$	= p-$CF_3C_6H_4$
$Ar_3Sn{\cdot}NPOE^+$	8.2	10.0
$(M\text{-}F)^+$	1.1	3.3
Ar_3Sn^+	73.1	51.7
$(Ar_3Sn\text{-}F)^+$	-	5.3
$(Ar_3Sn\text{-}CHF_3)^+$	-	2.0
$(Ar_2Sn\text{-}H)^+$	-	1.6
$ArSn^+$	17.6	22.7
Sn^+	-	3.4

* Percentage of the total positive ion current carried by tin-containing ions.

(4) $(3,5\text{-}X_2C_6H_3)_4Sn$ (X=F, Cl , CH_3)

ION^+	Ar= 3,5-$F_2C_6H_3$	= 3,5-$Cl_2C_6H_3$	= 3,5-$(CH_3)_2C_6H_3$
$Ar_3Sn{\cdot}NPOE^+$	No spectrum	25.6	2.4
M^+	available.	-	3.6
$Ar_3SnCH_2^+$		-	2.9
Ar_3Sn^+		74.4	39.2
$(Ar_3Sn\text{-}CH_2)^+$		-	1.3
Ar_2SnOH^+		-	2.1
$(Ar_2Sn\text{-}H)^+$		-	7.2
$(Ar_2Sn\text{-}CH_5)^+$		-	1.2
$ArSn^+$		-	17.3
$(ArSn\text{-}CH_4)^+$		-	4.4
$SnCH_3^+$		-	2.7
Sn^+		-	15.8

* Percentage of the total positive ion current carried by tin-containing ions.

Table VI (cont.) (5) $(p\text{-}XC_6H_4)_4Sn$ (X=CH_3, CF_3, CH_3O, CH_3S)

ION$^+$	Ar=p-$CH_3C_6H_4$	=p-$CF_3C_6H_4$	= p-$CH_3OC_6H_4$	= p-$CH_3SC_6H_4$
$(Ar_3Sn{\cdot}NPOE{+}C_6H_5)^+$	-	-	-	3.8
$(Ar_3Sn{\cdot}NPOE{-}2H)^+$	-	-	2.5	1.3
$Ar_3Sn{\cdot}NPOE^+$	2.1	10.0	-	-
M^+	-	-	2.5	10.0
$(M\text{-}F)^+$	-	3.3	-	-
$Ar_3SnCH_2^+$	1.9	-	-	3.3
Ar_3Sn^+	68.2	51.7	55.0	49.8
$(Ar_3Sn\text{-}F)^+$	-	5.3	-	-
$(Ar_3Sn\text{-}CH_2)^+$	-	-	3.8	-
$(Ar_3Sn\text{-}CH_4)+$	-	-	-	3.5
$(Ar_3Sn\text{-}2CH_3)^+$	-	-	3.0	-
$(Ar_3Sn\text{-}SCH_4)^+$	-	-	-	1.5
$(Ar_3Sn\text{-}CHF_3)^+$	-	2.0	-	-
$Ar_2SnCH_3^+$	2.6	-	-	-
Ar_2Sn^+	-	-	8.8	-
$(Ar_2Sn\text{-}CH_3)^+$	-	-	-	6.3
$(Ar_2Sn\text{-}H)^+$	7.1	1.6	-	-
$(Ar_2Sn\text{-}CH_3)^+$	-	-	3.5	-
$ArSn^+$	18.2	22.7	15.1	16.8
$(ArSn\text{-}CH_3)^+$	-	-	-	1.3
CH_3SSn^+	-	-	-	2.8
$SnCH_3^+$	-	-	2.3	-
Sn^+	-	3.4	3.5	-

* Percentage of the total positive ion current carried by tin-containing ions.

Table VI (cont.) (6) $(m\text{-}XC_6H_4)_4Sn$ (X=F, CF_3, CH_3, CH_3O)

ION$^+$	Ar=m-FC_6H_4	=m-$CF_3C_6H_4$	= m-$CH_3C_6H_4$	= m-$CH_3OC_6H_4$
$Ar_3Sn{\cdot}NPOE^+$	-	8.2	4.4	-
M^+	-	-	-	3.4
$(M\text{-}F)^+$	-	1.1	-	-
$(M\text{-}H)^+$	-	-	3.4	-
$Ar_3SnCH_2^+$	-	-	28.5	-
Ar_3Sn^+	57.1	73.1	48.7	78.1
$(Ar_3Sn\text{-}CH_3)^+$	-	-	1.2	-
Ar_2SnOH^+	-	-	3.6	-
$Ar_2Sn{\cdot}HF^+$	14.4	-	-	-
Ar_2Sn^+	-	-	-	2.3
$(Ar_2Sn\text{-}H)^+$	-	-	5.5	-
$(Ar_2Sn\text{-}CH_3)^+$	-	-	-	2.1
$ArSn^+$	28.5	17.6	17.7	14.1
Sn^+	-	-	12.6	-

* Percentage of the total positive ion current carried by tin-containing ions.

(7) Ar_3SnI (Ar=o-$CH_3C_6H_4$, o-$CH_3OC_6H_4$, 2,4,6-$(CH_3)_3C_6H_2$)

ION$^+$	Ar=o-$CH_3C_6H_4$	=o-$CH_3OC_6H_4$	=2,4,6-$(CH_3)_3C_6H_2$
$Ar_2SnI{\cdot}NPOE^+$	1.2	-	-
$Ar_3Sn{\cdot}NPOE^+$	1.2	-	-
$Ar_2Sn{\cdot}NPOE^+$	0.7	-	-
M^+	1.6	-	-
Ar_2SnI^+	25.4	32.3	-
Ar_3Sn^+	31.4	55.5	79.1
$Ar_3SnCH_2^+$	1.1	-	-
Ar_2SnOH^+	2.7	-	-
$(Ar_2Sn\text{-}H)^+$	6.2	-	-
SnI^+	2.7	-	-
$ArSn^+$	25.9	6.1	20.9
Sn^+	3.5	6.1	-

* Percentage of the total positive ion current carried by tin-containing ions.

Table VI (cont.) (8) $(o\text{-}CH_3OC_6H_4)_3SnX$ (X=Br, I, $o\text{-}CH_3OC_6H_4$)

ION^+	X=Br	=I	$=o\text{-}CH_3OC_6H_4$
Ar_3Sn^+	60.0	55.5	98.4
Ar_2SnX^+	40.0	32.3	-
$ArSn^+$	-	6.1	1.6
Sn^+	-	6.1	-

* Percentage of the total positive ion current carried by tin-containing ions.

(9) $(2,4,6\text{-}(CH_3)_3C_6H_2)_3SnX$ (X=Cl, Br,I, O_2CCH_3)

ION^+	X= Cl	=Br	= I	$=O_2CCH_3$
$Ar_2Sn{\cdot}NPOE^+$	-	-	-	0.6
$(M\text{-}H)^+$	2.8	3.9	-	-
Ar_3Sn^+	33.0	27.9	79.1	31.4
$Ar_2SnXCH_2^+$	-	2.4	-	-
Ar_2SnX^+	48.3	37.9	-	18.3
$Ar_2Sn{\cdot}H_2O^+$	-	-	-	6.2
$(Ar_2Sn\text{-}H)^+$	-	2.6	-	6.4
$ArSn^+$	13.7	22.6	20.9	12.1
$CHSnNO^+$	-	-	-	4.3
$SnCH_3^+$	-	-	-	8.1
Sn^+	2.2	2.8	-	12.7

* Percentage of the total positive ion current carried by tin-containing ions.

3.1.3. Negative Ion FAB MS Studies

To observe the negative ion FAB mass spectral behavior of aryltin compounds, all of the compounds in Table I were run in an NBA matrix. However, only (m-$CF_3C_6H_4)_4Sn$, (p-$CF_3C_6H_4)_4Sn$, (3,5-$F_2C_6H_3)_4Sn$, (3,5-$Cl_2C_6H_3)_4Sn$, (3,5-$(CH_3)_2C_6H_3)_4Sn$, (o-$CH_3OC_6H_4)_4Sn$, (m-$CH_3OC_6H_4)_4Sn$, (2,4,6-$(CH_3)_3C_6H_3)_3SnCl$, (2,4,6-$(CH_3)_3C_6H_3)_3SnO_2CCH_3$, (o-$CH_3OC_6H_4)_3SnBr$, (o-$CH_3OC_6H_4)_3SnI$ and (o-$CH_3C_6H_4)_3SnI$ produce good spectra. Due to the low sensitivity of negative ion FAB MS and the poor solubility of these samples in NBA, the rest of the compounds give either fewer very tiny tin-containing peaks or no sample related peak at all. Presumably, this phenomenon is related to the steric effects and the polarity of the ligands as well as the electronegativity of the compounds. The negative ion FAB spectral data are listed in Table VII.

The negative ion FAB MS spectra of these compounds show some distinct features, in contrast to their counterparts in positive ion FAB MS spectra (Table V) and EI MS spectra (Table IV). In general, negative ion FAB spectra have much lower ion intensities than their positive ion FAB and EI counterparts. In Table VII(1), both (m-$CF_3C_6H_4)_4Sn$ and (p-$CF_3C_6H_4)_4Sn$ have strong matrix related peaks in their spectra, $(M{\cdot}NBA+H)^-$, $M{\cdot}CH_3^-$ for (p-$CF_3C_6H_4)_4Sn$ and $M{\cdot}NBA^-$ for (m-$CF_3C_6H_4)_4Sn$. Both of them also have low abundance Ar_2Sn^- and $ArSn^-$ peaks and intense Ar_2SnF^- peaks, but do have abundant Ar_3Sn^- peaks. Such phenomena are also observed in spectra of (3,5-$F_2C_6H_3)_4Sn$ and (3,5-$Cl_2C_6H_3)_4Sn$ (Table VII(2)). (3,5-$F_2C_6H_3)_4Sn$ and (3,5-$Cl_2C_6H_3)_4Sn$ both have strong $Ar_2Sn{\cdot}X^-$ and matrix related peaks, $(M{\cdot}NBA-H)^-$ for (3,5-$F_2C_6H_3)_4Sn$ and $(M{\cdot}NBA-2H)^-$ for (3,5-$Cl_2C_6H_3)_4Sn$. They also have very strong Ar_3Sn^- peaks. For (3,5-$(CH_3)_2C_6H_3)_4Sn$, more similarities exist between its positive ion and negative ion FAB MS spectra. They all have intense $Ar_3Sn^{+/-}$ and $ArSn^{+/-}$ peaks. However, the negative ion

FAB MS spectrum has strong matrix related peaks (like $(M{\cdot}NBA\text{-}3H)^-$ and $M{\cdot}CH_3^-$) and Ar_2Sn^-.

The negative ion FAB MS spectra of $(o\text{-}CH_3OC_6H_4)_4Sn$ and $(m\text{-}CH_3OC_6H_4)_4Sn$ are very different from their positive ion spectra (Table VII(3)). Both of them have strong $(Ar_3Sn\text{-}2H)^-$ peaks instead of Ar_3Sn^- peaks. Moreover, negative ion FAB MS spectrum of $(o\text{-}CH_3OC_6H_4)_4Sn$ shows more tin-containing peaks than the +ve FAB MS spectrum does. The spectra of $(2,4,6\text{-}(CH_3)_3C_6H_2)_3SnCl$ and $(2,4,6\text{-}(CH_3)_3C_6H_2)_3SnO_2CCH_3$ in Table VII(4) also show a bigger difference with their +ve FAB and EI spectra. The negative ion FAB spectrum of $(2,4,6\text{-}(CH_3)_3C_6H_2)_3SnCl$ shows only a few peaks, and these peaks are quite different from those peaks in its +ve FAB spectrum (Table V(9)). The negative ion FAB spectrum of $(2,4,6\text{-}(CH_3)_3C_6H_2)_3SnO_2CCH_3$ has a very strong matrix related peak $(Ar_3Sn{\cdot}NO_2\text{-}CH_2)^-$ and few strong peaks in low mass range, like $ArSnCH_5^-$, $ArSn^-$ and Sn^-. No intense Ar_3Sn^- or Ar_2SnX^- or Ar_2Sn^- show in this spectrum. Big differences also show in the negative ion FAB spectra of $(o\text{-}CH_3OC_6H_4)_3SnBr$, $(o\text{-}CH_3OC_6H_4)_3SnI$ and $(o\text{-}CH_3C_6H_4)_3SnI$ in Table VII(5) compared with their +ve FAB spectra in Table V(7), (8). Both spectra of $(o\text{-}CH_3OC_6H_4)_3SnBr$ and $(o\text{-}CH_3OC_6H_4)_3SnI$ have intense $(Ar_3Sn\text{-}2H)^-$, $(Ar_2Sn\text{-}CH_3)^-$ and $(CH_3O)_2Sn^-$ peaks, while these peaks don't show in their corresponding +ve FAB spectra. The negative ion FAB spectrum of $(o\text{-}CH_3C_6H_4)_3SnI$ only shows one tin-containing peak, i.e. Ar_2SnI^- peak.

The spectral data in Table VII also indicate that the substituent type of the ligands has a bigger effect than the substituent position does. The spectra of $(m\text{-}CF_3C_6H_4)_4Sn$ and $(p\text{-}CF_3C_6H_4)_4Sn$ are quite similar, while the spectra of $(3,5\text{-}F_2C_6H_3)_4Sn$ and $(3,5\text{-}Cl_2C_6H_3)_4Sn$ show noticeable differences, both in intensity and in number of fragment peaks. Compared with these spectra, $(3,5\text{-}(CH_3)_2C_6H_3)_4Sn$ has a much different spectral form, with very intense Ar_2Sn^- and $ArSn^-$ peaks. The biggest effect of ligand type on the negative ion FAB spectra can be seen from Table VII(4) and (5). Both intensity and fragment pattern of $(2,4,6\text{-}(CH_3)_3C_6H_3)_3SnCl$ and $(2,4,6\text{-}(CH_3)_3C_6H_3)_3SnO_2CCH_3$ are

quite different. The spectrum of (o-$CH_3C_6H_4)_3SnI$ is also quite different from those of (o-$CH_3OC_6H_4)_3SnBr$ and (o-$CH_3OC_6H_4)_3SnI$.

* Note: text continues on page 77.

Table VII. Negative Ion FAB Mass Spectral Data* of Aryltin Compounds in NBA Matrix

(1) $(x\text{-}CF_3C_6H_4)_4Sn$ (x=m, p)

ION^-	Ar= m-$CF_3C_6H_4$	= p-$CF_3C_6H_4$
$(M\cdot NBA+H)^-$	-	26.6
$M\cdot NBA^-$	23.0	-
$M\cdot NO_2^-$	6.8	8.3
$M\cdot CH_3^-$	9.2	12.7
M^-	2.2	2.2
$(Ar_3SnF_2)^-$	3.0	0.5
$Ar_3Sn\cdot O^-$	6.9	8.7
Ar_3Sn^-	22.2	41.1
$Ar_2Sn\cdot F^-$	14.0	15.2
Ar_2Sn^-	3.9	4.8
$ArSnO^-$	4.1	4.0
$ArSn^-$	4.7	2.6

* Percentage of the total negative ion current carried by tin-containing ions.

Table VII (cont.) (2) $(3,5\text{-}X_2C_6H_3)_4Sn$ (X=F, Cl, CH_3)

ION$^-$	Ar= 3,5-$F_2C_6H_3$	= 3,5-$Cl_2C_6H_3$	= 3,5-$(CH_3)_2C_6H_3$
$(M\cdot NBA\text{-}H)^-$	14.1	-	-
$(M\cdot NBA\text{-}2H)^-$	-	27.6	-
$(M.NBA\text{-}3H)^-$	-	-	9.4
$(Ar_3Sn\cdot NBA\text{-}NO_2\text{-}H_2O\text{-}3H)^-$	10.9	-	-
$M\cdot NO_2^-$	4.4	-	-
$(M\cdot NO_2\text{- }2H)^-$	-	9.9	-
$M\cdot CH_3^-$	-	-	14.3
M^-	5.2	3.1	1.1
$(M\text{-}C_6H_5)^-$	-	7.0	-
$Ar_3SnF\cdot C_6H_5^-$	-	7.7	-
Ar_3SnF^-	6.5	-	-
$Ar_3Sn\cdot CH_2^-$	-	4.8	2.3
Ar_3Sn^-	24.1	23.6	44.1
$Ar_2Sn\cdot X^-$	11.1	11.5	8.2
Ar_2Sn^-	8.1	3.0	12.9
$(Ar_2Sn\text{-}C_6H_4)^-$	-	5.1	-
$(ArSn\text{-}2F)^-$	7.9	-	-
$ArSn^-$	-	-	11.0

* Percentage of the total negative ion current carried by tin-containing ions.

(3) $(x\text{-}CH_3OC_6H_4)_4Sn$ (x=o, m)

ION$^-$	Ar= o-$CH_3OC_6H_4$	= m-$CH_3OC_6H_4$
$(Ar_3Sn\cdot NBA\text{-}2H)^-$	-	5.0
$(Ar_3Sn\cdot NBA\text{-}H)^-$	6.5	-
$M\cdot CH_3^-$	-	4.2
$(M\text{-}CH_3)^-$	-	17.2
$(Ar_3Sn\text{-}2H)^-$	30.1	31.4
$(Ar_2Sn\text{-}CH_3)^-$	28.4	17.4
$(Ar_2Sn\text{-}CH_3O\text{-}CH_2)^-$	11.3	-
$CH_2Sn\cdot NBA^-$	-	7.1
$(CH_3O)_2Sn^-$	18.5	-
$OSn\cdot NO_2^-$	-	12.5
Sn^-	5.2	5.1

* Percentage of the total negative ion current carried by tin-containing ions.

Table VII (cont.) (4) $(2,4,6\text{-}(CH_3)_3C_6H_2)_3SnX$ (X=Cl, O_2CCH_3)

ION$^-$	X= Cl	= O_2CCH_3
$(M{\cdot}NBA\text{-}NO_2\text{-}C_7H_{13})^-$	-	8.6
$(Ar_3Sn{\cdot}NO_2\text{-}CH_2)^-$	-	25.8
$(Ar_2SnX{\cdot}NBA{+}NO_2)^-$	6.9	-
Ar_2SnX^-	57.7	5.5
$Ar_2SnH_2{\cdot}H_2O^-$	-	9.4
$CH_2Sn{\cdot}NBA^-$	24.8	-
$(Ar_2Sn\text{-}H)^-$	-	4.5
$ArSnCH_5^-$	-	18.7
$ArSn^-$	-	13.5
Sn^-	10.5	14.9

* Percentage of the total negative ion current carried by tin-containing ions.

(5) Ar_3SnX (Ar=o-$CH_3C_6H_4$, o-$CH_3OC_6H_4$; X=Br, I)

ION$^-$	$(o\text{-}CH_3OC_6H_4)_3Sn$ Br	$(o\text{-}CH_3OC_6H_4)_3SnI$	$(o\text{-}CH_3C_6H_4)_3SnI$
$(Ar_3Sn{\cdot}NBA\text{-}2H)^-$	4.2	6.5	-
Ar_2SnI^-	-	-	100.0
$(Ar_3Sn\text{-}2H)^-$	35.9	35.3	-
$(Ar_2Sn\text{-}CH_3)^-$	25.6	29.4	-
$(Ar_2Sn\text{-}CH_3\text{-}CH_3OH)^-$	11.9	-	-
$ArSn^-$	2.1	4.9	-
$(CH_3O)_2Sn^-$	18.0	20.0	-
Sn^-	2.2	3.9	-

* Percentage of the total negative ion current carried by tin-containing ions.

3.1.4. Fragmentation Mechanism Studies

Schemes 1-20 are the detailed fragmentation patterns of aryltin compounds under EI. For comparison, the fragmentation mechanism of these compounds under positive ion FAB in NBA matrix was studied. These detailed +ve FAB fragmentation patterns are given in Schemes 21-40. Scheme 67 shows the fragmentation pattern of $(3,5\text{-}Cl_2C_6H_3)_4Sn$/NBA under CA positive ion FAB with helium as the collisional gas. In all of these schemes, solid lines indicate the transitions verified by linked scans (B/E, B^2/E and $B^2/(1\text{-}E)/E^2$), while dotted lines are supposed transitions. In all of the transitions, the lost part is a neutral molecule or a neutral radical, whose formula can be directly derived from the precursor ion(s).

For the EI schemes, the major decomposition patterns of the aryltin compounds of Ar_4Sn and Ar_3SnX type in Table I are as follows, just as the results reported previously [52-53]:

$$M^{+\cdot} \longrightarrow Ar_2Sn^{+\cdot} + Ar_2$$

$$Ar_3Sn^{+} \longrightarrow ArSn^{+} + Ar_2$$

$$ArSn^{+} \longrightarrow Ar + Sn^{+}$$

However, for the +ve FAB schemes of these compounds, such decomposition patterns are not wholly applicable, even though for some compounds these patterns are observed. Moreover, it is difficult to find general fragmentation schemes for the +ve FAB spectra, although there are some similarities between the EI schemes and +ve FAB schemes.

Among the EI and +ve FAB schemes, generally, most of the +ve FAB schemes give more complex fragmentation patterns than their EI counterparts. Only the EI schemes

of $(p\text{-}CH_3SC_6H_4)_4Sn$, $(3,5\text{-}Cl_2C_6H_3)_4Sn$, $(o\text{-}CH_3OC_6H_4)_3SnBr$ and $(o\text{-}CH_3OC_6H_4)_3SnI$ produce more detailed fragmentation pattern than their +ve FAB schemes. The fragmentation of EI and +ve FAB schemes also show some other difference. For instance, in most of the +ve FAB schemes, the Ar_3Sn^+ peaks are observed directly from molecular ion peak fragmentation; while in EI schemes only a few such cases are observed. It is consistent with the reported EI results of other aryltin compounds [52, 53, 55].

Due to the poor solubility of $(3,5\text{-}Cl_2C_6H_3)_4Sn$ in NBA matrix, not more information about the fragmentation patterns is provided by Scheme 67 under CA positive ion FAB, with helium as the collisional gas, compared with Scheme 11 under plain +ve FAB condition. This perhaps suggests that direct linked scan studies of the aryltin compounds without the use of CA can also provide enough information on the fragmentation pattern studies for general purposes.

The following discussion will focus on the more detailed fragmentation patterns of six groups of compounds in EI linked scan and +ve FAB linked scan experiments.

(1) $(x\text{-}CH_3C_6H_4)_4Sn$ (x= o, m, p)

In Section 3.1.1. we have seen that the EI spectra of this group of compounds are quite similar to that of Ph_4Sn [52] in that even electron ions (e.g. Ar_3Sn^+, $ArSn^+$) are dominant in the spectra, odd electron ions (e.g. M^+, Ar_2Sn^+, Sn^+) unusually having low abundance. The EI linked scan studies (Schemes 1-3) of these compounds also show some similarities of the decomposition patterns with that of Ph_4Sn [52]. For these compounds, unimolecular decomposition reactions are the major mechanism. Molecular ions give Ar_2Sn^+ ion as the major peak in the metastable ion spectra by loss of an Ar_2 neutral. Ar_3Sn^+ ions (usually noted as the base peaks in the normal EI spectra), only observed as the direct decomposition product of molecular ion in Scheme 1 of $(o\text{-}CH_3C_6H_4)_4Sn$, eliminate an Ar_2 neutral giving $ArSn^+$ ions as the major product, while $ArSn^+$ ions are the

only ions to produce Sn^+ ions for all of these three compounds. Rearrangement reactions are of minor importance for these compounds. Only a few rearrangement peaks are observed. The Ar_2^+ ion is noted as the decomposition product of Ar_2Sn^+ by loss of Sn radical in the scheme of $(m\text{-}CH_3C_6H_4)_4Sn$. The $(Ar_2\text{-}H)^+$ ions are detected as rearrangement products of both Ar_3Sn^+ by loss of an ArSnH neutral and $(Ar_2Sn\text{-}H)^+$ ion by elimination of a Sn radical in the scheme of $(o\text{-}CH_3C_6H_4)_4Sn$, while in scheme of $(m\text{-}CH_3C_6H_4)_4Sn$ it is the product of Ar_2Sn^+ by loss of a SnH neutral. It is of interest that no migration of methyl group from phenyl to tin is observed for these compounds in both normal EI spectra and the linked scan spectra. Only a SnH_4^+ ion, which does not appear in the normal EI spectrum, is observed in the scheme of $(m\text{-}CH_3C_6H_4)_4Sn$. Similar rearrangement mechanisms have been studied by Occolowitz [52]. Both the similarities of spectral forms and the decomposition patterns suggest that the replacement of a hydrogen (no matter its position) on each the phenyl of Ph_4Sn by a methyl group has little effect on the EI spectra and its fragmentation modes under EI conditions, and also suggest these Ar_4Sn compounds have fairly similar structure with Ph_4Sn.

For the +ve FAB linked scan studies (Schemes 21-23) of these compounds, neither Ar_3Sn^+ nor Ar_2Sn^+ are observed from the direct decomposition of the molecular ions in the first field region. The $(Ar_2Sn\text{-}H)^+$ is noted in all of the schemes as the direct decomposition product of Ar_3Sn^+ ion by loss of a (Ar+H) molecule. The following transitions,

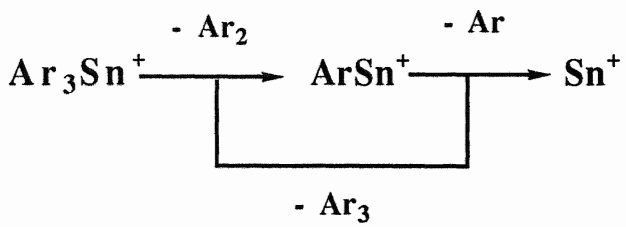

are observed in all of the schemes and as the major decomposition modes. Compared with

the EI linked scan studies, the +ve FAB schemes provide more detailed fragmentation patterns. The migration of methyl groups from the phenyl groups to tin is quite common in these samples, similar to the H migration of R_4Sn compounds [52] and the fluorine migration of $(C_6F_5)_4Sn$ [54]. Such migration peaks observed, not detected in the normal +ve FAB spectra, include CH_3SnH^+ (Scheme 21), $Ar_2SnCH_3^+$ (Scheme 22), $Ar_3SnCH_3^+$, CH_3Sn^+, $ArSn(CH_2)_3^+$, $(CH_3)_3Sn^+$ and $H_2Sn(CH_3)_2^+$ (Scheme 23). Rearrangement peaks, such as Ar_2^+, $(Ar_2\text{-}H)^+$ and $(Ar_2\text{-}CH_4)^+$, etc., are noted. Both the transition from Ar_3Sn^+ to Sn^+ and the migration of methyl groups suggest that the use of NBA matrix under +ve FAB has changed the bond strength between carbon atoms and tin atoms in the samples, due to the partial complexation of matrix molecule (or part of it) into the sample molecule (or piece of it).

(2) $(x\text{-}CF_3C_6H_4)_4Sn$ (x= m, p)

The EI linked scan studies (Schemes 4-5) show the detailed decomposition patterns of these two compounds. Both transitions leading to Ar_3Sn^+ generated from the molecular ion by loss of a neutral Ar and to $(M\text{-}F)^+$ are not verified by the metastable ion studies. It is quite interesting that Ar_2Sn^+ is also not observed as the direct decomposition product of molecular ion in the scheme of $(p\text{-}CF_3C_6H_4)_4Sn$, though it is the major peak of the decomposition of the molecular ion by loss of an Ar_2 molecule in the scheme of $(m\text{-}CF_3C_6H_4)_4Sn$. In both of the schemes, Ar_2SnF^+ is the common direct product of the molecular ions by elimination of a $(Ar_2\text{-}F)$ neutral, demonstrating the migration of fluorine from methyl group to tin atom. No information on the generation of SnF^+ and Sn^+ ions is provided by the linked scan studies. The mechanism of fluorine migration and formation of SnF^+ should be similar to those proposed by Miller [54, 55, 65] for other fluorine containing aryltin compounds (see discussion in (4)). The fragmentation patterns of Ar_3Sn^+, Ar_2SnF^+, Ar_2Sn^+, and $ArSn^+$ are shown in the schemes and are similar to the

previous studies [52].

In the +ve FAB linked scan studies (Schemes 24-25) of $(m\text{-}CF_3C_6H_4)_4Sn$ and $(p\text{-}CF_3C_6H_4)_4Sn$, no information on the generation of Ar_2Sn^+ and Sn^+ ions is provided. Ar_3Sn^+ is the direct decomposition product of $(M\text{-}F)^+$ by loss of a $CF_2C_6H_4$ neutral and $Ar_3Sn{\cdot}NBA^+$ by elimination of NBA molecule in Scheme 24 and of M^+ by loss of Ar neutral, $(M\text{-}F)^+$ and $Ar_3Sn{\cdot}NBA^+$ in Scheme 25. Ar_2SnF^+ is only found from the $(Ar_3Sn+2H+HF)^+$ decomposition in Scheme 25. SnF^+ is found from the fragmentation of $Ar_3Sn{\cdot}NBA^+$ (loss of a $(Ar_3\text{-}F){\cdot}NBA$ radical) and $ArSn^+$ (loss of a $CF_2C_6H_2$) in Scheme 24. The presence of Ar_2SnF^+ and SnF^+ indicate the migration of fluorine from methyl on phenyl to central atom tin under +ve FAB conditions. Under +ve FAB, the decomposition pattern of Ar_3Sn^+ is different from that under EI in that the major transition of Ar_3Sn^+ to $ArSn^+$ is common for organotin compounds under EI [52], while such a transition is not observed in the +ve FAB scheme of $(m\text{-}CF_3C_6H_4)_4Sn$.

(3) $(x\text{-}CH_3OC_6H_4)_4Sn$ (x= o, m, p), $(p\text{-}CH_3SC_6H_4)_4Sn$

The EI linked scan studies (Schemes 6-9) of this group of compounds show Ar_3Sn^+ and Ar_2Sn^+ (not observed in the scheme of $(p\text{-}CH_3SC_6H_4)_4Sn$) ions are generated from the molecular ion decomposition by loss of Ar and Ar_2 neutrals, separately. Fragment peaks with loss of methyl group(s), such as $(Ar_2Sn\text{-}2CH_3)^+$, $(Ar_2Sn\text{-}CH_3)^+$, $(Ar_3Sn\text{-}2CH_3)^+$ and $(ArSn\text{-}CH_3)^+$, are common for these compounds, suggesting a weaker bond strength between methyl and oxygen in the ligands due to the interaction of π orbital on benzene ring and the *p* orbital on O atom and *d* orbital on Sn atom. All of the $ArSn^+$ ions are observed as the disintegration products of Ar_3Sn^+ ions by elimination of an Ar_2 neutral for $(m\text{-}CH_3OC_6H_4)_4Sn$, $(p\text{-}CH_3OC_6H_4)_4Sn$ and $(p\text{-}CH_3SC_6H_4)_4Sn$. While for $(o\text{-}CH_3OC_6H_4)_4Sn$, $ArSn^+$ is the decomposition product of Ar_3Sn^+ and Ar_2Sn^+ just by loss of an Ar radical. Rearrangement peaks observed, such as $ArSn(OCH_3)_2^+$ (Scheme 6), $ArSn(OCH_3)_2^+$, CH_3OSnOH^+, CH_3OSn^+ (Scheme 7) and $SnSCH_3^+$ (Scheme 9), suggest

the migration of OCH_3 and SCH_3 group from phenyl to tin in the samples with similar mechanism of migration of fluorine to tin in $(C_6F_5)_4Sn$ [54].

The +ve FAB linked scan studies (Schemes 26-29) of this group of compounds indicate that the generation of Ar_3Sn^+ and Ar_2Sn^+ (not observed in the scheme of (p-$CH_3SC_6H_4)_4Sn$) ions under +ve FAB is the same as that under EI, namely Ar_3Sn^+ and Ar_2Sn^+ generated from the molecular ion decomposition by loss of an Ar and Ar_2 neutrals, separately. Fragment peaks, like $(Ar_2Sn\text{-}CH_3)^+$, $(Ar_3Sn\text{-}CH_3)^+$ and $(ArSn\text{-}CH_3)^+$, are found in the linked scan spectra of (m-$CH_3OC_6H_4)_4Sn$, (p-$CH_3OC_6H_4)_4Sn$ and (p-$CH_3SC_6H_4)_4Sn$, while for (o-$CH_3OC_6H_4)_4Sn$, $(Ar_3Sn\text{-}OCH_3)^+$ and ($Ar_2Sn\text{-}OCH_3)^+$ are observed. The presence of such peaks suggests weak bond strength between O and C atoms in NBA matrix. Only in the scheme of (p-$CH_3OC_6H_4)_4Sn$ is $ArSn^+$ observed as product of Ar_3Sn^+ (loss of an Ar_2 neutral) and Ar_2Sn^+ (loss of a Ar neutral) decomposition. The migration of OCH_3 from phenyl to tin is observed in those transitions which give rise to the peaks, like CH_3OSnOH^+, CH_3OSn^+ and $ArSnO(CH_3)_2^+$ (Scheme 26), CH_3OSn^+, $ArSnO(CH_3)_2^+$ (Scheme 27) and $SnOCH_3^+$ (Scheme 28). Such migration should have a similar mechanism to that under EI for other organotin compounds [52, 54] (c.f. discussion in (4)).

(4) (m-$FC_6H_4)_4Sn$, (3,5-$X_2C_6H_3)_4Sn$ (X= Cl, F, CH_3)

In the EI linked scan studies (Schemes 10-13) of this group of compounds, the transition leading to Ar_3Sn^+ ion from molecular ion decomposition by loss of an Ar neutral is not verified only in the case of (3,5-$(CH_3)_2C_6H_3)_4Sn$. Ar_2Sn^+ ions are found as the direct decomposition products of molecular ions of (3,5-$F_2C_6H_3)_4Sn$ and (3,5-$Cl_2C_6H_3)_4Sn$ by elimination of an Ar_2 neutral. Fragment peaks, with loss of a substituent group from the precursor ion(s), is only observed for (3,5-$(CH_3)_2C_6H_3)_4Sn$ as $(Ar_2Sn\text{-}CH_3)^+$. The migration of F and Cl atoms to the tin atom is observed in Scheme 10 (SnF^+), Scheme 11 (Ar_2SnCl^+, $SnCl^+$), and Scheme 13 (SnF^+). The $ArSn^+$ ion is found from the

Ar_2Sn^+ decomposition in Scheme 12. The following transitions,

$$Ar_3Sn^+ \xrightarrow{-\,Ar_2} ArSn^+ \xrightarrow{-\,(Ar\text{-}X)} SnX^+ \quad (X=\ F,\ Cl)$$

are verified in all of the schemes of halogen atom containing compounds. Miller et al. have discussed [101] ring fluorine-to-metal transfers for many pentafluorophenyl compounds including those with tin and lead [54,102] and a mechanism involving a 1,3-migration of the ortho-fluorine was proposed (A).

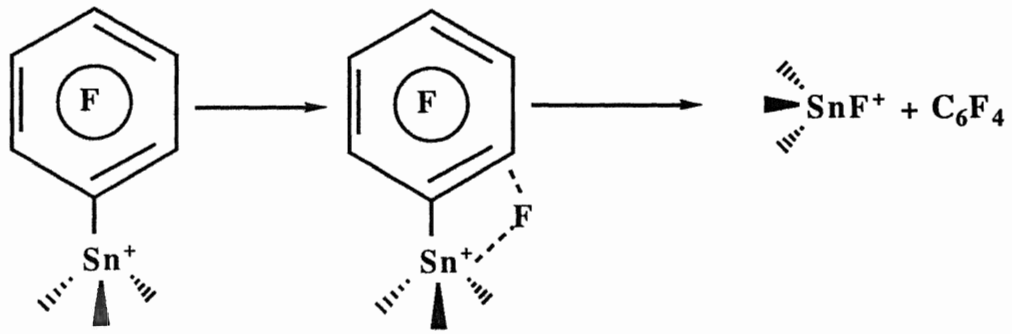

(A)

π-Bonded intermediates were suggested earlier [103] to account for fluorine migration from the para-position in the mass spectrum of p-$FC_6H_4Mn(CO)$ [104]. A similar mechanism was proposed to explain the migration of the para-position halogen to tin in mass spectra of $(p\text{-}XC_6H_4)_3SnY$ (X =F, Cl; Y = Cl, Br, I) by Miller et al.[65] (B).

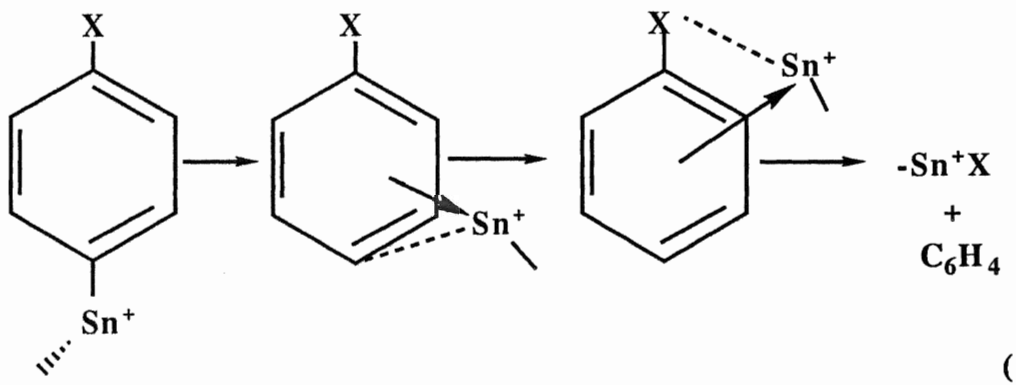

(B)

Mechanism (B) can be used to explain the migration of meta-position fluorine and chlorine to tin in the titled compounds, and also the migration of CH_3, CH_3O and CH_3S groups on phenyls to tin.

The +ve FAB linked scan studies (Schemes 30-33) of these compounds show that no transitions leading to fragment peaks from molecular ion decomposition are verified. All of the fragment peaks come from the disintegration of adducts of the matrix (or part of it) as the precursor ion. Due to poor solubility of $(3,5\text{-}Cl_2C_6H_3)_4Sn$ in NBA, Scheme 31 provides very little information on fragmentation pattern of the compound. In contrast to the EI studies, the migration of methyl group(s) from the ligand(s) to tin, like peaks $Ar_3SnCH_2^+$, $Ar_2SnCH_3^+$ and $(CH_3)_4Sn^+$, is observed in Scheme 32 of $(3,5\text{-}(CH_3)_2C_6H_3)_4Sn$. In this scheme, more fragment peaks by loss of methyl group(s) from precursor ions is also observed, such as $(M\text{-}4CH_3)^+$, $(M\text{-}5CH_3)^+$, $(ArSn\text{-}CH_3)^+$, $(Ar_2Sn\text{-}CH_3)^+$. In Scheme 30 of $(3,5\text{-}F_2C_6H_3)_4Sn$, the interesting peaks are $ArSnF_3^+$ and SnF^+, indicating the migration of the meta-position fluorine to tin under +ve FAB with the same mechanism as that under EI. Ar_2Sn^+, which also produces an $ArSn^+$ peak, is only found in the scheme of $(3,5\text{-}(CH_3)_2C_6H_3)_4Sn$ and comes from the decomposition of Ar_3Sn^+ by loss of an Ar radical.

(5) $(2,4,6\text{-}(CH_3)_3C_6H_2)_3SnX$ (X= Cl, Br, I, O_2CCH_3)

The EI linked scan studies (Schemes 17-20) of this group of compounds show that no transitions from molecular ion to fragment ion are verified for $(2,4,6\text{-}(CH_3)_3C_6H_2)_3SnBr$ and $(2,4,6\text{-}(CH_3)_3C_6H_2)_3SnI$. $(Ar_2Sn\text{-}H)^+$, instead of Ar_2Sn^+, is observed as the direct decomposition product of Ar_3Sn^+ by loss of an (Ar-H) neutral (Schemes 17, 19, 20), $(Ar_2SnX\text{-}H)^+$ (X = Cl, Br) (Schemes 17, 18), $Ar_2SnO_2CCH_3^+$ (Scheme 20) and molecular ion (Schemes 17, 20). $(Ar_2SnCl\text{-}H)^+$ (Scheme 17) and $Ar_2SnO_2CCH_3^+$ (Scheme 20) are found from molecular ion decomposition. No Ar_3SnI^+ or $(Ar_3SnI\text{-}H)^+$ is observed in Scheme 19. $SnCl^+$ (Scheme 17) generated from $(Ar_2SnCl\text{-}$

$CH_4)^+$ and $(ArSnCl-H)^+$ and $SnBr^+$ (Scheme 18) generated from $(Ar_2SnBr-H)^+$, $(Ar_2SnBr-CH_4)^+$ and $(ArSnBr-2H)^+$ are observed; and the mechanism of formation of these ions is similar to that of $SnPh_3X$ (X = F, Cl, Br, or I) proposed by Chambers et al. [53]. Fragment peaks with methyl group loss from precursor ion(s) is not common (only $(Ar_2SnO_2CCH_3-CH_3)^+$ in Scheme 20 is observed). As reported earlier [64, 65] by Miller et al., the loss of a phenyl preferred over the loss of a halide in EI is also detected in both the normal EI spectra and the EI linked scan spectra of these compounds.

In the +ve FAB linked scan studies (Schemes 37-40) of these compounds, no transitions from molecular ions to fragment peaks are proved. Ar_3Sn^+ ions come from $(M-2H)^+$ in Scheme 38 and $(Ar_3Sn{\cdot}NBA-2H)^+$ in Scheme 40. Ar_2SnCl^+, instead of $(Ar_2SnCl-H)^+$, comes from $(M-H)^+$ in Scheme 37, while $(Ar_2SnBr-H)^+$ comes from $(M-2H)^+$ in Scheme 38. $(Ar_2Sn-H)^+$ ions are the direct decomposition product of Ar_3Sn^+ (Schemes 37-40), $(M-H)^+$ and Ar_2SnCl^+ (Scheme 37), $(M-2H)^+$ and $(Ar_2SnBr-H)^+$ (Scheme 38). $SnCl^+$ generated from Ar_3SnCl^+ and $SnBr^+$ from $(Ar_2SnBr-H)^+$, $(ArSnBr-2H)^+$ and $(Ar_2SnBr-CH_5)^+$ are also observed. Some rearrangement peaks, such as $((CH_3)_4SnH^+$ (Scheme 37), $ArSn(CH_2)_2^+$, $(CH_3)_4Sn^+$ (Scheme 38), $Ar_2SnCH_2^+$ (Scheme 39), CH_3Sn^+, $Ar_3SnCH_3^+$, Ar_2SnCH^+, $C_6H_2SnCCH_3^+$ (Scheme 40), are found. Fragment peaks with loss of methyl groups from the precursor ion(s) are common, $(Ar_2Sn-CH_3)^+$ (Scheme 37), $(ArSn-2CH_3)^+$, $(Ar_2Sn-2CH_3-H)^+$ (Scheme 38), $(Ar_2Sn-2CH_3-H)^+$ (Scheme 40). The formation mechanism of these ions are similar to the previous discussion.

(6) $(o\text{-}CH_3OC_6H_4)_3SnX$ (X=Br, I), $(o\text{-}CH_3C_6H_4)_3SnI$

In the EI linked scan studies (Schemes 14-16) of these compounds, the transition of Ar_3Sn^+ ions from molecular ion decomposition is verified in Schemes 15-16, while in Scheme 14, it is from $(M-2H)^+$ decomposition. Ar_2SnI^+ comes from M^+ (Scheme 16) and $(M-2H)^+$ (Scheme 14), $(Ar_2SnBr-H)^+$ is observed as the direct product of molecular ion

decomposition. $(Ar_2Sn\text{-}H)^+$ comes from Ar_3Sn^+, instead of M^+, decomposition in Schemes 14-16, while in Scheme 14, it also comes from $(M\text{-}2H)^+$. SnI^+ is only observed in Scheme 14 from $(M\text{-}2H)^+$ and Ar_2SnI^+. Rearrangement peaks, like $Ar_2SnCH_3^+$ (Scheme 14), $SnOH^+$ (Scheme 15), $SnOCH_3^+$, $H_2SnCH_3^+$ (Scheme 16), are observed. Fragment peaks, such as $(Ar_2Sn\text{-}CH_3)^+$ (Scheme 15), $(Ar_3Sn\text{-}OCH_3)^+$, $(Ar_2Sn\text{-}CH_3)^+$, are found.

The +ve FAB linked scan studies (Schemes 34-36) of this group of compounds show no transitions from molecular ion to fragment ion. In Scheme 34, $(Ar_2Sn\text{-}H)^+$, instead of Ar_2Sn^+, and Ar_2SnI^+ are the direct product of molecular ion decomposition in the first field free region. No SnX^+ (X = Br, I) ions are observed in these schemes. Rearrangement peaks, such as $(CH_2O)_2SnAr^+$, $C_6H_4SnCH_2^+$, are observed in Scheme 36 of $(o\text{-}CH_3OC_6H_4)_3SnI$. Fragment peaks, like $(Ar_2Sn\text{-}2CH_3)^+$, $(Ar_3Sn\text{-}3CH_3)^+$ and $(Ar_3Sn\text{-}2CH_3)$ (Scheme 34), $(Ar_2Sn\text{-}CH_3)^+$ (Scheme 35), $(Ar_2Sn\text{-}CH_3)^+$, $(Ar_3Sn\text{-}CH_3)^+$ (Scheme 36), are common. $(Ar_2SnI\text{-}CH_3I)^+$ is observed in Scheme 34 of $(o\text{-}CH_3C_6H_4)_3SnI$.

The fragmentation mechanism of this group of compounds under EI and +ve FAB is same as the discussed before and reported results for other aryltin halides [53,64,65].

* Note: text continues on page 122.

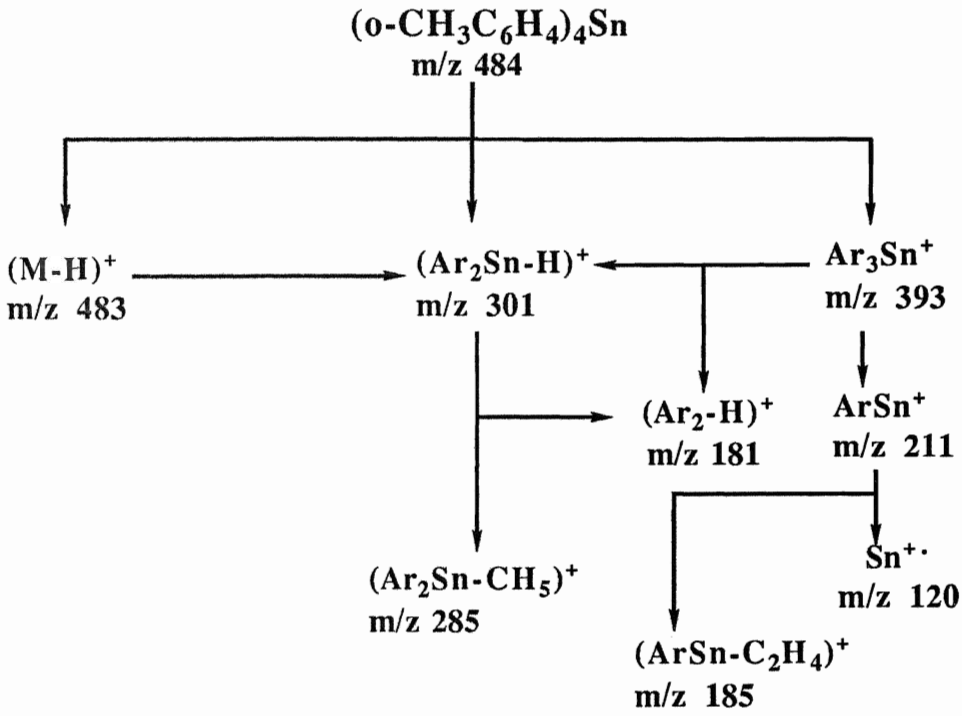

SCHEME 1 Fragmentation pattern of $(o\text{-}CH_3C_6H_4)_4Sn$ under EI

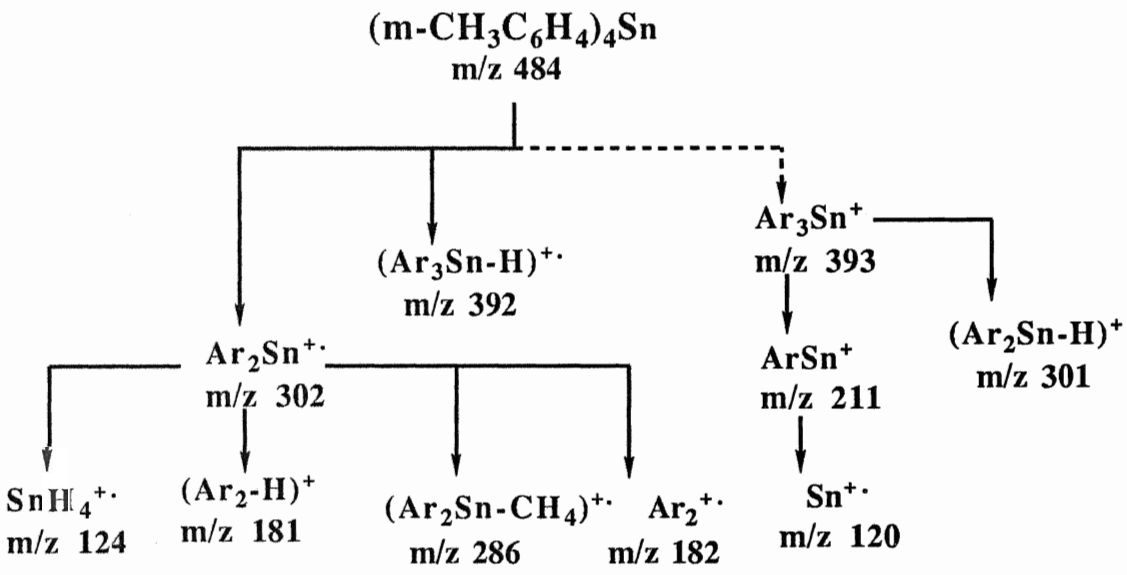

SCHEME 2 Fragmentation pattern of $(m\text{-}CH_3C_6H_4)_4Sn$ under EI

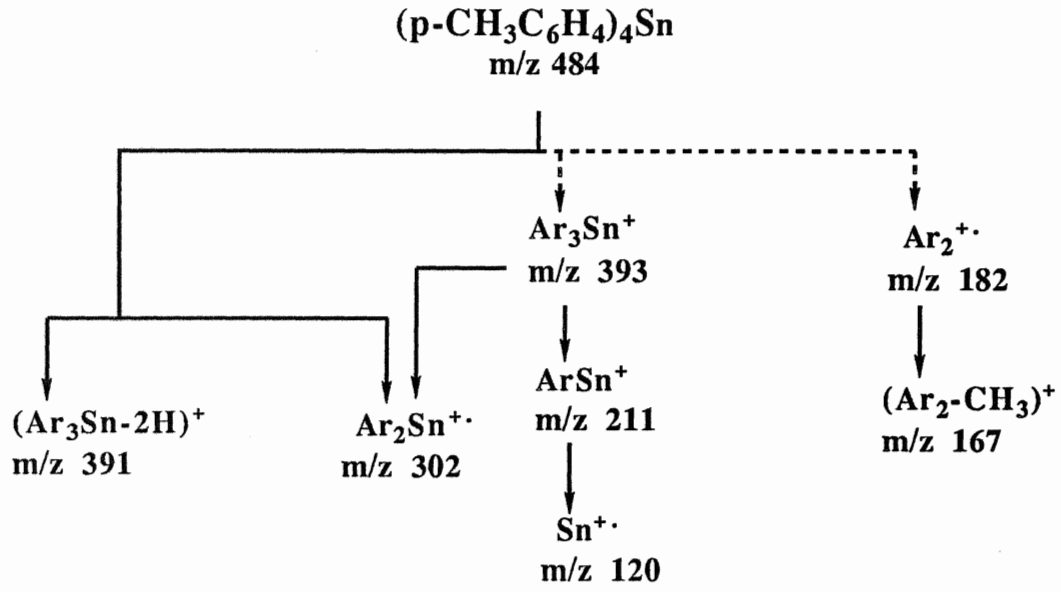

SCHEME 3 Fragmentation pattern of $(p\text{-}CH_3C_6H_4)_4Sn$ under EI

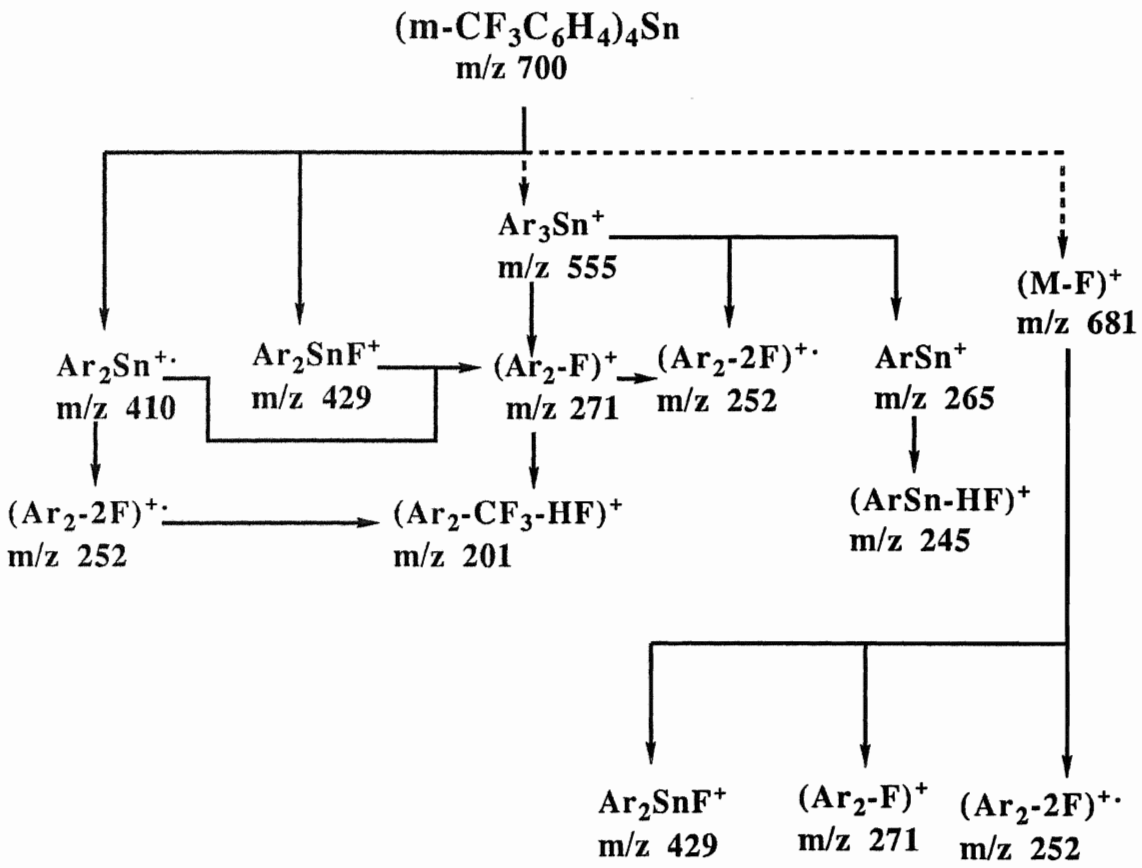

SCHEME 4 Fragmentation pattern of $(m\text{-}CF_3C_6H_4)_4Sn$ under EI

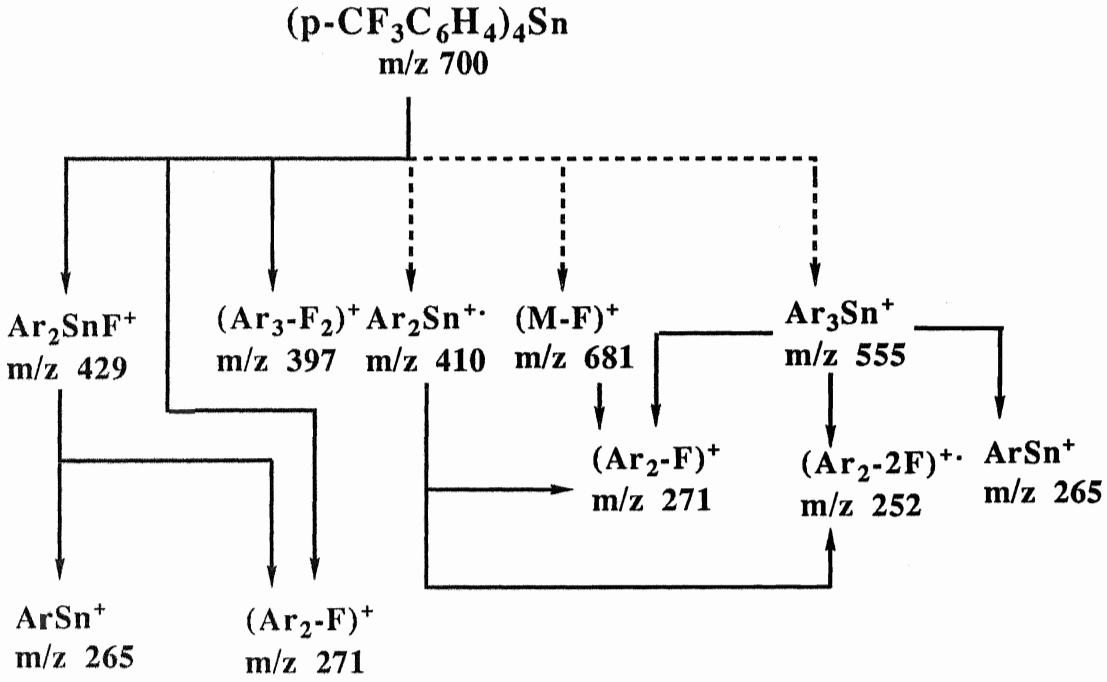

SCHEME 5 Fragmentation pattern of $(p\text{-}CF_3C_6H_4)_4Sn$ under EI

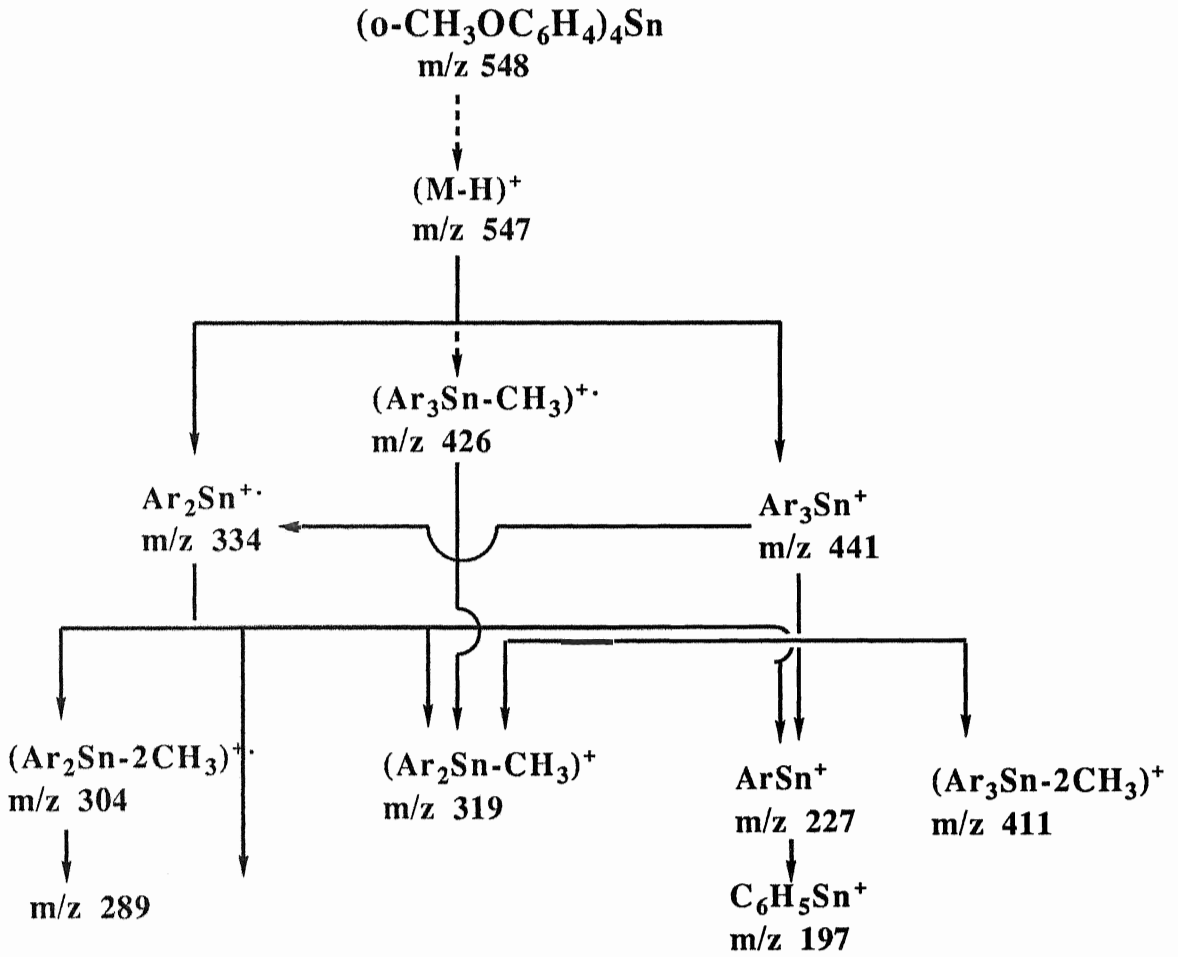

SCHEME 6 Fragmentation pattern of $(o\text{-}CH_3OC_6H_4)_4Sn$ under EI

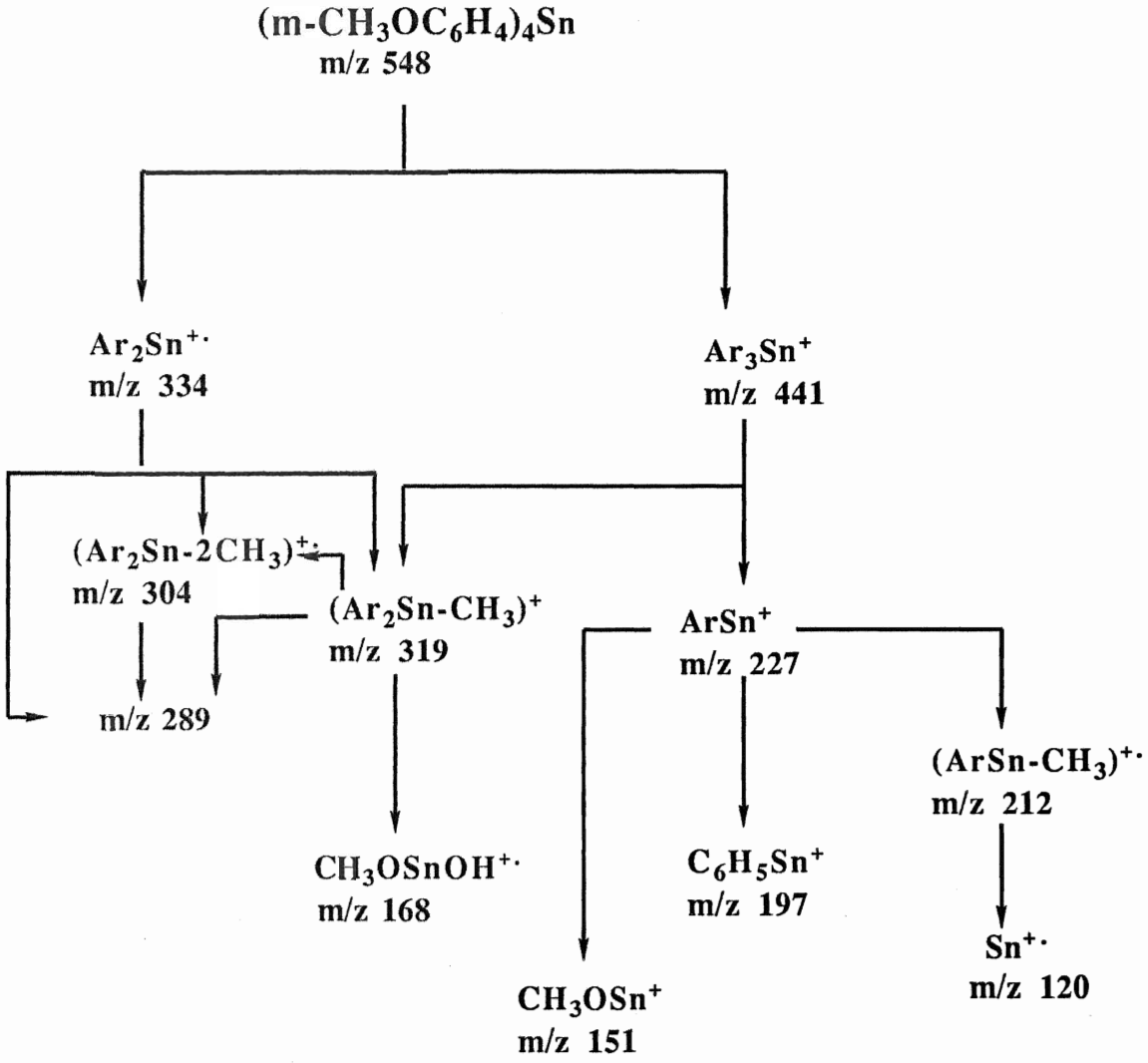

SCHEME 7 Fragmentation pattern of (m-$CH_3OC_6H_4$)$_4$Sn under EI

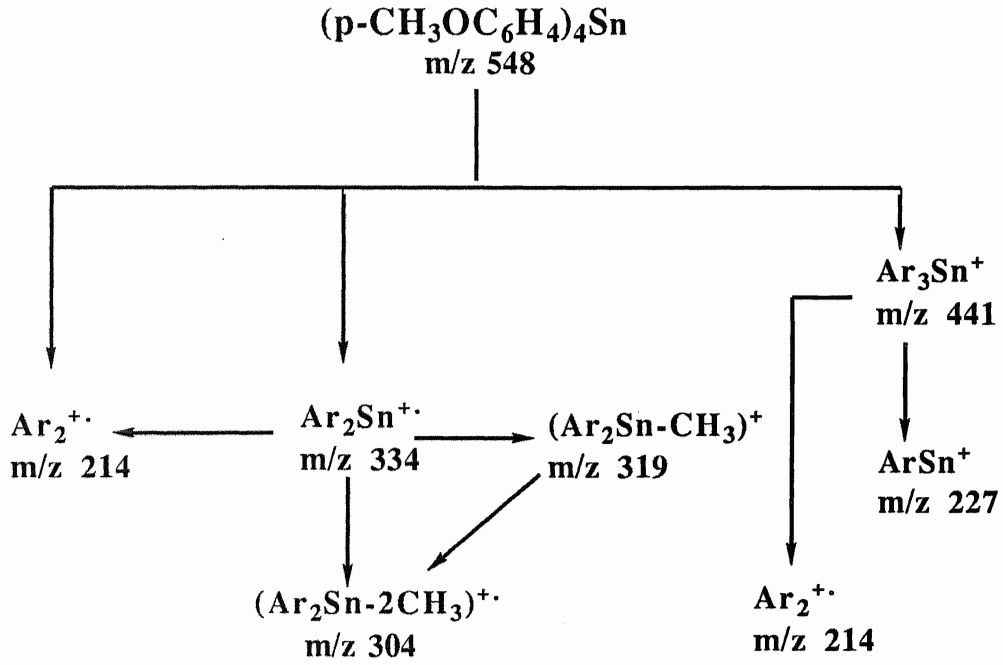

SCHEME 8 Fragmentation pattern of $(p\text{-}CH_3OC_6H_4)_4Sn$ under EI

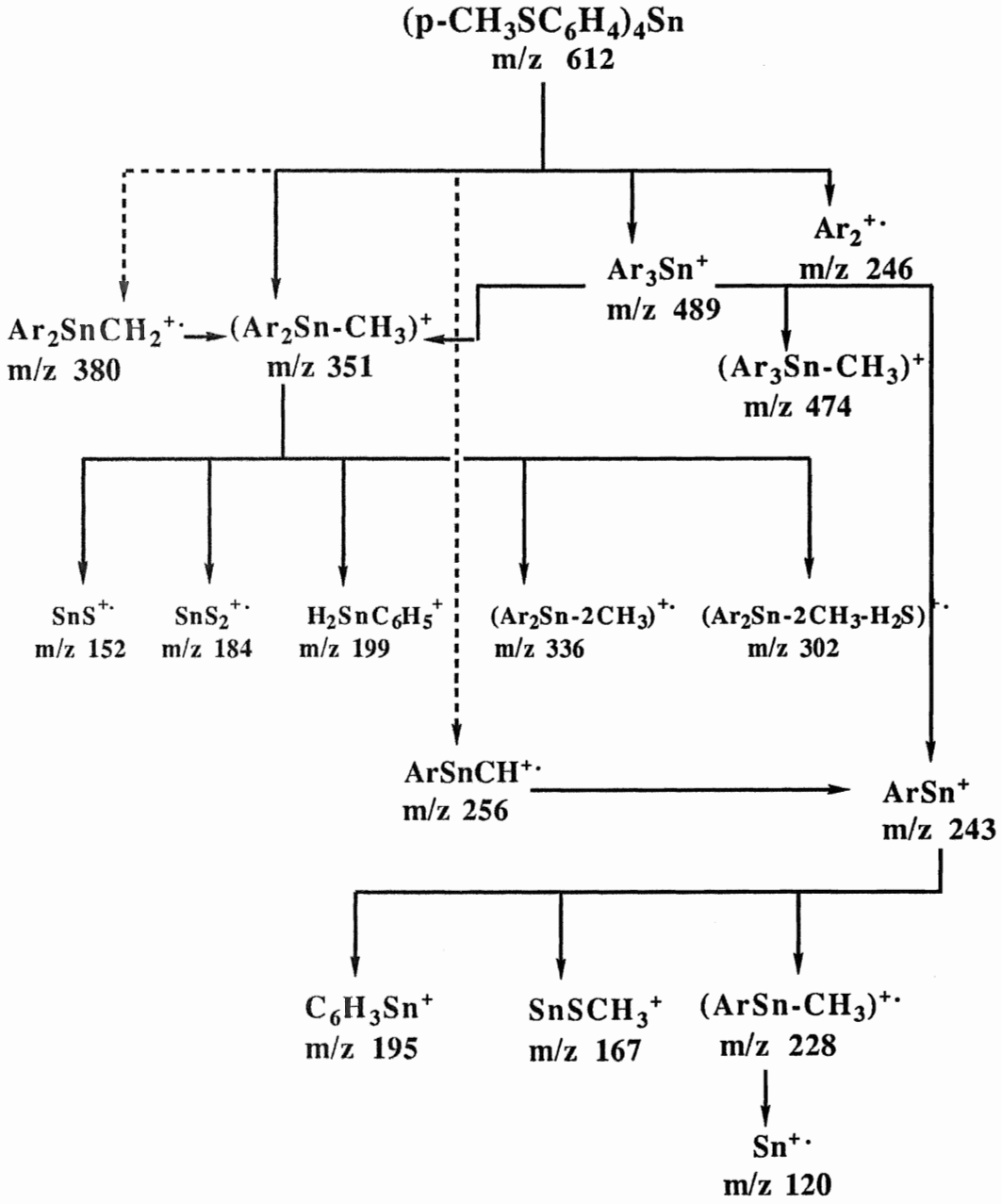

SCHEME 9 Fragmentation pattern of $(p\text{-}CH_3SC_6H_4)_4Sn$ under EI

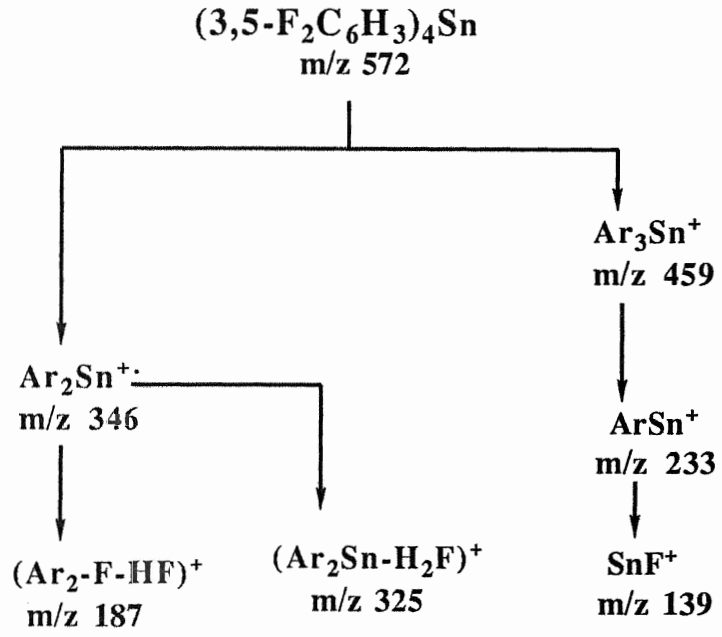

SCHEME 10 Fragmentation pattern of $(3,5\text{-}F_2C_6H_3)_4Sn$ under EI

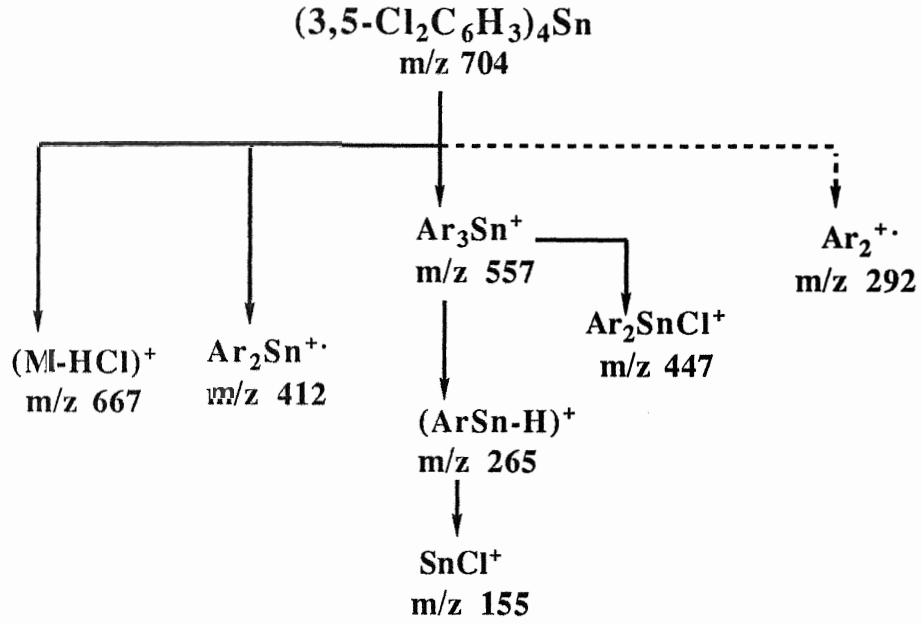

SCHEME 11 Fragmentation pattern of $(3,5\text{-}Cl_2C_6H_3)_4Sn$ under EI

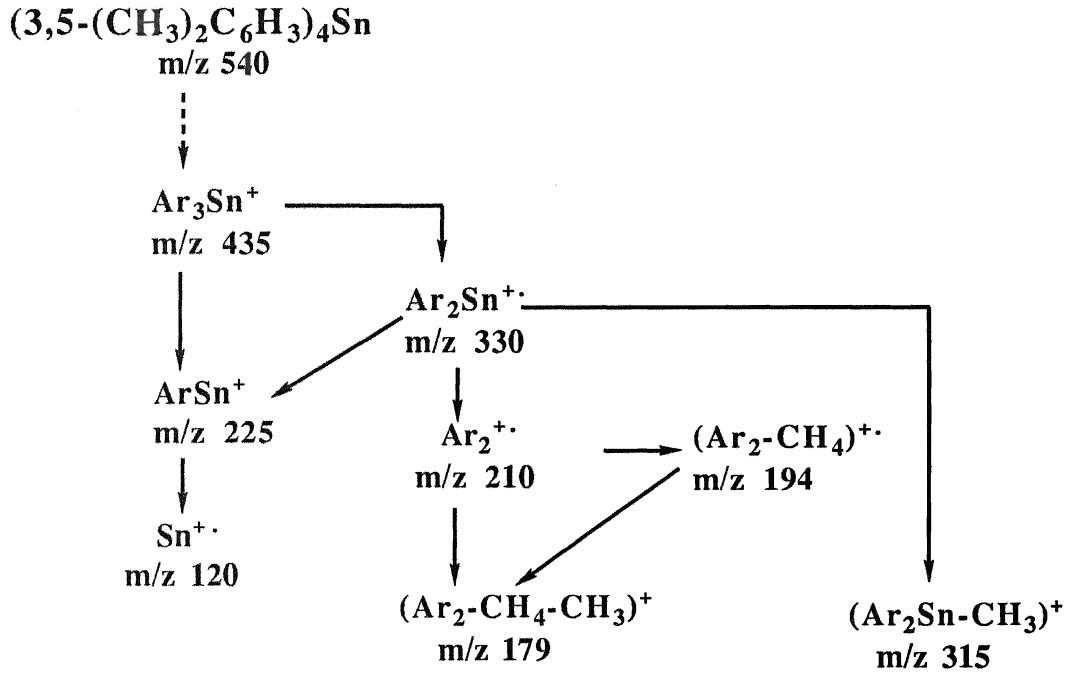

SCHEME 12 Fragmentation pattern of $(3,5\text{-}(CH_3)_2C_6H_3)_4Sn$ under EI

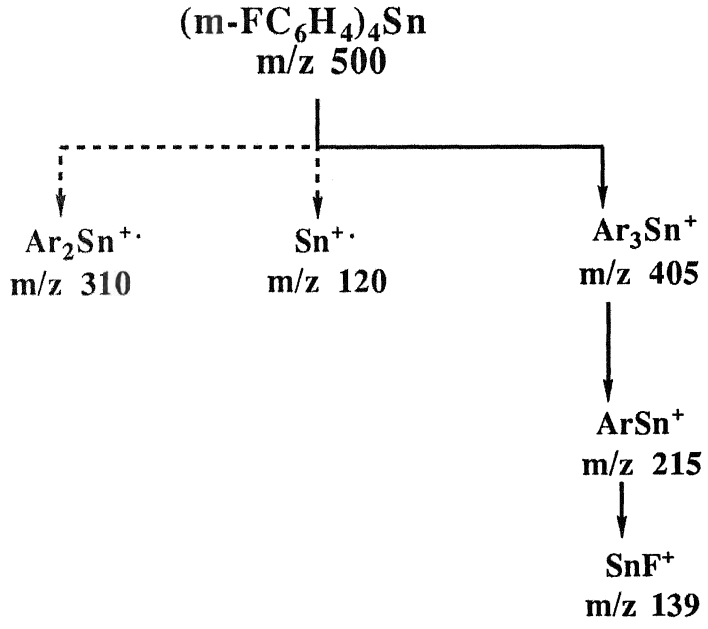

SCHEME 13 Fragmentation pattern of $(m\text{-}FC_6H_4)_4Sn$ under EI

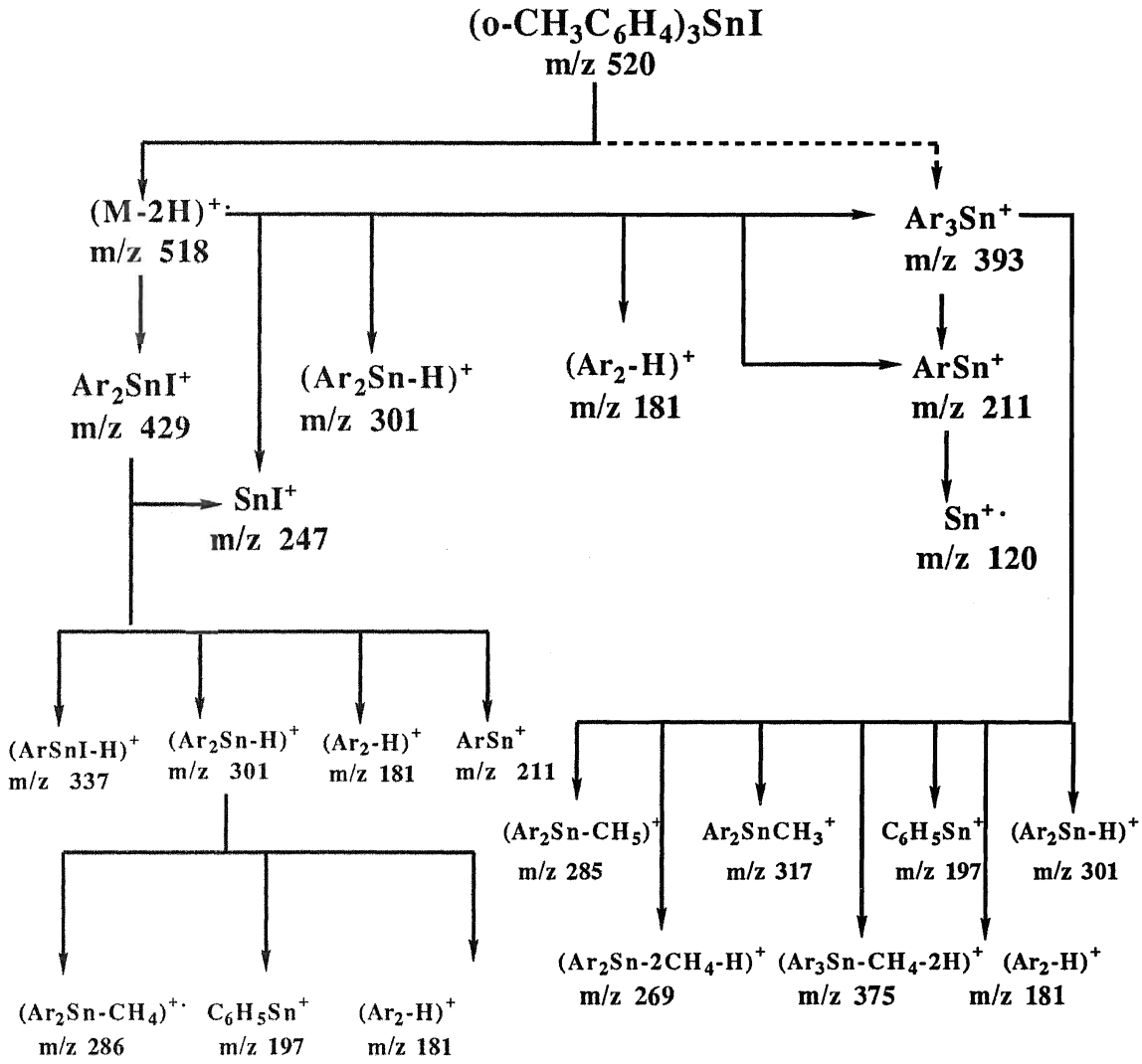

SCHEME 14 Fragmentation pattern of $(o\text{-}CH_3C_6H_4)_3SnI$ under EI

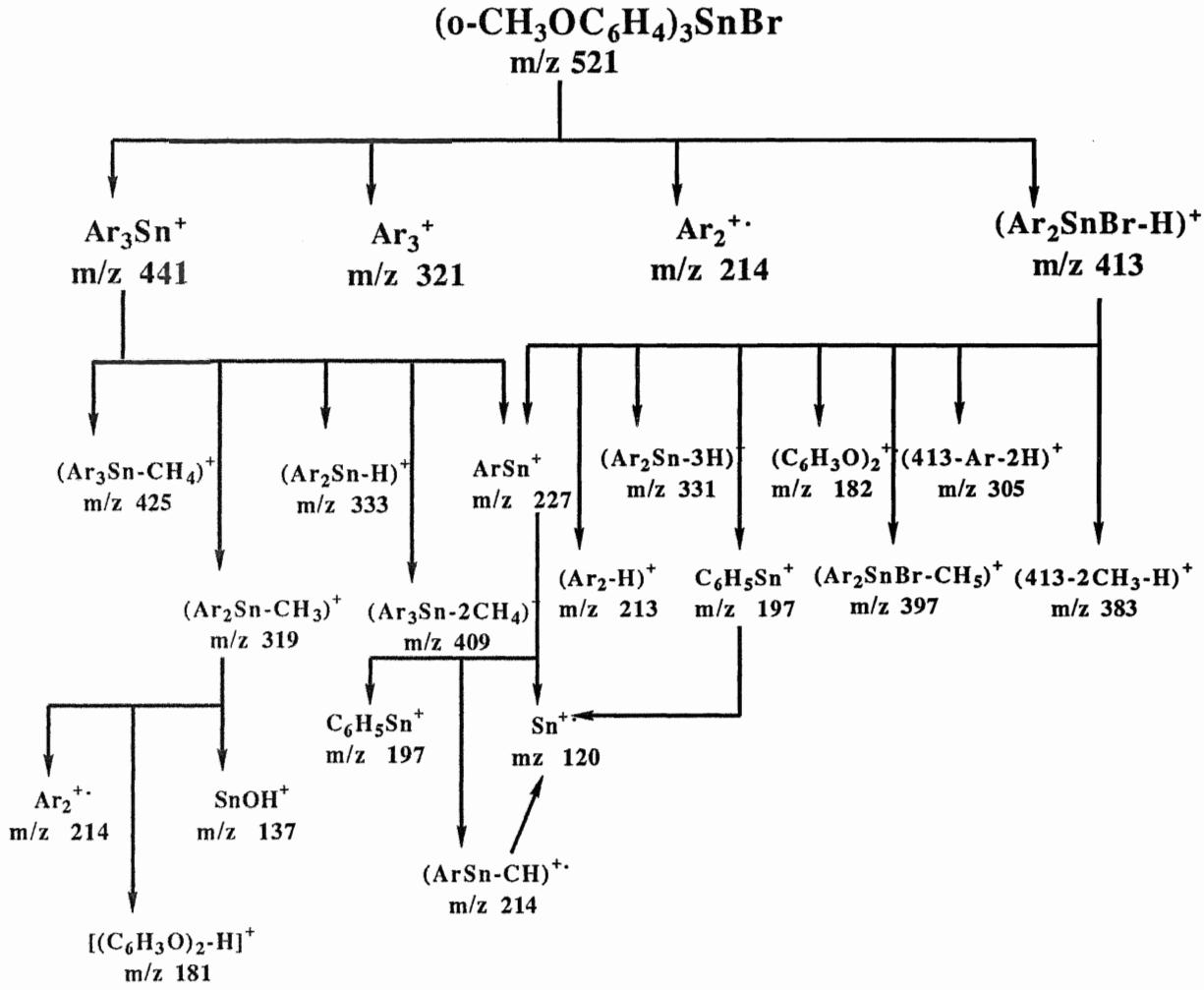

SCHEME 15 Fragmentation pattern of (o-$CH_3OC_6H_4)_3SnBr$ under EI

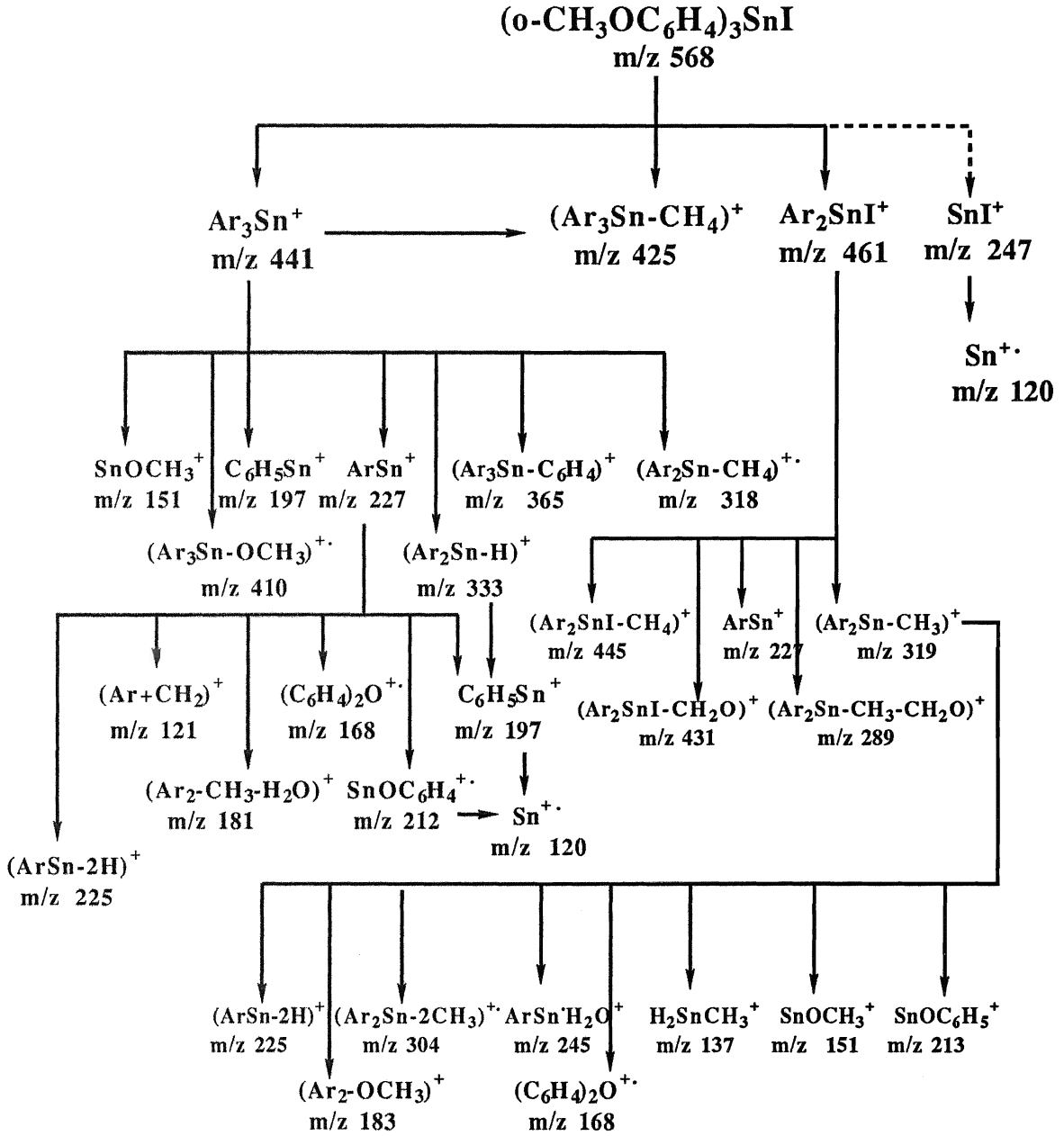

SCHEME 16 Fragmentation pattern of $(o\text{-}CH_3OC_6H_4)_3SnI$ under EI

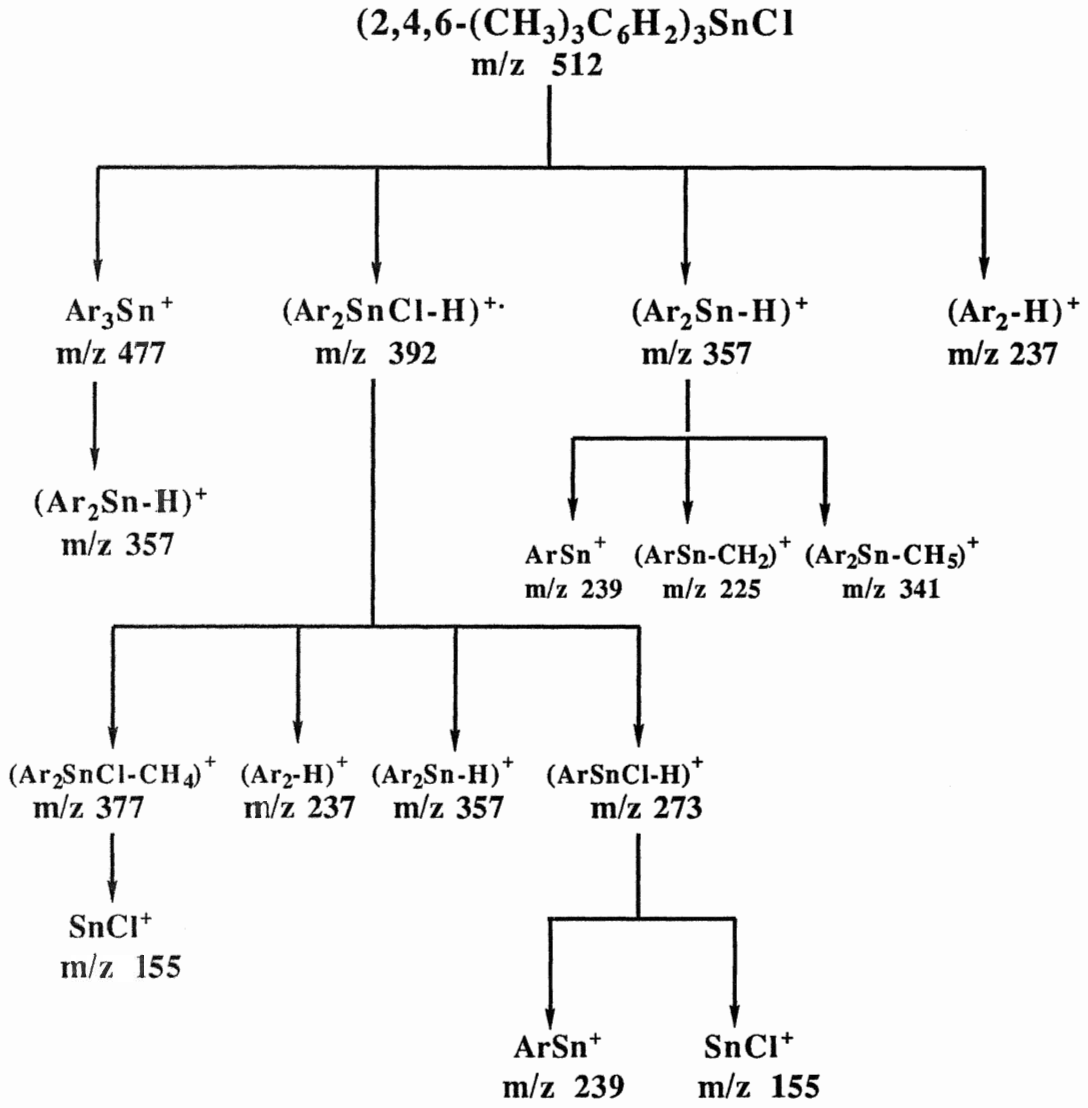

SCHEME 17 Fragmentation pattern of $(2,4,6\text{-}(CH_3)_3C_6H_2)_3SnCl$ under EI

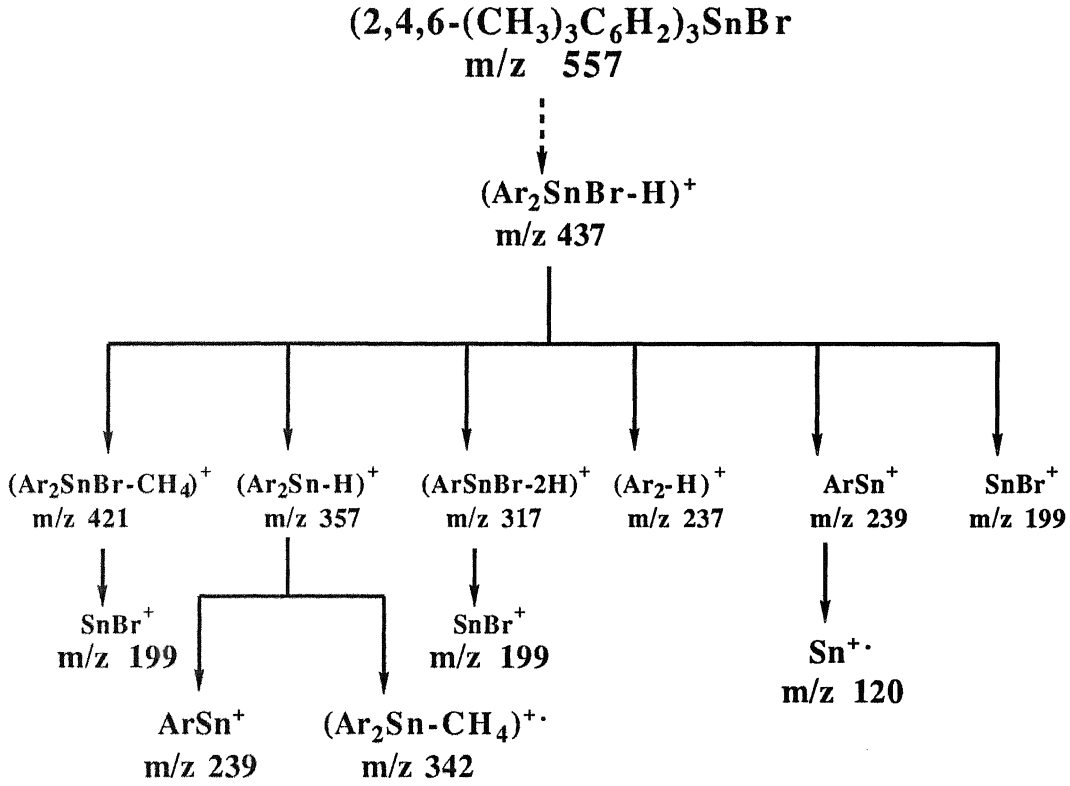

SCHEME 18 Fragmentation pattern of $(2,4,6\text{-}(CH_3)_3C_6H_2)_3SnBr$ under EI

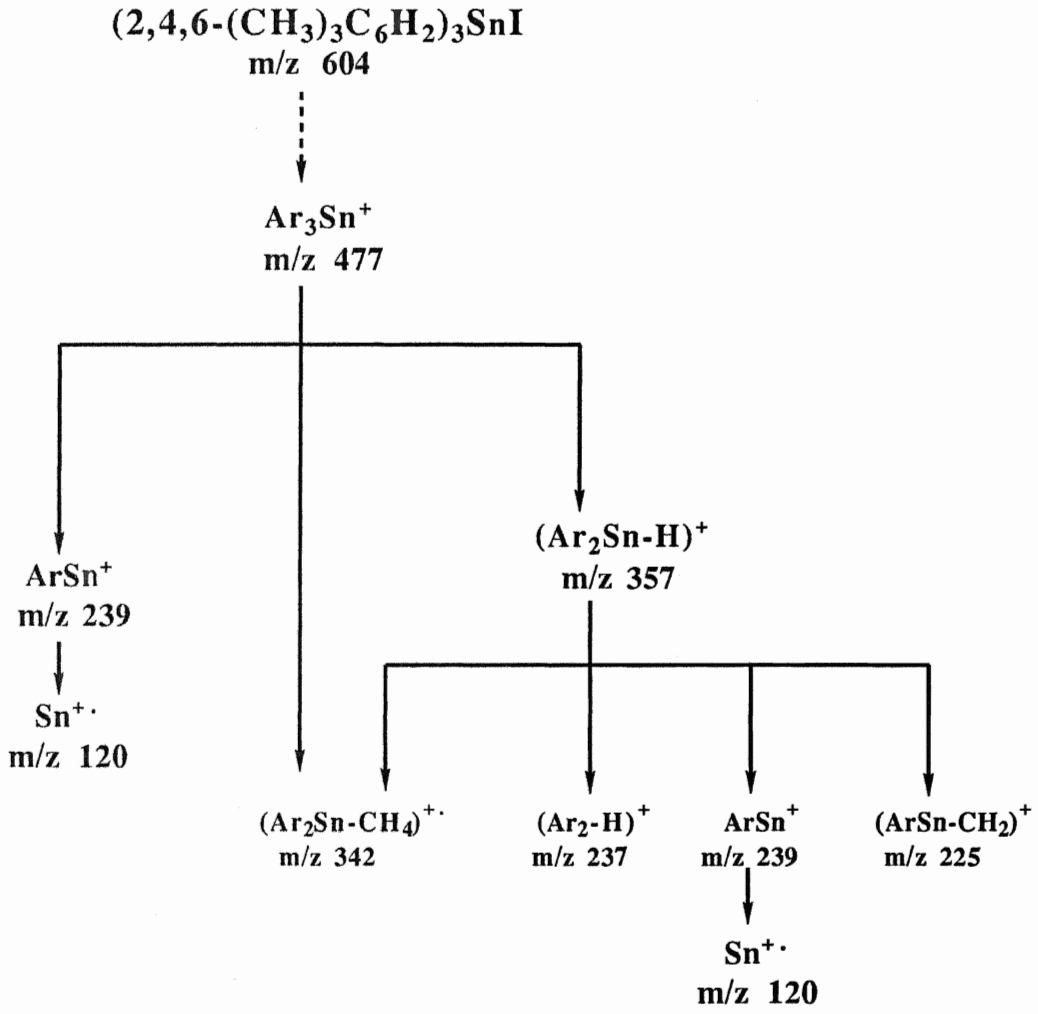

SCHEME 19 Fragmentation pattern of $(2,4,6\text{-}(CH_3)_3C_6H_2)_3SnI$ under EI

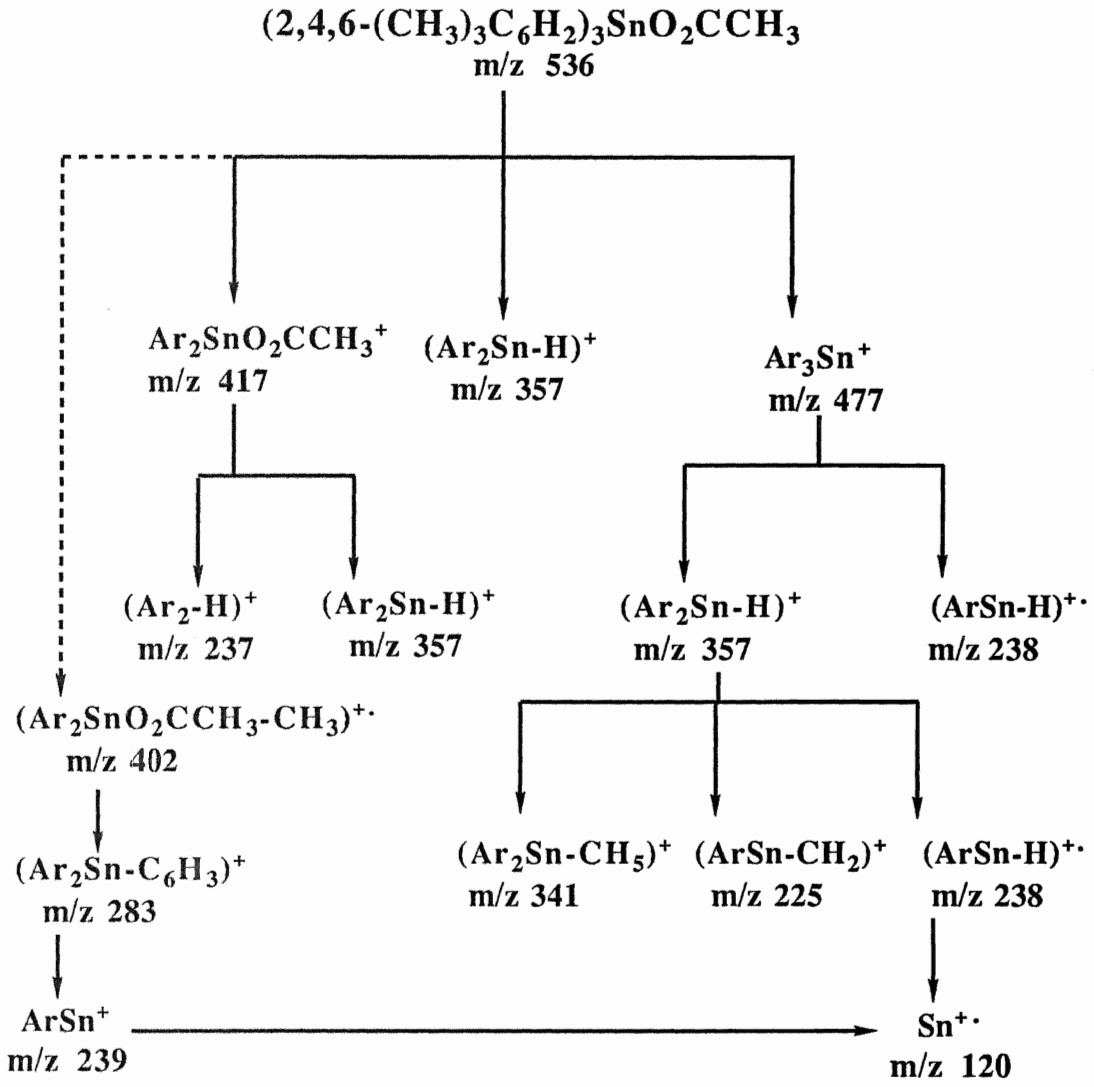

SCHEME 20 Fragmentation pattern of $(2,4,6\text{-}(CH_3)_3C_6H_2)_3SnO_2CCH_3$ under EI

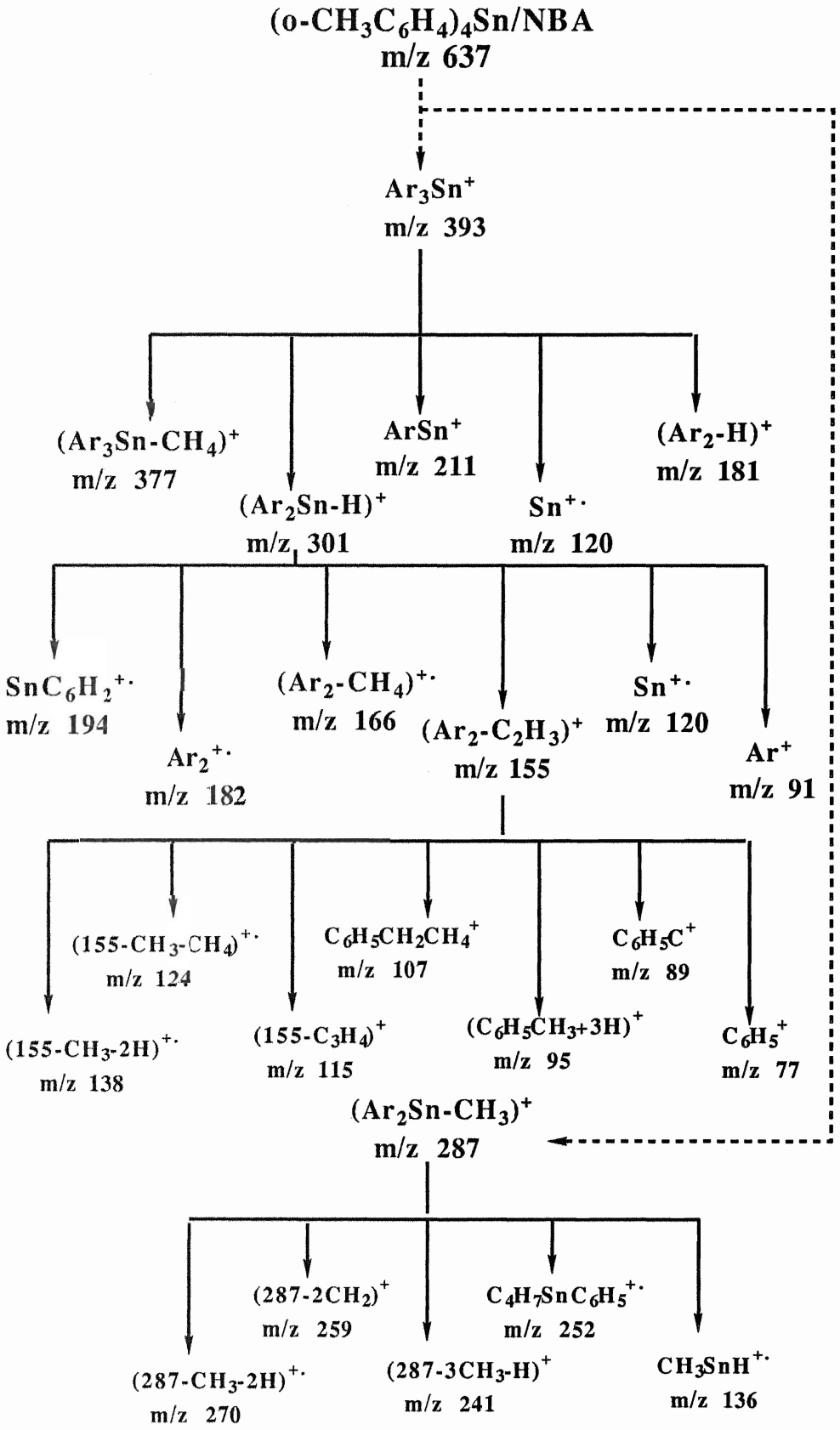

SCHEME 21 Fragmentation pattern of $(o\text{-}CH_3C_6H_4)_4Sn$/NBA under positive ion FAB

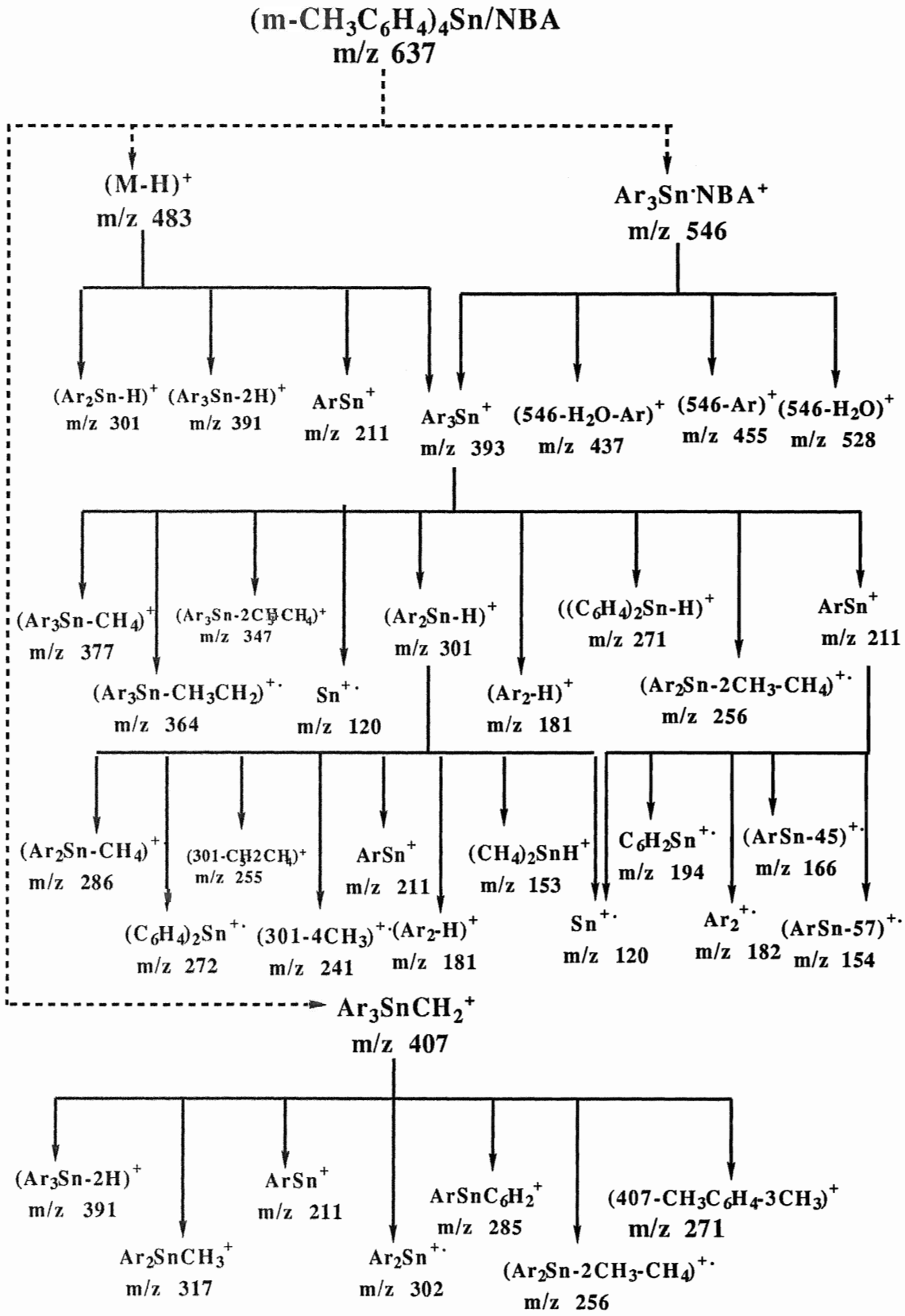

SCHEME 22 Fragmentation pattern of $(m\text{-}CH_3C_6H_4)_4Sn$/NBA under positive ion FAB

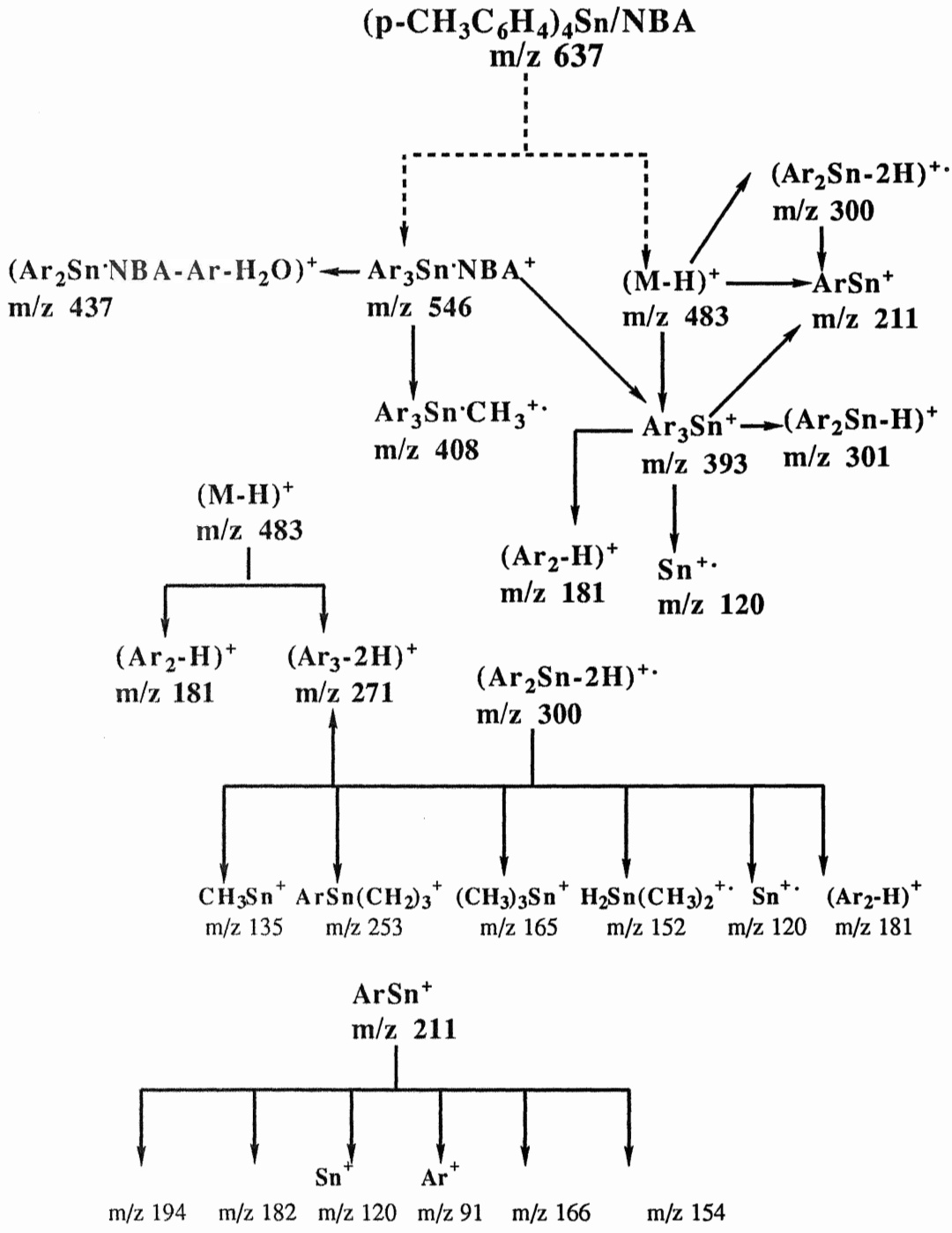

SCHEME 23 Fragmentation pattern of $(p\text{-}CH_3C_6H_4)_4Sn$/NBA under positive ion FAB

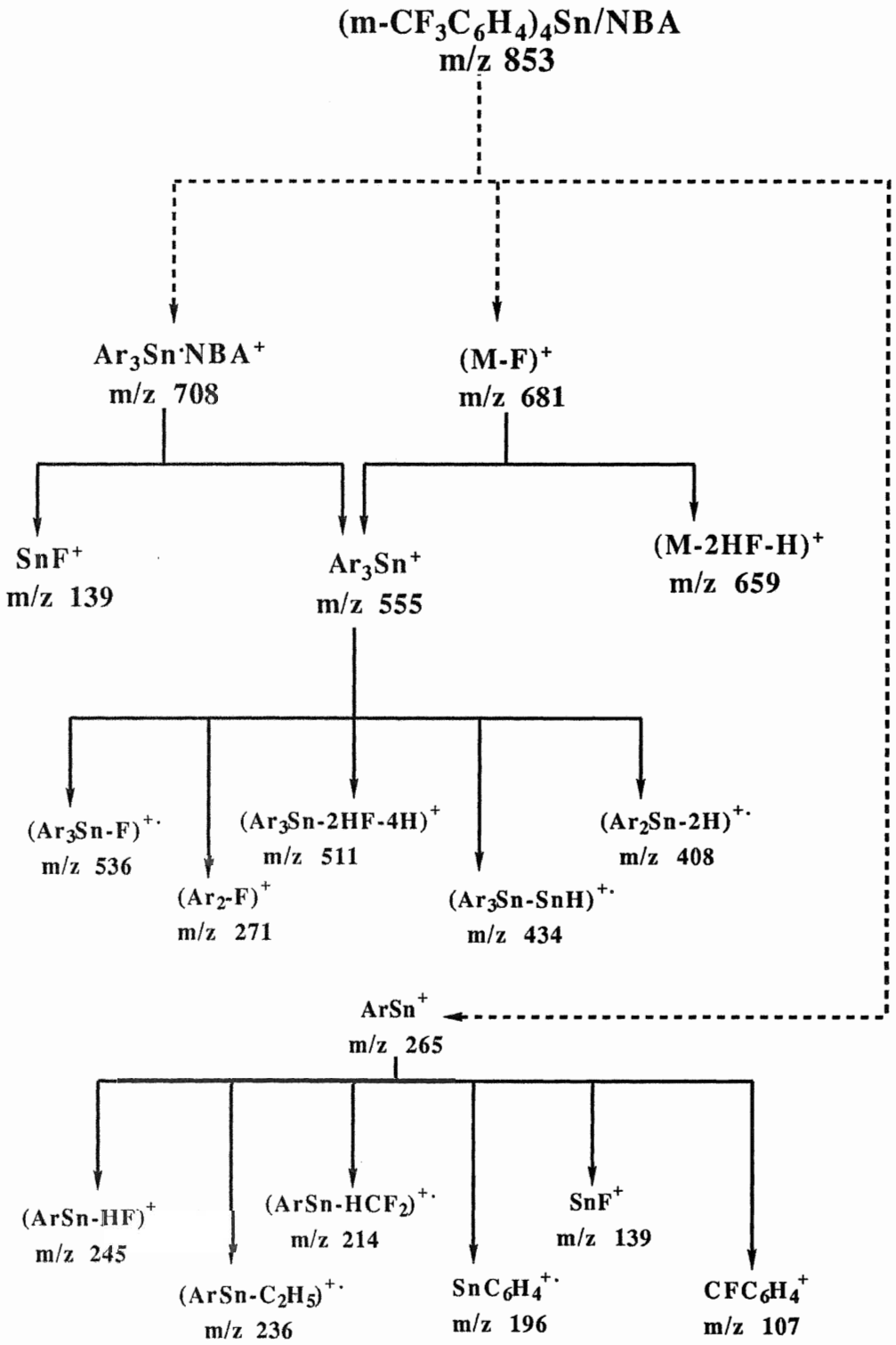

SCHEME 24 Fragmentation pattern of $(m\text{-}CF_3C_6H_4)_4Sn$/NBA under positive ion FAB

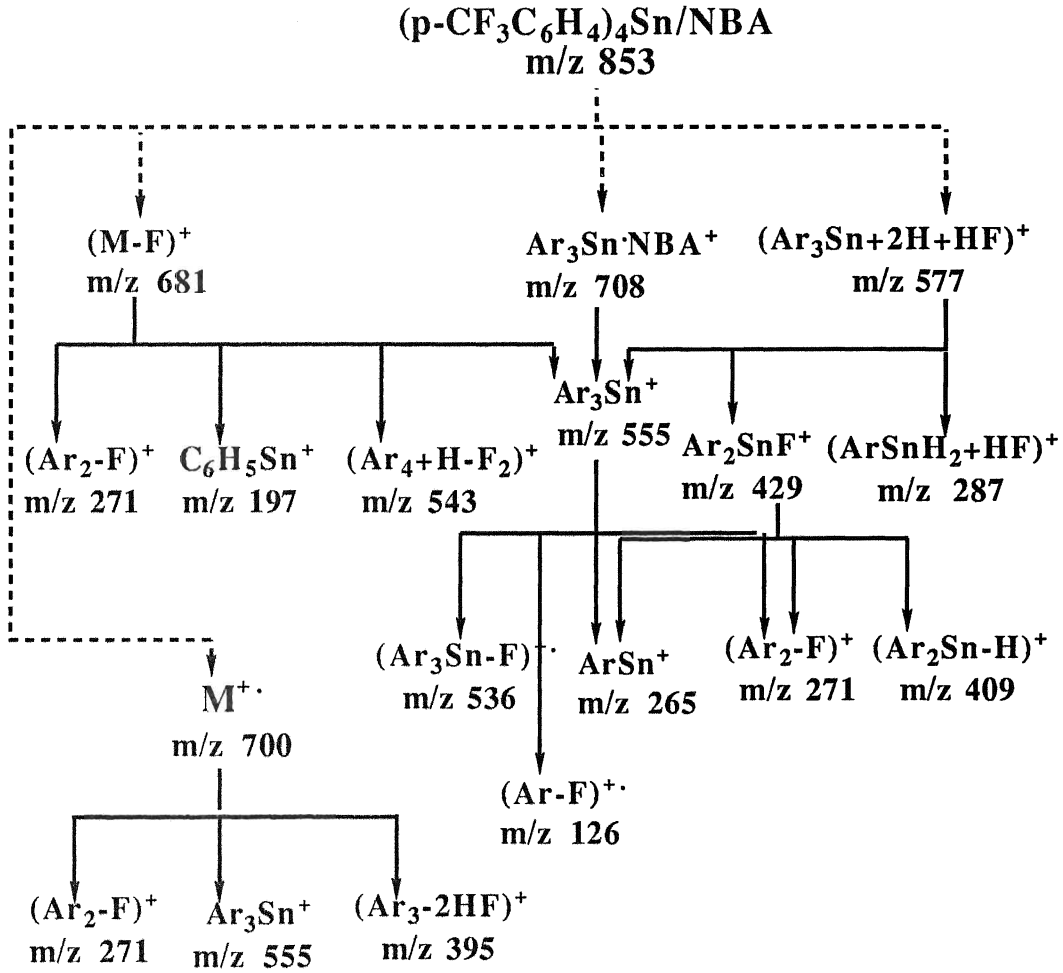

SCHEME 25 Fragmentation pattern of $(p\text{-}CF_3C_6H_4)_4Sn$/NBA under positive ion FAB

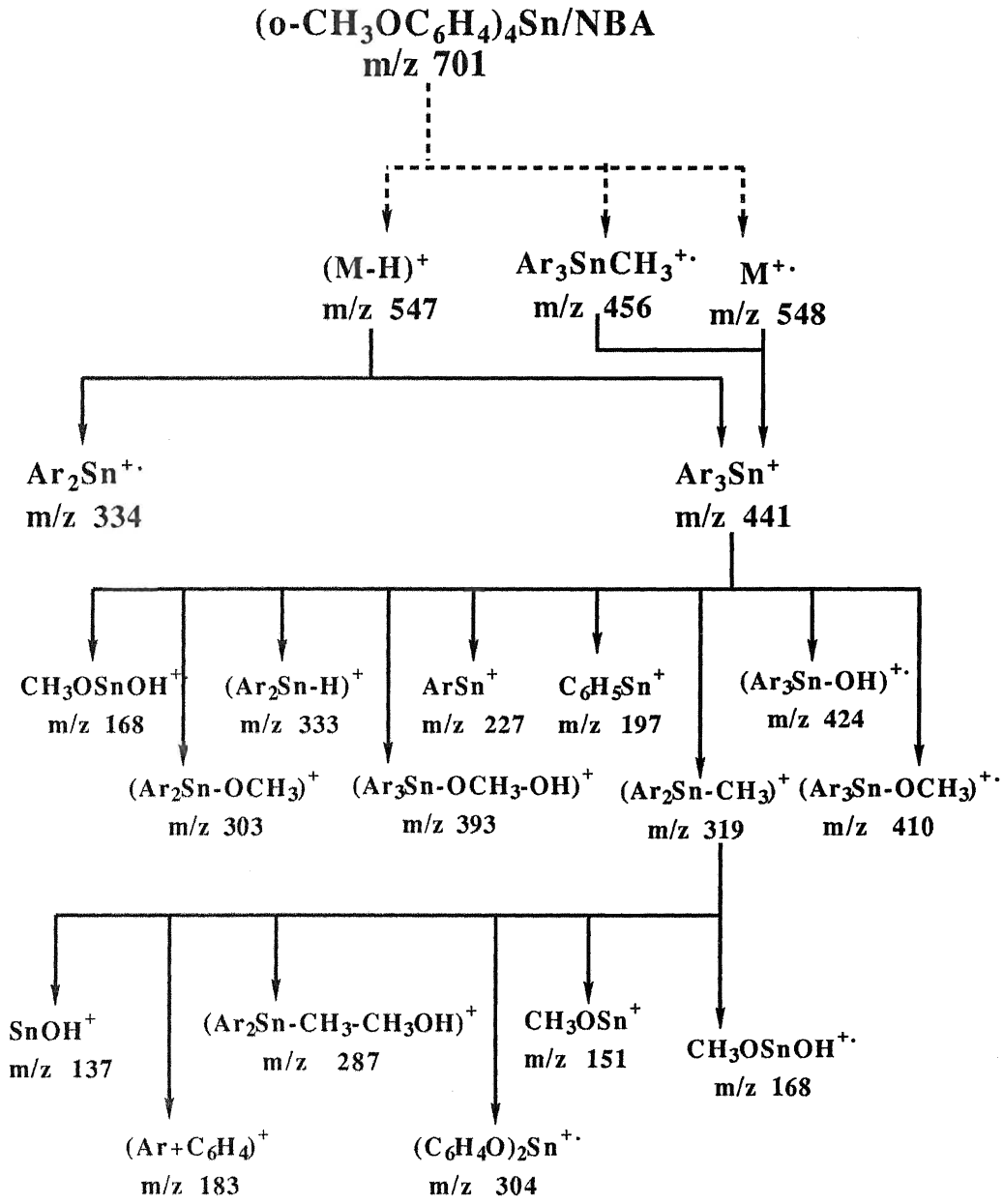

SCHEME 26 Fragmentation pattern of $(o\text{-}CH_3OC_6H_4)_4Sn$/NBA under positive ion FAB

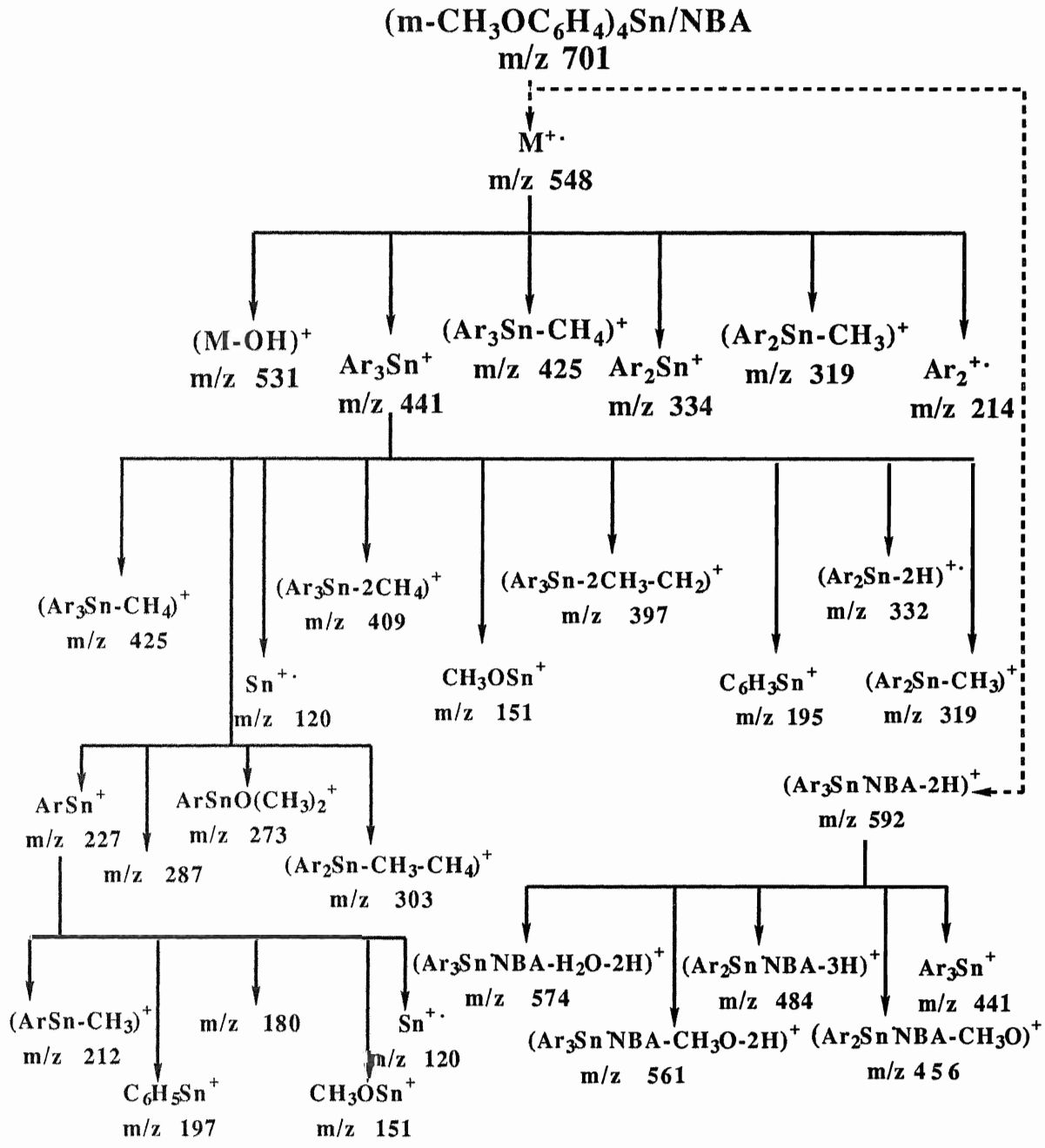

SCHEME 27 Fragmentation pattern of $(m\text{-}CH_3OC_6H_4)_4Sn$/NBA under positive ion FAB

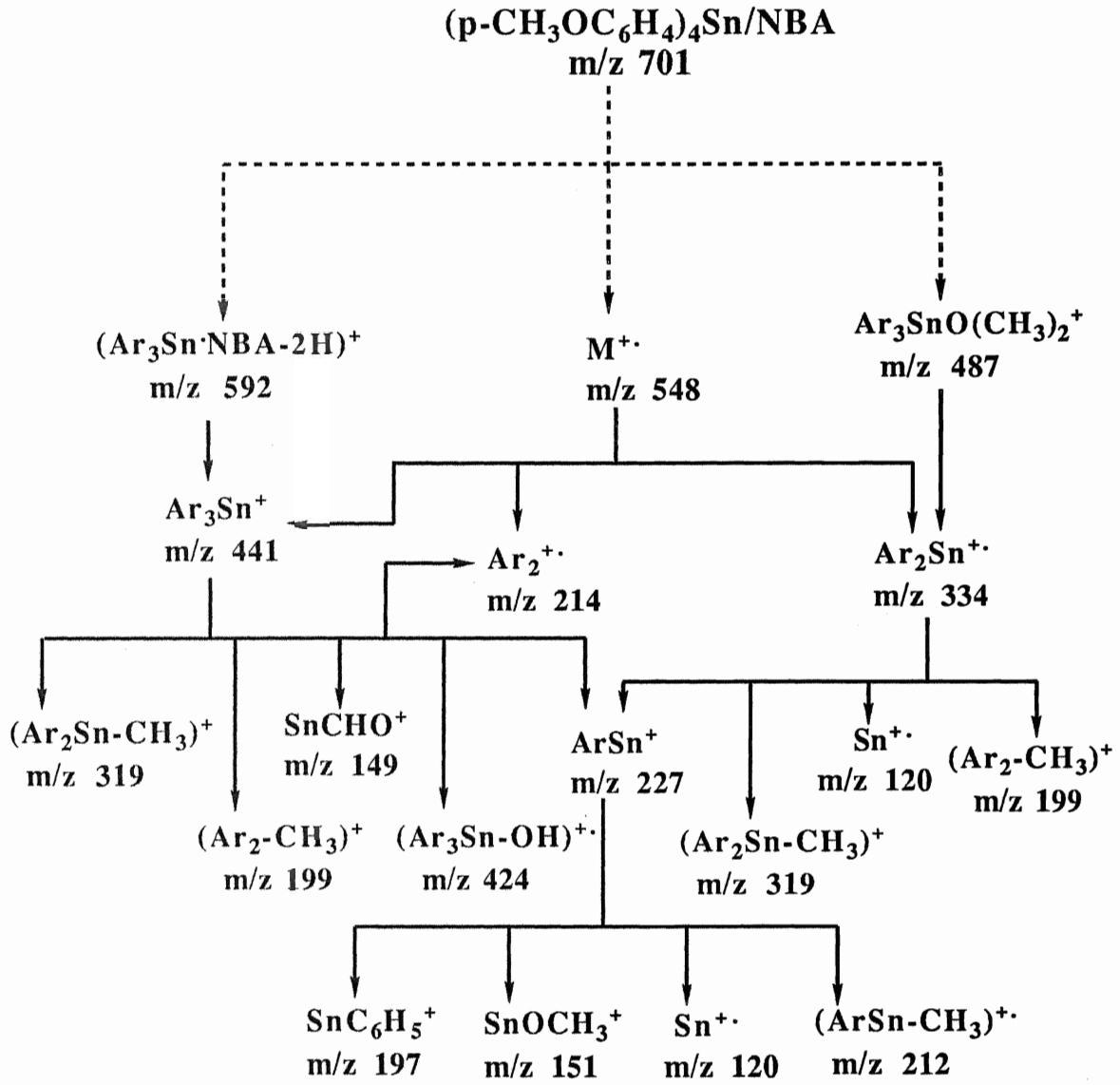

SCHEME 28 Fragmentation pattern of $(p\text{-}CH_3OC_6H_4)_4Sn$/NBA under positive ion FAB

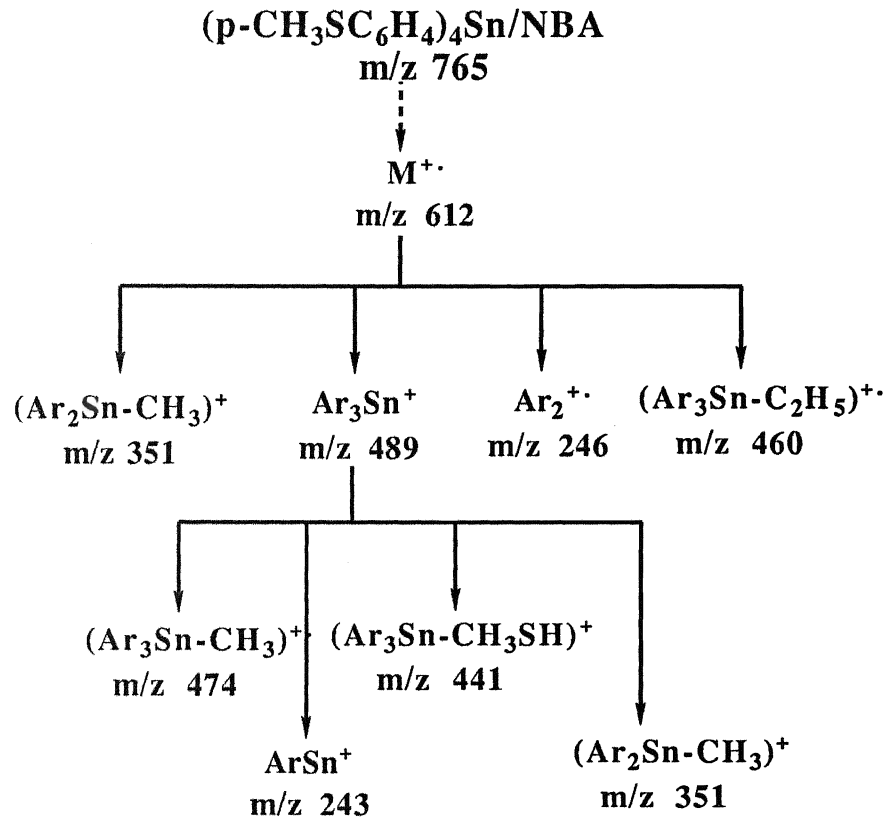

SCHEME 29 Fragmentation pattern of $(p\text{-}CH_3SC_6H_4)_4Sn$/NBA under positive ion FAB

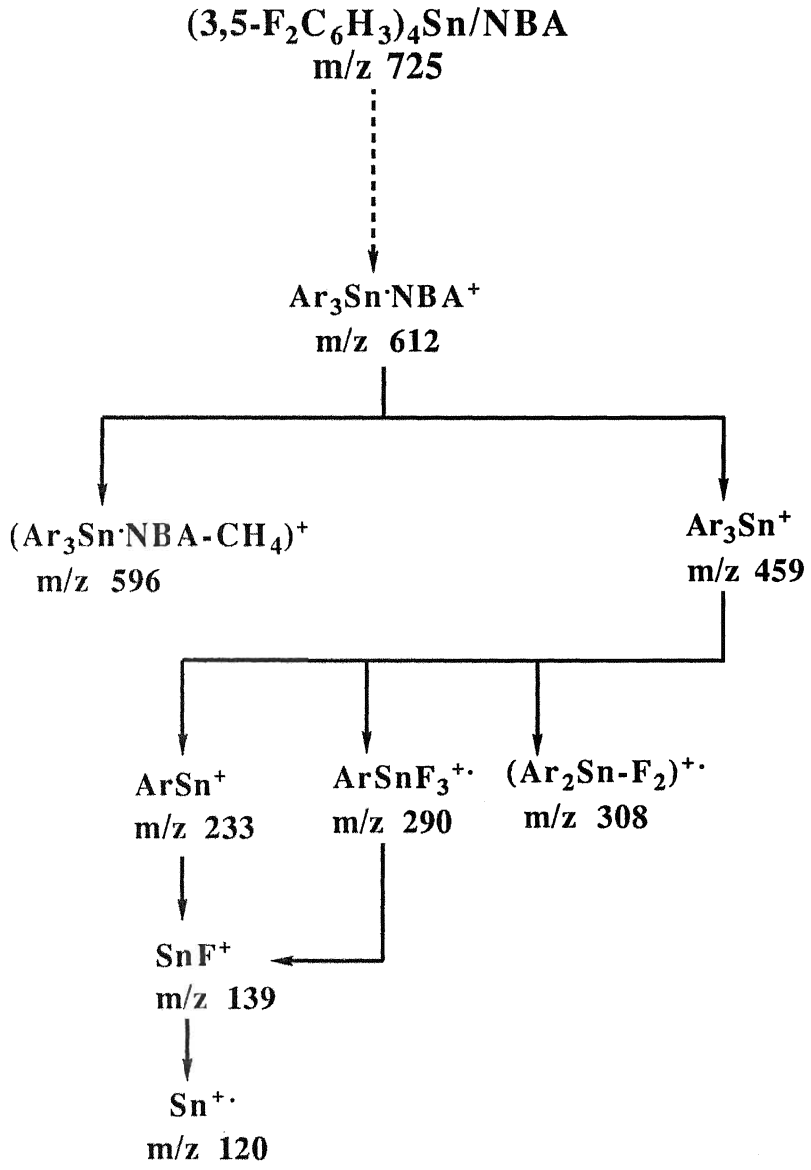

SCHEME 30 Fragmentation pattern of $(3,5\text{-}F_2C_6H_3)_4Sn$/NBA under positive ion FAB

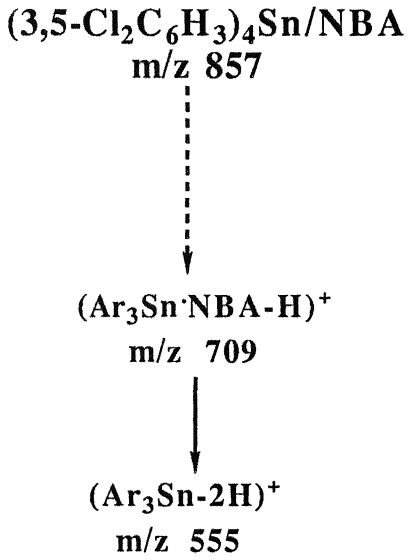

SCHEME 31 Fragmentation pattern of $(3,5\text{-}Cl_2C_6H_3)_4Sn$/NBA under positive ion FAB

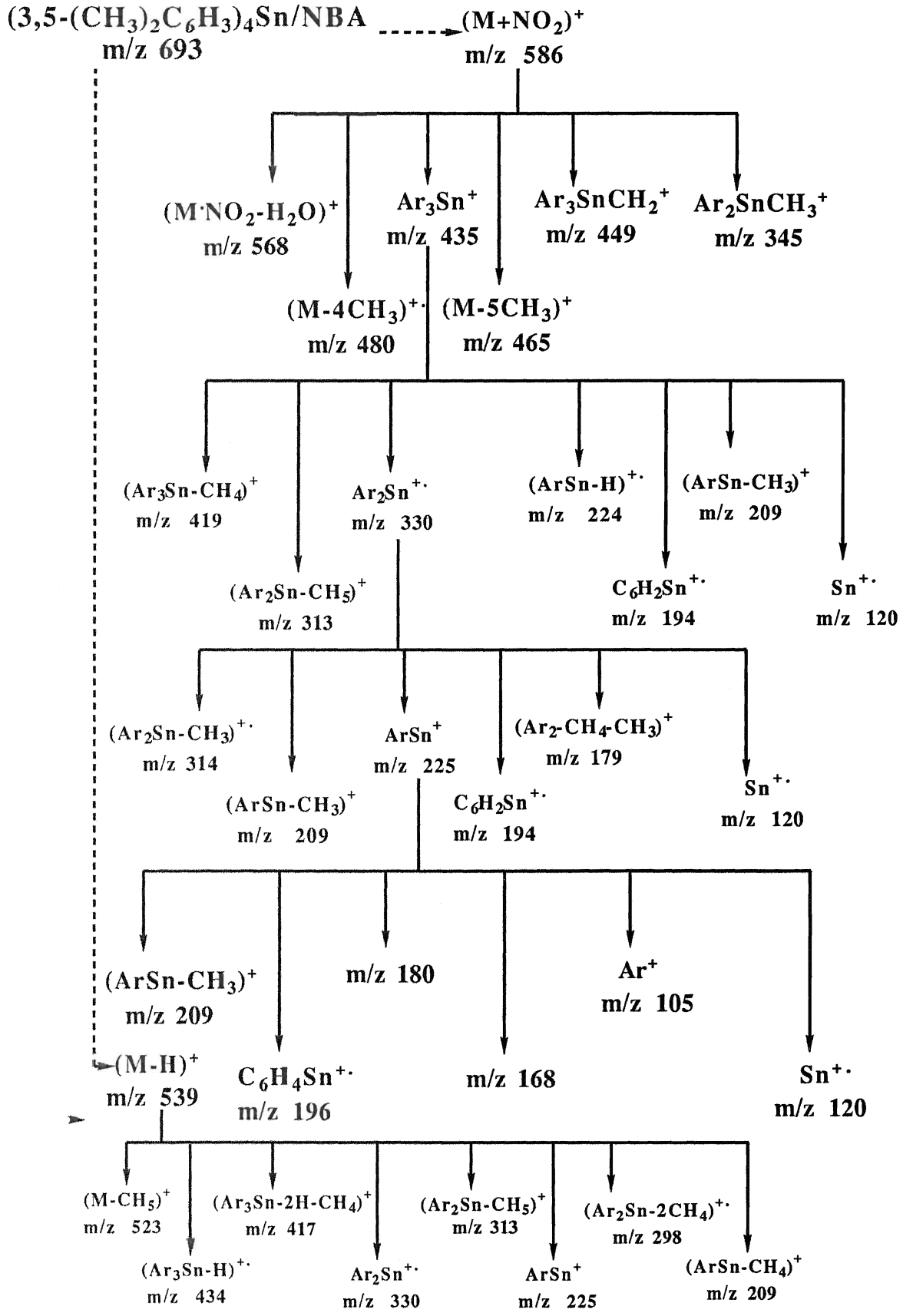

SCHEME 32 Fragmentation pattern of $(3,5\text{-}(CH_3)_2C_6H_3)_4Sn$/NBA under positive ion FAB

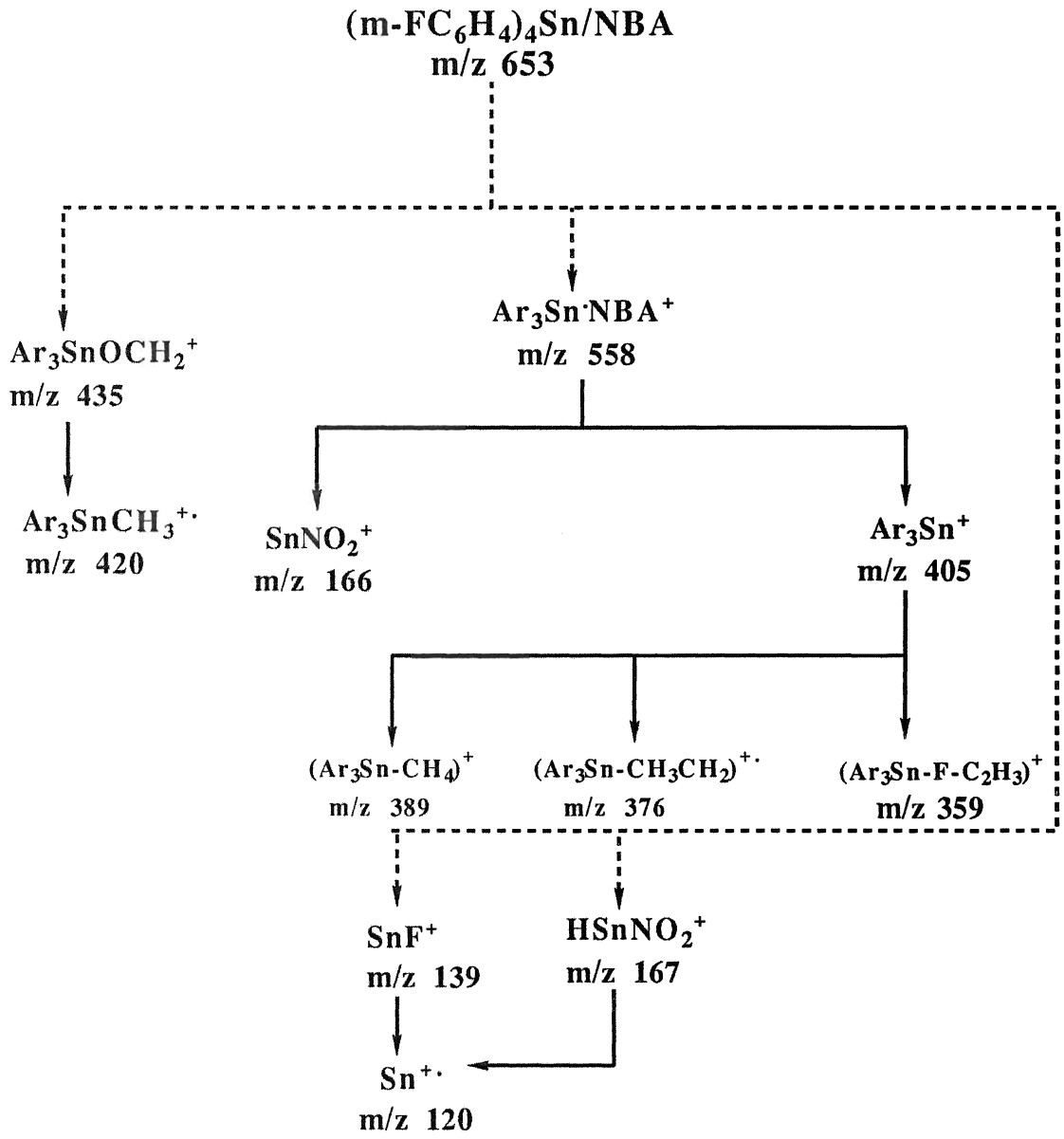

SCHEME 33 Fragmentation pattern of $(m\text{-}FC_6H_4)_4Sn/NBA$ under positive ion FAB

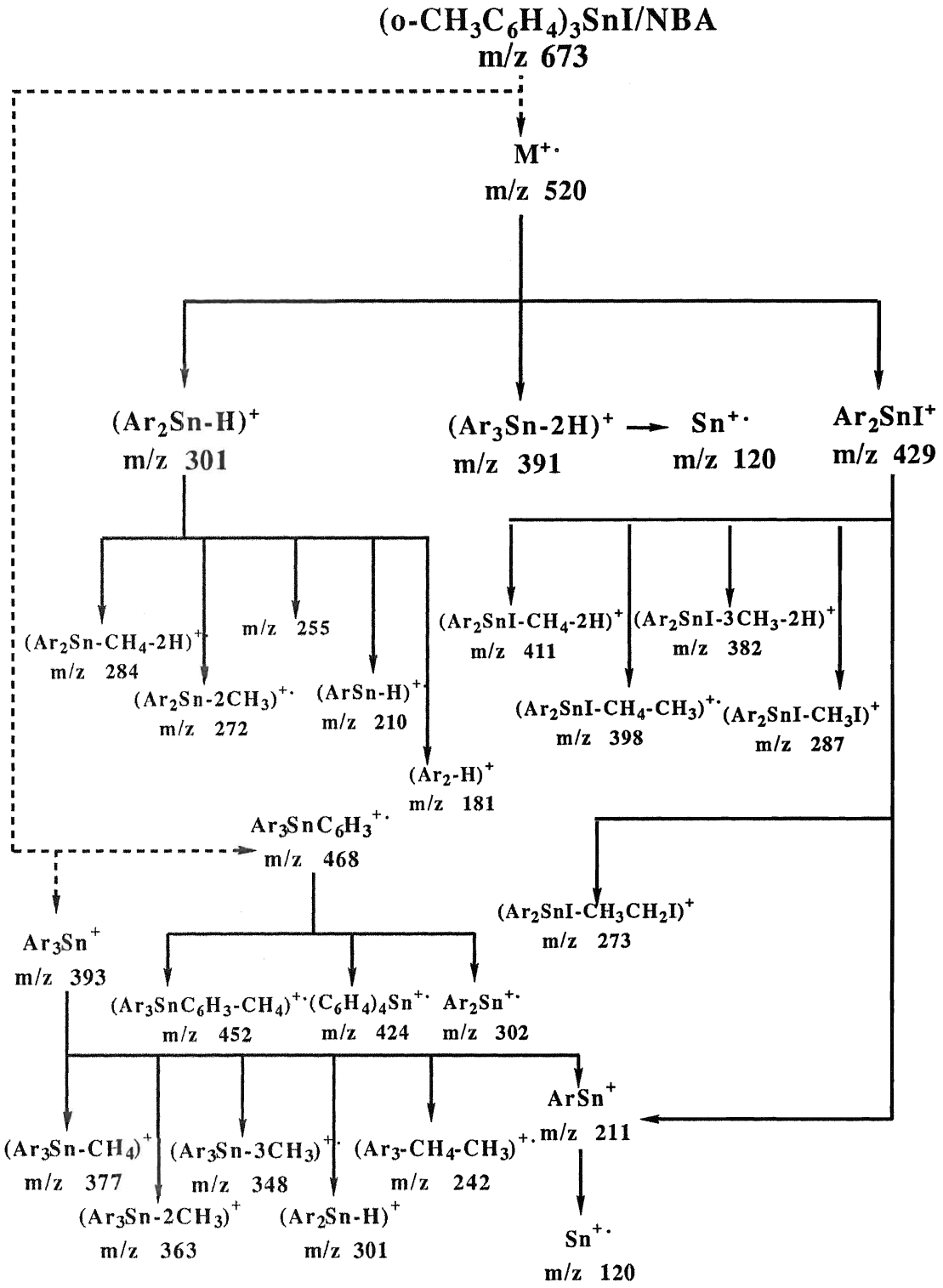

SCHEME 34 Fragmentation pattern of $(o\text{-}CH_3C_6H_4)_3SnI$/NBA under positive ion FAB

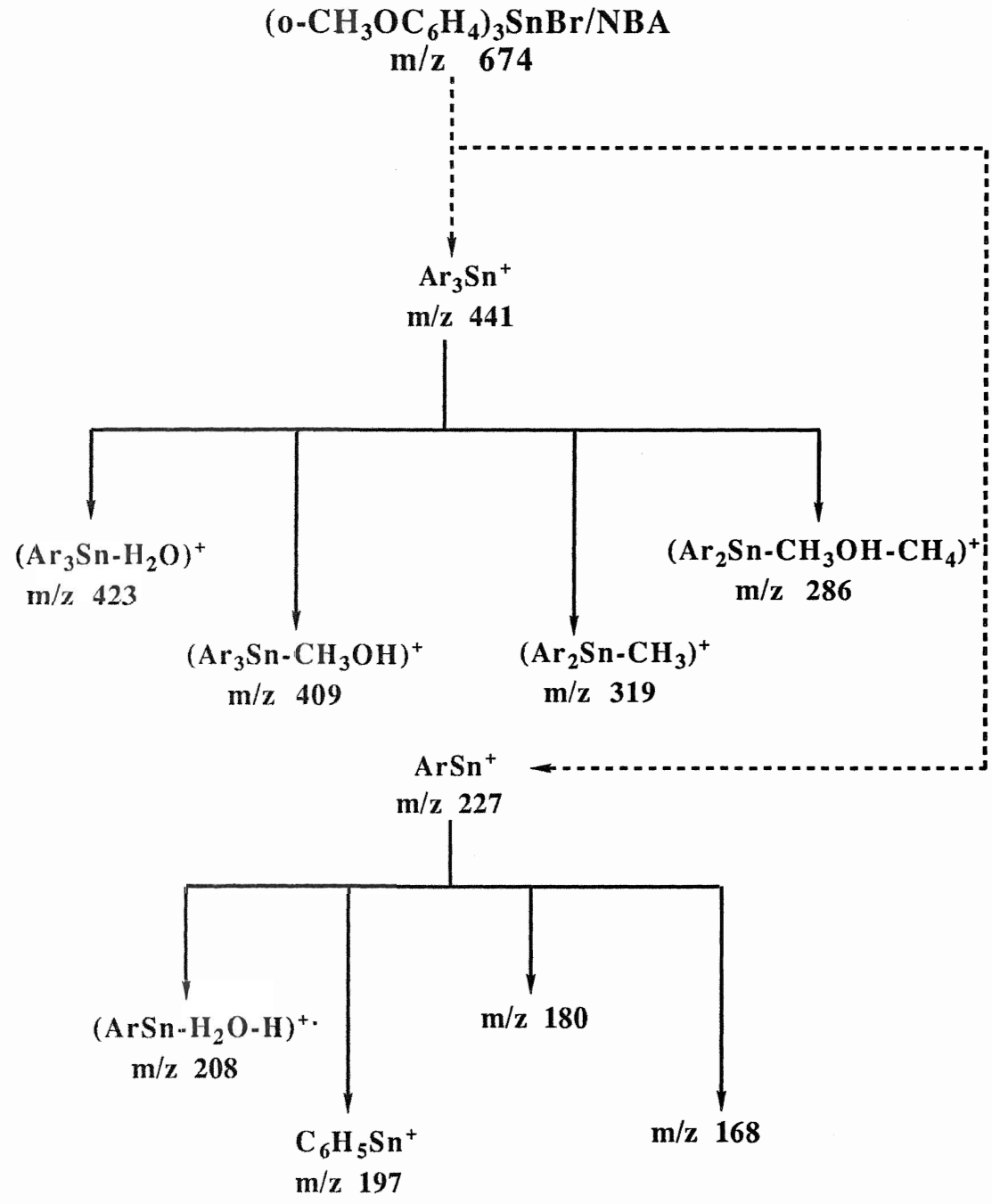

SCHEME 35 Fragmentation pattern of $(o\text{-}CH_3OC_6H_4)_3SnBr$/NBA under positive ion FAB

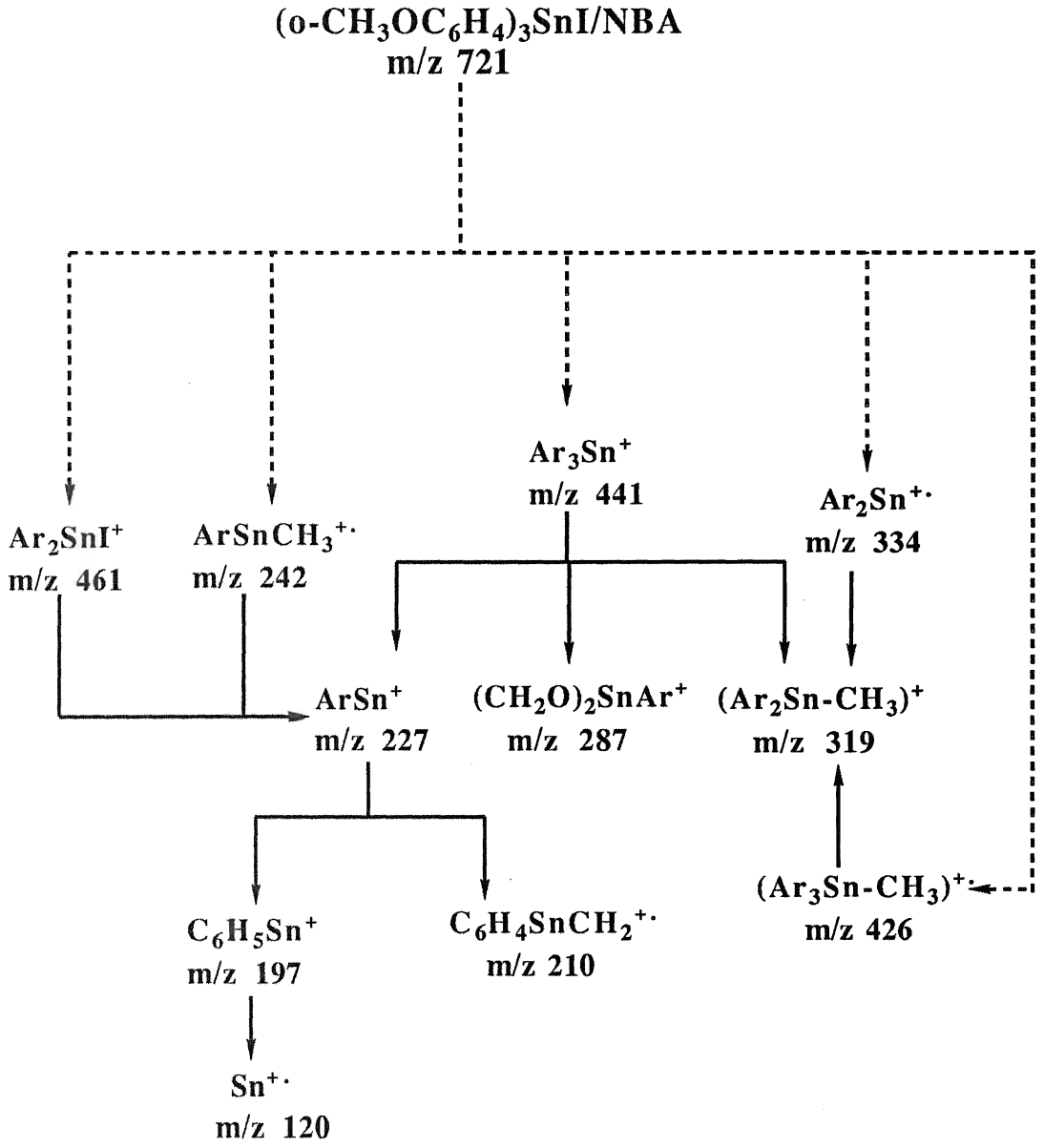

SCHEME 36 Fragmentation pattern of (o-$CH_3OC_6H_4)_3SnI$/NBA under positive ion FAB

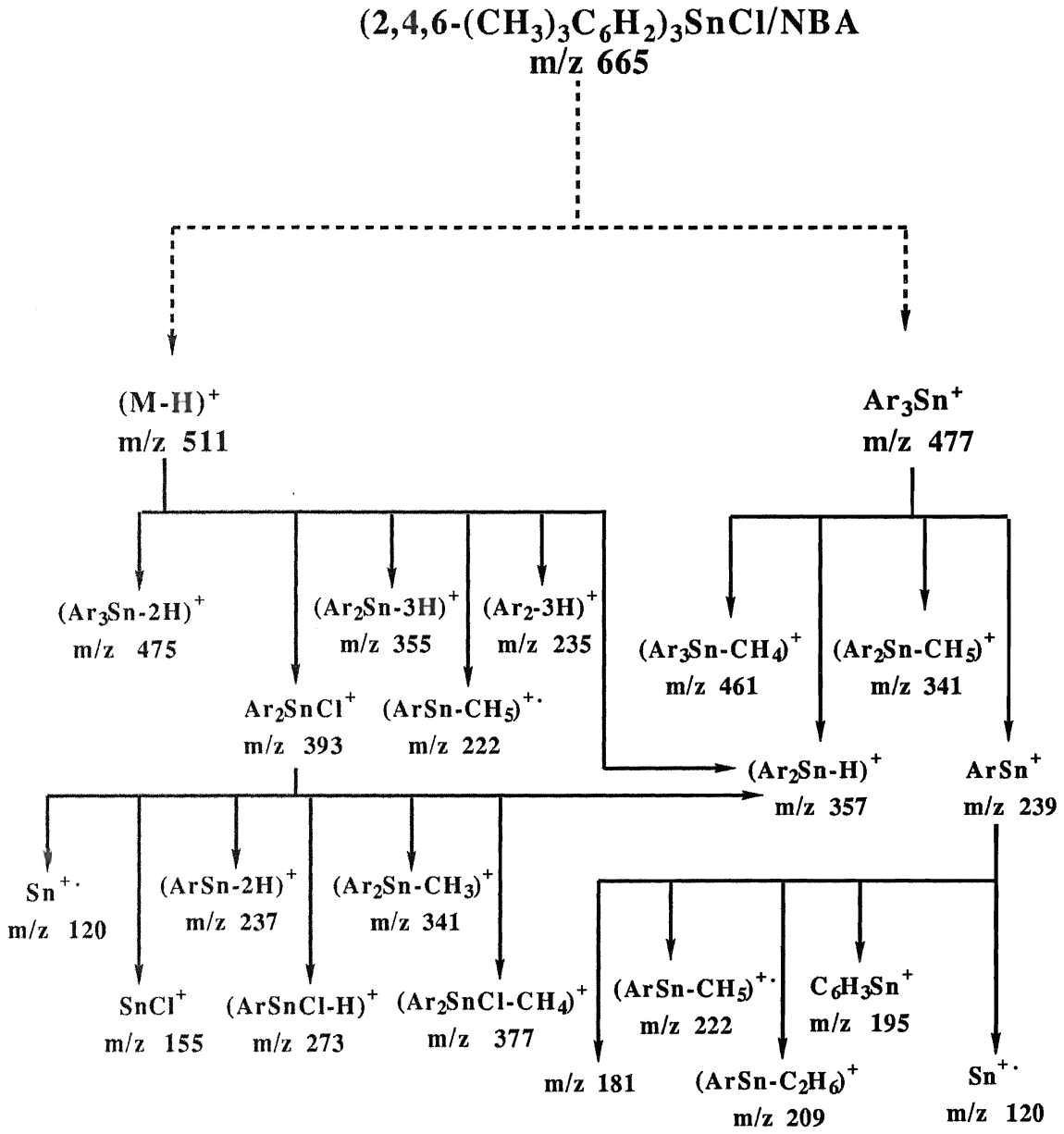

SCHEME 37 Fragmentation pattern of (2,4,6-$(CH_3)_3C_6H_2)_3SnCl$/NBA under positive ion FAI

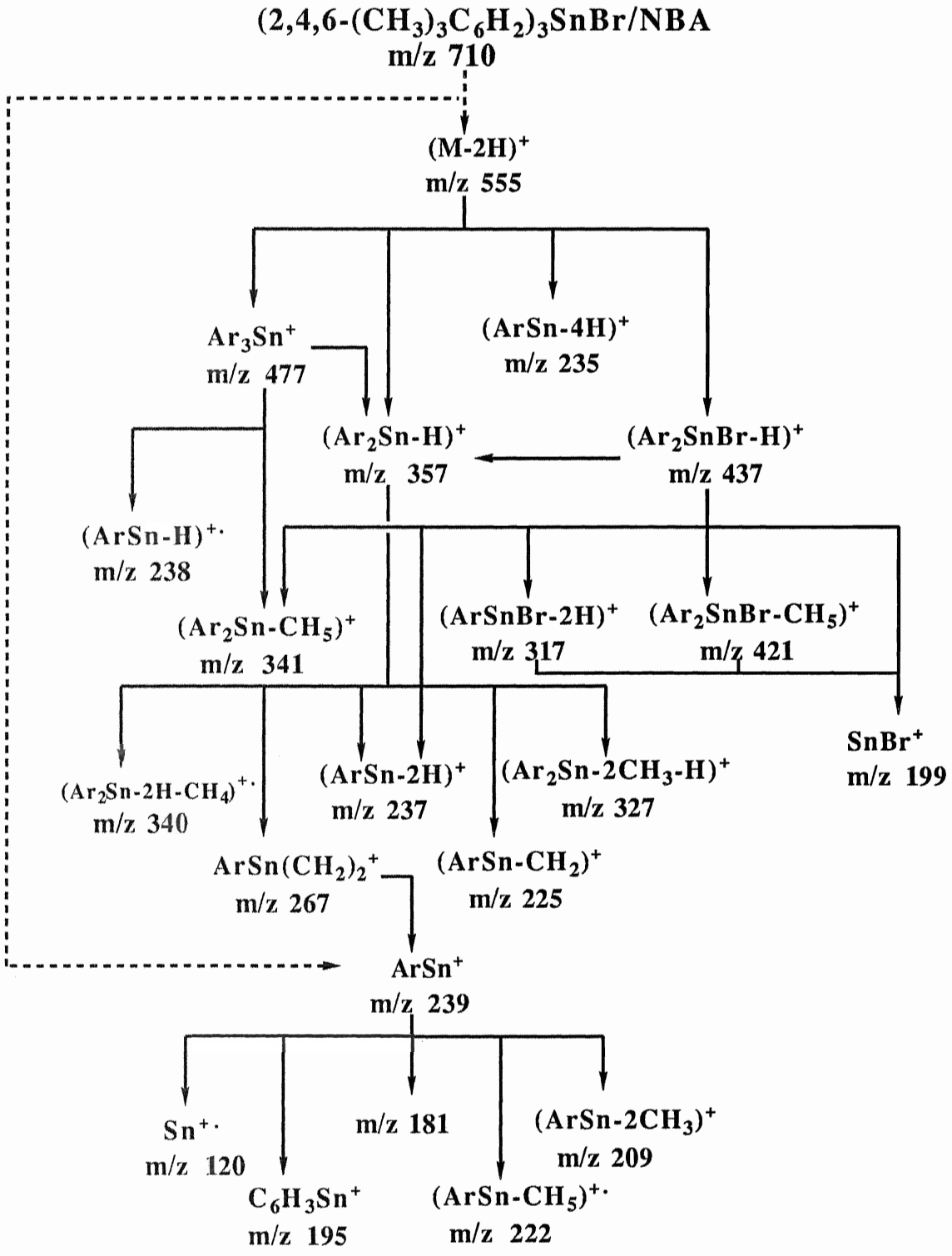

SCHEME 38 Fragmentation pattern of (2,4,6-$(CH_3)_3C_6H_2)_3SnBr$/NBA under positive ion FAB

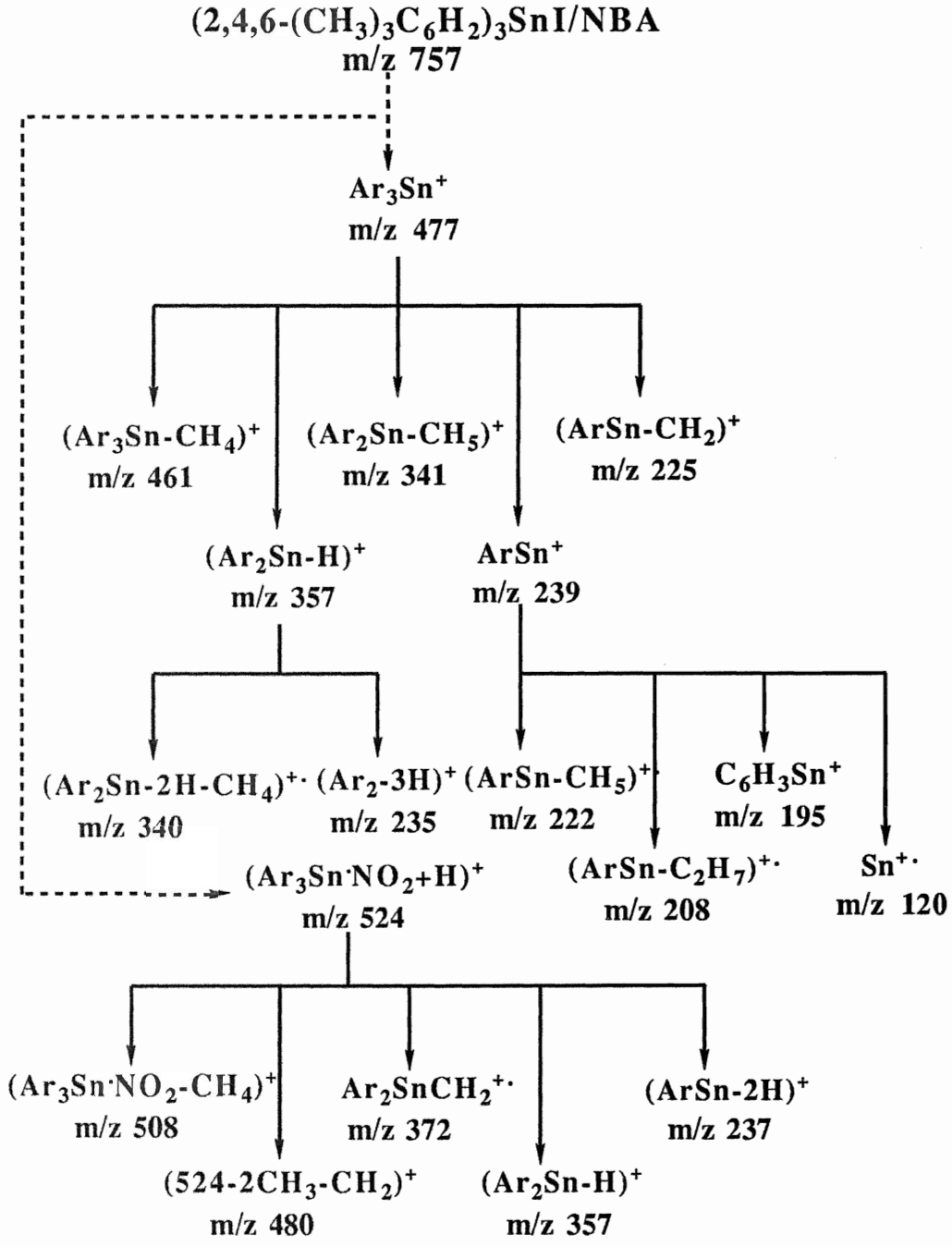

SCHEME 39 Fragmentation pattern of $(2,4,6\text{-}(CH_3)_3C_6H_2)_3SnI$/NBA under positive ion FAB

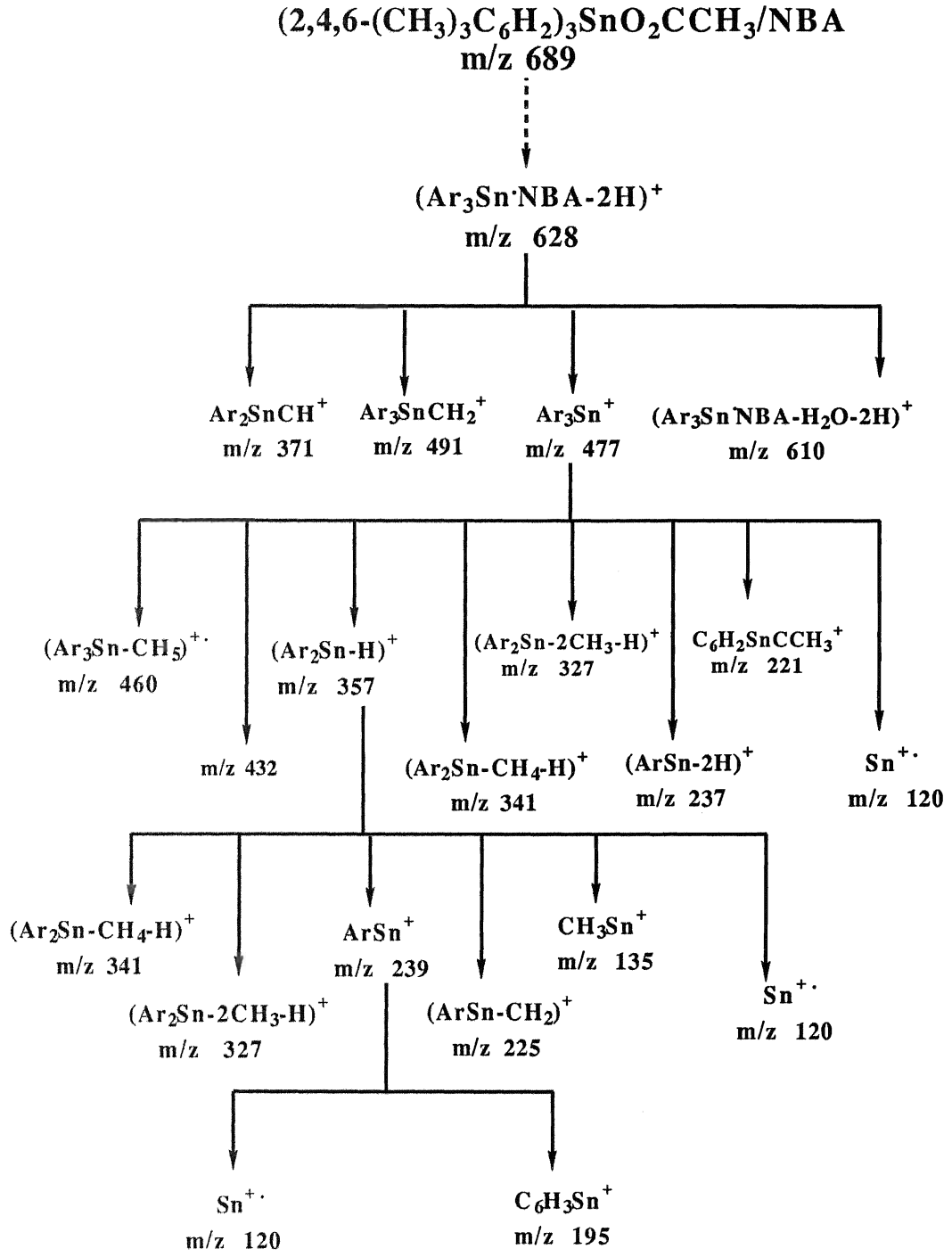

SCHEME 40 Fragmentation pattern of $(2,4,6\text{-}(CH_3)_3C_6H_2)_3SnO_2CCH_3$/NBA under positive ion FAB

3.1.5. Comparison of the Ionization Techniques

For comparison, Table VIII lists both the EI mass spectral data and +ve FAB mass spectral data in NBA matrix of all of the aryltin compounds in Table I.

From the data in Table VIII and the discussion in Section 3.1.1. and Section 3.1.2., we can find that many similarities exist between EI spectra of aryltin compounds and their +ve FAB spectra in NBA. More than half of the compounds in Table I have not produced molecular ion peaks in their EI and +ve FAB spectra. Even in those cases in which molecular ion peaks appear, both EI and +ve FAB spectra show only very low abundance of molecular ion. The only exception to this is that $(p\text{-}CH_3SC_6H_4)_4Sn$ has fairly intense molecular ion peaks in its EI and +ve FAB spectra. In most of these spectra, even ion peaks, such as Ar_3Sn^+ and $ArSn^+$, are dominant peaks, as has been observed [50-66] with other organotin compounds. The fragmentation patterns under EI and +ve FAB are somewhat similar, although usually +ve FAB give more fragment peaks.

However, some differences are also obvious. In EI spectra, Ar_2Sn^+ peaks are intense in most cases, if they show up, while in their +ve FAB spectra if they appear, they have very low abundance. All of the EI spectra give Sn^+ peaks; in some of the +ve FAB spectra, Sn^+ peaks totally disappear (e.g. $(o\text{-}CH_3OC_6H_4)_4Sn$, $(m\text{-}CF_3C_6H_4)_4Sn$, $(p\text{-}CH_3SC_6H_4)_4Sn$, $(p\text{-}CH_3C_6H_4)_4Sn$ and $(3,5\text{-}Cl_2C_6H_3)_4Sn$). In +ve FAB spectra, Ar_2SnI^+ (of $(o\text{-}CH_3C_6H_4)_3SnI$ and $(o\text{-}CH_3OC_6H_4)_3SnI$), Ar_2SnBr^+ (of $(o\text{-}CH_3OC_6H_4)_3SnBr$) and SnF^+ (of $(p\text{-}CF_3C_6H_4)_4Sn$) are strong. However, when they show in EI spectra, they have lower abundance. Except that more tin-containing peaks are observed in EI spectrum of $(o\text{-}CH_3C_6H_4)_4Sn$ than in its +ve FAB spectrum, all +ve FAB spectra have more tin-containing peaks than their EI counterparts do.

Both the similarities and the differences can find some reason from either the nature of ionization techniques or from the chemical properties of the sample themselves. The

similarities illustrate the bonding between tin atoms and their ligands in samples are weak, since for the same sample both EI and +ve FAB spectra show similar fragment peaks, while FAB is a lower energy ionization technique. The differences indicate the use of liquid matrices in FAB MS partially changes the bond strength between tin atoms and their ligands so that some fragment peaks are intense in EI spectra, but weak in +ve FAB, or reverse.

Based on these similarities and differences, EI and FAB can complement each other in getting detailed mass spectral information on structure and chemical properties of sample. Thus FAB MS has also proved a very good technique in analyzing this group of aryltin compounds just as for other aryltin compounds reported earlier [52-66].

*Note: text continues on page 131.

Table VIII Comparison of EI and Positive Ion FAB/NBA Mass Spectra* of Aryltin Compounds

(1) $(x\text{-}CH_3C_6H_4)_4Sn$ (x=o, m, p)

ION$^+$	Ar= o-$CH_3C_6H_4$		= m-$CH_3C_6H_4$		= p-$CH_3C_6H_4$	
	EI	FAB	EI	FAB	EI	FAB
$Ar_3Sn{\cdot}NBA^+$	-	-	-	2.3	-	2.1
$(M\text{-}H)^+$	0.2	-	0.9	1.5	0.1	0.7
$Ar_3Sn{\cdot}CH_2^+$	-	-	-	2.1	-	-
Ar_3Sn^+	58.7	73.9	47.1	53.6	49.2	81.6
$Ar_2Sn{\cdot}OH^+$	-	-	-	2.9	-	-
Ar_2Sn^+	-	-	24.6	-	23.1	-
$(Ar_2Sn\text{-}H)^+$	11.1	-	-	5.9	-	-
$(Ar_2Sn\text{-}2H)^+$	-	-	-	-	-	1.1
$ArSn^+$	19.3	15.0	12.5	17.5	12.5	14.6
Sn^+	10.7	11.1	14.9	14.3	15.0	-

* Percentage of the total positive ion current carried by tin-containing ions.

(2) $(x\text{-}CF_3C_6H_4)_4Sn$ (x=m, p)

ION$^+$	Ar= m-$CF_3C_6H_4$		= p-$CF_3C_6H_4$	
	EI	FAB	EI	FAB
$Ar_3Sn{\cdot}NBA^+$	-	5.5	-	5.3
$(M\text{-}F)^+$	4.1	4.0	3.6	1.5
$(Ar_3SnHF+2H)^+$	-	4.3	-	8.0
Ar_3Sn^+	55.3	54.9	68.5	39.6
$(Ar_3Sn\text{-}F)^+$	-	2.7	-	2.4
$(Ar_3Sn\text{-}CHF_3)^+$	-	1.1	-	1.4
$Ar_2Sn{\cdot}F^+$	3.3	-	2.4	-
$(Ar_2Sn{\cdot}F\text{-}2H)^+$	-	4.0	-	3.0
Ar_2Sn^+	1.8	-	1.2	-
$(Ar_2Sn\text{-}HF\text{-}H)^+$	-	2.9	-	0.6
$ArSn^+$	20.4	20.6	16.1	17.5
$(ArSn\text{-}HF)^+$	4.0	-	-	-
SnF^+	7.7	-	5.0	11.3
Sn^+	3.4	-	3.3	9.6

* Percentage of the total positive ion current carried by tin-containing ions.

Table VIII (cont.) (3) $(x\text{-}CH_3OC_6H_4)_4Sn$ (x=o, m, p)

ION$^+$	Ar= o-$CH_3OC_6H_4$		= m-$CH_3OC_6H_4$		= p-$CH_3OC_6H_4$	
	EI	FAB	EI	FAB	EI	FAB
$(Ar_3Sn\cdot NBA\text{-}H)^+$	-	0.3	-	-	-	-
$(M\cdot NBA\text{-}2H)^+$	-	-	-	0.5	-	0.9
M^+	-	-	7.9	2.7	0.7	1.3
$(M\text{-}H)^+$	0.7	0.4	-	-	-	-
$Ar_3SnO(CH_3)_2^+$	-	-	-	-	2.3	0.6
$Ar_3Sn\cdot CH_2^+$	-	-	-	-	-	1.4
Ar_3Sn^+	54.2	96.9	51.9	55.2	33.8	60.2
$(Ar_3Sn\text{-}CH_4)^+$	-	-	-	1.3	0.4	1.8
$(Ar_3Sn\text{-}OCH_3)^+$	-	-	-	-	-	2.1
$(Ar_3Sn\text{-}2CH_3)^+$	0.6	-	-	-	-	-
$Ar_2Sn\cdot OH^+$	-	-	-	1.5	-	-
$Ar_2SnCH_3^+$	-	-	-	-	-	1.9
Ar_2Sn^+	10.1	-	7.7	4.6	9.3	5.9
$(Ar_2Sn\text{-}CH_3)^+$	6.8	2.4	8.0	4.4	5.1	3.1
$(Ar_2Sn\text{-}OCH_3)^+$	-	-	1.0	-	2.6	-
$(Ar_2Sn\text{-}2CH_3)^+$	4.3	-	-	-	-	-
$(Ar_3Sn\text{-}CH_3O\text{-}CH_2)^+$	2.1	-	-	-	-	-
$ArSn(OCH_3)_2^+$	-	-	0.9	0.9	-	-
$ArSnOCH_3\cdot H_2O^+$	-	-	-	-	4.6	-
$ArSn^+$	4.7	-	11.4	14.5	17.1	16.3
$(ArSn\text{-}CH)^+$	3.2	-	-	-	-	-
$(ArSn\text{-}CH_3)^+$	-	-	-	-	2.6	-
$(ArSn\text{-}OCH_3)^+$	6.6	-	-	-	6.3	-
$C_6H_5SnH_2^+$	-	-	-	-	-	2.0
$C_6H_3Sn^+$	-	-	3.2	2.3	-	-
$H_2Sn(OCH_3)_2^+$	-	-	-	-	2.8	-
$SnOCH_3^+$	2.6	-	-	-	4.1	-
$C_2H_5Sn^+$	-	-	3.1	2.8	-	-
$SnCH_3^+$	1.1	-	-	6.9	-	-
Sn^+	2.8	-	5.0	6.6	8.5	2.3

* Percentage of the total positive ion current carried by tin-containing ions.

Table VIII (cont.) (4) $(3,5\text{-}X_2C_6H_3)_4Sn$ (X=F, Cl , CH_3)

ION$^+$	Ar= 3,5-$F_2C_6H_3$		= 3,5-$Cl_2C_6H_3$		= 3,5-$(CH_3)_2C_6H_3$	
	EI	FAB	EI	FAB	EI	FAB
$Ar_3Sn{\cdot}NBA^+$	-	6.2	-	-	-	-
$(Ar_3Sn{\cdot}NBA\text{-}H)^+$	-	-	-	10.2	-	-
$M{\cdot}NO_2^+$	-	-	-	-	-	1.1
M^+	0.1	-	-	-	-	-
$(M\text{-}H)^+$	-	-	-	-	0.9	4.0
$(M\text{-}3H)^+$	-	-	1.9	-	-	-
$(M\text{-}CH_3)^+$	-	-	-	-	0.3	-
$Ar_3Sn{\cdot}CHO^+$	-	-	-	1.6	-	-
$Ar_3Sn{\cdot}CH_2^+$	-	-	-	-	0.6	4.8
Ar_3Sn^+	34.8	48.1	35.1	61.5	25.9	46.0
$(Ar_3Sn\text{-}CH_3)^+$	-	-	-	-	1.2	1.2
$(Ar_3Sn\text{-}Cl)^+$	-	-	-	3.2	-	-
$(Ar_3Sn\text{-}HCl)^+$	-	-	0.5	-	-	-
Ar_2SnX^+	-	-	1.0	0.9	-	3.0
Ar_2Sn^+	2.1	-	-	-	20.5	8.9
$(Ar_2Sn\text{-}2H)^+$	-	-	1.1	-	-	-
$(Ar_2Sn\text{-}CH_3)^+$	-	-	-	-	1.0	1.4
$ArSnCH_3^+$	-	-	-	-	-	1.1
$ArSn^+$	19.8	20.3	18.1	22.7	14.0	16.1
$(ArSn\text{-}CH_3)^+$	-	-	-	-	7.5	5.2
$(ArSn\text{-}2CH_3)^+$	-	-	-	-	7.5	-
SnX^+	23.4	14.4	35.1	-	-	-
Sn^+ (X=F, Cl, CH_3)	19.8	11.0	7.0	-	20.7	7.1

* Percentage of the total positive ion current carried by tin-containing ions.

Table VIII (cont.) (5) $(p\text{-}XC_6H_4)_4Sn$ (X=CH_3, CF_3, CH_3O, CH_3S)

ION$^+$	Ar=p-$CH_3C_6H_4$		=p-$CF_3C_6H_4$		= p-$CH_3OC_6H_4$		= p-$CH_3SC_6H_4$	
	EI	FAB	EI	FAB	EI	FAB	EI	FAB
$(M\cdot NBA\text{-}2H)^+$	-	-	-	-	-	0.9	-	-
$(M\cdot NBA\text{-}NO_2)^+$	-	-	-	-	-	-	-	9.6
$Ar_3Sn\cdot NBA^+$	-	2.1	-	5.3	-	-	-	-
M^+	-	-	-	-	0.7	1.3	10.5	18.4
$(M\text{-}H)^+$	0.1	0.7	-	-	-	-	-	-
$(M\text{-}F)^+$	-	-	3.6	1.5	-	-	-	-
$Ar_3SnO(CH_3)_2^+$	-	-	-	-	2.3	0.6	-	-
$(Ar_3SnHF+2H)^+$	-	-	-	8.0	-	-	-	-
$Ar_3Sn\cdot CH_2^+$	-	-	-	-	-	1.4	-	-
Ar_3Sn^+	49.2	81.6	68.5	39.6	33.8	60.2	48.4	72.0
$(Ar_3Sn\text{-}CH_4)^+$	-	-	-	-	0.4	1.8	-	-
$(Ar_3Sn\text{-}F)^+$	-	-	-	2.4	-	-	-	-
$(Ar_3Sn\text{-}OCH_3)^+$	-	-	-	-	-	2.1	-	-
$(Ar_3Sn\text{-}CHF_3)+$	-	-	-	1.4	-	-	-	-
$Ar_2SnCH_3^+$	-	-	-	-	-	1.9	0.2	-
$Ar_2Sn\cdot F^+$	-	-	2.4	-	-	-	-	-
$(Ar_2Sn\cdot F\text{-}2H)^+$	-	-	-	3.0	-	-	-	-
Ar_2Sn^+	23.1	-	-	-	9.3	5.9	-	-
$(Ar_2Sn\text{-}2H)+$	-	1.1	-	-	-	-	-	-
$(Ar_2Sn\text{-}CH_3)^+$	-	-	-	-	5.1	3.1	17.0	-
$(Ar_2Sn\text{-}OCH_3)^+$	-	-	-	-	2.6	-	-	-
$(Ar_2Sn\text{-}HF\text{-}H)^+$	-	-	-	0.6	-	-	-	-
$(Ar_2Sn\text{-}2HF)^+$	-	-	1.2	-	-	-	-	-
$ArSnOCH_3\cdot H_2O)^+$	-	-	-	-	4.6	-	-	-
$ArSn^+$	12.5	14.6	16.1	17.5	17.1	16.3	12.3	-
$(ArSn\text{-}CH_3)^+$	-	-	-	-	2.6	-	-	-
$(ArSn\text{-}OCH_3^+$	-	-	-	-	6.3	-	-	-
$SnOCH_3^+$	-	-	-	-	4.1	-	-	-
$C_6H_5SnH_2^+$	-	-	-	-	-	2.0	-	-
$(CH_3O)_2SnH_2^+$	-	-	-	-	2.8	-	-	-
SnF^+	-	-	5.0	11.3	-	-	-	-
Sn^+	15.0	-	3.3	9.6	8.5	2.3	11.5	-

* Percentage of the total positive ion current carried by tin-containing ions.

Table VIII (cont.) (6) $(m\text{-}XC_6H_4)_4Sn$ (X=F, CF_3, CH_3, CH_3O)

ION^+	Ar=m-FC_6H_4		=m-$CF_3C_6H_4$		= m-$CH_3C_6H_4$		= m-$CH_3OC_6H_4$	
	EI	FAB	EI	FAB	EI	FAB	EI	FAB
$Ar_3Sn{\cdot}NBA^+$	-	4.5	-	5.5	-	2.3	-	0.5
M^+	-	-	-	-	-	-	7.9	2.7
$(M\text{-}H)^+$	-	-	-	-	0.9	1.5	-	-
$(M\text{-}F)^+$	-	-	4.1	4.0	-	-	-	-
$Ar_3Sn{\cdot}OCH_2^+$	-	7.1	-	-	-	-	-	-
$(Ar_3SnHF+2H)^+$	-	-	-	4.3	-	-	-	-
$Ar_3Sn{\cdot}CH_2^+$	-	-	-	-	-	2.1	-	-
Ar_3Sn^+	28.4	43.5	55.3	54.9	47.1	53.6	51.9	55.2
$(Ar_3Sn\text{-}CH_4)^+$	-	-	-	-	-	-	-	1.3
$(Ar_3Sn\text{-}F)^+$	-	-	-	2.7	-	-	-	-
$(Ar_3Sn\text{-}CHF_3)^+$	-	-	-	1.1	-	-	-	-
$Ar_2Sn{\cdot}F^+$	-	-	3.3	-	-	-	-	-
$(Ar_2Sn{\cdot}F\text{-}2H)^+$	-	-	-	4.0	-	-	-	-
$Ar_2Sn{\cdot}OH^+$	-	-	-	-	-	2.9	-	1.5
Ar_2Sn^+	2.6	-	1.8	-	24.6	-	7.7	4.6
$(Ar_2Sn\text{-}H)^+$	-	-	-	-	-	5.9	-	-
$(Ar_2Sn\text{-}CH_3)^+$	-	-	-	-	-	-	8.0	4.4
$(Ar_2Sn\text{-}OCH_3)^+$	-	-	-	-	-	-	1.0	-
$(Ar_2Sn\text{-}F)^+$	-	-	-	2.9	-	-	-	-
$ArSn(OCH_3)_2^+$	-	-	-	-	-	-	0.9	0.9
$ArSn^+$	19.7	28.2	20.4	20.6	12.5	17.5	11.4	14.5
$(ArSn\text{-}HF)^+$	-	-	4.0	-	-	-	-	-
$C_6H_3Sn^+$	-	-	-	-	-	-	3.2	2.3
$C_2H_5Sn^+$	-	-	-	-	-	-	3.1	-
SnF^+	22.2	-	7.7	-	-	-	-	-
$SnCH_3^+$	-	-	-	-	-	-	-	6.9
Sn^+	27.1	16.7	3.4	-	14.9	14.3	5.0	6.6

* Percentage of the total positive ion current carried by tin-containing ions.

Table VIII (cont.) (7) Ar_3SnI (Ar=o-$CH_3C_6H_4$, o-$CH_3OC_6H_4$, 2,4,6-$(CH_3)_3C_6H_2$)

ION^+	Ar=o-$CH_3C_6H_4$		=o-$CH_3OC_6H_4$		=2,4,6-$(CH_3)_3C_6H_2$	
	EI	FAB	EI	FAB	EI	FAB
$(Ar_3Sn{\cdot}NBA+C_2H_2)^+$	-	-	-	0.9	-	-
$Ar_3Sn{\cdot}NBA^+$	-	0.7	-	-	-	-
$Ar_2SnI{\cdot}NBA^+$	-	0.6	-	-	-	-
$(Ar_3Sn{\cdot}NBA-H_2O)^+$	-	-	-	-	-	0.7
M^+	-	0.6	-	-	-	-
$(M-H)^+$	0.1	-	-	-	0.1	-
$Ar_3SnC_6H_3^+$	-	1.8	-	-	-	-
$(Ar_3Sn{\cdot}NO_2+CH)^+$	-	-	-	1.3	-	-
$(Ar_3Sn{\cdot}NO_2+H)^+$	-	-	-	-	-	6.1
$Ar_3Sn{\cdot}CH_4^+$	-	-	-	-	-	3.2
Ar_3Sn^+	59.2	37.0	63.5	54.7	62.1	35.3
Ar_2SnI^+	6.4	18.9	3.4	18.6	-	-
$(Ar_3Sn-3CH_3)^+$	-	-	0.7	-	-	-
$(ArSnI+CH_3)^+$	-	-	0.5	-	-	-
$Ar_2SnCH_3^+$	-	1.4	-	-	-	-
$(Ar_2Sn-H)^+$	3.0	4.5	-	-	13.2	7.6
$(Ar_2Sn-CH_3)^+$	-	-	2.7	1.0	-	-
$(ArSnI-H)^+$	1.9	-	-	-	-	-
SnI^+	4.5	2.7	2.3	-	-	-
$ArSnCH_2^+$	-	-	-	-	-	3.0
$ArSn^+$	18.3	22.3	6.7	8.4	18.0	28.0
$SnC_6H_5^+$	-	-	10.9	-	-	-
$SnOCH_3^+$	-	-	4.7	3.8	-	-
Sn^+	6.8	9.4	4.7	11.2	6.7	16.0

* Percentage of the total positive ion current carried by tin-containing ions.

Table VIII (cont.) (8) $(o\text{-}CH_3OC_6H_4)_3SnX$ (X=Br, I, $o\text{-}CH_3OC_6H_4$)

ION^+	X=Br		=I		$=o\text{-}CH_3OC_6H_4$	
	EI	FAB	EI	FAB	EI	FAB
$(Ar_3Sn{\cdot}NBA+C_2H_2)^+$	-	1.8	-	0.9	-	-
$Ar_3Sn{\cdot}NBA^+$	-	-	-	-	-	0.3
$(Ar_3Sn{\cdot}NO_2+CH)^+$	-	0.5	-	1.3	-	-
M^+	0.4	-	-	-	-	-
$(M-H)^+$	-	-	-	-	0.7	0.4
Ar_3Sn^+	51.4	51.8	63.5	54.7	54.2	96.9
Ar_2SnX^+	12.8	32.7	3.4	18.6	-	-
$(Ar_3Sn\text{-}2CH_3)^+$	-	-	-	-	0.6	-
$(Ar_3Sn\text{-}3CH_3)^+$	-	-	0.7	-	-	-
Ar_2Sn^+	-	-	-	-	10.1	-
$(ArSnX+CH_3)^+$	-	-	0.5	-	-	-
$(Ar_2Sn\text{-}CH_3)^+$	2.4	-	2.7	1.0	6.8	2.4
$(Ar_2Sn\text{-}2CH_3)^+$	-	-	-	-	4.3	-
$(Ar_2Sn\text{-}CH_3O\text{-}CH_2)^+$	-	-	-	-	2.1	-
$(ArSn\text{-}CH)^+$	-	-	-	-	3.2	-
$(ArSn\text{-}OCH_3)^+$	-	-	-	-	6.6	-
$ArSn^+$	7.4	6.8	6.7	8.4	4.7	-
$\sim SnX^+$	15.1	2.4	2.3	-	1.1	-
$C_6H_3Sn^+$	-	-	10.9	-	-	-
$SnOCH_3^+$	4.9	-	4.7	3.8	2.6	-
Sn^+	5.6	4.0	4.7	11.2	2.8	-

X= Br, I, CH_3

* Percentage of the total positive ion current carried by tin-containing ions.

~ For EI mass spectrum of $(o\text{-}CH_3OC_6H_4)_3SnBr$, this abundance includes those of $C_6H_5Sn^+$ and $SnBr^+$.

Table VIII (cont.) (9) $(2,4,6\text{-}(CH_3)_3C_6H_2)_3SnX$ (X=Cl, Br, I, O_2CCH_3)

ION$^+$	X= Cl		=Br		= I		= O_2CCH_3	
	EI	FAB	EI	FAB	EI	FAB	EI	FAB
$(Ar_3Sn{\cdot}NBA\text{-}2H)^+$	-	-	-	-	-	-	-	0.5
$(Ar_3Sn{\cdot}NBA\text{-}H_2O)^+$	-	-	-	-	-	0.7	-	-
$(M{\cdot}X\text{-}H)^+$	-	-	-	-	-	-	-	-
M^+	-	-	-	-	-	-	0.7	-
$(M\text{-}H)^+$	0.3	3.6	0.2	2.8	0.1	-	-	-
$(Ar_3Sn{\cdot}NO_2{+}H)^+$	-	-	-	-	-	6.1	-	2.2
$(Ar_3Sn{\cdot}NO_2\text{-}CH_2)^+$	-	-	-	-	-	-	-	1.5
$Ar_3Sn{\cdot}CH_4^+$	-	0.1	-	-	-	3.2	-	-
$Ar_3Sn{\cdot}CH_2^+$	-	-	-	1.5	-	-	-	2.0
$(M\text{-}C_6H_3)^+$	0.9	-	-	-	-	-	-	-
Ar_3Sn^+	2.0	21.8	3.1	20.8	62.1	35.3	7.8	39.2
$(Ar_3Sn\text{-}CH_4)^+$	-	-	-	-	-	-	-	0.8
$Ar_2SnXCH_2^+$	-	2.2	-	1.9	-	-	-	-
Ar_2SnX^+	-	21.7	-	-	-	-	22.2	1.8
$(Ar_2SnX\text{-}H)^+$	40.4	-	39.7	17.6	-	-	-	-
$(Ar_2SnX\text{-}CH_3)^+$	-	-	-	-	-	-	2.5	-
$Ar_2Sn{\cdot}H_2O^+$	-	-	-	-	-	-	2.3	4.1
$(Ar_2SnX\text{-}CH_4)^+$	6.2	2.4	3.9	0.6	-	-	-	-
$(Ar_2SnX\text{-}3CH_3)^+$	-	-	3.7	-	-	-	-	-
$Ar_2SnCH_3^+$	-	-	-	2.5	-	-	-	-
$(Ar_2Sn\text{-}H)^+$	4.7	3.2	4.7	5.0	13.2	7.6	22.5	10.4
$(Ar_2Sn\text{-}OH)^+$	-	-	-	-	-	-	1.4	-
$(Ar_2Sn\text{-}CH_5)^+$	-	0.1	-	1.2	-	-	-	1.4
$(ArSnX\text{-}H)^+$	2.9	1.8	2.4	1.5	-	-	-	-
$ArSnCH_2^+$	-	1.4	-	2.6	-	3.0	1.0	2.1
$ArSn^+$	21.8	18.4	19.2	18.9	18.0	28.0	18.8	23.7
SnX^+	10.6	5.3	12.6	4.7	-	-	4.1	-
$SnCH_3^+$	-	8.5	-	10.3	-	-	3.7	4.6
Sn^+	10.3	7.8	11.4	8.2	6.7	16.0	9.6	6.0

* Percentage of the total positive ion current carried by tin-containing ions.

3.2. Ferrocenes

3.2.1. Comparison of EI MS Spectra and Positive Ion FAB MS Spectra

Most of the EI spectra of the ferrocenes studied in this thesis have been reported in literature. For comparison with their counterparts of positive ion FAB mass spectra, the EI spectra of these compounds were recorded again, with the Concept IS double focusing mass spectrometer. Good agreement with those reported results is reached. The spectral data are listed in Table IX.

Generally, all of these spectra show very intense molecular ion peaks, most of them being base peaks, though exceptions exist. Ferrocenemethanol and ferrocenecarboxylic acid both have $C_5H_5FeOH^+$ (m/z 138) as base peak, 1,1'-ferrocenedimethanol has $C_6H_6^+$ (m/z 78), and 1,1'-bis(diphenylphosphino)ferrocene $FePH^+$ (m/z 88) as base peak. In those cases where molecular ion peaks are not base peaks, however, they are still the second strongest peaks. The fragment peaks usually have very low abundance, except for the few peaks such as $(C_5H_5)_2Fe^+$ (m/z 186), $C_5H_5FeOH^+$ (m/z 138), $C_5H_5Fe^+$ (m/z 121), $FeOH^+$ (m/z 73) and Fe^+ (m/z 56). Most of fragment peaks are iron-containing peaks. Peaks coming from ligand(s) are not only weaker (only ferroceneacetonitril, 1,1'-ferrocenedimethanol and 1,1'-ferrocenedicarboxylic acid have strong ligands related peaks), but also fewer. Most of the intense fragment peaks are direct products of molecular ion decomposition (see section 3.2.2), although a few rearrangement peaks are observed.

Under EI conditions, unimolecular reaction is the major type of reaction. The second one is rearrangement reaction. Migration of substituent group from ligands to iron is common, for example, $C_5H_5FeOH^+$ and $FeOH^+$ in ferrocenemethanol, ferrocene-carboxylic acid, ferroceneacetic acid, 1,1'-ferrocenedimethanol, and 1,1'-

ferrocenedicarboxylic acid, $C_5H_5FeCN^+$ and $FeCN^+$ in ferroceneacetonitrile, $FeCH_3^+$ in acetylferrocene, $FeC_6H_5^+$ in benzoylferrocene and 1,1'-dibenzoylferrocene.

The EI spectra of ferrocenes are comparatively simple. The fact that all spectra of these compounds have very strong molecular ion peaks indicates small ferrocene derivatives are very stable and both the bonds between iron and ligands and those within ligand(s) are quite strong.

To observe the positive ion FAB MS behavior of ferrocenes in NBA matrix, all samples in Table II were studied with the Concept IS double focusing mass spectrometer. Ferrocene and 1,1'-ferrocenedicarboxylic acid did not produce any sample peaks, only the peaks of NBA matrix. In order to get positive ion spectrum of ferrocene, other matrix liquids, such as NPOE, glycerol, monothioglycerol, sulfolane, 2,2'-thiodiethanol, 1,3-dimethyl-pyrimidinone and diamylphenol, have been used. However, all these attempts failed to produce a spectrum. The fact that ferrocene can't give +ve FAB spectrum is perhaps related to its poor solubility in these matrices and its higher ionization energy. As one soft ionization technique, the positive ion FAB could not provide enough energy to ionize ferrocene and make it decompose. For 1,1'-ferrocenedicarboxylic acid, the reason why it can't yield +ve FAB spectrum in NBA is probably due to some reactions occurring between the analyte and matrix. All of the rest of this group of compounds give good spectra. The +ve FAB spectral data of these compounds are listed in Table IX.

The +ve FAB spectra of these compounds have the following features. All compounds but 1,1'-bis(diphenylphosphino)ferrocene (whose EI spectrum indicates this compound deliquesces) have shown molecular ion peaks as base peaks in their spectra. Compared with the very intense molecular ion peaks, fragment peaks have lower abundance, even those intense fragment peaks observed in the EI spectra (e.g. $(C_5H_5)_2Fe^+$ (m/z 186), $C_5H_5FeOH^+$ (m/z 138), $C_5H_5Fe^+$ (m/z 121), $FeOH^+$ (m/z 73), Fe^+ (m/z 56)). Some fragment peaks which are very weak in the EI spectra, however, give higher abundance in their positive ion FAB spectra (e.g. $(M\text{-}OH)^+$ (m/z 199) of

ferrocenemethanol, $C_6H_5CO^+$ (m/z 105) of benzoylferrocene and 1,1'-dibenzoylferrocene, $(M\text{-}OH)^+$ (m/z 229) of 1,1'-ferrocenedimethanol, $(M\text{-}OCH_3)^+$ (m/z 271) of 1,1'-dimethylferrocenedicarboxylate, $C_5H_5FeC_5H_4CH_2^+$ (m/z 199) of ferroceneacetonitrile, $(C_5H_5)_2Fe^+$ (m/z 186) of acetylferrocene, $C_5H_4COOFeCO^+$ (m/z 192) of ferrocenecarboxylic acid, $(M\text{-}COCH_2)^+$ (m/z 228) of 1,1'-diacetylferrocene, $C_5H_4PPh_2FeO^+$ (m/z 321) of 1,1'-bis(diphenylphosphino)ferrocene). Except for $C_6H_5CO^+$ (m/z 105) of benzoyl ferrocene and 1,1'-dibenzoylferrocene and $C_6H_6^+$ (m/z 78) of 1,1'-ferrocenedimethanol, all intense fragment peaks in their spectra are iron-containing peaks. This can be explained with the strong bonding between iron and pieces of ligand(s) or ligand itself and the low ionization energy of iron (7.90eV)).

Unfortunately, only low abundance (relative abundance 8.5) molecular ion of 1,1'-bis(diphenylphosphino)ferrocene is observed in its positive ion FAB spectrum, while in its EI spectrum the relative abundance is 14.3. The $(M{\cdot}CH_3OH{+}H)^+$ is the base peak in the +ve FAB spectrum. The bigger difference between the spectra of this derivative and those of ferrocenes is attributed to its larger ligands which make ferrocenyl group function differently under both EI and positive ion FAB conditions. Another factor contributing the difference might be the deliquescence of the sample, and thus contaminates.with water.

In the +ve FAB spectra of the ferrocenes, migration of substituent group from ligands to iron still occurs, however, it is not as common as in EI spectra. The migrating peaks, if they appear, have much lower abundance than their EI counterparts.

Generally, the positive ion FAB of these compounds are simple and clear. They are quite similar to their EI counterparts. This indicates that +ve FAB can be a very good choice of ionization technique when studying ferrocene derivative with mass spectrometry if available. Like EI, +ve FAB can also provide a lot of information on fragmentation which is very useful in deducing molecular structure. Moreover, +ve FAB can yield more strong molecular ion peaks, which make it easier to determine the molecular weight of the sample. For some ferrocene derivatives (like ferrocene itself), however, choosing suitable

matrix liquid is still a big problem.

The negative ion FAB experiments of all these compounds in NBA matrix were performed. However, no one compound gives any sample related peaks. This perhaps is due to the low sensitivity of the negative ion FAB technique or because NBA is not a good matrix for the negative ion FAB experiments.

*Note: text continues on page 143.

Table IX. Comparison of EI and Positive Ion FAB/NBA Mass Spectra of Ferrocenes

Ferrocene				1,1'-ferrocenedicarboxylic acid			
		EI	FAB			EI	FAB
Ions	**m/z**	**r.abd**	**r.abd**	**Ions**	**m/z**	**r.abd**	**r.abd**
M^+	186	100.0		M^+	274	100.0	
$C_5H_5Fe^+$	121	29.3		$(M-2H)^+$	272	31.3	
$C_3H_3Fe^+$	95	4.4		$(M-O)^+$	258	6.0	
$C_3H_2Fe^+$	94	3.6		$(M-H_2O-OH)^+$	239	2.0	
M^{++}	93	4.8		$(M-COOH-OH)^+$	212	54.9	
C_2HFe^+	81	3.6		$(M-COOHO_2H)^+$	196	2.4	
$C_5H_5^+$	65	0.7		$C_5H_4COOFeO^+$	180	17.5	
Fe^+	56	18.7		$FeC_5H_4COOH^+$	165	17.4	
				$FeC_5H_2COO^+$	162	6.1	
				$C_5H_4COFe^+$	148	3.6	
				$C_5H_3FeCO^+$	146	6.7	
				$C_5H_4FeOH^+$	137	7.1	
				$C_{10}H_8^+$	128	8.9	
				$C_5H_4Fe^+$	120	6.2	
				$C_5H_3Fe^+$	119	6.4	
				$C_6H_5CO^+$	105	40.8	
				$C_5H_4CO^+$	92	55.1	
				C_2HFe^+	81	8.4	
				$C_6H_5^+$	77	17.1	
				$FeOH^+$	73	15.6	
				$C_5H_4^+$	64	17.0	
				Fe^+	56	22.7	

Table IX(cont.)

Ferrocenecarboxaldehyde				Ferrocenemethanol			
		EI	FAB			EI	FAB
Ions	m/z	r.abd	r.abd	Ions	m/z	r.abd	r.abd
$(M+H)^+$	215	-	36.9	M^+	216	55.7	100.0
M^+	214	100.0	100.0	$(M-OH)^+$	199	-	22.3
$(C_5H_5)_2Fe^+$	186	62.7	12.0	$(M-H_2O)^+$	198	1.4	-
$HOFeC_5H_4COH^+$	165	-	1.4	$(C_5H_5)_2Fe^+$	186	5.0	2.7
$C_5H_4COFeCH_2^+$	162	-	1.5	$CH_2FeC_5H_4CH_2OH^+$	165	-	0.6
$C_5H_5FeOH^+$	138	-	2.4	$C_5H_5FeCHOH^+$	151	8.7	2.6
$C_5H_4FeO^+$	136	-	4.1	$C_5H_5FeOH^+$	138	100.0	15.0
$C_{10}H_9^+$	129	8.9	2.5	$C_5H_4FeO^+$	136	-	4.6
$C_{10}H_8^+$	128	7.3	-	$C_5H_5Fe^+$	121	15.4	54.0
$C_5H_5Fe^+$	121	70.2	10.7	$C_5H_4Fe^+$	120	4.3	1.3
$C_5H_4Fe^+$	120	15.4	2.7	$C_6H_5CO^+$	105	-	0.8
$C_5H_4COCH_3^+$	107	5.1	1.5	$C_3H_3Fe^+$	95	4.6	-
$C_3H_3Fe^+$	95	12.9	-	$C_3H_2Fe^+$	94	4.5	-
$C_3H_2Fe^+$	94	14.6	-	$C_7H_7^+$	91	-	1.4
$(C_5H_5)_2Fe^{++}$	93	6.2	-	$C_7H_6^+$	90	-	2.1
$C_5H_4CO^+$	91	-	1.9	$CH_3OFeH_2^+$	89	-	1.7
$C_5H_3CO^+$	90	-	3.5	C_2HFe^+	81	5.0	2.0
$H_2FeOCH_3^+$	89	-	2.6	$C_6H_6^+$	78	8.2	2.2
C_2HFe^+	81	12.8	3.1	$C_6H_5^+$	77	-	2.1
$C_6H_6^+$	78	-	1.5	$FeOH^+$	73	31.6	-
$C_6H_5^+$	77	-	3.0	$C_5H_5^+$	65	3.0	1.0
$FeOH^+$	73	-	2.3	$C_5H_3^+$	63	-	1.1
$C_6H_6^+$	65	10.5	1.7	Fe^+	56	26.6	5.2
HFe^+	57	-	2.9				
Fe^+	56	71.7	8.9				

Table IX(cont.)

Ferroceneacetonitrile				Acetylferrocene			
		EI	FAB			EI	FAB
Ions	**m/z**	**r.abd**	**r.abd**	**Ions**	**m/z**	**r.abd**	**r.abd**
$(M+NO_2+3H)^+$	274	-	2.3	M^+	228	100.0	100.0
$(M+O)^+$	241	-	4.0	$(M-CH_3)^+$	213	2.2	-
$(M+2H)^+$	227	-	2.3	$C_5H_5FeC_5H_4CH_2^+$	199	8.2	2.7
$(M+H)^+$	226	-	19.5	$(C_5H_5)_2Fe^+$	186	5.5	10.8
M^+	225	100.0	100.0	$C_5H_5FeC_5H_4^+$	185	24.0	3.0
$(M-H)^+$	224	8.3	8.5	$C_5H_5FeC_5H_3^+$	184	2.2	-
$(M-2H)^+$	223	-	7.0	$FeC_5H_4COCH_3^+$	163	3.6	3.5
$C_5H_5FeC_5H_4CH_2OH^+$	216	-	2.1	$C_6H_3COFe^+$	159	1.1	-
$C_5H_4FeC_5H_4CH_2O^+$	214	-	3.7	$FeC_5H_4CO^+$	148	1.4	-
$C_5H_5FeC_5H_4CH_2^+$	199	-	7.5	$C_5H_4FeO^+$	136	-	3.6
$C_5H_4CH_2CNFeH^+$	160	7.6	3.3	$C_6H_5Fe^+$	133	1.2	-
$C_5H_4CH_2CNFe^+$	159	7.1	-	$C_5H_4C_5H_5^+$	129	15.3	2.1
$C_5H_5FeCN^+$	147	7.9	-	$(C_5H_4)_2^+$	128	3.7	-
$C_5H_5FeCH_3^+$	136	-	7.4	$C_5H_5Fe^+$	121	12.2	6.2
$C_5H_4FeCH_2^+$	134	10.1	-	$C_5H_4Fe^+$	120	3.6	-
$C_5H_5Fe^+$	121	27.7	7.0	$C_6H_3CO^+$	103	1.3	-
M^{++}	112	2.8	-	$C_3H_3Fe^+$	95	2.5	-
$C_3H_3Fe^+$	95	5.4	-	$C_3H_2Fe^+$	94	3.7	-
$C_3H_2Fe^+$	94	4.9	-	$C_5H_3CO^+$	90	-	2.5
$C_5H_4CN^+$	90	-	2.7	C_2HFe^+	81	3.3	-
$FeCN^+$	82	10.6	-	$C_6H_5^+$	77	-	2.1
C_2HFe^+	81	6.9	-	CH_3Fe^+	71	4.4	-
$C_5H_4CH_3^+$	79	3.5	3.3	Fe^+	56	13.4	3.1
$C_5H_4CH_2^+$	78	41.8	-				
$C_5H_4CH^+$	77	7.0	-				
$C_5H_5^+$	65	2.8	-				
Fe^+	56	57.7	4.9				

Table IX(cont.)

Ferrocenecarboxylic acid				Ferroceneacetic acid			
		EI	FAB			EI	FAB
Ions	m/z	r.abd	r.abd	Ions	m/z	r.abd	r.abd
$(M+CO_2)^+$	274	-	2.5	$C_5H_5Fe{\cdot}NBA^+$	274	-	2.0
$(M+CO)^+$	258	-	1 .7	M^+	244	100.0	100.0
$(M+O)^+$	246	-	1.3	$(M-H_2O)^+$	226	0.8	0.8
$(M+H)^+$	231	-	26.2	$(M-COOH)^+$	199	24.7	12.4
M^+	230	76.6	100.0	$(C_5H_5)_2Fe^+$	186	0.7	-
$(M-O)^+$	214	2.7	-	$HFeC_5H_4CH_2COOH^+$	180	-	5.6
$(M-OH)^+$	213	-	4.7	$FeC_5H_4CH_2COOH^+$	179	5.9	7.6
$C_5H_4COOFeCO^+$	192	-	9.9	$HFeC_5H_4CH_2COH_2^+$	165	-	1.3
$(C_5H_5)_2Fe^+$	186	5.9	-	$FeC_5H_4CH_2CO^+$	162	1.3	-
$FeC_5H_4COOH^+$	165	17.7	3.6	$C_5H_4CH_2FeOH^+$	151	24.3	8.7
$C_5H_5Fe(OH)_2H^+$	156	1.6	-	$C_5H_5FeOH^+$	138	10.0	-
$C_5H_5FeOH^+$	138	100.0	7.7	$C_5H_4FeO^+$	136	-	10.0
$C_5H_4FeOH^+$	137	7.1	-	$FeC_5H_4CH_2^+$	134	6.4	-
$C_{10}H_8^+$	128	5.8	-	$C_5H_5Fe^+$	121	36.8	11.6
$C_5H_5Fe^+$	121	8.6	2.6	$C_9H_7^+$	115	-	1.9
$C_5H_4Fe^+$	120	4.9	-	$C_5H_4CH_2COH^+$	107	-	5.4
M^{++}	115	3.1	-	$C_5H_4CH_2CO^+$	106	8.3	-
$C_3H_3Fe^+$	95	3.5	-	$C_3H_3Fe^+$	95	3.8	-
$C_3H_2Fe^+$	94	6.4	-	$C_3H_2Fe^+$	94	3.0	-
$(C_5H_5)_2Fe^{++}$	93	3.7	1.1	$C_5H_4CH_2C^+$	90	-	3.0
$C_5H_4CO^+$	92	13.5	-	$C_5H_4CHC^+$	89	-	10.6
C_2HFe^+	81	11.0	1.0	C_2HFe^+	81	4.5	-
$FeOH^+$	73	40.4	1.7	$C_6H_6^+$	78	8.7	-
$C_5H_5^+$	65	3.7	-	$C_6H_5^+$	77	4.1	12.8
$C_5H_4^+$	64	7.7	-	$FeOH^+$	73	16.8	-
$C_5H_3^+$	63	5.9	-	$C_5H_5^+$	65	1.6	-
Fe^+	56	27.7	3.0	$C_5H_3^+$	63	-	9.7
				Fe^+	56	22.9	8.2

Table IX(cont.)

Benzoylferrocene			1,1'-ferrocenedimethanol		
	EI	FAB		EI	FAB
Ions	m/z	r.abd	Ions	m/z	r.abd	r.abd
$(M+2H)^+$	292	-	7.2	$(C_5H_4CH_2OHFe{\cdot}NBA-3H)^+$	301	-	2.3
$(M+H)^+$	291	-	41.6	M^+	246	72.6	100.0
M^+	290	100.0	100.0	$(M-OH)^+$	229	-	37.1
$(M-2H)^+$	288	-	6.6	$(M-H_2O)^+$	228	5.1	-
$C_5H_4FeC_5H_4C_6H_4^+$	260	1.3	-	$(C_5H_4C)_2Fe^+$	208	-	4.7
$FeC_5H_4COC_6H_5^+$	225	1.4	3.2	$C_5H_4CH_3FeC_5H_5^+$	200	2.0	2.4
$C_5H_4COC_6H_5COH^+$	198	1.1	-	$C_5H_5FeC_5H_4CH_2^+$	199	3.7	3.8
$C_5H_4COC_6H_5CO^+$	197	3.2	-	$C_5H_4CH_2OHFeOH^+$	168	4.8	-
$C_5H_3COC_6H_5CO^+$	196	2.1	-	$C_5H_4CH_2OFeO^+$	166	-	3.8
$C_5H_5FeC_5H_4^+$	185	2.0	-	$C_5H_4CH_2OHFe^+$	151	6.6	19.4
$C_6H_5OHFeOH_2^+$	168	-	6.3	$C_5H_4CH_2OFe^+$	150	13.6	-
$(C_5H_4FeOH_2+H_2)^+$	141	4.3	-	$C_5H_5FeOH^+$	138	0.9	-
$H_2FeC_5H_4OH^+$	139	1.3	-	$C_5H_4FeO^+$	136	-	14.1
$FeC_6H_5^+$	133	7.4	2.3	$C_5H_4CH_2Fe^+$	134	4.4	-
$C_5H_4C_5H_5^+$	129	3.1	-	$C_5H_5Fe^+$	121	7.5	4.7
$C_{10}H_8^+$	128	1.3	-	$C_5H_4Fe^+$	120	1.8	3.7
$C_5H_5Fe^+$	121	4.8	-	$C_9H_7^+$	115	2.4	2.3
$C_6H_5C_3H_2^+$	115	2.6	-	$C_3H_3Fe^+$	95	1.5	-
$C_6H_5CO^+$	105	1.3	17.1	$C_3H_2Fe^+$	94	1.7	-
$C_3H_2Fe^+$	94	1.3	-	$C_5H_4CO^+$	91	-	4.7
C_2HFe^+	81	1.4	-	$C_5H_4CO^+$			
$C_6H_5^+$	77	3.5	-	$H_2FeOCH_3^+$	90	-	6.3
Fe^+	56	7.2	4.7	C_2HFe^+	89	-	5.4
				$C_6H_7^+$	81	2.0	-
					79	-	8.0
				$C_6H_6^+$	78	100.0	23.6
				$C_6H_5^+$	77	-	6.7
				$FeOH^+$	73	13.4	5.6
				$C_5H_5^+$	65	1.8	2.9
				$C_5H_3^+$	63	-	3.3
				Fe^+	56	8.9	6.2

Table IX(cont.)

1,1'-diacetylferrocene				1,1'-dimethylferrocenedicarboxylate			
		EI	FAB			EI	FAB
Ions	m/z	r.abd	r.abd	Ions	m/z	r.abd	r.abd
$(M+H)^+$	271	-	59.7	M^+	302	100.0	100.0
M^+	270	100.0	100.0	$(M-OCH_3)^+$	271	5.2	30.4
$(M-CH_3)^+$	255	3.8	2.1	$(M-CH_2)^+$	288	-	2.3
$(M-HCO)^+$	241	-	2.0	$(M-2OCH_3)^+$	240	-	1.2
$(M-COCH_2)^+$	228	-	9.6	$C_5H_4COOCH_3FeOCH_3^+$	210	1.9	-
$(M-COCH_3)^+$	227	9.2	-	$C_5H_4COOCH_2FeOCH_2^+$	208	-	2.0
$(M-COCH_3-CO)^+$	199	21.1	3.9	$C_5H_4COOCH_3FeH^+$	180	19.4	4.7
$(C_5H_5)_2Fe^+$	186	-	4.7	$C_5H_4COOCH_3Fe^+$	179	-	4.6
$C_{10}H_8Fe^+$	184	2.9	-	$C_5H_4COOFeH^+$	165	-	7.3
$C_5H_4COCH_3FeOH^+$	180	-	4.5	$C_5H_5FeOCH_3^+$	152	18.2	1.9
$C_5H_4COCH_3FeO^+$	179	-	2.8	$C_5H_4COFeH^+$	149	6.0	4.8
$C_6H_4COFeOH^+$	165	-	2.9	$C_5H_4COFe^+$	148	4.3	-
$C_5H_4COCH_3Fe^+$	163	10.9	12.1	$C_5H_4FeO^+$	136	-	5.3
$C_5H_4COCH_2Fe^+$	162	-	2.8	$C_5H_5FeH^+$	122	15.5	5.2
$C_5H_4COFe^+$	148	3.0	-	$C_5H_5Fe^+$	121	13.0	3.4
$C_5H_4FeO^+$	136	-	5.9	$C_5H_4Fe^+$	120	4.8	5.2
$C_5H_4FeCH_2^+$	134	-	2.1	$C_6H_5CO^+$	105	-	2.6
$C_5H_5Fe^+$	121	6.8	4.1	$C_3H_3Fe^+$	95	2.7	-
$C_5H_4Fe^+$	120	6.8	2.6	$C_3H_2Fe^+$	94	3.2	-
$C_3H_2Fe^+$	94	4.5	-	$C_5H_4COH^+$	93	5.2	2.2
$C_5H_4CO^+$	91	-	2.6	$C_5H_4CO^+$	92	12.1	5.9
$C_5H_3CO^+$	90	-	3.5	$C_5H_3CO^+$	90	-	2.9
$CH_3OFeH_2^+$	89	-	2.2	$CH_3OFeH_2^+$	89	-	2.7
C_2HFe^+	81	2.6	-	CH_3OFe^+	87	2.2	-
$FeOH^+$	73	-	2.2	$C_5H_5^+$	65	3.2	4.7
$FeCH_3^+$	71	11.4	4.6	$C_5H_4^+$	64	3.7	-
Fe^+	56	14.1	6.5	Fe^+	56	15.7	6.3

Table IX(cont.)

1,1'-dibenzoylferrocene				1,1'-bis(diphenylphosphino)ferrocene			
		EI	FAB			EI	FAB
Ions	m/z	r.abd	r.abd	Ions	m/z	r.abd	r.abd
$(M{\cdot}NBA\text{-}C_5H_4\text{-}2OH)^+$	449	-	2.1	$(M{\cdot}NBA+H)^+$	708	-	9.1
M^+	394	100.0	100.0	$(M{\cdot}NBA\text{-}CH)^+$	692	-	5.8
$(M\text{-}O)^+$	378	-	2.6	$(M{\cdot}NBA\text{-}CH_2)^+$	691	-	11.4
$(M\text{-}CO)^+$	366	0.2	-	$(M{\cdot}NBA\text{-}CH_3)^+$	690	-	5.5
$(M\text{-}2CO+2H)^+$	340	1.0	-	$(M\text{-}C_6H_4+2H_2O)^+$	594	-	8.4
$(M\text{-}C_6H_5)^+$	317	-	2.2	$(M\text{-}C_5H_5+2H_2O)^+$	593	-	20.9
$C_6H_6FeC_5H_4COC_6H_5^+$	290	-	5.3	$(M{\cdot}CH_3OH+H)^+$	587	-	100.0
$C_6H_5FeC_5H_4COC_6H_5^+$	289	1.9	-	$(M{\cdot}CH_3OH)^+$	586	-	58.6
$C_6H_4FeC_5H_4C_6H_4^+$	273	1.9	-	$(M{\cdot}OH)^+$	571	-	10.6
$(M\text{-}FeC_6H)^+$	260	3.6	2.2	$(M+O)^+$	570	-	10.8
$HFeC_5H_4COC_6H_5^+$	226	-	2.0	$(M+H)^+$	555	-	5.1
$FeC_5H_4COC_6H_5^+$	225	3.0	11.6	M^+	554	14.3	8.5
$C_5H_5FeC_5H_4COH_2^+$	215	1.1	-	$(C_5H_4PPh_2FeC_5H_4Ph+NO_2+OH)^+$	509	-	5.2
$C_5H_5FeC_5H_4CO^+$	212	1.6	-	$(509\text{-}O)^+$	493	-	5.5
$C_5H_5FeC_5H_4OH_2^+$	203	1.4	-	$(M\text{-}Ph)^+$	477	1.1	-
$C_5H_5FeC_5H_4OH^+$	202	1.3	-	$C_5H_4PPh_2FeC_5H_4OH_2^+$	387	-	6.8
$C_5H_4COC_6H_5CO^+$	197	4.2	5.1	$C_5H_4PPh_2FeC_5H_4OH^+$	386	6.0	13.4
$C_5H_3COC_6H_5CO^+$	196	2.4	3.8	$(387\text{-}2H)^+$	385	-	7.1
$C_6H_6Fe{\cdot}NO_2^+$	180	-	8.3	$C_5H_5FeC_5H_4PPh_2^+$	370	75.9	-
$C_9H_6Fe^+$	170	1.3	-	$HOFeC_5H_4PPh_2^+$	322	-	9.7
$C_6H_5C_5H_4^+$	141	5.0	4.7	$OFeC_5H_4PPh_2^+$	321	2.1	57.0
$H_2FeC_5H_4OH^+$	139	1.6	-	$FeC_5H_4PPh_2^+$	305	-	9.4
$C_6H_5FeH_2^+$	135	-	3.5	$C_5H_5FeC_5H_4PPh^+$	293	15.9	-
$C_6H_5Fe^+$	133	11.5	9.6	$C_5H_4PPh_2{\cdot}H_2O^+$	267	-	9.8
$C_6H_5C_3H_2^+$	115	3.1	-	$C_5H_5FeC_5H_4Ph^+$	262	5.4	-
$C_6H_5CO^+$	105	6.6	64.6	$C_5H_5FePHPh^+$	230	25.0	10.1
$C_3H_2Fe^+$	94	1.0	-	$C_6H_4FeC_5H_3P^+$	226	6.7	-
$C_6H_5^+$	77	4.7	-	Ph_2PO^+	201	-	5.5
Fe^+	56	4.5	8.2	$C_5H_4FeC_6H_5^+$	197	-	6.2

Table IX(cont.)

1,1'-bis(diphenylphosphino)ferrocene **(continued from page 143)**

		EI	FAB
Ions	**m/z**	**r.abd**	**r.abd**
$(C_5H_5)_2Fe^+$	186	4.2	6.2
$C_5H_5FeC_5H_4^+$	185	7.3	-
$C_5H_4FeC_5H_4^+$	184	2.3	-
$C_5H_4FeC_5H_3^+$	183	6.5	-
$C_5H_4PC_6H_5^+$	171	13.2	-
$C_5H_3PC_6H_4^+$	170	12.0	-
$C_6H_5PFeH^+$	165	6.0	-
$C_5H_5FeOH^+$	138	26.6	-
$C_6H_5Fe^+$	133	7.1	-
$C_{10}H_9^+$	129	3.9	-
$C_{10}H_8^+$	128	5.1	-
$C_{10}H_7^+$	127	2.1	-
$C_5H_5Fe^+$	121	22.7	-
$C_6H_5C_3H_2^+$	115	7.4	-
$C_6H_4P^+$	107	5.0	-
$C_5H_4P^+$	95	3.8	-
$C_5H_3P^+$	94	4.8	-
$C_5H_2P^+$	93	2.2	-
$C_6H_5CH_3^+$	92	6.0	-
$C_6H_5CH_2^+$	91	2.2	-
$FePH^+$	88	100.0	-
C_2HFe^+	81	6.8	-
$FeOH^+$	73	9.1	-
FeH_2^+	58	71.8	-
Fe^+	56	29.8	-

3.2.2. Fragmentation Mechanism Studies

Schemes 41-54 are the detailed fragmentation patterns of the ferrocenes in Table II under EI. Schemes 55-66 are the +ve FAB fragmentation patterns of those ferrocenes which can produce good +ve FAB spectra in NBA matrix. For comparison, Scheme 68 shows the fragmentation patterns of ferrocenecarboxaldehyde/NBA under CA positive ion FAB with helium as the collisional gas. In all of these schemes, solid line transitions are verified with linked scans (B/E, B^2/E and $B^2(1-E)/E^2$). The dotted line transitions are not certified by these experiments. In all of the transitions, the lost part is a neutral molecule or a neutral radical, whose formula can be directly derived from the precursor ion(s).

The EI schemes show that most of the major fragment peaks in their EI spectra are direct products of molecular ion decomposition. This fact indicates that unimolecular reaction is the dominant reaction form under EI conditions. Few of intense fragment peaks come from the decomposition of other fragment peaks. Some rearrangement peaks are also observed in these schemes.

Among this group of ferrocenes, the fragmentation patterns of $(C_5H_5)_2Fe$, $C_5H_5FeC_5H_4CHO$, $C_5H_5FeC_5H_4CH_2OH$, $C_5H_5FeC_5H_4COCH_3$, $C_5H_5FeC_5H_4COOH$, $C_5H_5FeC_5H_4COC_6H_5$, $(C_5H_4COCH_3)_2Fe$ and $(C_5H_4COOH)_2Fe$ under EI have been studied previously [69, 74, 89, 99, 100]. Good agreement between this study and those previous studies has been reached. However, some minor differences are also observed. Compared with Innorta et al.'s fairly simple decomposition modes [89] in the second field free region under EI with a Finnigan-MAT 112S mass spectrometer, more complex fragmentation patterns are observed for $C_5H_5FeC_5H_4CHO$, $C_5H_5FeC_5H_4CH_2OH$, $C_5H_5FeC_5H_4COCH_3$, $C_5H_5FeC_5H_4COOH$, and $C_5H_5FeC_5H_4COC_6H_5$ in our experiments in the first field free region. All of the detailed fragmentation patterns are shown in Schemes 41-43, 45-46, 48, 50-51. The differences may come from the fact that

different field free regions and a different mass spectrometer are used in the studies.

For $C_5H_5FeC_5H_4CH_2CN$, $C_5H_5FeC_5H_4CH_2COOH$, $(C_5H_4CH_2OH)_2Fe$, $(C_5H_4COOCH_3)_2Fe$, $(C_5H_4COC_6H_5)_2Fe$ and $(C_5H_4PPh_2)_2Fe$, to my knowledge, their EI mass spectra and fragmentation patterns have not been previously published, even though these compounds are the most accessible ferrocene derivatives. The EI and FAB spectral data of these compounds are presented in Table IX. The detailed fragmentation patterns are shown in Schemes 44, 47, 49, 52-54. Unlike the other schemes, the metastable ion studies of $(C_5H_4PPh_2)_2Fe$ under EI only provide limited information on the generation of fragment peaks due to deliquescence of the sample.

All of the +ve FAB schemes give more detailed fragmentation patterns than their EI counterparts. More low mass range peaks are generated in +ve FAB linked scans than in EI mode. Like the EI schemes, most of the major fragment peaks in +ve FAB spectra are direct products of molecular ion decomposition. However, more rearrangement peaks are observed in +ve FAB schemes. The more detailed fragmentation patterns of ferrocenes in +ve FAB further indicate utilities of +ve FAB ionization for this group of compounds.

The following discussion will focus on the more detailed fragmentation patterns of two groups of compounds in EI linked scans and +ve FAB linked scan experiments.

(1) $C_5H_5FeC_5H_4R$ (R= CHO, CH_2OH, CH_2CN, $COCH_3$, COOH, CH_2COOH, COC_6H_5)

The EI linked scan studies (Schemes 42-48) of this group of monosubstituent ferrocenes show that most of the intense peaks, (e.g. $C_5H_5Fe^+$, $(C_5H_5)_2Fe^+$, $C_5H_5FeOH^+$, $C_5H_5FeCN^+$) in the normal EI spectra are the direct products of molecular ions decomposition in the first field free region. Most of the sub-fragment peaks are the products of fragment peaks decomposition. This suggests that decomposition is the major form of reaction under EI. Typical rearrangement peaks, such as $C_5H_5FeOH^+$ (Schemes 43,45-46), $C_5H_5FeCN^+$ (Scheme 44), C_3HFePh^+ (Scheme 48), are observed. The peaks

with loss of a C_5H_5 group from the molecular ion are found in Scheme 45 of $C_5H_5FeC_5H_4COCH_3$ ($FeC_5H_4COCH_3^+$), Scheme 46 of $C_5H_5FeC_5H_4COOH$ ($FeC_5H_4COOH^+$), Scheme 47 of $C_5H_5FeC_5H_4CH_2COOH$ ($FeC_5H_4CH_2COOH^+$), and Scheme 48 of $C_5H_5FeC_5H_4COC_6H_5$ ($FeC_5H_4COPh^+$). No Fe^+ ions are observed in these linked scan spectra. The mechanism of decomposition and rearrangement of these compounds is similar to the previous discussion and the literature reports.

In the +ve FAB linked scan studies (Schemes 55-61) of these compounds, like the EI studies, most of the intense peaks in their normal +ve FAB spectra are the direct products of molecular ion decomposition. Compared with the EI studies, the +ve FAB schemes show that more fragment peaks come from molecular ion decomposition in the first field free region. All of the molecular ions give out $(C_5H_5)_2Fe^+$, $C_5H_5Fe^+$ (but $C_5H_5FeC_5H_4CH_2COOH$, $C_5H_5FeC_5H_4COPh$), Fe^+ (but $C_5H_5FeC_5H_4CH_2COOH$, $C_5H_5FeC_5H_4COPh$) as the direct decomposition product. Rearrangement peaks, like $(M\text{-}H_2O)^+$, $C_5H_2FeO^+$, $C_5H_4FeO^+$ (Scheme 55), $(M\text{-}H_2O)^+$, $FeOH^+$, $C_5H_5FeOH^+$, $C_5H_5FeCHOH^+$, $Fe(OH)_2^+$ (Scheme 56), $(M\text{-}NH_3)^+$, $C_5H_5FeCN^+$, $C_5H_3FeCN^+$ (Scheme 57), $C_5H_5FeOHCH_3^+$, $C_5H_5FeOH^+$, $FeCH_3^+$ (Scheme 58), $C_5H_5FeOH^+$, $FeOH^+$, $C_5H_4FeO^+$, H_2OFeOH^+, C_5HFeCO^+ (Scheme 59), $(M\text{-}H_2O)^+$, $C_5H_4CH_2FeOH^+$, $C_5H_5FeOH^+$, $FeOH^+$ (Scheme 60), $(M\text{-}H_2O)^+$, $C_5H_5FePh^+$, $C_5H_4FeO^+$, $FeC_6H_6^+$, $C_5H_4OFe^+$ (Scheme 61), are common. The peaks with loss of a C_5H_5 group from the molecular ion are found in Scheme 56 ($FeC_5H_4CH_2OH^+$), Scheme 58 ($FeC_5H_4COCH_3^+$), Scheme 59 ($FeC_5H_4COOH^+$), Scheme 60 ($FeC_5H_4CH_2COOH^+$), Scheme 61 ($FeC_5H_4COPh^+$). The +ve FAB schemes provide more detailed information on fragmentation patterns, especially the generation information of certain ions, such as $FeOH^+$, Fe^+, $FeCH_3^+$ and $FeC_6H_6^+$, etc. Fe^+ ions, which are not found in the EI schemes, but are observed in all of the +ve FAB schemes. This indicates that the +ve FAB linked scan techniques are very useful to study the formation of low mass fragment peaks.

(2) $(C_5H_4R)_2Fe$ (R = CH_2OH, $COCH_3$, $COOCH_3$, COC_6H_5)

For this group of disubstituent ferrocenes, the EI linked scan studies (Schemes 49-50, 52-53) still show that most of the intense peaks come from molecular ion direct decomposition. However, in these schemes, no $(C_5H_5)_2Fe^+$ peaks are found. $C_5H_5Fe^+$ ions are only observed in Scheme 49 of $(C_5H_4CH_2OH)_2Fe$ and Scheme 50 of $(C_5H_4COCH_3)_2Fe$. Only in Scheme 47, peaks with loss of a ligand group from molecular ion do not show up. Rearrangement peaks are observed as $C_5H_4CH_2OHFeOH^+$, $(M-H_2O)^+$ (Scheme 49), $HFeC_5H_5^+$, $(180-H_2O)^+$, $(180-CO-H_2O)^+$ (Scheme 52).

The +ve FAB linked scan studies (Schemes 62-65) of these compounds indicate that no $(C_5H_5)_2Fe^+$ ions are the direct product of molecular ion decomposition in the first field free region, although most of the intense peaks also come from the decomposition. $C_5H_5Fe^+$ ions are observed in Scheme 63 of $(C_5H_4COCH_3)_2Fe$ and Scheme 64 of $(C_5H_4COOCH_3)_2Fe$. Rearrangement peaks are found as: $C_5H_4CH_2OHFeOH^+$, $C_5H_4FeO^+$, $C_5H_5FeH^+$, $FeOH^+$ (Scheme 62), $C_5H_4COCH_3FeOH^+$, $FeCH_3^+$ (Scheme 63), $C_5H_4COOCH_3FeH^+$, $C_5H_5FeOCH_3^+$ (Scheme 64), and $C_5H_4COC_6H_5FeOH^+$, $FeC_6H_5^+$ (Scheme 65). Fe^+ ions show up in Schemes 62-63. Peaks with loss of a ligand group from the molecular ion are observed as $C_5H_4COCH_3Fe^+$ (Scheme 63), $(M-C_5H_4COC_6H_5)^+$ (Scheme 65).

*Note: text continues on page 175.

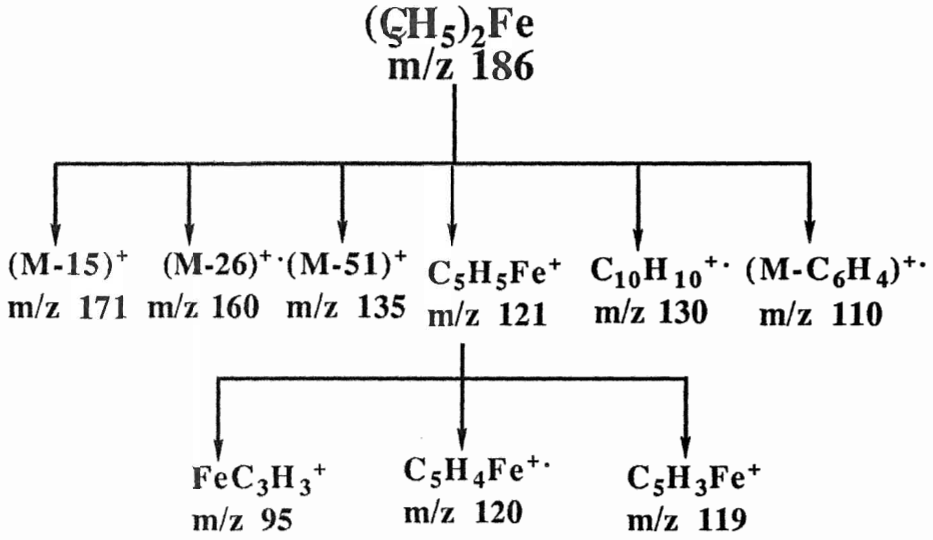

SCHEME 41 Fragmentation pattern of ferrocene under +EI

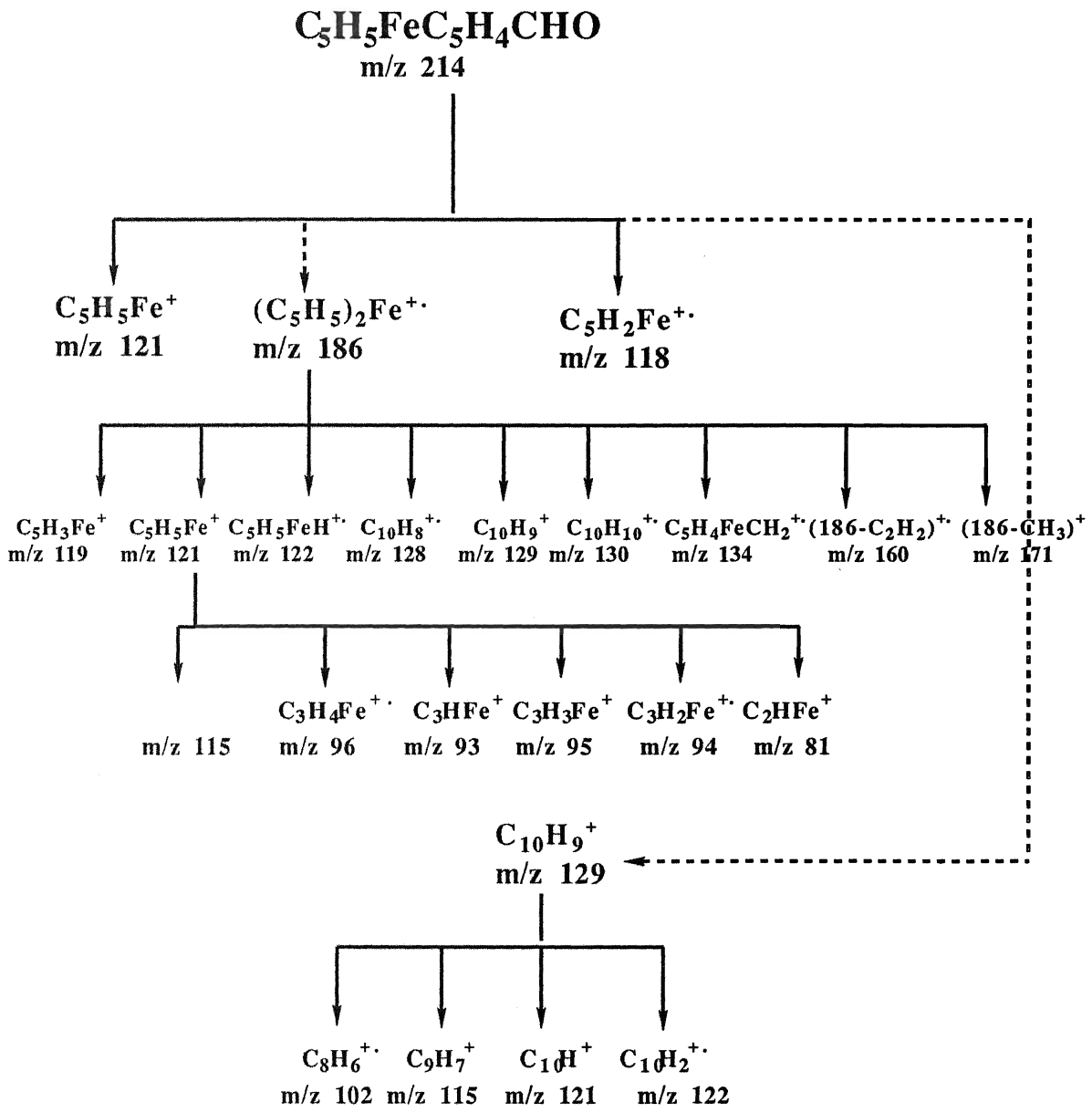

SCHEME 42 Fragmentation pattern of ferrocenecarboxaldehyde under EI

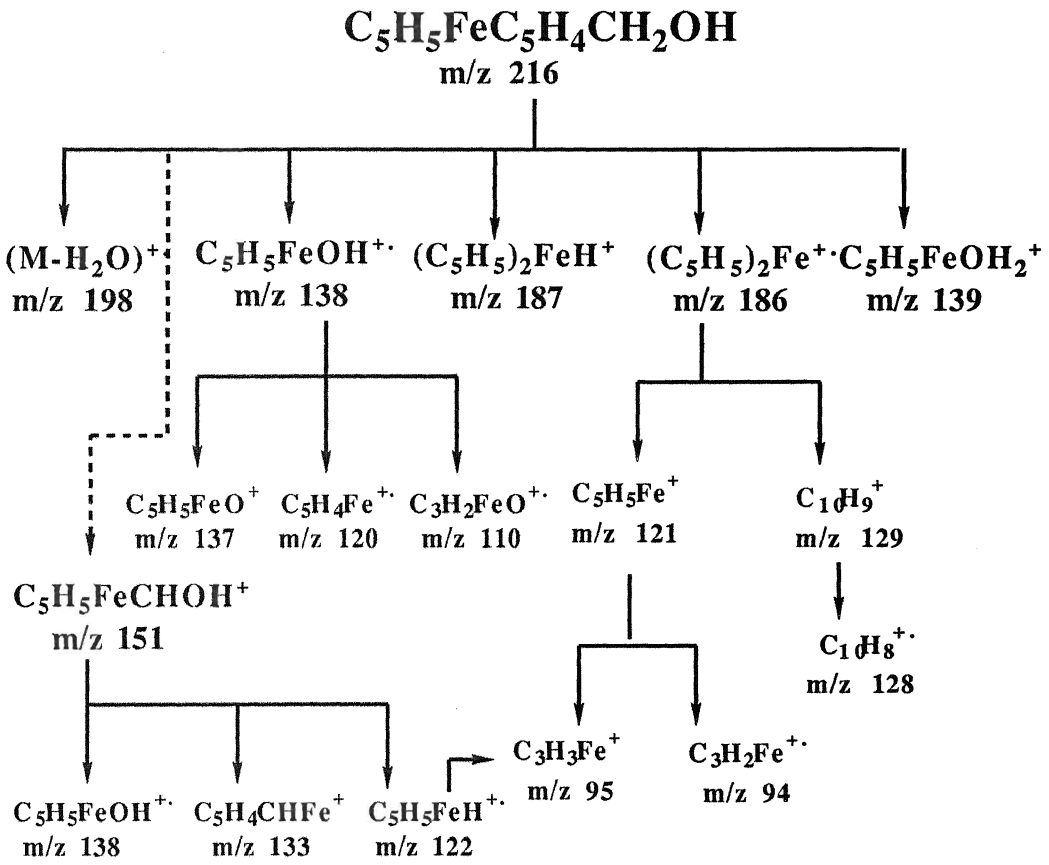

SCHEME 43 Fragmentation pattern of ferrocenemethanol under EI

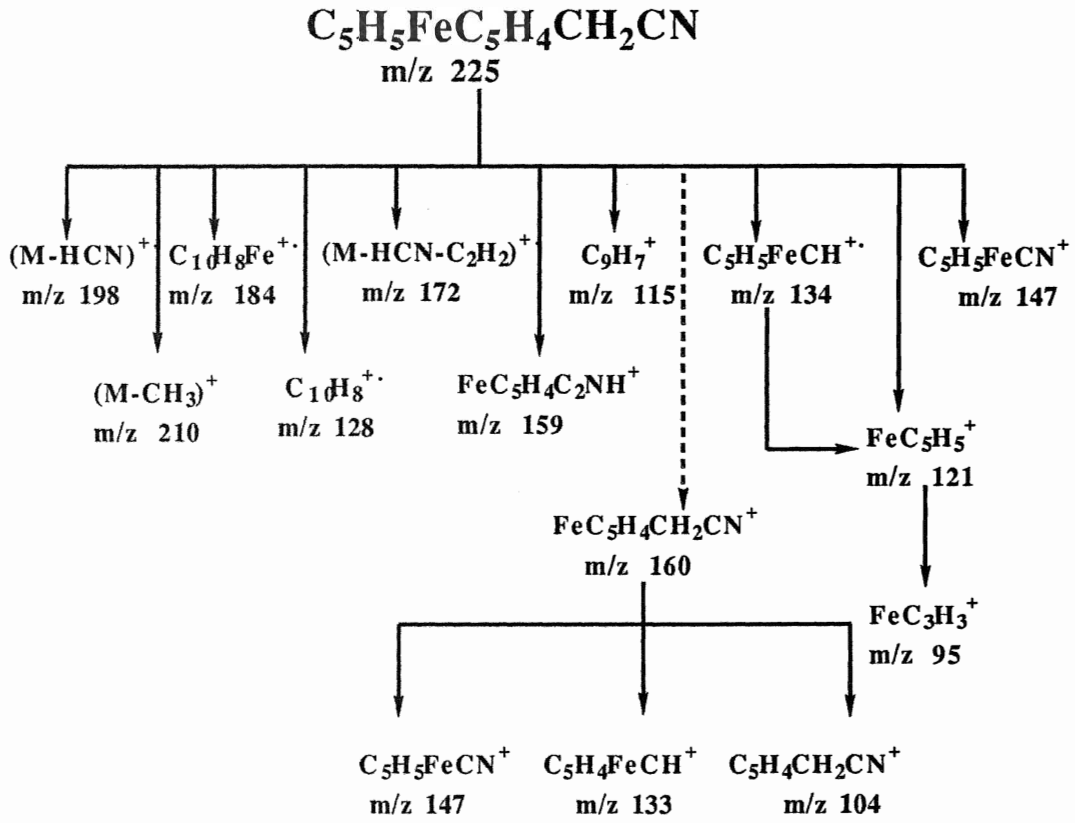

SCHEME 44 Fragmentation pattern of ferroceneacetonitrile under EI

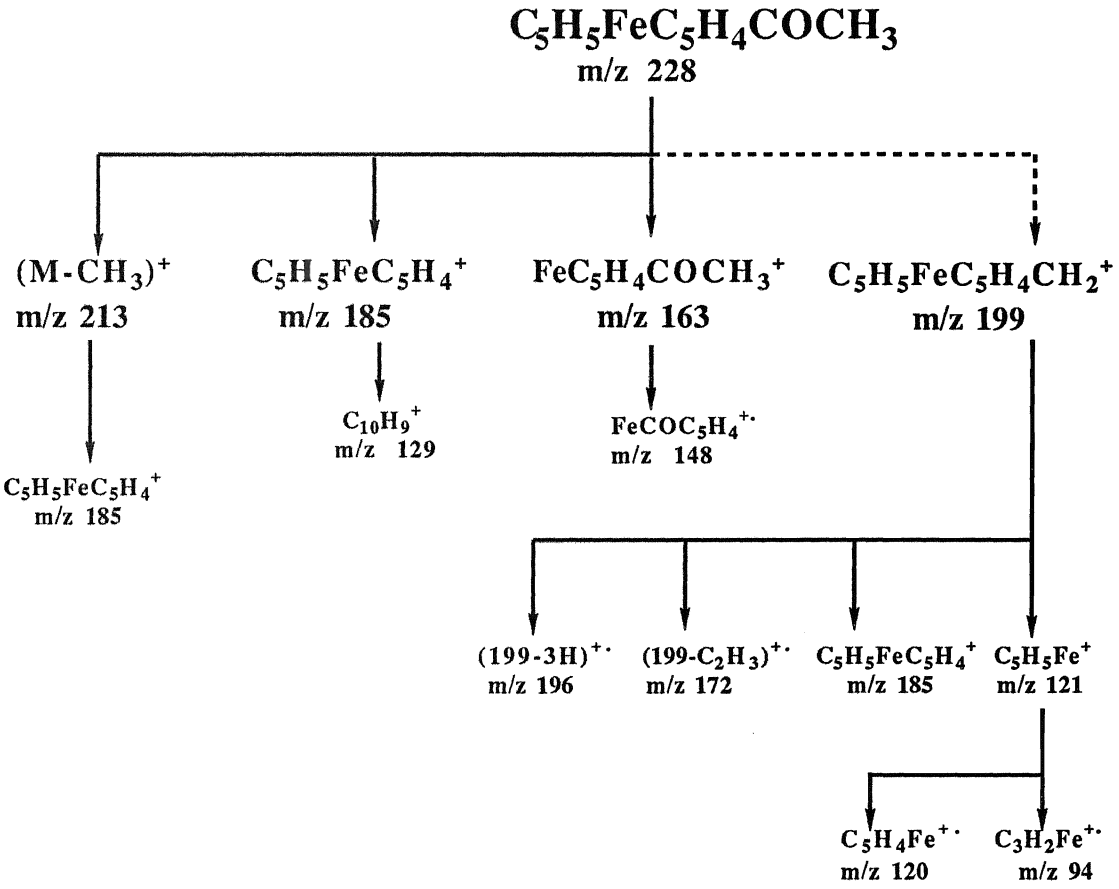

SCHEME 45 Fragmentation pattern of acetylferrocene under EI

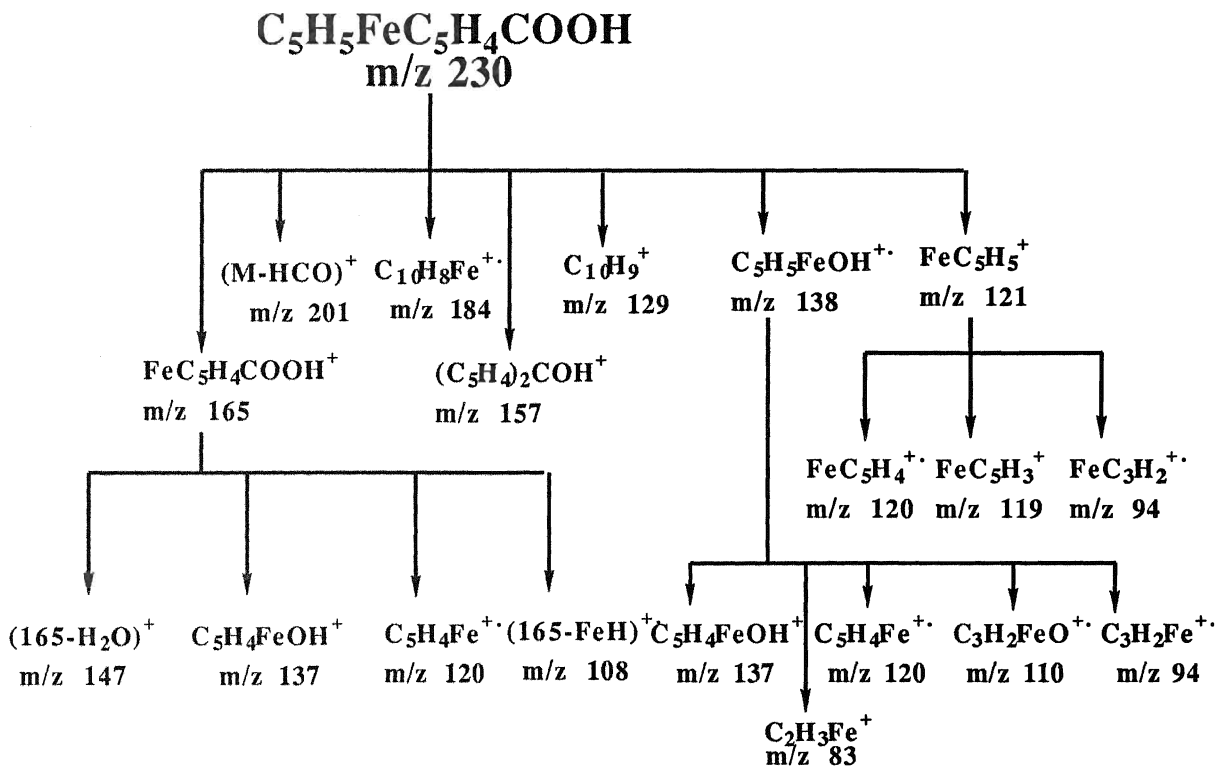

SCHEME 46 Fragmentation pattern of ferrocenecarboxylic acid under EI

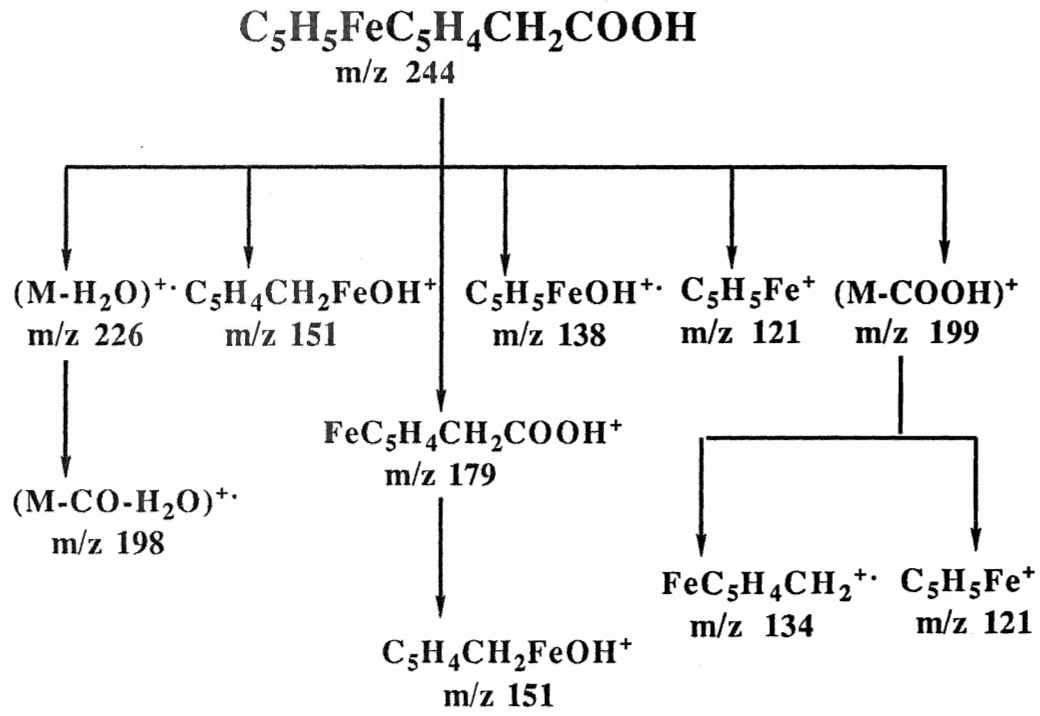

SCHEME 47 Fragmentation pattern of ferroceneacetic acid under EI

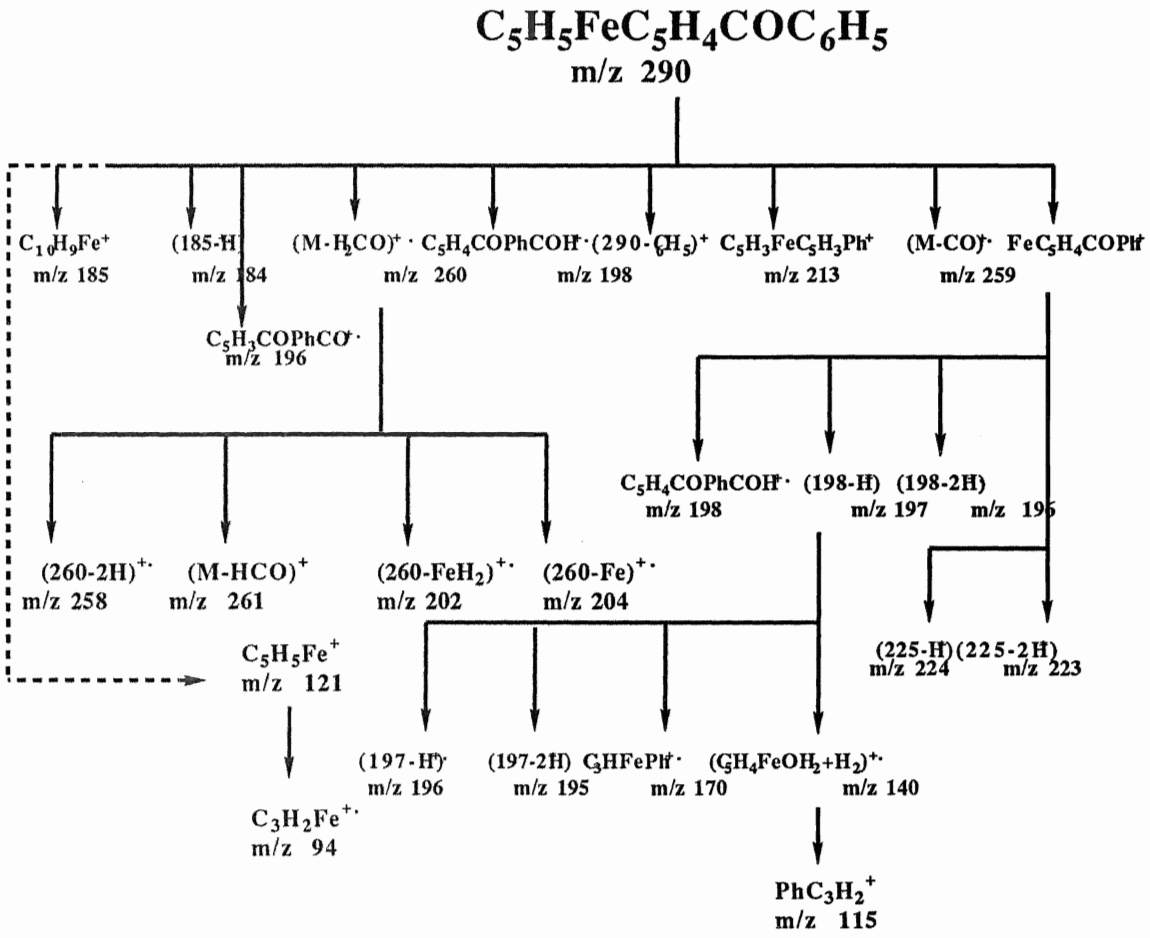

SCHEME 48 Fragmentation pattern of benzoyferrocene under EI

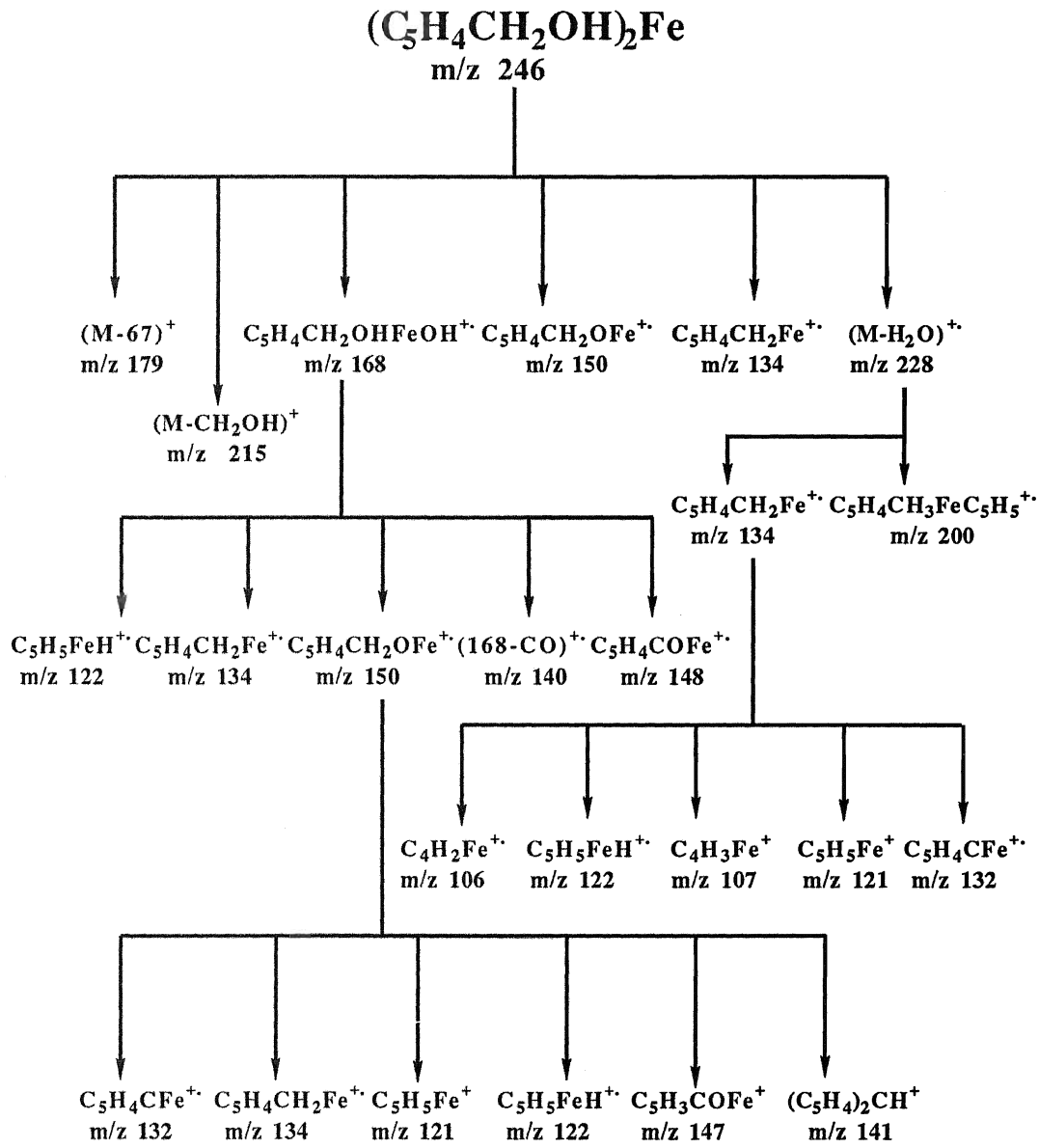

SCHEME 49 Fragmentation pattern of 1,1'-ferrocenedimethanol under EI

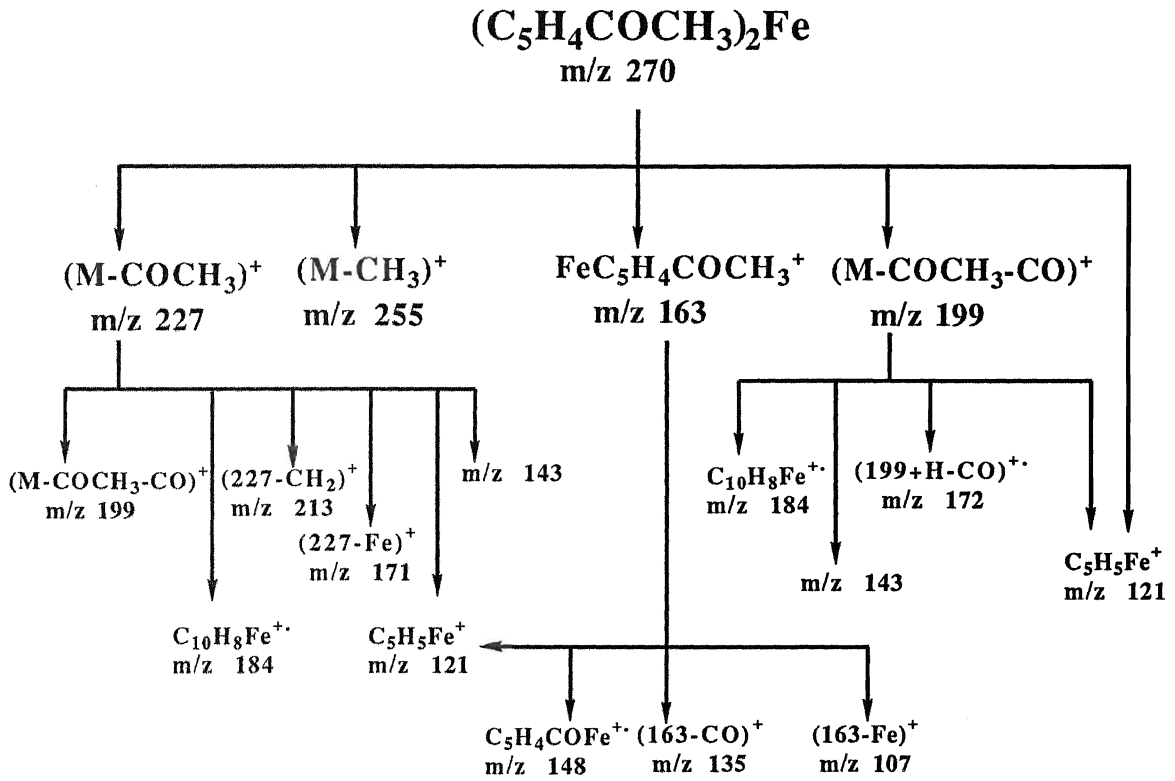

SCHEME 50 Fragmentation pattern of 1,1'-diacetylferrocene under +EI

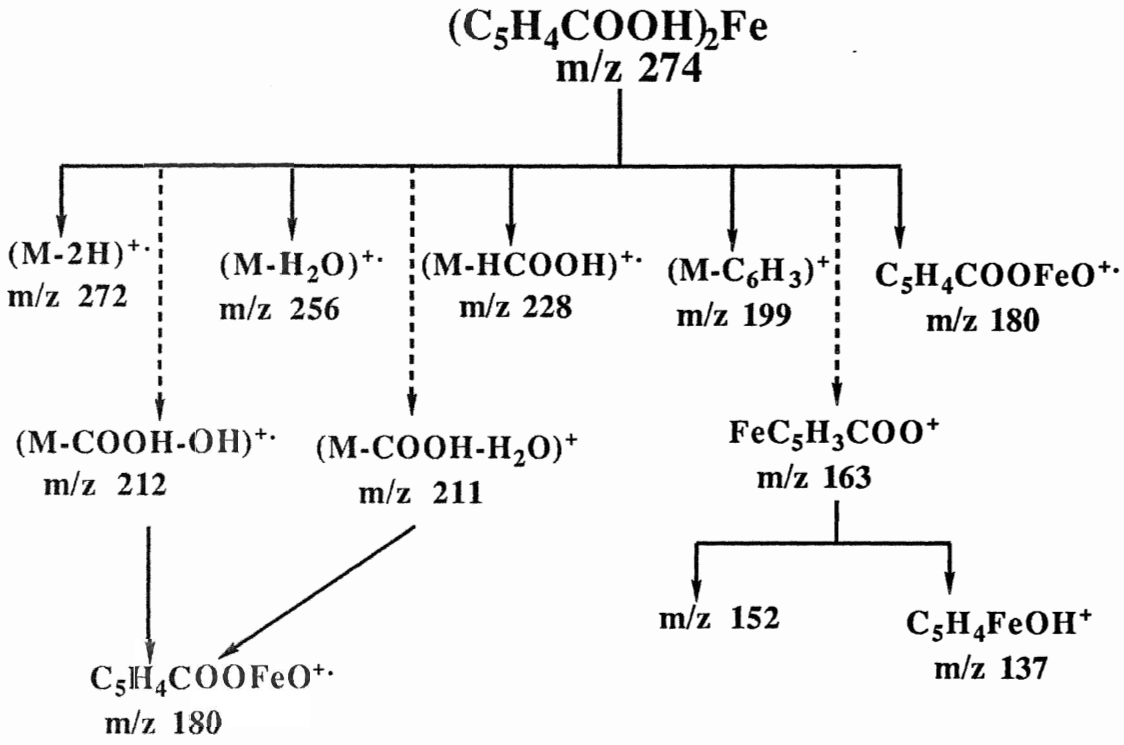

SCHEME 51 Fragmentation pattern of 1,1'-ferrocenedicarboxylic acid under EI

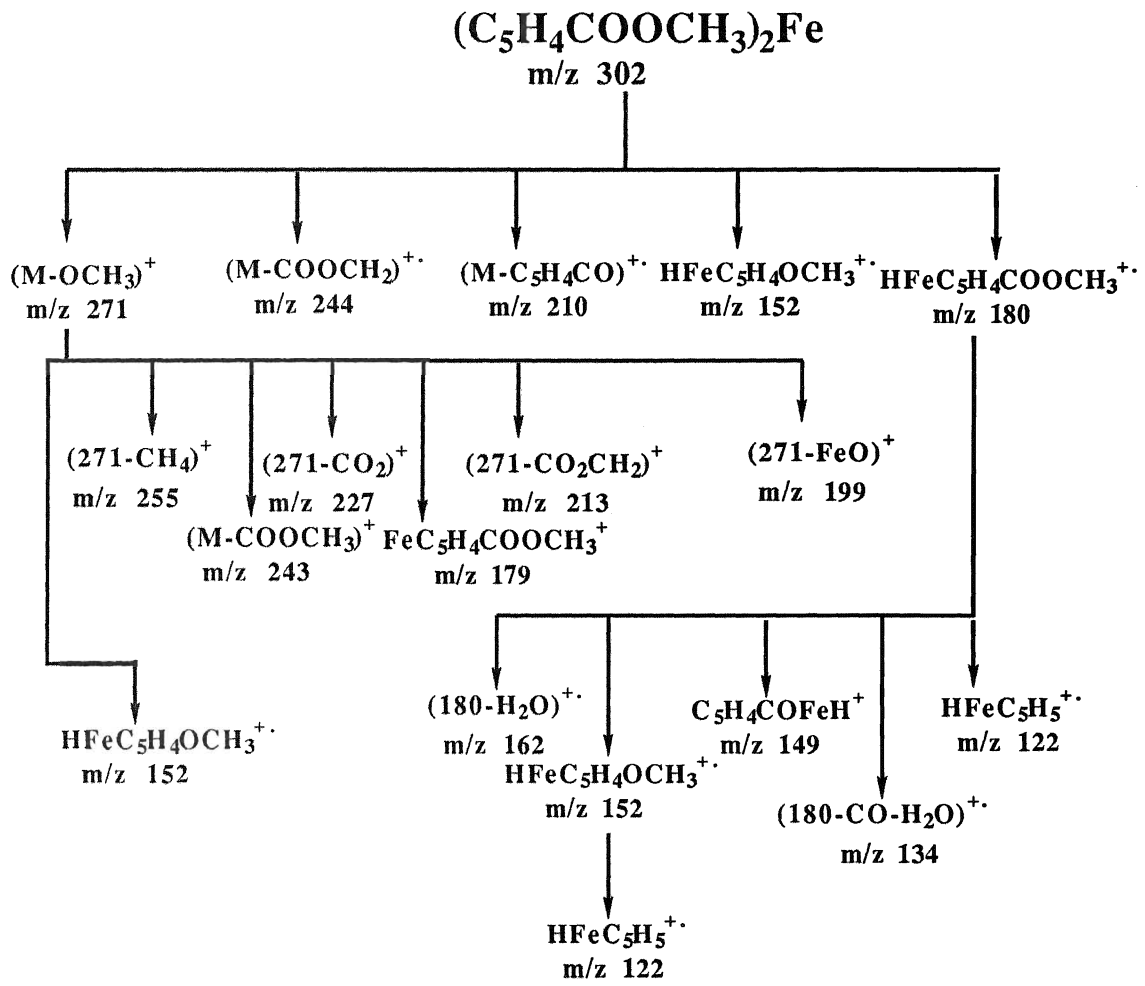

SCHEME 52 Fragmentation pattern of 1,1'-dimethylferrocenedicarboxylate under EI

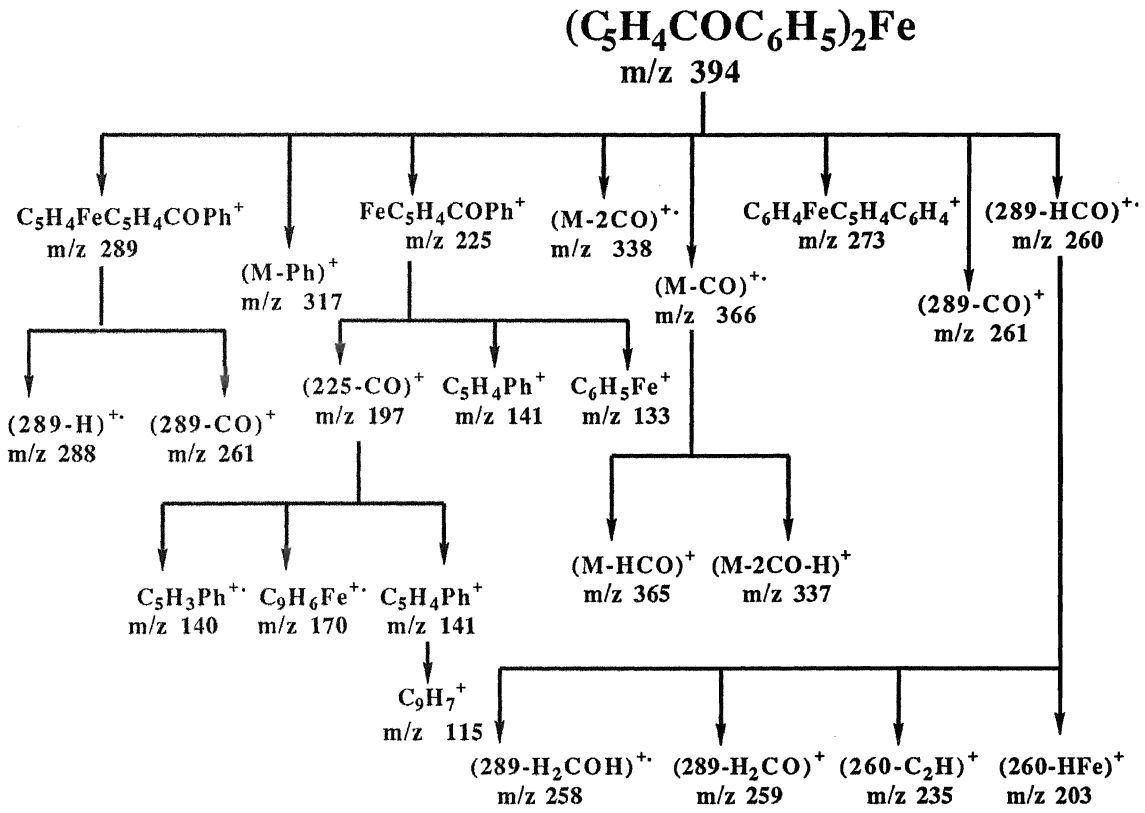

SCHEME 53 Fragmentation pattern of 1,1'-dibenzoylferrocene under EI

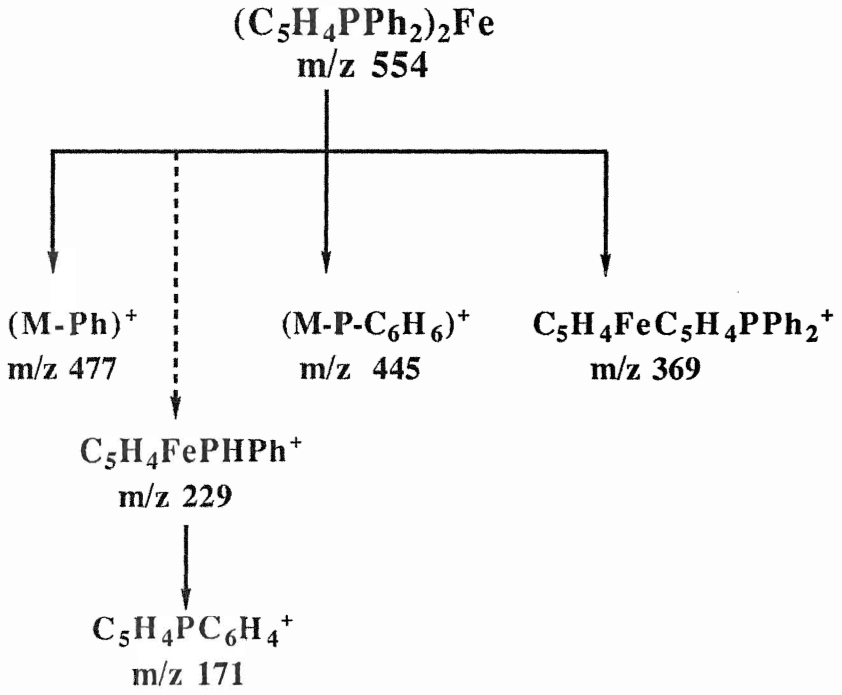

SCHEME 54 Fragmentation pattern of 1,1'-bis(diphenylphosphino)-ferrocene under EI

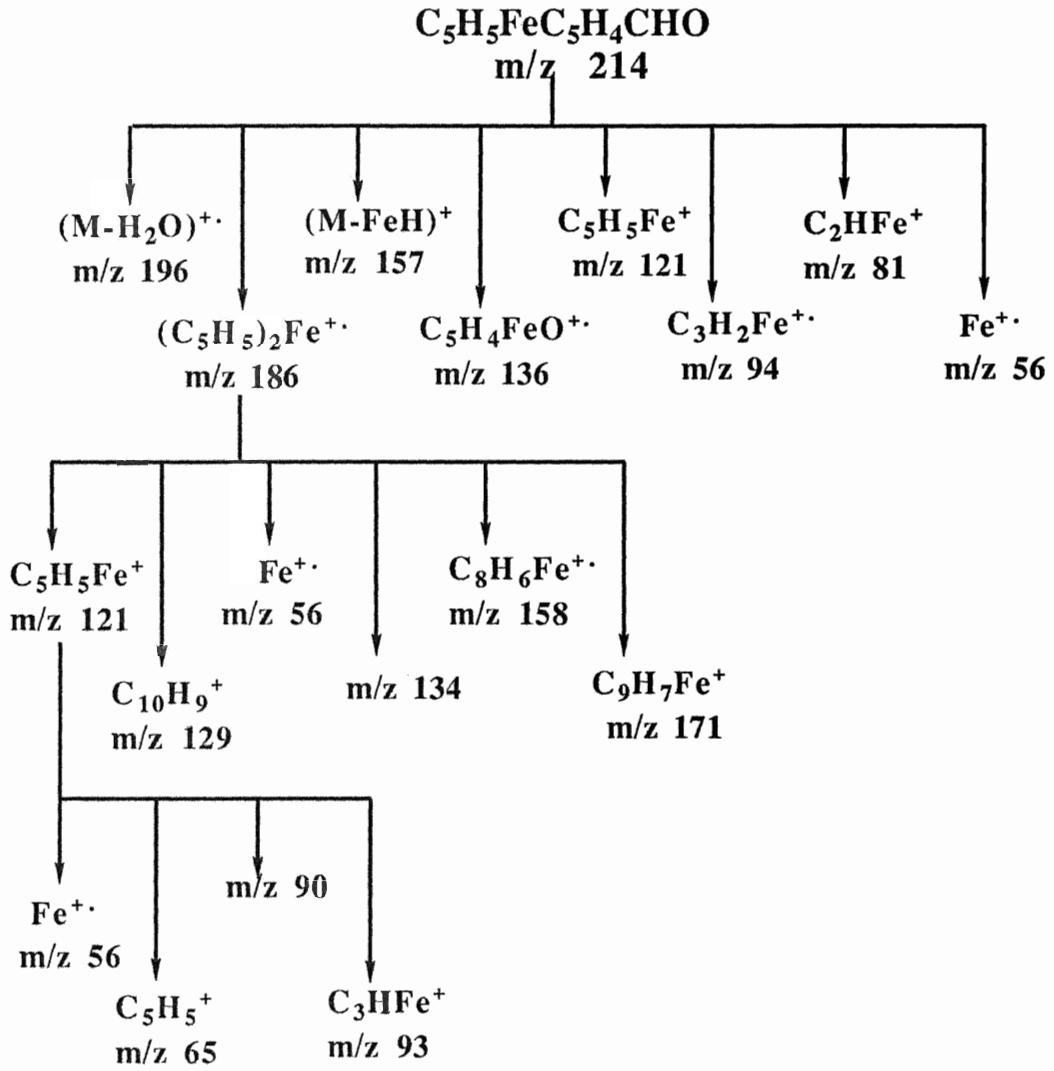

SCHEME 55 Fragmentation pattern of ferrocenecarboxaldehyde/NBA under positive ion FAB

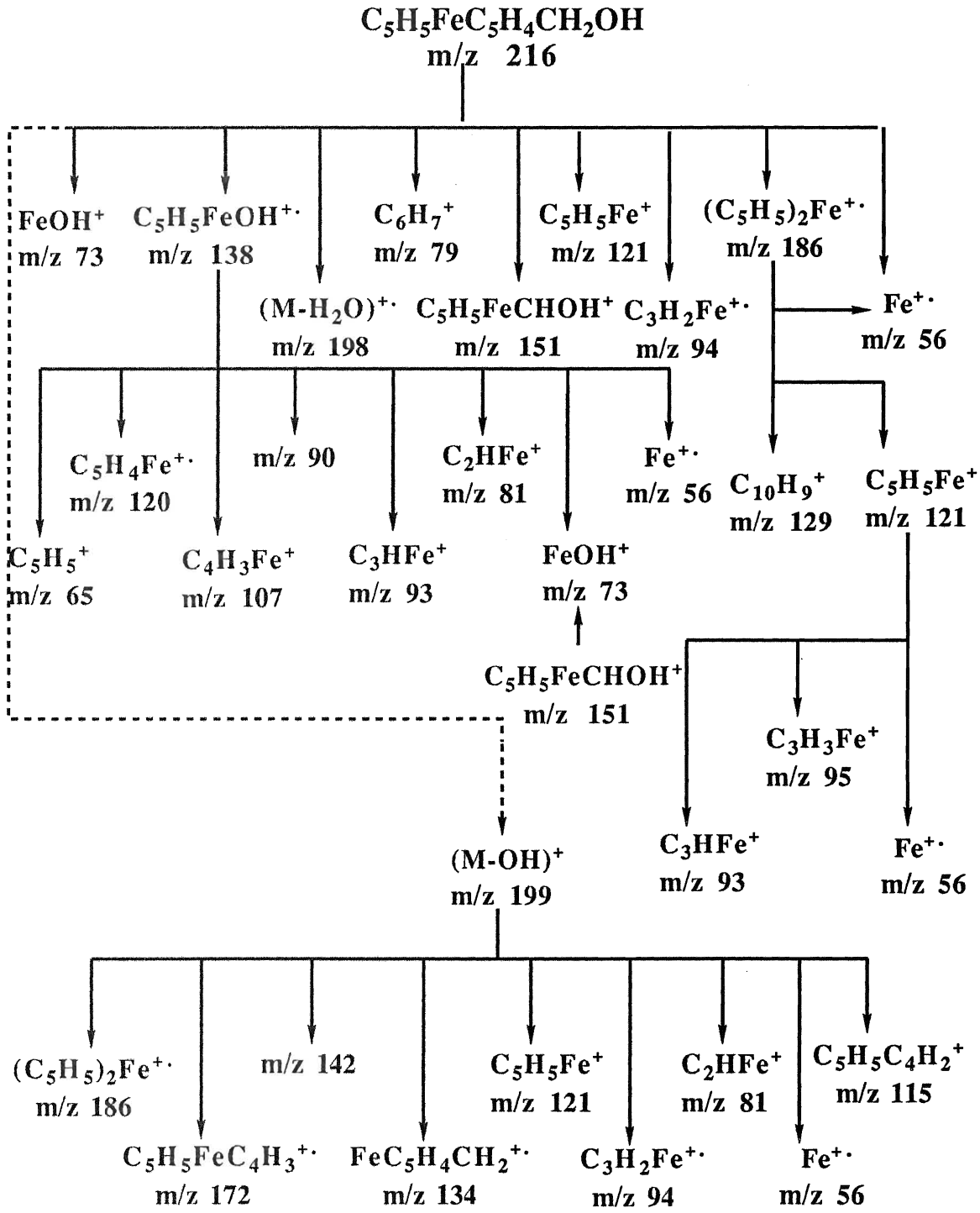

SCHEME 56 Fragmentation pattern of ferrocenemethanol/NBA under positive ion FAB

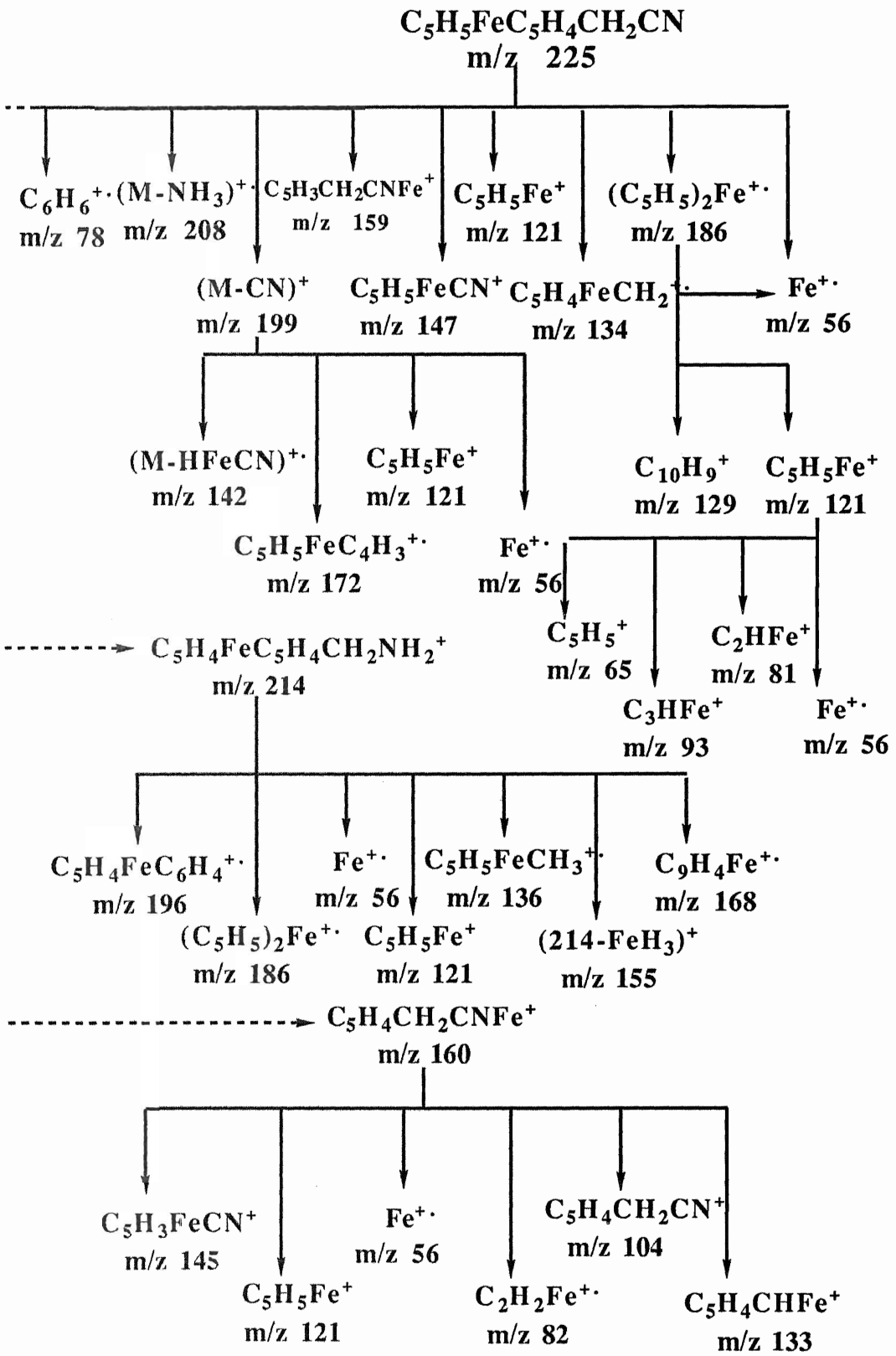

SCHEME 57 Fragmentation pattern of ferroceneacetonitrile/NBA under positive ion FAB

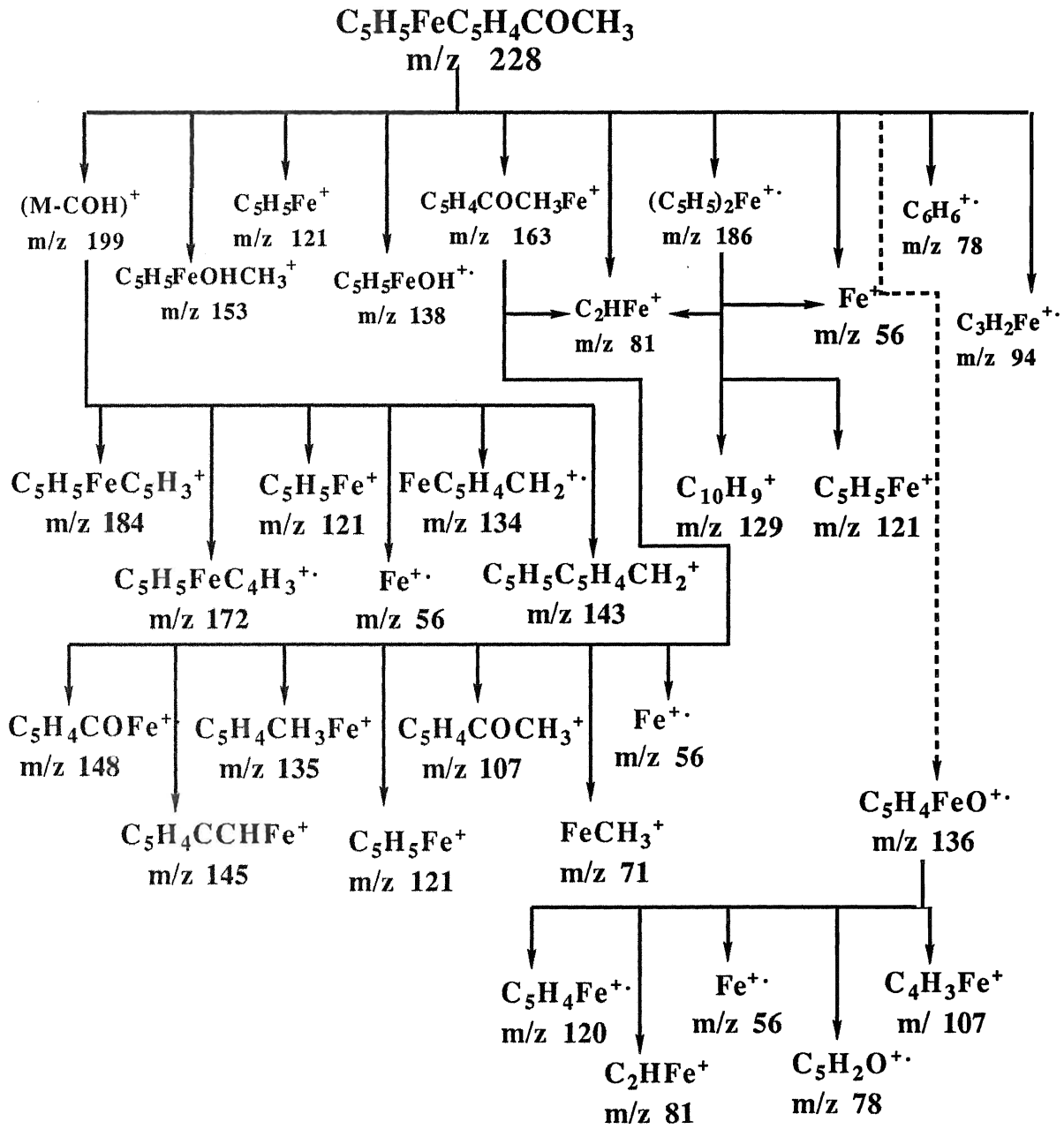

SCHEME 58 Fragmentation pattern of acetylferrocene/NBA under positive ion FAB

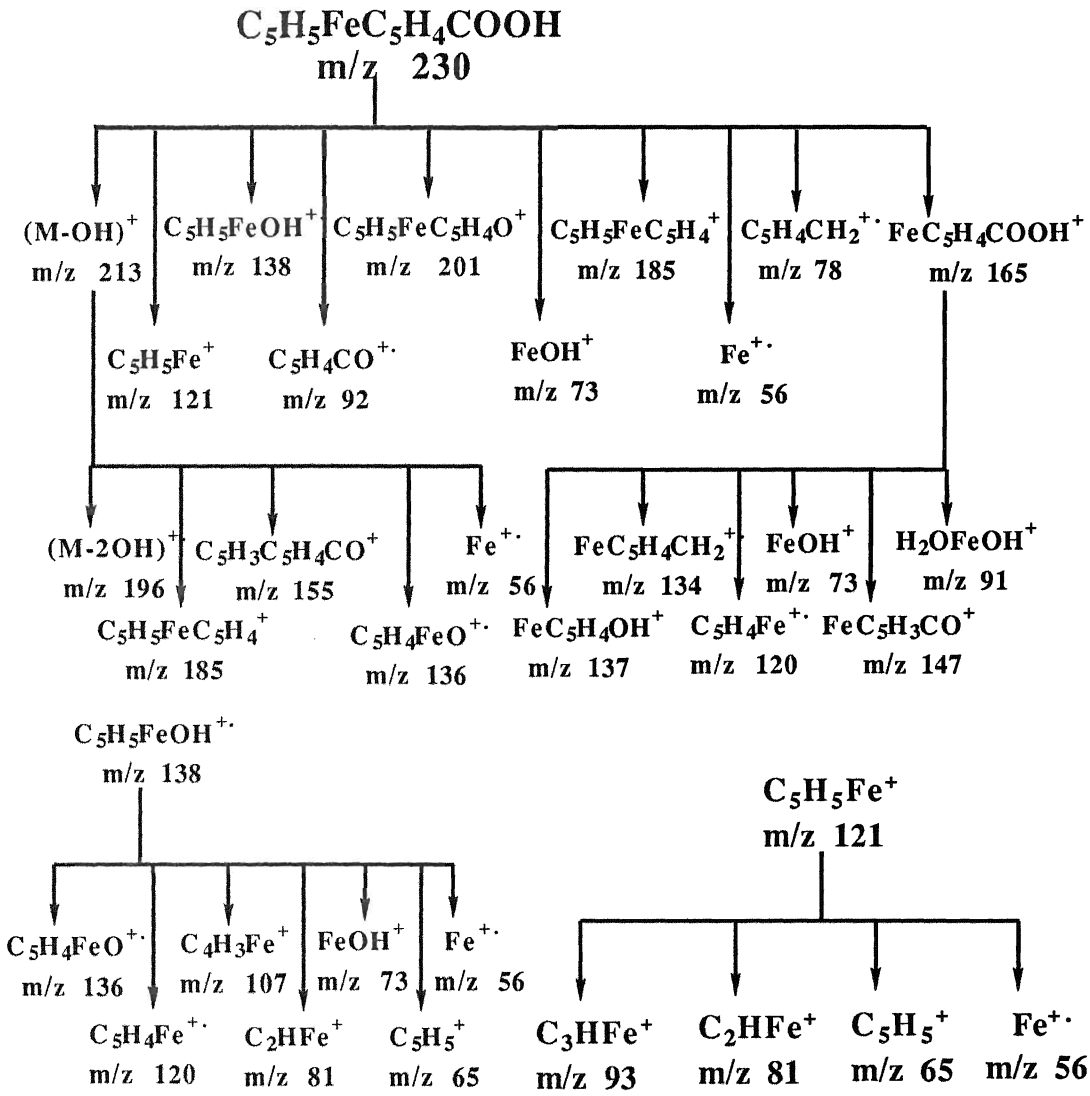

SCHEME 59 Fragmentation pattern of ferrocenecarboxylic acid/NBA under positive ion FAB

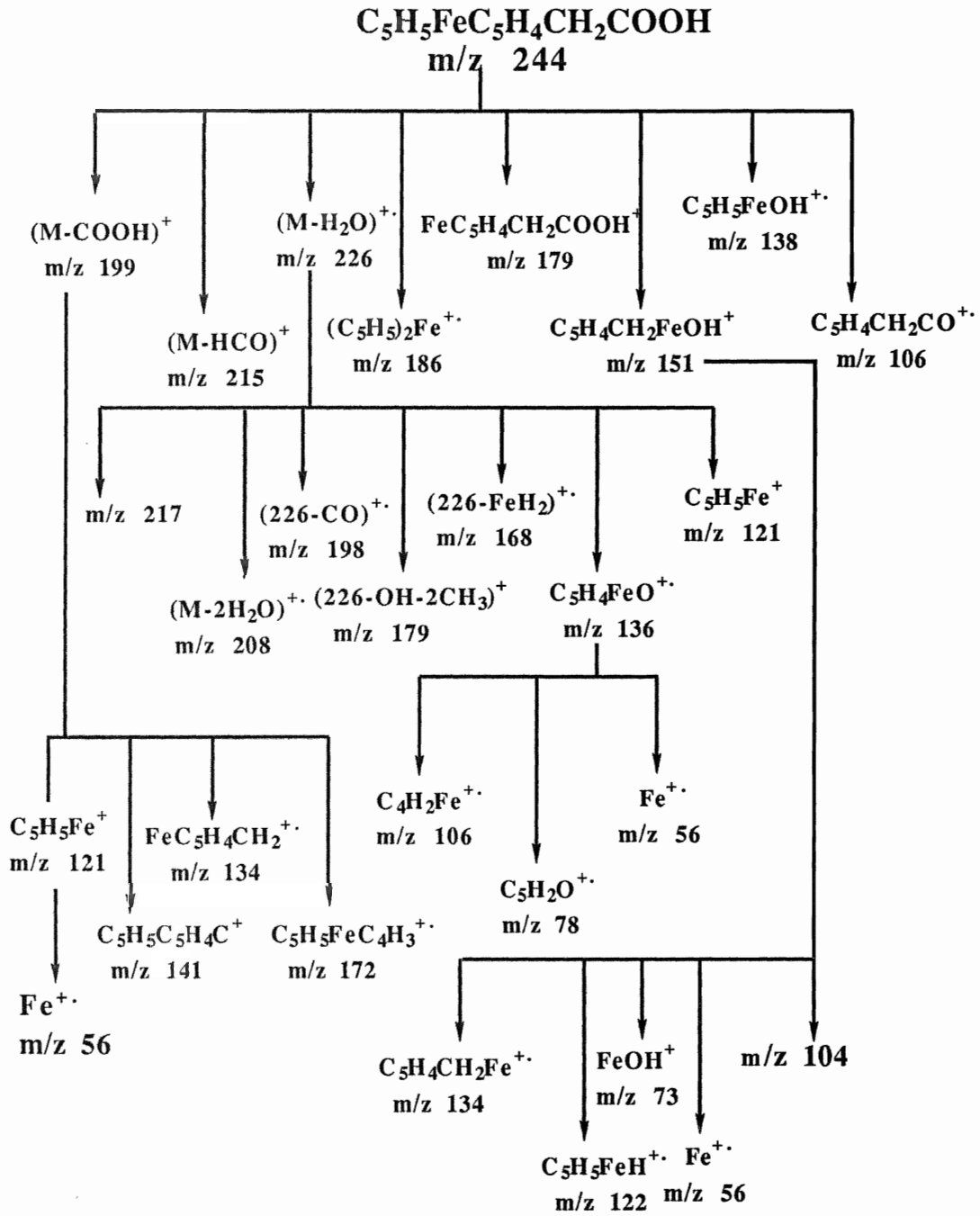

SCHEME 60 Fragmentation pattern of ferroceneacetic acid/NBA under positive ion FAB

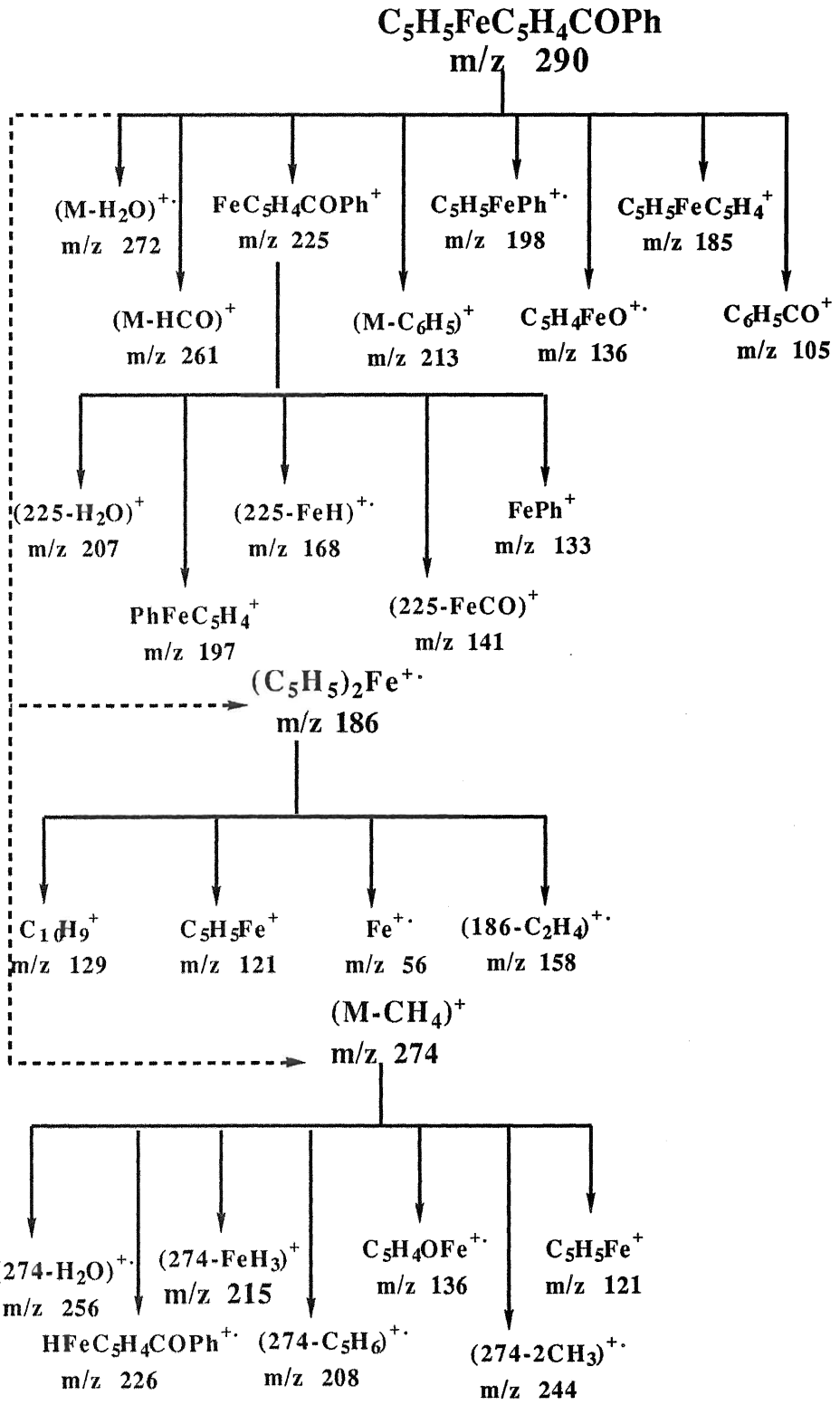

SCHEME 61 Fragmentation pattern of benzoylferrocene/NBA under positive ion FAB

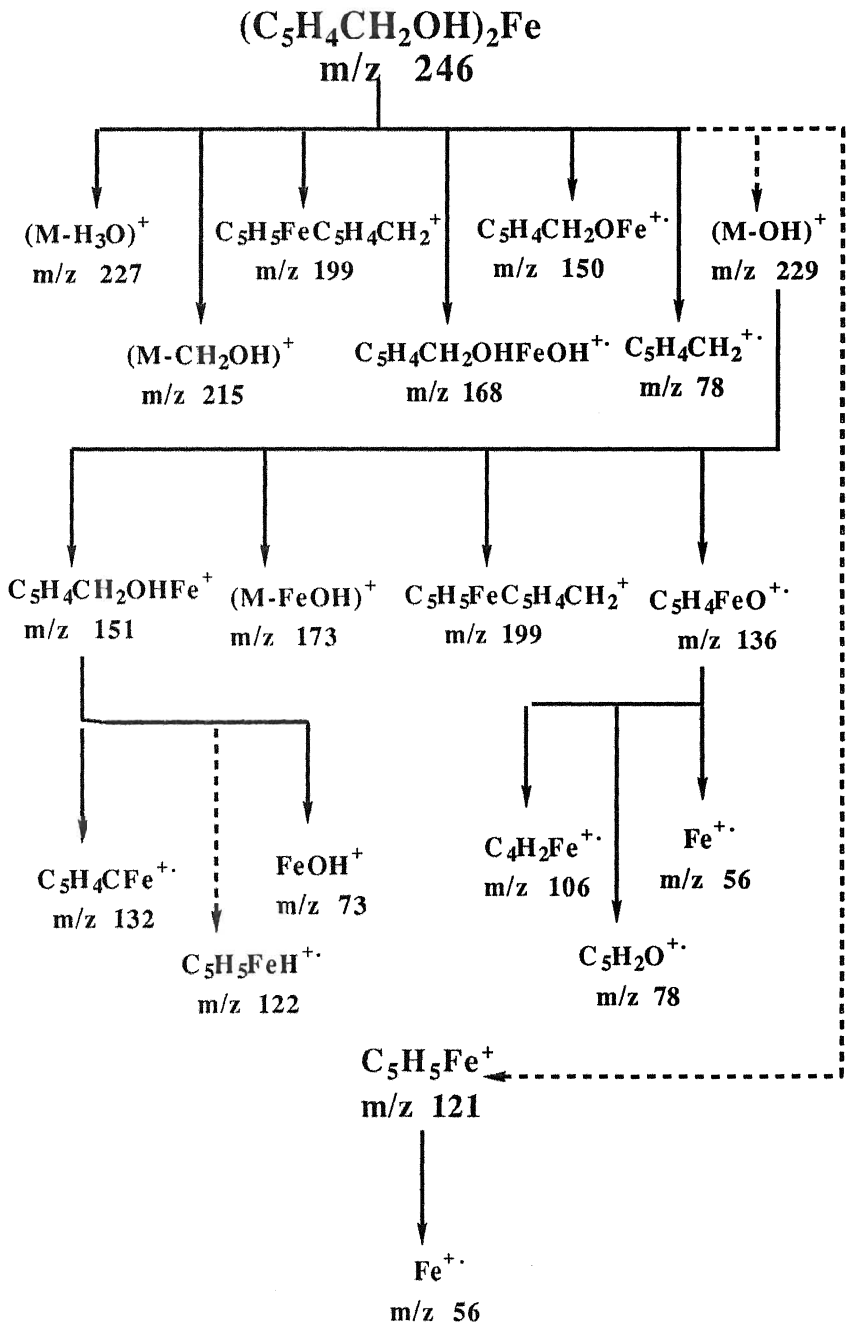

SCHEME 62 Fragmentation pattern of 1,1'-ferrocenedimethanol/NBA under positive ion FAB

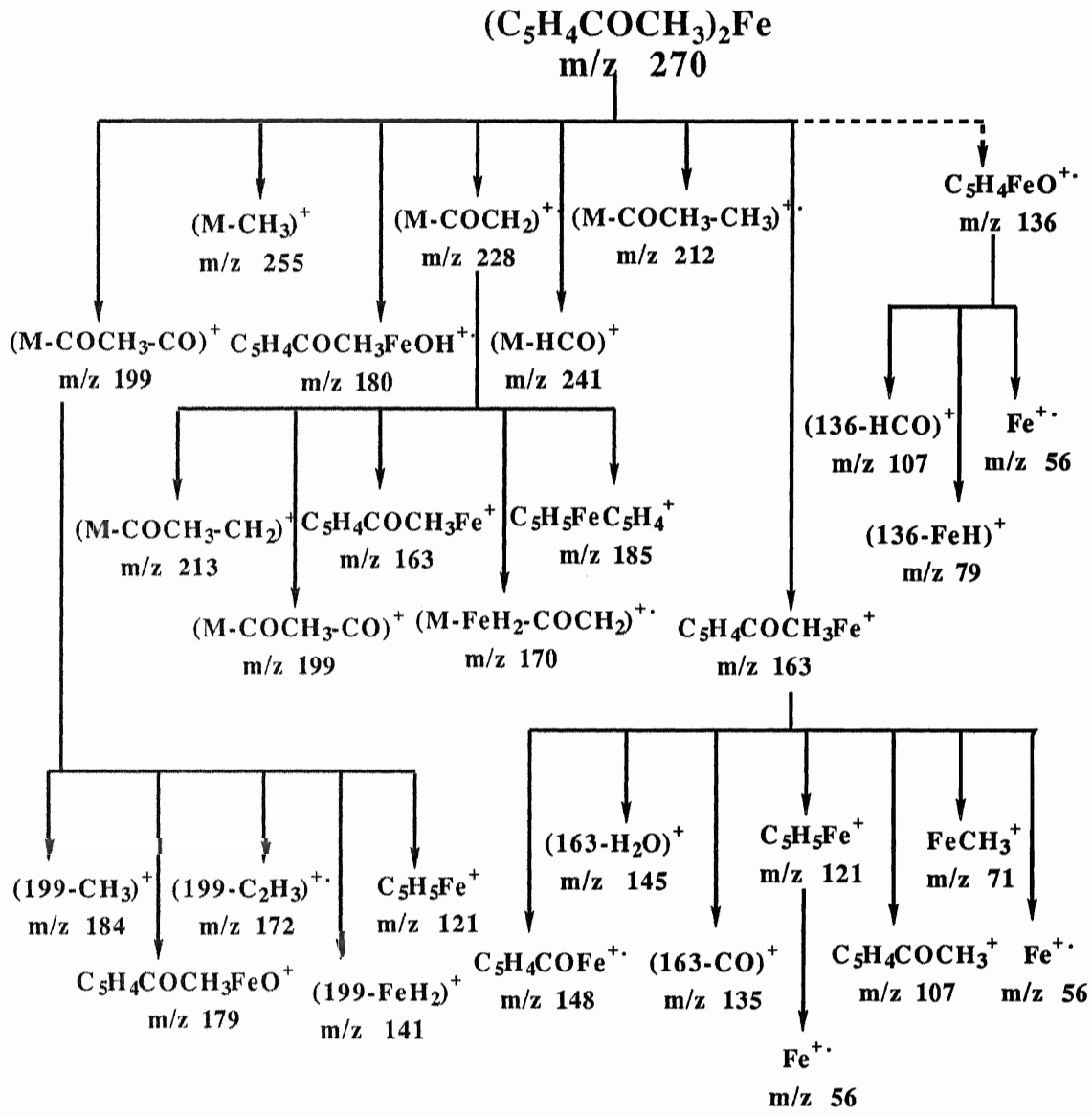

SCHEME 63 Fragmentation pattern of 1,1'-diacetylferrocene/NBA under positive ion FAB

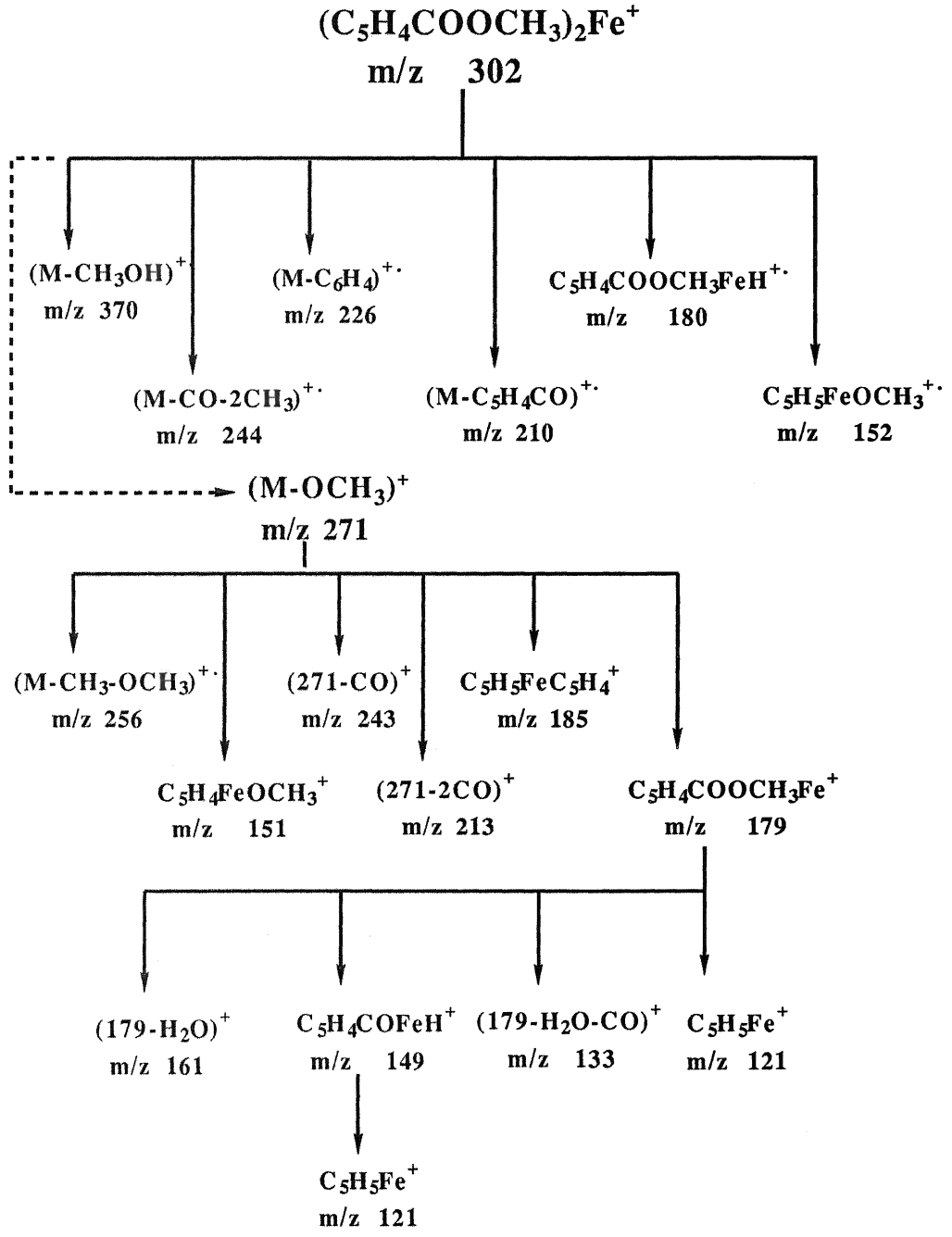

SCHEME 64 Fragmentation pattern of 1,1'-dimethylferrocenedicarboxylate/NBA under positive ion FAB

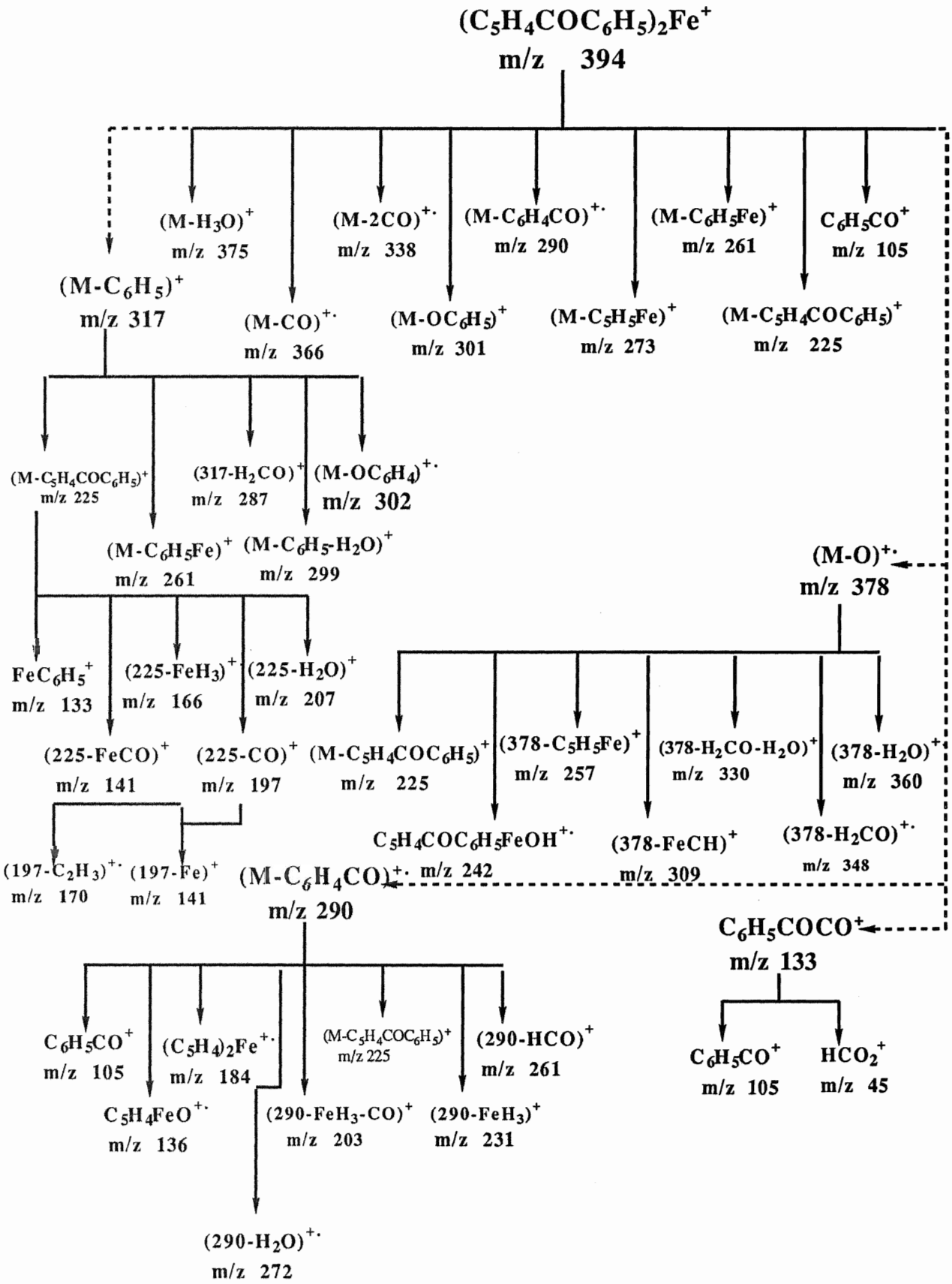

SCHEME 65 Fragmentation pattern of 1,1'-dibenzoylferrocene/NBA under positive ion FAB

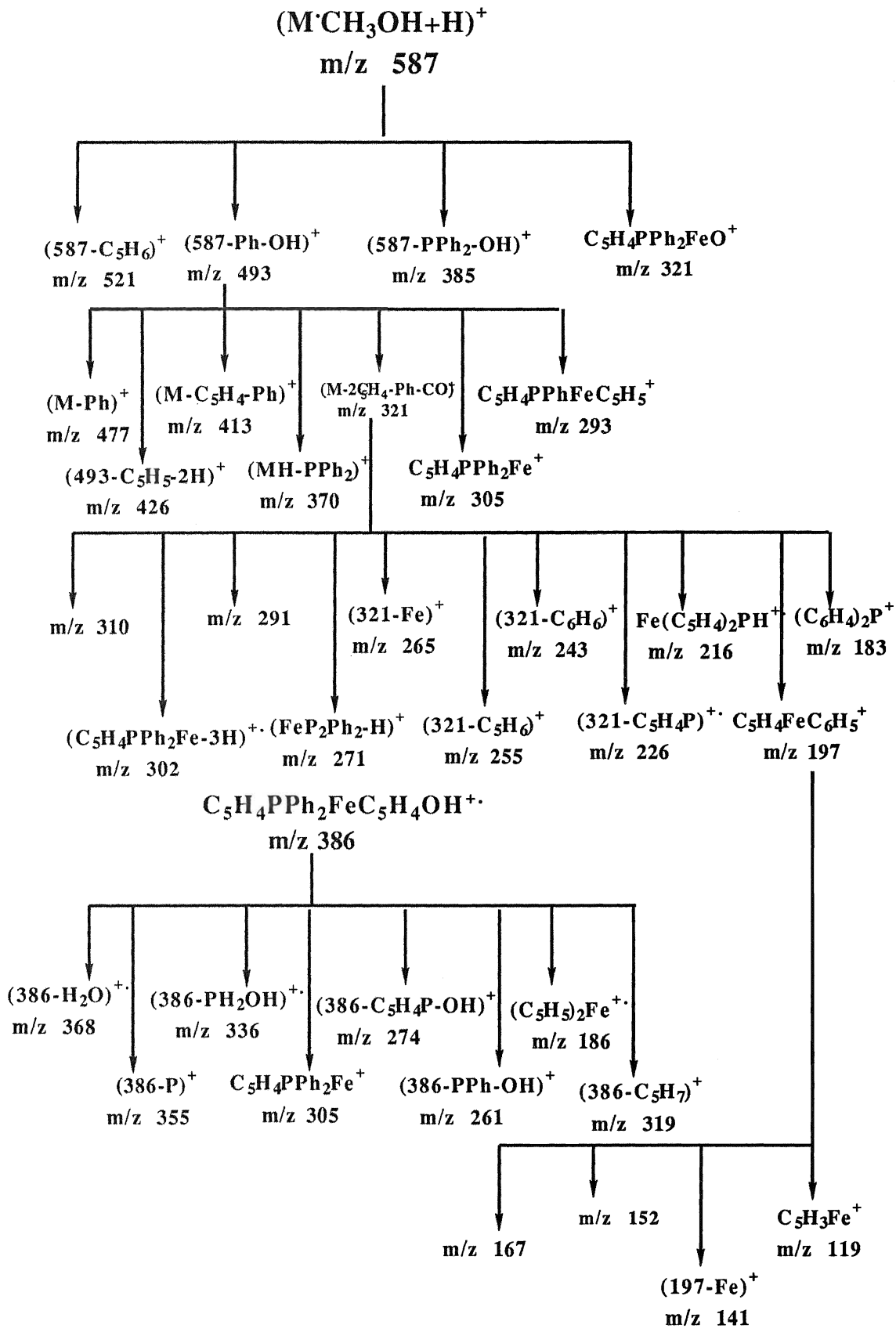

SCHEME 66 Fragmentation pattern of 1,1'-bis(diphenylphosphino)ferrocene/NBA under positive ion FAB

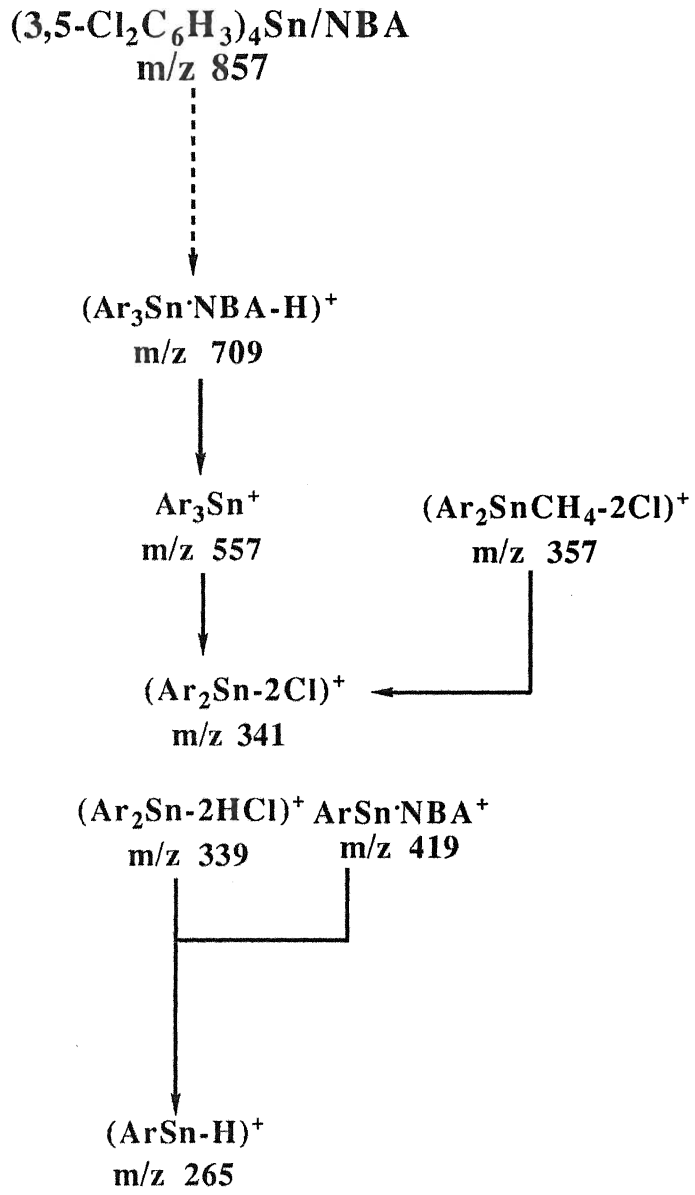

SCHEME 67 Fragmentation pattern of $(3,5\text{-}Cl_2C_6H_3)_4Sn$/NBA under CA positive ion FAB

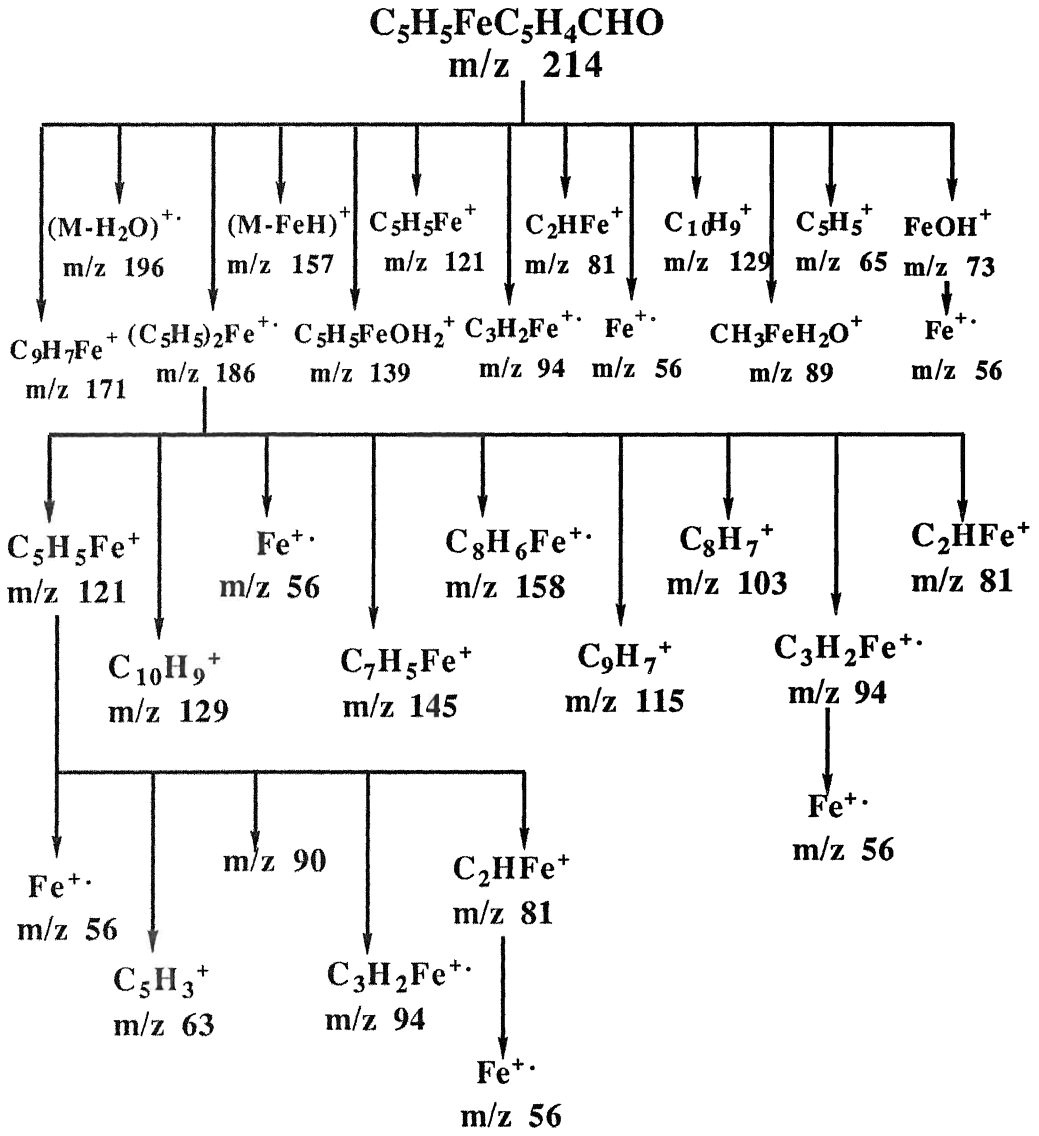

SCHEME 68 Fragmentation pattern of ferrocenecarboxaldehyde/NBA under CA positive ion FAB

.4.

CONCLUSIONS

Aryltin Compounds

Both EI MS and FAB MS studies on this group of compounds have been done. In all of the EI spectra of aryltin compounds, tin-containing peaks are dominant. Ligand related peaks are few and usually of low abundance. More than half of the spectra have not shown molecular ion peaks. If they appear, they usually have very low abundance. Ar_3Sn^+ ion peaks are the most intense metal-containing peaks in all EI spectra except in those of $(2,4,6\text{-}(CH_3)_3C_6H_2)_3SnCl$ and $(2,4,6\text{-}(CH_3)_3C_6H_2)_3SnBr$, in which $(Ar_2SnX\text{-}H)^+$ are the most intense peaks. In most cases, even-electron ions, such as Ar_3Sn^+ and $ArSn^+$, dominate the spectra. However, in some cases, odd-electron ion Ar_2Sn^+ and Sn^+ peaks have very high abundance. In fact, Sn^+ peaks appear in all EI spectra. This phenomenon doesn't occur in the positive ion FAB spectra.

The EI MS studies of this group of compounds show that the ligand type has the biggest effect on the corresponding spectra, then the substituent group type, and finally the substituent group position on benzene ring. Such effects can be seen from both the intensities of peaks in these spectra and the fragmentation patterns of each compound.

The fragmentation pattern studies under EI with linked scans indicate the major decomposition modes of these compounds as the following:

$$M^{+\cdot} \longrightarrow Ar_2Sn^{+\cdot} + Ar_2$$

$$Ar_3Sn^{+} \longrightarrow ArSn^{+} + Ar_2$$

$$ArSn^{+} \longrightarrow Ar + Sn^{+}$$

However, detailed fragmentation patterns are different from one compound to another.

In FAB MS studies of this group of compounds, matrix optimization showed that 3-nitrobenzyl alcohol (NBA) and 2-nitrophenyloctylether (NPOE) can give good FAB MS spectra. Of these two, NBA can provide much better spectra.

Like their EI counterparts, metal-containing peaks are dominant in all positive ion FAB spectra in matrix NBA. In most of the +ve FAB spectra, no molecular ion peaks show up. Even in those spectra in which molecular ion peaks appear, they usually are of low abundance. Even-electron ion peaks are very intense, such as Ar_3Sn^+ and $ArSn^+$. Compared with EI spectra, odd-electron ion peaks Ar_2Sn^+ and Sn^+ are in low abundance, if they do show up. Both ligand related and matrix related peaks are of low abundance.

The effect of the substituent group position, the substituent group type on benzene ring, and the ligand type, on the positive ion FAB spectra in NBA have been studied. The results show that the ligand type has the biggest effect, then the substituent group type, finally the substituent group position. However, when the substituent group becomes larger, substituent group position also has a bigger effect on the +ve FAB spectra in NBA.

The fragmentation mechanism studies under +ve FAB with linked scans show that there are some similarities between the EI and the +ve FAB fragmentation patterns. However, the major decomposition modes of these compounds under EI are not wholly applicable under +ve FAB. Generally, the +ve FAB mode can provide more detailed fragmentation patterns.

The negative ion FAB MS studies of all of these compounds have been carried out.

The negative ion FAB spectra of these compounds are quite different, compounds either giving good spectra or none whatsoever, depending upon substituents. The negative ion FAB spectra show bigger differences with their +ve FAB counterparts. The major one is that matrix related metal-containing peaks are relatively more intense in negative ion FAB spectra.

Ferrocene Compounds

For this group of compounds, both EI MS and positive/negative ion FAB MS in NBA matrix studies have been done. Good agreement between the recorded EI spectra and those results reported earlier [69, 74, 89, 99, 100] is reached. The fragmentation mechanism studies under EI with linked scans in the first field free region show that most of the intense peaks in the EI spectra are the direct products of molecular ion decomposition. Some differences are observed between the first field free region linked scans and the second field free region linked scans reported elsewhere [89] of some ferrocene derivatives. Generally, the first field free region linked scans can provide more detailed information on the fragmentation patterns. In EI spectra, molecular ion peaks are of high abundance. In most cases, they are base peaks.

All but two of the compounds give very good + ve FAB spectra. In all of the positive ion FAB spectra, but that of 1,1'-bis(diphenylphosphino)ferrocene, molecular ion peaks are base peaks. Fragment peaks are usually of low abundance, just like that in EI spectra. These FAB spectra also produce some fragment peaks which are not available in EI spectra. The fragmentation mechanism studies of the ferrocenes under positive ion FAB with linked scans techniques in the first field free region indicate that, under FAB mode, more detailed information on the decomposition patterns can be obtained. These studies also show that most of the intense peaks in the +ve FAB spectra are the direct products of molecular ion decomposition, which suggests the unimolecular reaction is the dominant form, just as that in EI mode. Thus, the positive ion FAB MS proves its applicability to the ferrocene compounds.

The negative ion FAB MS studies of these ferrocenes in NBA matrix, however, did not produce any sample related peaks.This probably is the result of the poor sensitivity of the negative ion FAB MS.

.5 .

REFERENCES

[1]. E. Goldstein, Berl. Ber., 39, 691 (1886).

[2]. W. Wien, Ann. Physik, 65, 440 (1898).

[3]. J. J. Thomson, "Rays of Positive Electricity and Their Application to Chemical Analysis" (Longmans and Green Co., London, 1913).

[4]. J. J. Thomson, Phil. Mag., 21, 225 (1911).

[5]. A. J. Dempster, Phys. Rev., 11, 316 (1918).

[6]. F. W. Aston, Phil. Mag., 38, 707 (1919).

[7]. R. Herzog, Z. Phys., 89, 447 (1934).

[8]. R. Herzog and J. H. E. Mattacuch, Annalen der Physik. Leipzig., 19, 345 (1934).

[9]. M. J. O'Neal and T. P. Wier, Anal. Chem., 23, 830 (1951).

[10]. H. E. Duckworth, R. C. Barber, V. S. Venkatasubramanian, "Mass Spectroscopy", 2nd edition (Cambridge University Press, 1986).

[11]. T. Matsuo, Org. Mass Spectom., 26, 374 (1991).

[12]. Ian Howe, Dudley H. Williams, Richard D. Bowen, "Mass Spectrometry: Principles and Applications", 2nd edition (McGraw-Hill Inc. 1981).

[13]. J. M. Miller and G. L. Wilson, Adv. Inorg. Chem. Radiochem., 18, 229 (1976).

[14]. M. Barber, R. S. Bordoli, R. D. Sedgwick and A. N. Tyler, Nature, 293, 270 (1981).

[15]. M. Barber, R. S. Bordoli, R. D. Sedgwick, and A. N. Tyler, J. Chem. Soc.

Chem. Comm., 325 (1984).

[16]. J. M. Miller, Adv. Inorg. Chem. Radiochem., 28, 1 (1984).

[17]. E. De Pauw, Mass Spectrom. Rev., 5, 191 (1986).

[18]. M. Barber, R. S. Bordoli, R. D. Sedgwick, and A. N. Tyler, Nature (London), 293, 270 (1981).

[19]. M. Barber, R. S. Baldwin, R. D. Sedgwick, A. N. Tyler, Biomed. Mass Spectrom., 492, 8 (1981).

[20]. J. M. Miller, J. Organomet. Chem., 249, 299 (1983).

[21]. H. R. Schulten and H. M. Schiebel, Naturwissenschaften, 65, 223 (1978).

[22]. F. W. Aston, Proc. Roy. Soc., Ser. A 149, 396 (1935).

[23]. H. R. Morris, M. Panico, and N. J. Haskins, Int. J. Mass Spectrom. Ion Phys., 26, 363 (1983).

[24]. Richard M. Caprioli, Anal. Chem., 62, 477A (1990).

[25]. M. S. B. Munson and F. H. Field, J. Am. Chem. Soc., 88, 2621 (1966).

[26]. E. C. Huang, T. Wachs, J. J. Conboy, and J. D. Henion, Anal. Chem., 62, 713A (1990).

[27]. C. Merritt, Jr. and C. N. McEwen, "Field Desorption Mass Spectrometry" , pp1-2, (Marcel Dekker Inc., New York, 1990).

[28]. P. Lattimer Robert, Hans-Rolf Schulten, Anal. Chem., 61, 1210 (1989).

[29]. R. D. Macfarlane, R. P. Skowroski, D. F. Torgerson, Biochem. Biophys. Res. Commun., 60, 616 (1974).

[30]. J. Cotter Robert, Anal. Chem., 60, 781A (1988).

[31]. R. E. Honig and J. R. Woolston, Appl. Phys. Lett., 2, 138 (1963).

[32]. R. J. Cozemius, J. M. Capellen, Int. J. Mass Spectrom. Ion Phys., 34, 197 (1980).

[33]. F. Hillenkamp, and M. Karas, "Methods in Enzymology", V193, 280-294, Edited by J. A. McCloskey (Academic Press, 1990).

[34]. K. Tanaka, H. Waki, Y. Ido, S. Skita, Y. Yoshida, and T. Yoshida, Rapid Commun. Mass Spectrom. 2, 151 (1988).

[35]. D. M. Hercules, R. J. Day, K. Balasanmugam, T. A. Dang, C. P. Li , Anal. Chem., 54, 280A (1982).

[36]. H. W. Werner, "Developments in Applied Spectroscopy" 7A, P 239 (Plenum, New York, N. Y. , 1969).

[37]. A. Fulcher, M.Sc. Thesis, Dept. of Chem. Brock U., 1988.

[38]. S. J. Pachuta and R. G. Cooks, Chem. Rev. 87, 647 (1987).

[39]. D. H. Williams, A. F. Findeis, S. Naylor and B. W. Gibson, J. Am. Chem. Soc. 109, 1980 (1987).

[40]. J. Sunner, A. Morales and P. Kebarle, Anal. Chem. 60, 98 (1988).

[41]. C. A. Evans, Jr., Anal. Chem., 44, 67A (1972).

[42]. A. G. Harrison and R. J. Cotter, "Methods in Enzymology", V193, 1-37, Edited by J. A. McCloskey (Academic Press, 1990).

[43]. E. de Pauw, Mass Spectrom. Rev., 5, 191 (1986).

[44]. K. L. Busch, G. L. Glish and Scott A. McLuckey, "Mass Spectrometry /Mass Spectrometry: Techniques and Applications of Tandem Mass Spectrometry" , P59 (VCH Publishers Inc. , 1988).

[45]. K. R. Jennings, Int. J. Mass Spec. Ion Phys., 1, 227 (1968).

[46]. F. W. McLafferty, P. F. Bente, R. Kornfeld, S-C. Tsai, and I. Howe, J. Am. Chem. Soc., 95, 2120 (1973).

[47]. D. J. Douglas, J. Phys. Chem., 185, 86 (1982).

[48]. J. H. Beynon, R. G. Cooks, T. Keough, Int. J. Mass Spectrom. Ion Phys., 14, 437 (1974).

[49]. Yong-Chen Ning, "Structural Identification of Organic Compounds and Organic Spectrometry", (QingHua University Press, 1989).

[50]. V. H. Dibeler, J. Res. Natn. Bur. Stand., 49, 235 (1953).

[51]. B. G. Hobrock and R.W. Kiser, J. Phys. Chem., 65, 2186 (1961).

[52]. J. L. Occolowitz, Tetrahedron Letters, 43, 5291 (1966).

[53]. D. B. Chambers, F. Glockling and M. Weston, J. Chem. Soc. A, 1759 (1967).

[54]. J. M. Miller, Can. J. Chem., 47, 1613 (1969).

[55]. G. F. Lanthier, J. M. Miller and A. J. Oliver, Can. J. Chem., 51, 1945 (1973).

[56]. M. Gielen and G. Mayence, J. Organomet. Chem., 46,281 (1972).

[57]. P. G. Harrison and S. R. Stobart, J. Organomet. Chem., 47, 89 (1973).

[58]. I. Wharf, M. Onyszchuk, D. M. Tallet, and J. M. Miller, Can.J. Spect., 24, 123 (1979).

[59]. I. Wharf, M. Onyszchuk, J. M. Miller and T. R. B. Jones, J. Organomet. Chem., 190, 417 (1980).

[60]. J. M. Miller, H. Mondal, I. Wharf and M. Onyszchuk, J. Organomet. Chem., 306, 193 (1986).

[61]. G. K. Bratspies, J. F. Smith and J. O. Flill, J. Anal. Appl. Pyrolysis, 2 , 35 (1980).

[62]. M. Gielen, Org. Mass Spectrom., 18, 453 (1983).

[63]. F. A. Bottino, P. Finocchiaro, E. Libertin, and A. Recca, J. Coord. Chem., 12, 303 (1983).

[64]. J. M. Miller and A. Fulcher, Can. J. Chem., 63, 2308 (1985).

[65]. J. M. Miller and I. Wharf, Can. J. Spect., 32, 1 (1987).

[66]. M. F. Iskander, L. Labib, M. M. Z. Nour El-Din, M. Tawfik, Polyhedron, 8, 2755 (1989).

[67]. L. Friedman, A. P. Irsa, and G. Wilkinson, J. Amer. Chem. Soc., 77, 3689 (1955).

[68]. M. Cais, and M. S. Lupin, Advances in Organometallic Chemistry, Vol.8, P 211, Edited by F. G. A. Stone and R. West (Academic Press, 1970).

[69]. G. A. Junk and H. J. Svec, Recent Top. Mass Spectro., Lect., NATO Study Inst.,

85 (1969).

[70]. M. Cais, M. S. Lupin and J. Sharvit, Israel J. Chem., 7, 73 (1969).

[71]. D. T. Roberts, Jr., Diss. Abstr. B., 27, 2365 (1969).

[72]. I. J. Spilners, J. C. Larson, Org. Mass Spectrom., 3 , 915 (1970).

[73]. Curtis F. Sheley, Derry l. Fishel, Org. Mass Spectrom., 6, 1131 (1972).

[74]. Hiromu Imai, Bull. Chem. Soc. Hap., 45, 1264 (1972).

[75]. K. Yamakawa and M. Hisatome, Org. Mass Spectrom., 6, 167 (1972).

[76]. E. L. Mysove, I. R. Lyatifov, R. B. Materikova and N. S. Kochetkova, J. Organomet. Chem., 169, 301 (1979).

[77]. M. Hisatome, and K. Yamakawa, Organic Mass Spectrometry, 13, 1 (1978).

[78]. D. V. Zagoreskii, N. M. Loim, Yu. S. Nekrasov, V. F. Sizoi, and Yu.N. Sukharev, J. Organomet. Chem., 202, 201 (1980).

[79]. B. V. Zhuk, G. A. Domrachev, N. M. Semenov, E. I. Mysov, R. B. Materikova, N. S. Kochelkova, J. Organomet. Chem., 184, 231 (1980).

[80]. S. Chen, J. Organomet. Chem., 202, 183 (1980).

[81]. S. R. Patil, U. N. Kantak, and D. N. Sen, Organic Mass Spectrometry, 18, 136 (1983).

[82]. V. Rapic', and N. Filipovic'-Marinic', Organic Mass Spectrometry, 20, 688 (1985).

[83]. V. Rapic', and N. Filipovic'-Marinic', Organic Mass Spectrometry, 20, 104 (1985)

[84]. K-H. Thiele, C. Kruger, T. Bartik, M. Dargatz, J. Organomet. Chem., 352, 115 (1988).

[85]. J. Mirek, S. Rachwal, T. Gorecki, B. Kawaleck, P. Mirat and E. Szneler, J. Organomet. Chem., 344, 363 (1988).

[86]. C. Kruger, H-K. Thiele, M. Dargatz, and T. Bartik, J. Organomet. Chem., 362,

147 (1989).

[87]. K. L. Rinheart, Abstr. 16th Southeastern Regional Meeting Amer. Chem. Soc., Charleston, West Virginia Paper 120 (1964).

[88]. S. M. Shildcrout, J. Amer. Chem. Soc., 95, 3846 (1973).

[89]. G. Innorta, F. Scagnolari, A. Modelli, S. Torroni, A. Foffani, and S. Sorriso, J. Organometal. Chem., 241, 375 (1983).

[90]. N. Filipovic'-Marinic', V. Rapic', V. Kramer and B. Kralj, J. Organomet. Chem., 298, 405 (1985).

[91]. P. R. Nelson, J. R. Appling, E. K. Barefield and R. F. Moran, Inorg. Chem., 25, 1510 (1986).

[92]. T. Drewello and H. Schwarz, Inter. J. Mass spectrom. Ion Processes, 93, 177 (1989).

[93]. F. G. N. Cloke, A. M. Greenway, K. R. Seddon, A. A. Shimran, A. C. Swain, J. Organomet. Chem., 372, 231 (1989).

[94]. F. M. Lappert, M. J. McGeary, R. V. Parish, J. Organomet. Chem., 373, 107 (1989).

[95]. S. Barfuss, K. H. Emrich, W. Hirschwald, P. A. Dowben, N. M. Boag, J. Organomet. Chem., 391, 209 (1990).

[96]. I. Wharf, and M. G. Simard, Act. Cryst C (47), 1314 (1991); and references therein.

[97]. I. Wharf, Inorg. Chim., 159, 41 (1989).

[98]. J. S. Ni, M.Sc. Thesis, Dept. of Chem. Brock U., 1991.

[99]. A. Mandelbaum and M. Cais, Tetrahedron Letters, N0. 51, 3847 (1964).

[100]. D. V. Zagorevskii, T. V. Volkova, S. O. Yakushin, B. G. Antipov and Y. S. Nekrasov, Org. Mass Spectrom., 26, 748 (1991).

[101]. J. M. Miller and G. L. Wilson, Adv. Inorg. Chem. and Radiochem., 18, 229 (1976) and references therein.

[102]. T. Chivers, G.F. Lanthier, and J. M. Miller, J. Chem. Soc. (A), 2556 (1971).

[103]. M.J.S. Dewar, G.L.Grady, D.R.Kuhn and K.M.Merz, Jr., J. Amer. Chem. Soc., 106, 6773 (1984) and references therein.

[104]. J.D.Hawthorne, M.J.Mays and R.N.F. Simpson, J. Organomet. Chem., 12, 407 (1968).

[105]. F.W.McLafferty, Interpretation of Mass Spectra, 3rd edition(University Science Books, 1980).